

STUDIES IN COHERENT PUMP-PROBE SPECTROSCOPY OF THREE AND FOUR LEVEL SYSTEMS

By

NIHARIKA SINGH

(PHYS01200704030)

Bhabha Atomic Research Centre, Mumbai

*A thesis submitted to the
Board of Studies in Physical Sciences
In partial fulfillment of requirements
For the Degree of*

DOCTOR OF PHILOSOPHY

of

HOMI BHABHA NATIONAL INSTITUTE



November, 2012

Homi Bhabha National Institute

Recommendations of the Viva Voce Board

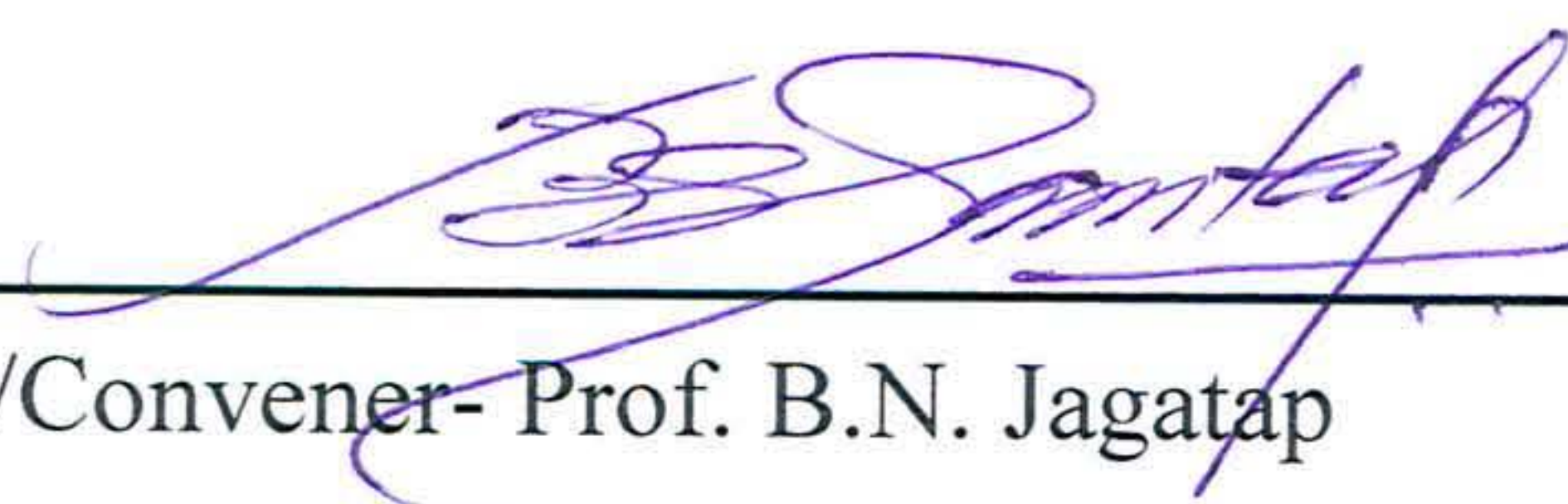
As members of the Viva Voce Board, we certify that we have read the dissertation prepared by **Niharika Singh** entitled “**Studies in coherent pump-probe spectroscopy of three and four level systems**” and recommend that it may be accepted as fulfilling the dissertation requirement for the Degree of Doctor of Philosophy.



20-3-2013

Chairman- Dr. G.P. Kothiyal

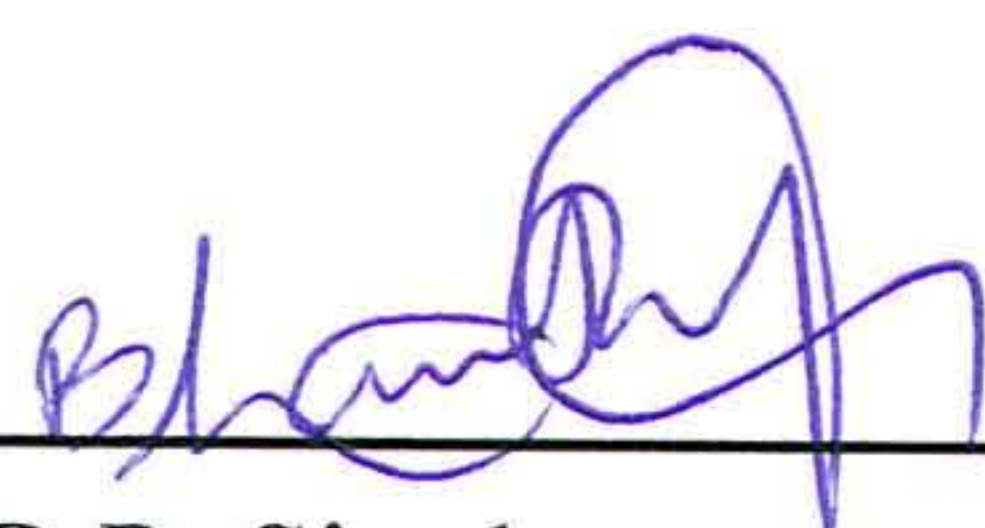
Date:



20-03-2013

Guide/Convener- Prof. B.N. Jagatap

Date:

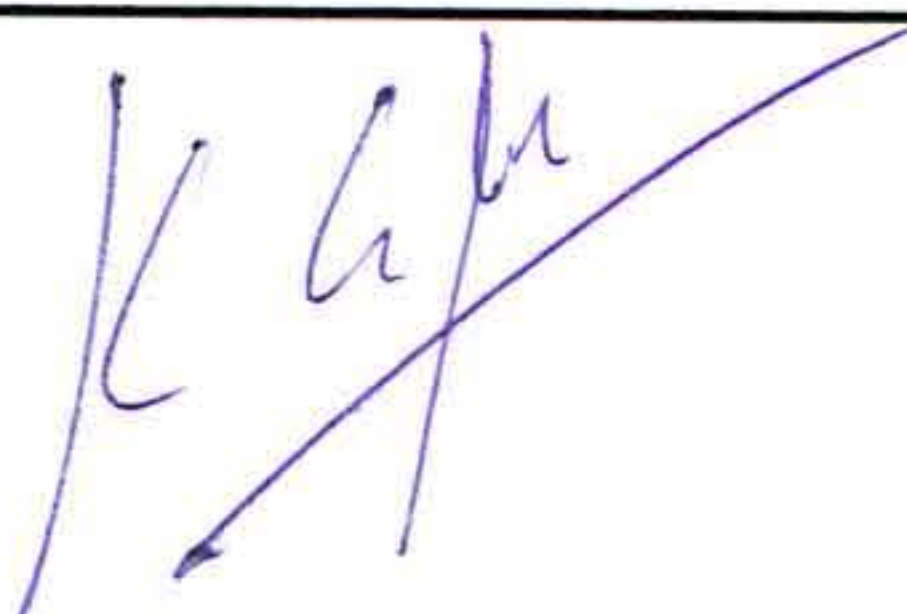


20 March, 2013

Member 1- Prof. B.P. Singh

Date:

Member 2- Dr. K.G. Manohar



Date: 20/3/2013

Final approval and acceptance of this dissertation is contingent upon the candidate's submission of the final copies of the dissertation to HBNI.

I hereby certify that we have read this dissertation prepared under our direction and recommend that it may be accepted as fulfilling the dissertation requirement.

Date: 20 March 2013

Place: Bhabha Atomic Research Centre, Mumbai, India

STATEMENT BY AUTHOR

This dissertation has been submitted in partial fulfillment of requirements for an advanced degree at Homi Bhabha National Institute (HBNI) and is deposited in the Library to be made available to borrowers under rules of the HBNI.

Brief quotations from this dissertation are allowable without special permission, provided that accurate acknowledgement of source is made. Requests for permission for extended quotation from or reproduction of this manuscript in whole or in part may be granted by the Competent Authority of HBNI when in his or her judgment the proposed use of the material is in the interests of scholarship. In all other instances, however, permission must be obtained from the author.

Niharika Singh

DECLARATION

I, hereby declare that the investigation presented in the thesis has been carried out by me.

The work is original and has not been submitted earlier as a whole or in part for a degree/
diploma at this or any other Institution/University.

Niharika Singh

Dedicated to.....

.....My Parents

ACKNOWLEDGMENTS

I would like to express my heartfelt gratitude and regards to my supervisor, Prof. B.N. Jagatap, for his luminous guidance and encouragement in executing this project from conception to completion. Fortunate to be one of his students I have learnt a tremendous amount of physics and benefited from his teaching and unwavering support. He helped me a lot in developing better insight of the problems and most of my work during the research years has been a recapitulation of his ideas. Also I could not stress enough the contribution made by Dr. R. D'Souza and Dr. Q.V. Lawande who have been influential mentors to me during these foundation years. Their invaluable support and guidance were integral to the successful completion of this thesis. Sometimes when calculations became too hazy for me to make any sense, Dr. D'Souza explained the intricacies involved with great enthusiasm. Lawande Sir was generous enough to travel all the way from Goregaon even after his retirement just to help me whenever I got stuck. These three persons have instilled in me the importance of hard work, unrelenting patience, perseverance and composure.

I extend many thanks to my doctoral committee members, Dr. G.P. Kothiyal, Prof. B.P. Singh and Dr. K.G. Manohar for their encouragement, keen assessment and invaluable suggestions. Special thanks to Dr. K.G. Manohar who helped me clarify several doubts.

Though for a short time I had the privilege to work with Dr. Ayan Ray who taught me various aspects of experimental quantum optics. Thanks to Ayan and Y.B. Kale for their help with the experiments.

My sincerest thanks are for my friends Rita, Charu, Manju, Neelam, Saroj, Seema and Susheel for their moral support and providing a sympathetic ear whenever needed. Special thanks to Susheel for

bolstering me through many tough times. I would also like to thank Dr. S. Pradhan, Dr. Asawari Rath, Dr. Aparna Shastri, Paramjeet Singh, Shitanshu and Anubhav for several fruitful discussions.

I would also like to recognize some great teachers who taught me a good deal of science and encouraged me to pursue a research career, Late Prof. B.P. Asthana, Prof. B.P. Mandal, Dr. R.K. Singh and Prof. S. Singh. Thanks are due to the HBNI program for funding my doctoral studies.

Finally I am extremely grateful to my parents, my brother Shammi and sister Gunjan to whom I am eternally indebted, for always believing in me and making this a reality. They have been considerate of my demands, pressure and erratic mood swings through these years. Words are not enough to express my gratitude for their love, unconditional support and blessings.

CONTENTS

	Page no.
A. SYNOPSIS	xiv
B. LIST OF PUBLICATIONS	xxiv
C. LIST OF FIGURES	xxix
D. LIST OF TABLES	xxxvii
1. CHAPTER 1: INTRODUCTION	1-22
1.1 Coherence and Interference in Atom-Field Interaction	2
1.1.1 Rabi Oscillations and Dressed States	4
1.1.2 Autler-Townes Splitting	5
1.1.3 Coherent Population Trapping	6
1.1.4 Electromagnetically Induced Transparency	7
1.1.5 Electromagnetically Induced Absorption	9
1.2 Role of Incoherence	10
1.2.1 Collisional Relaxation	10
1.2.2 Spontaneously Generated Coherence	11
1.2.3 Laser Phase Fluctuations	12
1.3 Scope and Perspectives	13
1.3.1 Ultra-Precision Measurements	13
1.3.2 Amplification without Inversion	15

1.3.3	Slow, Fast and Stopped Light	16
1.3.4	Negative Refraction	17
1.3.5	Enhancement of Nonlinear Processes	18
1.4	Organization of the Thesis	19
2.	CHAPTER 2: MASTER EQUATION APPROACH TO LASER MATTER INTERACTION	23-43
2.1	Introduction	23
2.2	Derivation of the Master Equation for Three-Level Systems	25
2.2.1	Hamiltonian	25
2.2.2	Time Evolution of the System	27
2.2.3	Master Equation for Λ , V and Ξ Systems	36
2.3	Master Equation for Four-Level Systems	37
2.3.1	Degenerate Double Lambda System	38
2.3.2	Tripod System	39
2.3.3	N- Resonance System	39
2.4	Master Equation for Dipolar Molecular Systems	40
3.	CHAPTER 3: COHERENCE AND INTERFERENCE IN THREE-LEVEL DIPOLAR MOLECULE	44-66
3.1	Introduction	44
3.2	Theoretical Formulation	46
3.3	Absorption Spectrum and Dispersion	49

3.4 Doppler Averaging	55
3.4.1 Linewidth of EIT in a Doppler Broadened Medium	56
3.4.2 Dispersion at EIT Resonance	60
3.5 Role of Virtual Mechanism	62
3.6 Configuring a Three-level Molecular System	65
4. CHAPTER 4: COHERENCE IN DEGENERATE DOUBLE A SYSTEM	67-90
4.1 Introduction	67
4.2 Theoretical Formulation	69
4.3 Perturbative Analysis and Dressed States	71
4.4 Suppression of Subnatural Resonance	76
4.5 Electromagnetically Induced Transparency	79
4.6 Coherent Spectroscopy in Six-Level Configuration	83
4.7 Experimental Realization of Simultaneous Dressing	85
4.7.1 Experimental Scheme	85
4.7.2 Results and Discussion	88
5. CHAPTER 5: AMPLIFICATION WITHOUT INVERSION IN DEGENERATE DOUBLE A SYSTEM	91-108
5.1 Introduction	91
5.2 Model and Numerical Results	92
5.3 Perturbative Analysis	96

5.4 Doppler Averaging	101
5.5 Quantum Jump Approach to AWI	103
6. CHAPTER 6: COHERENCE AND INTERFERENCE IN	109-138
DOUBLE DARK RESONANT SYSTEMS	
6.1 Introduction	109
6.2 Double Control EIT Resonances in Tripod System	110
6.2.1 Model and Basic Formulation	110
6.2.2 Results and Discussion	113
6.3 Pump - probe spectroscopy of N-resonance system	118
6.3.1 Variants of N System	118
6.3.2 Theoretical Formulation	119
(a) <i>Model A</i>	120
(b) <i>Model B</i>	120
(c) <i>Model C</i>	120
6.3.3 Absorption Spectra	121
(a) <i>Absorption in Model A</i>	121
(b) <i>Absorption in Model B</i>	123
(c) <i>Absorption in Model C</i>	125
6.3.4 Switching Between EIA and EIT in Model C	126
6.4 Spontaneously Generated Coherence in N system	128
6.4.1 Theoretical Formulation	128
6.4.2 Perturbative Analysis	129

6.4.3 Results and Discussion	130
6.5 EIT in Λ and N System: Experimental	135
7. CHAPTER 7: PHASE FLUCTUATIONS IN COHERENT DYNAMICS OF N-RESONANCE	139-164
7.1 Introduction	139
7.2 Theoretical Formulation	141
7.2.1 Numerical Analysis	145
7.2.2 One Time Averages	146
7.3 Effect of Phase Fluctuations on Three- and 2+1- Photon Resonances	147
7.3.1 Steady - State Population Distribution	148
(a) <i>Three-Photon Resonance</i>	148
(b) <i>2+1-Photon Resonance</i>	155
7.3.2 Time Dependent Behaviour of the Population Distribution	159
7.4 Effect of Phase Fluctuations on Absorption	163
8. CHAPTER 8: COHERENCE INDUCED NEGATIVE REFRACTIVE INDEX IN FOUR-LEVEL ATOMIC MEDIUM	165-184
8.1 Introduction	165
8.2 Approaches for Realization of Negative Refraction Index	167
8.3 Description of the Models	170
8.4 Realization of Negative Refractive Index in Model (a)	171

8.4.1	Theoretical Formulation	171
(a)	Density Matrix Equations and Coherences	171
(b)	Electric and Magnetic Response	173
8.4.2	Results and Discussion	175
8.5	Realization of Negative Refractive Index in Model (b)	179
8.5.1	Theoretical Formulation	179
8.5.2	Results and Discussion	181
9.	CHAPTER 9: CONCLUSIONS AND FUTURE SCOPE OF THE WORK	185-193
9.1	Conclusions	185
9.2	Future Scope of the Work	192
	<i>APPENDIX</i>	194-205
<i>A-1</i>	<i>Zero Order Polarizations of Degenerate Double Λ System</i>	194
<i>A-2</i>	<i>Absorption and Dispersion in Degenerate Double Λ System</i>	195
<i>A-3</i>	<i>Low Frequency Coherence in Degenerate Double Λ System</i>	197
<i>A-4</i>	<i>Probability Amplitudes for Quantum Jump Approach</i>	199
<i>A-5</i>	<i>Steady State Populations in Tripod System</i>	200
<i>A-6</i>	<i>Steady State Populations in N System</i>	201
<i>A-7</i>	<i>Non-Zero Elements of Matrix M^{pqS} in N System</i>	204
	<i>BIBLIOGRAPHY</i>	206-221



Homi Bhabha National Institute

Ph.D. PROGRAMME

1. Name of the Student:	Niharika Singh
2. Name of the Constituent Institution:	Homi Bhabha National Institute
3. Enrolment No. :	PHYS01200704030
4. Title of the Thesis:	Studies in coherent pump-probe spectroscopy of three and four level systems
5. Board of Studies:	Physical Sciences

SYNOPSIS

Manipulation and control of atomic/molecular response by electromagnetic fields is one of the central themes of quantum optics research in recent years [1-15]. These control strategies rely on quantum coherence and interference in multi-level atomic/molecular systems that are coherently driven by two or more electromagnetic fields [1-4]. In this context, phenomena such as electromagnetically induced transparency (EIT), electromagnetically induced absorption (EIA), coherent population trapping (CPT), amplification without inversion (AWI) etc. have been discussed in great details [1-5]. Apart from generating renewed interest in the understanding of subtle effects in coherent

photon-atom interactions, these studies have created a new technological frontier based on photon engineering in a dressed atomic medium. Current interest in this area is driven by several important metrological applications, i.e., atomic frequency standards, miniaturized atomic clock, ultra-precision atomic magnetometry, atomic frequency offset locking, which are primarily derived from sub-natural linewidths of the dark resonances associated with EIT and CPT phenomena [5-7]. In more recent years, increasing attention is being paid to several other closely related phenomena which include for example, subluminal and superluminal light propagation, storage of light, quantum information processing and also the search for metamaterials, i.e., innovative systems that display negative refractive index [8-10].

The present thesis deals with coherent dynamics of multi-level atomic/molecular systems and its manifestation in the observation of several of the above referred phenomena, i.e., EIT, EIA, AWI and negative refractive index, together with the issues connected with spontaneously generated coherence (SGC), Kerr nonlinearity and the effect of finite bandwidths of driving fields. The major part of the thesis is concerned with theoretical aspects of coherent laser-atom/molecule interaction and predictions of novel effects arising from the field induced coherence and interference. These studies have been done in the framework of master equation and the systems investigated are three- and four-level atoms in various level configurations, i.e., Λ , double Λ , tripod, N-resonance etc [10]. Hyperfine manifolds of D_1 and D_2 transitions of alkali atoms are primarily used for constructing these level schemes. In order to provide a flavor of the coherent pump-probe spectroscopy for precision measurements, a few experimental results are also reported for a medium of alkali atoms [11].

The thesis is organized in nine chapters according to the various atomic/molecular systems studied and the quantum coherence phenomena associated with them.

Chapter-1 presents a brief introduction to the subject of quantum coherence and interference in driven multi-level systems and their manifestations in tailoring optical properties of an atomic/molecular medium [1-10]. The underlying concepts, the current status of the field and the fascinating applications of these phenomena in basic and applied sciences are briefly discussed here. The contents of this chapter, thus, provide both the motivation and the basis for the work presented in the subsequent chapters.

Chapter-2 provides the discussion on the master equation framework used for addressing the interaction of multi-level system with coherent multi-frequency electromagnetic field. A prototype system for investigating quantum coherence and interference phenomena is a three-level atomic system in Λ , V or Ξ configurations [1-5]. An explicit derivation of the semiclassical master equation in electric dipole and rotating wave approximations is discussed here for a three-level atomic system interacting with two external coherent fields and incoherent vacuum fields. The total system of atom and vacuum reservoir is described by a Hamiltonian in the second quantized form whereas the external fields are assumed to be classical. The technique of projection operators is used to eliminate the field modes and obtain the master equation for reduced atomic density operator from the Liouville equation. The discussion is then generalized for various four-level schemes of interest. Permanent dipole moments associated with molecular transitions provide pathways for multi-photon transitions and consequently their inclusion in the master equation is of paramount importance while dealing with coherent pump-probe spectroscopy of molecular systems [12]. In this context, we

develop and discuss the necessary master equation framework for a three-level molecular Λ system with permanent dipole moments and undergoing m - and n -photon transitions on pump and probe resonances. The master equation applicable to pertinent level schemes is then used as a starting point for analysis of steady state as well as time dependent behaviour of quantum systems and associated interference effects in the subsequent chapters. Connection to the experimental systems is established by averaging atomic/molecular response over Maxwell-Boltzmann velocity distribution.

Chapter-3 deals with the study of coherent pump-probe spectroscopy of three-level molecular Λ system with permanent moments. The motivation for these studies is provided by the very recent interest in EIT in the molecular domain [13]. A particular issue that is unique for molecules is the existence of diagonal or permanent dipole moments. It is therefore interesting to explore the role of permanent dipole moments on the observation of EIT and its connection to the issue of subluminal and superluminal light propagation. Master equation for a three-level Λ system including the permanent dipole moments is used to obtain analytical expressions for $m+n$ photon EIT and dispersion for a medium of stationary as well as Doppler broadened molecular medium. Contrary to the earlier reported work [13], we observe no amplification in 2+2 photon process when the sign of the permanent moments is reversed. Reasons for these contrasting observations are discussed. Our study shows that the permanent moments essentially damp the laser-molecule Rabi frequency to result in narrower EIT line width and larger group velocity index. These effects are further enhanced when the order of the multi-photon process is increased. While considering the multi-photon EIT mediated by permanent dipole mechanism, it is important to include the effect of virtual mechanism.

This issue is discussed by considering the special case of 2+1-photon EIT. The discussion presented in this chapter, thus, provides an integrated view of coherent pump-probe spectroscopy of a medium of dipolar molecules and its comparison with atomic case.

Chapter-4 presents detailed analysis of coherent pump-probe spectroscopy of Λ system with an additional adjacent excited level. The level scheme thus consists of two simultaneous Λ resonances with common ground levels and excited by the same pair of pump and probe fields, i.e., degenerate double lambda (DDL) resonance [6]. This level configuration is the simplest of the four-level systems and is experimentally relevant since it occurs naturally in all coherent spectroscopy experiments on D_1 and D_2 transitions of alkali atoms owing to the close spacing of excited hyperfine levels. Detailed theoretical analysis is performed using relevant Master equation. The probe absorption spectrum and dispersion in the absence and presence of Doppler broadening are discussed. This analysis shows that the two simultaneously excited Λ resonances result in peculiar interference effects in the probe absorption spectrum and dispersion. These are illustrated using model four-level DDL scheme formed in D_2 transition of ^{85}Rb . In particular for stationary atoms we observe the suppression of the sub-natural resonance and the possibility of probe amplification under specific field-atom interaction parameters. Electromagnetically induced transparency (EIT) in a DDL system is studied and the effect of the neighbouring level on the shape, linewidth and position of EIT profile is discussed. The discussion is further augmented by the study of six-level model as applicable to D_2 transition of ^{85}Rb . The analysis presented in this chapter thus provides a realistic theoretical description of pump-probe spectroscopy of hyperfine transitions of alkali atoms. The chapter is completed with a discussion on an experimental scheme

employed for dressed state spectroscopy of DDL system in a Doppler broadened medium of ^{87}Rb atoms using two commercial single mode external cavity diode lasers. The experimental results are discussed in the light of the theoretical model [11].

Chapter-5 presents a detailed analysis and discussion on the phenomenon of amplification without inversion (AWI) [4] observed in the DDL system of Chapter-4. It is shown here that a four-level DDL system under specific conditions can exhibit AWI without the need of incoherent pumping [10]. The dependence of AWI on atom-field interaction parameters and spontaneous emission rates is investigated. It is observed that the AWI resonance can be tuned in a broad frequency range by varying pump detuning and its strength is maximized when the detuning is half the frequency separation between excited levels. AWI is observed to be critically dependent on the low frequency coherence established between the pair of ground levels and is observed to persist even after the inclusion of Doppler averaging. Approximate analytical expression for probe absorption is derived to corroborate the numerical results and to discuss the contrasting behavior, i.e., absorption *vs.* AWI, in the model DDL system in D_1 and D_2 transitions of ^{87}Rb . The discussion on AWI is further augmented using quantum jump formalism, which provides useful insight into the underlying mechanism responsible for amplification.

Chapter-6 deals with theoretical analysis of interference effects in general four-level configurations, i.e., tripod system [14] and N-resonance [3,10], driven by three coherent fields, i.e., pump, probe and control lasers, from the point of view of controlling of the coherent dynamics and its manifestations. For the tripod system, the behaviour of the pair of EIT resonances as a function of laser-atom interaction parameters is

investigated with an objective of controlling the EIT linewidths [14]. In case of N-resonance, we discuss issues pertaining to the inversion in dressed states, observation of more than one transparency window and switching between two different regimes of coherent laser atom interaction: EIT and EIA, by controlling the laser parameters. These effects are attributed to the population trapping in the dark state, competition between inherent Λ and V systems and transfer of coherence. The role of spontaneously generated coherence (SGC) on the linear and non-linear response of N-system is investigated, and the transformation of EIA into EIT and enhancement of Kerr nonlinearity along with suppression of absorption are discussed. On the experimental front, a set-up developed for realizing EIT resonance in N-system in Doppler broadened Rb atoms is discussed. Experimental results on EIT in N-resonance and its comparison with EIT in Λ system show that the EIT signal in N-resonance is significantly narrower than that in a Λ system. This observation is in agreement with the observation that N-resonance is superior to a Λ resonance, which makes the former system more attractive for applications relating to time and frequency standards.

Chapter-7 deals with the investigations of laser phase fluctuations [15] on the coherent dynamics of four-level systems with N-resonance as an example. N-resonance has been chosen specifically for these studies since the ‘dark’ resonances associated with it are of particular importance for atomic frequency standards. An important issue that has a direct bearing on the experiments is how finite bandwidths of the driving lasers affect the steady state as well as the time dependent spectroscopic properties of N-resonance. While such studies in three-level configurations have been done extensively [15] and are shown to have pronounced effects on the linewidths of the EIT and CPT

resonances, very little work is reported on N-resonance, probably due to the complex configuration of levels and coupling fields. The present chapter addresses this very problem employing the master equation approach. We assume here that the finite bandwidths arise from the phase fluctuations of the laser fields, the statistics of which is described in terms of the Wiener-Levy diffusion model. We derive an exact master equation for phase averaged atomic density operator using the theory of multiplicative stochastic processes. Numerical results for the steady state and time dependent populations are obtained for 3-photon and 2+1-photon resonance conditions for finite bandwidth of lasers and cross-correlations. In a similar manner the effect of phase fluctuations on the EIT and EIA resonances has been investigated [10]. We observe that in general the phase fluctuations tend to broaden and even destroy the sharp resonances, and dampen the Rabi oscillations; however the extent of this effect is critically dependent on the phase fluctuations associated with the three fields. It is also found that the introduction of cross-correlation helps to revive the coherent behaviour to some extent, albeit depending on correlation between specific pairs of coherent fields.

Chapter-8 is devoted to exploratory investigations on the observation of negative refractive index in four-level systems interacting with three coherent fields, a probe, a control and a *rf* field [8,10]. In the framework of Master equation and Classius-Mossotti relation, we obtain relative permittivity and permeability for a dense medium of such atoms. Analysis reflects the existence of probe frequency domains where permittivity and permeability can become simultaneously negative. The use of dispersion property of the negative refractive index to control the group velocity of the probe beam from subluminal

to superluminal is also discussed. Importance of coherent preparation in achieving negative refractive index in the optical frequency domain is highlighted in this work.

Finally the important conclusions of the present study and scope for future work are briefly summarized in Chapter-9.

References

1. Coherent population trapping in laser spectroscopy, edited by E. Wolf, Progress in Optics.
E. Arimondo, in Progress in Optics, **XXXV**, 258 (1996) and references therein.
2. Electromagnetically induced transparency: Optics in coherent media.
M. Fleischhauer, A. Imamoglu and J.P. Marangos, Rev. Mod. Phys. **77**, 633 (2005) and references therein.
3. Atomic four-level N systems.
C. Goren, A.D. Wilson-Gordon, M. Rosenbluh and H. Friedmann, Phys. Rev. A. **69**, 053818 (2004).
4. Lasing without inversion.
J. Mompart and R Corbalan, J. Opt. B: Quantum Semiclass. Opt. **2**, R7 (2000).
5. Precision spectroscopy with coherent dark states.
R. Wynands and A. Nagel, Appl. Phys. B **68**, 1 (1999).
6. Sub-natural linewidth resonances in coherently driven double Λ system.
Niharika Singh, Q.V. Lawande, R. D'Souza and B.N. Jagatap, Pramana- J. of Phys. **75**, 1151 (2010).
7. Atomic frequency offset locking in a Λ type three-level Doppler broadened Cs system.

Y.B. Kale, A. Ray, R. D'Souza, Q.V. Lawande and B.N. Jagatap, *Appl. Phys. B* **100**, 505 (2010).

8. Negative Refractive Index Materials.

V. Veselago, L. Braginsky, V. Shklover and C. Hafner, *J. Comput. Theor. Nanosci.* **3**, 189 (2006);

Physics of negative refractive index materials.

S.A. Ramakrishna, *Rep. Prog. Phys.* **68**, 449 (2005)

9. Slow and fast light: fundamentals and applications.

R.W. Boyd, *J. Mod. Opt.* **56**, 1908 (2009).

10. Coherent pump-probe spectroscopy of four level atomic systems.

Niharika Singh and B.N. Jagatap, *AIP Conf. Proc.* **1391**, 16 (2011).

11. Resonances in the pump-probe spectroscopy of Λ system in alkali atoms.

Niharika Singh, Y.B. Kale, A. Ray and B.N. Jagatap, *Indian J. Phys* **84**, 1119 (2010).

12. Two-level rotating-wave approximations for molecules in a static electric field with an application to rotationally averaged spectra.

M.A. Kmetc, R.A. Thuraisingham and W.J. Meath, *Phys. Rev. A* **33**, 1688 (1986).

13. Electromagnetically induced transparency in a three-level Λ system with permanent dipole moments.

F. Zhou, Y. Niu and S. Gong, *J. Chem. Phys.* **131**, 034105 (2009).

14. Double control electromagnetically induced transparency windows in a tripod system.

Niharika Singh, R. D'Souza, Q.V. Lawande and B.N. Jagatap, *Asian Journal of Physics* **20**, 221 (2011).

15. The effect of laser field fluctuations on coherent population trapping

B.J. Dalton and P.L. Knight, *J. Phys. B: At. Mol. Phys.* **15**, 3997 (1982).

Publications

I. Journal Publications

a. Published

1. Sub-natural linewidth resonances in coherently-driven double Λ system.

Niharika Singh, Q.V. Lawande, R. D'Souza and B.N. Jagatap, *Pramana- J. of Phys.* **75**, 1151 (2010).

2. Resonances in the pump-probe spectroscopy of Λ system in alkali atoms.

Niharika Singh, Y.B. Kale, A. Ray and B.N. Jagatap, *Indian J. Phys.* **84**, 1119 (2010).

3. Modulation transfer in Doppler broadened Λ system and its application to frequency offset locking.

Y.B. Kale, A. Ray, **Niharika Singh**, Q.V. Lawande and B.N. Jagatap, *Eur. Phys. J. D.* **61**, 221 (2011).

4. Coherent pump-probe spectroscopy of four level atomic systems.

Niharika Singh and B.N. Jagatap, *AIP Conf. Proc.* **1391**, 16 (2011).

5. Double control electromagnetically induced transparency windows in a tripod system.

Niharika Singh, R. D'Souza, Q.V. Lawande and B.N. Jagatap, *Asian Journal of Physics*, **20**, 221 (2011).

6. Electromagnetically induced transparency in a Λ -type molecular system with permanent dipole moments revisited.

Niharika Singh, Q.V. Lawande, R. D'Souza and B.N. Jagatap, *J. Chem. Phys.* **137**, 104309 (2012).

b. Communicated

1. Coherent pump-probe spectroscopy of a Λ system with a close lying excited level.

Niharika Singh, A. Ray, R. D'Souza, Q.V. Lawande and B.N. Jagatap.

2. Amplification without inversion in a four level atomic system in degenerate double Λ configuration.

Niharika Singh, R. D'Souza, Q.V. Lawande and B.N. Jagatap.

3. Laser phase fluctuations in a four-level atomic system in N-configuration.

Niharika Singh, R. D'Souza, Q.V. Lawande and B.N. Jagatap.

II. Books/Reports/General Articles

1. Ultrasensitive Magnetometry: Exploring Ultra-low Magnetic Fields in the Physical World.

Niharika Singh, A. Ray and B.N. Jagatap, *IWSA Newsletter*, p.13 (2010).

2. Spectroscopy of coherently prepared three and four level medium.

Niharika Singh, A. Ray, Y.B. Kale and B.N. Jagatap, *Emerging Trends in Laser and Spectroscopy and Applications*, published by Allied Publishers Private Limited, New Delhi, p.261 (2010).

3. Spectroscopy in coherently prepared atomic medium and its applications.

Y.B. Kale, **Niharika Singh**, A. Ray and B.N. Jagatap, *Kiran*, Vol. 21, 2, p.22 (2010).

4. Precision spectroscopy of coherently prepared three and four level atomic medium.
Niharika Singh, A. Ray, Y.B. Kale and B.N. Jagatap, BARC Newsletter, Founder's day special issue, p.271 (2010).
5. Electromagnetically induced transparency in a tripod atomic system.
Niharika Singh, Q.V. Lawande, R. D'Souza and B.N. Jagatap, Kiran, vol. 22, 1, p.21 (2011).
6. Electromagnetically induced transparency in a tripod atomic system.
Niharika Singh, R. D'Souza, Q.V. Lawande, and B.N. Jagatap, BARC Newsletter, Founder's day special issue, p.382 (2011).

III. Conferences/Symposia

1. Amplification without inversion in a degenerate double lambda system.
Niharika Singh, R. D'Souza, Q.V. Lawande and B.N. Jagatap, IEEE Conference Series, Conference on lasers and electro optics (CLEO) technical digest, Optical Society of America, art. no. 6326327, p. JTh2A.35 (May 6-11, 2012).
2. Coherence induced negative refractive index in a 4 level atomic medium.
Niharika Singh, Q.V. Lawande, R. D'Souza and B.N. Jagatap, Proceedings of International Conference on Quantum Optics and Quantum Computing (ICQOQC-2011), Department of Physics and Materials Science and Engineering, Jaypee Institute of Information Technology, Noida, p.70 (March 24-26, 2011).
3. Spectroscopy in coherent atomic medium.
Niharika Singh, A. Ray, Y.B. Kale and B.N. Jagatap, Proceedings of Meghnad Saha Memorial Symposium on Emerging Trends in Laser & Spectroscopy and

Applications (MMSETLSA-2009), University of Allahabad, (March 23-25, 2009).

(Best poster award).

4. Sub-natural linewidth resonances in coherently driven double Λ system.

Niharika Singh, Q.V. Lawande, R. D'Souza, A. Ray and B.N. Jagatap, Proceedings of National Laser Symposium (NLS-09), Bhabha Atomic Research Centre, Mumbai, p.68 (January 13-16, 2010).

5. Electromagnetically induced transparency in four and five level atomic systems.

Niharika Singh, Q.V. Lawande, B.N. Jagatap and R. D'Souza, Proceedings of Topical Conference on Interaction of EM Radiation with Atoms, Molecules and Cluster (TC-2010), Raja Ramanna Centre for Advanced Technology, Indore, p.72 (March 03–06, 2010).

6. Electromagnetically induced transparency in a tripod atomic system.

Niharika Singh, Q.V. Lawande, R. D'Souza and B.N. Jagatap, Proceedings of National Laser Symposium (NLS-19), Raja Ramanna Centre for Advanced Technology, Indore, p.75 (December 1-4, 2010). **(Best poster award).**

7. Realization of negative refractive index: Theoretical analysis for a coherently driven four-level system.

Niharika Singh, R. D'Souza, Q.V. Lawande and B.N. Jagatap, Proceedings of National Laser Symposium (NLS-19), Raja Ramanna Centre for Advanced Technology, Indore, p.76 (December 1-4, 2010).

8. Amplification without inversion in degenerate and non-degenerate double lambda system.

Niharika Singh, Q.V. Lawande, R. D'Souza, A. Ray and B.N. Jagatap, Proceedings of DAE-BRNS Symposium on Atomic, Molecular and Optical Physics, Karnatak University, Dharwad, p.102 (February 22-25, 2011). **(Best poster award)**.

9. Electromagnetically induced transparency and absorption in a four level N type atomic system.

Niharika Singh, Proceedings of 99th Indian Science Congress (ISCA 2011-12), KIIT Bhubaneswar, p.117 (January 3-7, 2012).

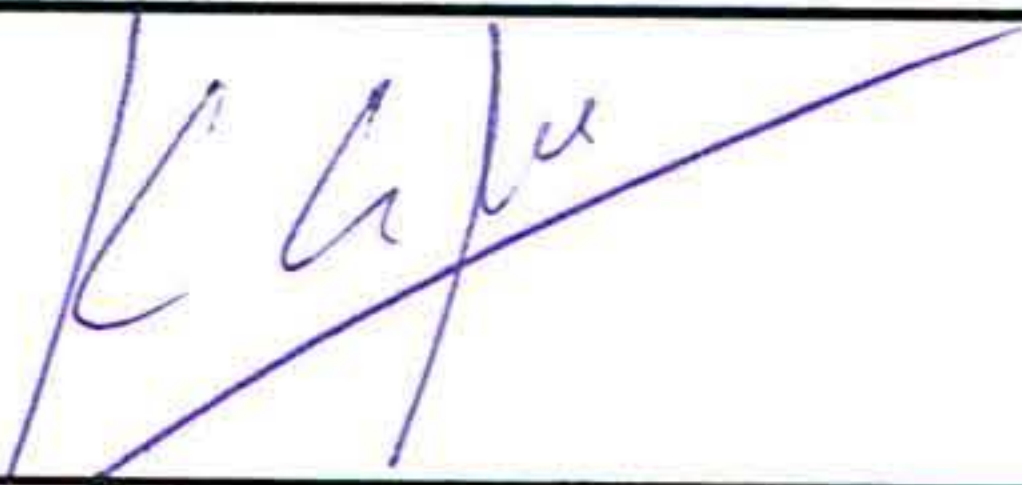
10. Effect of spontaneously generated coherence on the coherent dynamics of a four-level N system.

Niharika Singh, presented in 99th Indian Science Congress (ISCA 2011-12), KIIT Bhubaneswar, p.51 (January 3-7, 2012) for Young Scientist Award Programme.

Signature of Student:

Date: 3 August 2012

Doctoral Committee

S. No.	Name	Designation	Signature	Date
1.	Dr. G.P. Kothiyal	Chairman		3/08/2012
2.	Prof. B.N. Jagatap	Convener		3/08/2012
3.	Prof. B.P. Singh	Member		3/08/2012
4.	Dr. K.G. Manohar	Member		3/08/2012

LIST OF FIGURES

	Page no.
Fig. 1.1	Two-level atom coherently driven by a laser field of Rabi frequency α . 3
Fig. 1.2(a)	Level scheme representation of Λ system. 3
Fig. 1.2(b)	Level scheme representation of V system. 3
Fig. 1.2(c)	Level scheme representation of Ξ system. 3
Fig. 2.1(a)	Schematic representation of four-level system in DDL configuration. 38
Fig. 2.1(b)	Schematic representation of four-level system in tripod configuration. 38
Fig. 2.1(c)	Schematic representation of four-level system in N- configuration. 38
Fig. 3.1	Schematic representation of a molecular three-level Λ system. 46
Fig. 3.2(a)	Absorption (A) vs. Δ_p in Λ system for $(\alpha_c, \Delta_c) = (5\gamma, 0)$ and $m = 1, 2$. 54
Fig. 3.2(b)	Dispersion (η) vs. Δ_p in Λ system for $(\alpha_c, \Delta_c) = (5\gamma, 0)$ and $m = 1, 2$. 54
Fig. 3.3(a)	Doppler averaging ($2W_D = 100\gamma$) on the spectrum of Fig. 3.2(a). 56
Fig. 3.3(b)	Doppler averaging ($2W_D = 100\gamma$) on the spectrum of Fig. 3.2(b). 56
Fig. 3.4	EIT half-width (Γ_{EIT}) vs. $z_{23}^{(c)}$ for $(\alpha_c, \Delta_c) = (5\gamma, 0)$ and $2W_D = 100\gamma$. 60
Fig. 3.5	Slope of dispersion profile at the peak of EIT for the data of Fig. 3.4. 61
Fig. 4.1	Schematic of DDL system formed in D_2 transition of ^{85}Rb . 69
Fig. 4.2(a)	Dressed state energies vs. Δ_1 in DDL system for $\alpha_1 = 10$ MHz. 75
Fig. 4.2(b)	Widths of dressed level transitions vs. Δ_1 in DDL system. 75
Fig. 4.3(a)	Dressed state energies of $\Lambda^{(1)}$ and $\Lambda^{(2)}$ systems vs. Δ_1 . 75

Fig. 4.3(b)	Widths of dressed level transitions <i>vs.</i> Δ_1 in $\Lambda^{(1)}$ and $\Lambda^{(2)}$ systems.	75
Fig. 4.4(a)	A and η in DDL system for $(\alpha_1, \Delta_1) = (10, -40)$ MHz.	76
Fig. 4.4(b)	A and η in DDL system for $(\alpha_1, \Delta_1) = (10, 20)$ MHz.	76
Fig. 4.4(c)	A and η in DDL system for $(\alpha_1, \Delta_1) = (10, 100)$ MHz.	76
Fig. 4.5(a)	A and η for $(\alpha_1, \Delta_1) = (10, 25)$ MHz.	77
Fig. 4.5(b)	A and η for $(\alpha_1, \Delta_1) = (10, 38.37)$ MHz (suppression of absorption).	77
Fig. 4.5(c)	A and η for $(\alpha_1, \Delta_1) = (10, 50)$ MHz.	77
Fig. 4.6	Square of the dipole matrix element <i>vs.</i> Δ_1 for $\alpha_1 = 10$ MHz.	78
Fig. 4.7	Doppler averaged absorption spectrum for $\alpha_1 = 10$ MHz and $\Delta_1 = S$.	80
Fig. 4.8	Doppler averaging on the suppression of resonance in Fig. 4.5(b).	81
Fig. 4.9	EIT linewidths <i>vs.</i> pump Rabi frequency for $\Lambda^{(1)}$ and DDL systems.	81
Fig. 4.10	EIT linewidths <i>vs.</i> pump detuning for $\Lambda^{(1)}$ and DDL systems.	82
Fig. 4.11	Experimental set up for coherent pump-probe spectroscopy.	86
Fig. 4.12	Dressed state spectroscopy of ^{87}Rb D_2 transition for $\Delta_1 \approx 265$ MHz.	89
Fig. 4.13	Dressed state spectroscopy of ^{87}Rb D_2 transition for $\Delta_1 \approx -467$ MHz.	90
Fig. 5.1	AWI in DDL system of ^{87}Rb D_1 line for $(\alpha_1, \Delta_1) = (20, 430)$ MHz.	93
Fig. 5.2	Steady state populations in the bare levels for the data of Fig. 5.1.	94
Fig. 5.3	Effect of pump detuning (Δ_1) on AWI for the data of Fig. 5.1.	95
Fig. 5.4	Effect of pump Rabi frequency (α_1) on AWI for the data of Fig. 5.1.	95
Fig. 5.5	AWI <i>vs.</i> incoherent decay rates $\Gamma_{12}(=\Gamma_{21})$ and $\Gamma_{34}(=\Gamma_{43})$.	95
Fig. 5.6(a)	$\text{Re}(\chi_1)$ <i>vs.</i> probe detuning (δ_1) for data of Fig. 5.1.	96

Fig. 5.6(b)	Re(χ_2) vs. δ_1 for the data of Fig. 5.1.	96
Fig. 5.6(c)	Re(χ_3) vs. δ_1 for the data of Fig. 5.1.	96
Fig. 5.7	A in DDL system of ^{87}Rb D ₂ transition for $(\alpha_1, \Delta_1) = (20, 80)$ MHz.	99
Fig. 5.8	AWI in ^6Li D ₁ transition for $(\alpha_1, S, \Delta_1) = (4, 26.1, 14)$ MHz.	100
Fig. 5.9(a)	Doppler averaging ($2W_D = 250$ MHz) on the spectrum of Fig. 5.1.	101
Fig. 5.9(b)	Doppler averaging ($2W_D = 250$ MHz) on the spectrum of Fig. 5.1.	101
Fig. 5.10	Variation of AWI with Doppler width ($2W_D$) for the data of Fig. 5.1.	102
Fig. 5.11	Effect of Doppler broadening on A for the data of Fig. 5.7.	102
Fig. 5.12	Variation of the width of Doppler averaged AWI resonance with α_1 .	103
Fig. 5.13	Different manifolds of atom + photon system for a DDL scheme.	104
Fig. 5.14(a)	Relative probabilities of coherent periods for the data of Fig. 5.1.	108
Fig. 5.14(b)	Relative absorption at $\delta_1 = \Delta_1$ for the data of Fig. 5.1.	108
Fig. 5.15(a)	Relative probabilities of coherent periods for the data of Fig. 5.7.	108
Fig. 5.15(b)	Relative absorption at $\delta_1 = \Delta_1$ for the data of Fig. 5.7.	108
Fig. 6.1(a)	Absorption spectrum of Λ system for $(\alpha_1, \Delta_1) = (5, 0)$ MHz.	114
Fig. 6.1(b)	Absorption in tripod system for $(\alpha_1, \alpha_2, \Delta_1, \Delta_2) = (5, 1, 0, 3)$ MHz.	114
Fig. 6.2(a)	EIT in tripod system for $(\alpha_1, \Delta_1, \Delta_2) = (5, 0, 3)$ MHz, $\alpha_2 = 1$ MHz.	115
Fig. 6.2(b)	EIT in tripod system for $(\alpha_1, \Delta_1, \Delta_2) = (5, 0, 3)$ MHz, $\alpha_2 = 5$ MHz.	115
Fig. 6.2(c)	EIT in tripod system for $(\alpha_1, \Delta_1, \Delta_2) = (5, 0, 3)$ MHz, $\alpha_2 = 10$ MHz.	115
Fig. 6.2(d)	EIT in tripod system for $(\alpha_1, \Delta_1, \Delta_2) = (5, 0, 3)$ MHz, $\alpha_2 = 40$ MHz.	115
Fig. 6.3(a)	EIT linewidths vs. α_2 for $(\alpha_1, \Delta_1, \Delta_2) = (5, 0, 3)$ MHz.	116

Fig. 6.3(b)	EIT linewidths vs. Δ_2 for $(\alpha_1, \alpha_2, \Delta_1) = (5, 1, 50)$ MHz.	116
Fig. 6.4(a)	EIT linewidths vs. α_2 for $(\alpha_1, \Delta_1, \Delta_2) = (20, 0, 20)$ MHz.	116
Fig. 6.4(b)	EIT linewidths vs. Δ_2 for $(\alpha_1, \alpha_2, \Delta_1) = (20, 15, 100)$ MHz.	116
Fig. 6.5(a)	Absorption spectrum of model A for $\Delta_1 = \Delta_2 = 0$ and $2W_D = 0$.	121
Fig. 6.5(b)	Absorption spectrum for $\Delta_1 = \Delta_2 = 0$ and $2W_D = 510$ MHz.	121
Fig. 6.6(a)	Absorption spectrum for $(\alpha_1, \alpha_2, \Delta_1, \Delta_2) = (5, 5, 0, 50)$ MHz.	122
Fig. 6.6(b)	Absorption spectrum for $(\alpha_1, \alpha_2, \Delta_1, \Delta_2) = (5, 5, -50, 50)$ MHz.	122
Fig. 6.7(a)	Absorption in model B for $(\alpha_2, \alpha_3, \Delta_2, \Delta_3) = (5, 5, 0, 20)$ MHz.	123
Fig. 6.7(b)	Absorption in model B for $(\alpha_2, \alpha_3, \Delta_2, \Delta_3) = (1, 5, 0, 20)$ MHz.	123
Fig. 6.7(c)	Absorption spectrum for $(\alpha_2, \alpha_3, \Delta_2, \Delta_3) = (5, 1, 0, 20)$ MHz.	123
Fig. 6.8(a)	Absorption in model C for $(\alpha_1, \alpha_3, \Delta_1, \Delta_3) = (10, 50, 0, 50)$ MHz.	125
Fig. 6.8(b)	Absorption spectrum for $(\alpha_1, \alpha_3, \Delta_1, \Delta_3) = (10, 10, 0, 50)$ MHz.	125
Fig. 6.8(c)	Absorption spectrum for $(\alpha_1, \alpha_3, \Delta_1, \Delta_3) = (50, 10, 0, 50)$ MHz.	125
Fig. 6.9(a)	EIA in model C for $(\alpha_1, \alpha_3, \Delta_1, \Delta_3) = (5, 5, 0, 0)$ MHz.	127
Fig. 6.9(b)	EIT and EIA in model C for $(\alpha_1, \alpha_3, \Delta_1, \Delta_3) = (5, 6, 0, 0)$ MHz.	127
Fig. 6.9(c)	EIT in model C for $(\alpha_1, \alpha_3, \Delta_1, \Delta_3) = (5, 10, 0, 0)$ MHz.	127
Fig. 6.10	EIA linewidth as a function of $2W_D$ for the data of Fig. 6.9(a).	127
Fig. 6.11(a)	Absorption in model C for $(\alpha_1, \alpha_3, \Delta_1, \Delta_3) = (10, 10, 0, 0)$ MHz.	131
Fig. 6.11(b)	Effect of SGC on A of Fig. 6.11(a) for $(\Phi_1, \Phi_2) = (0.9, 0.0)$.	131
Fig. 6.11(c)	Effect of SGC on A of Fig. 6.11(a) for $(\Phi_1, \Phi_2) = (0.99, 0.99)$.	131

Fig. 6.12(a)	Linear absorption and dispersion for the data of Fig. 6.11(a).	132
Fig. 6.12(b)	Linear absorption and dispersion for the data of Fig. 6.11(b).	132
Fig. 6.12(c)	Linear absorption and dispersion for the data of Fig. 6.11(c).	132
Fig. 6.12(d)	Nonlinear absorption and Kerr nonlinearity for data of Fig. 6.11(a).	132
Fig. 6.12(e)	Nonlinear absorption and Kerr nonlinearity for data of Fig. 6.11(b).	132
Fig. 6.12(f)	Nonlinear absorption and Kerr nonlinearity for data of Fig. 6.11(c).	132
Fig. 6.13(a)	$\chi^{(3)}$ vs. Δ_2 for $(\alpha_1, \alpha_3, \Delta_1, \Delta_3) = (1, 10, 0, 0)$ MHz, $\Phi_1 = \Phi_2 = 0$.	133
Fig. 6.13(b)	$\chi^{(3)}$ vs. Δ_2 for $(\alpha_1, \alpha_3, \Delta_1, \Delta_3) = (1, 10, 0, 0)$ MHz, $\Phi_1 = \Phi_2 = 0.99$.	133
Fig. 6.14(a)	$\chi^{(1)}$ vs. Δ_2 for $(\alpha_1, \alpha_3, \Delta_1, \Delta_3) = (1, 10, 0, 10)$ MHz, $\Phi_1 = \Phi_2 = 0$.	134
Fig. 6.14(b)	$\chi^{(1)}$ vs. Δ_2 for the data of Fig. 6.14 (a) with $(\Phi_1, \Phi_2) = (0.9, 0.0)$.	134
Fig. 6.14(c)	$\chi^{(1)}$ vs. Δ_2 for the data of Fig. 6.14 (a) with $\Phi_1 = \Phi_2 = 0.99$.	134
Fig. 6.14(d)	$\chi^{(3)}$ vs. Δ_2 for $(\alpha_1, \alpha_3, \Delta_1, \Delta_3) = (1, 10, 0, 10)$ MHz, $\Phi_1 = \Phi_2 = 0$.	134
Fig. 6.14(e)	$\chi^{(3)}$ vs. Δ_2 for the data of Fig. 6.14 (d) with $(\Phi_1, \Phi_2) = (0.9, 0.0)$.	134
Fig. 6.14(f)	$\chi^{(3)}$ vs. Δ_2 for the data of Fig. 6.14 (d) with $\Phi_1 = \Phi_2 = 0.99$.	134
Fig. 6.15	Energy-level diagram for EIT experiment in ^{87}Rb D ₂ transition.	136
Fig. 6.16	EIT in Λ configuration of ^{87}Rb D ₂ transition for $\Delta_2 \approx 0$.	136
Fig. 6.17	Comparison of EIT in Λ and N configurations for $\Delta_2 \approx -78.5$ MHz.	138
Fig. 7.1(a)	Effect of laser phase fluctuations on ρ_{11} for three-photon resonance.	151
Fig. 7.1(b)	Effect of laser phase fluctuations on ρ_{22} for three-photon resonance.	151
Fig. 7.1(c)	Effect of laser phase fluctuations on ρ_{33} for three-photon resonance.	151
Fig. 7.1(d)	Effect of laser phase fluctuations on ρ_{44} for three-photon resonance.	151

Fig. 7.2(a)	Effect of individual bandwidths on ρ_{11} for two-photon resonance.	152
Fig. 7.2(b)	Effect of individual bandwidths on ρ_{11} for three-photon resonance.	152
Fig. 7.2(c)	Effect of individual bandwidths on ρ_{33} for two-photon resonance.	152
Fig. 7.2(d)	Effect of individual bandwidths on ρ_{33} for three-photon resonance.	152
Fig. 7.3(a)	Effect of critical cross correlations on ρ_{11} for two-photon resonance.	153
Fig. 7.3(b)	Behaviour in the vicinity of three-photon resonance.	153
Fig. 7.3(c)	Effect of critical cross correlations on ρ_{33} for two-photon resonance.	153
Fig. 7.3(d)	Behaviour in the vicinity of three-photon resonance.	153
Fig. 7.4(a)	Effect of laser phase fluctuations on ρ_{11} for 2+1-photon resonance.	156
Fig. 7.4(b)	Effect of laser phase fluctuations on ρ_{22} for 2+1-photon resonance.	156
Fig. 7.4(c)	Effect of laser phase fluctuations on ρ_{33} for 2+1-photon resonance.	156
Fig. 7.4(d)	Effect of laser phase fluctuations on ρ_{44} for 2+1-photon resonance.	156
Fig. 7.5(a)	Effect of individual bandwidths on ρ_{11} for 2+1-photon resonance.	157
Fig. 7.5(b)	Effect of individual bandwidths on ρ_{33} for 2+1-photon resonance.	157
Fig. 7.6(a)	Effect of critical cross correlations on ρ_{11} for 2+1-photon resonance.	158
Fig. 7.6(b)	Effect of critical cross correlations on ρ_{33} for 2+1-photon resonance.	158
Fig. 7.7(a)	Time evolution of ρ_{11} at three-photon resonance with initial state $ 1\rangle$.	160
Fig. 7.7(b)	Time evolution of ρ_{22} at three-photon resonance with initial state $ 1\rangle$.	160
Fig. 7.7(c)	Time evolution of ρ_{33} at three-photon resonance with initial state $ 1\rangle$.	160
Fig. 7.7(d)	Time evolution of ρ_{11} at three-photon resonance with initial state $ 3\rangle$.	160

Fig. 7.7(e)	Time evolution of ρ_{22} at three-photon resonance with initial state $ 3\rangle$.	160
Fig. 7.7(f)	Time evolution of ρ_{33} at three-photon resonance with initial state $ 3\rangle$.	160
Fig. 7.8(a)	Time evolution of ρ_{11} for 2+1-resonance with $ 1\rangle$ as initial state.	161
Fig. 7.8(b)	Time evolution of ρ_{22} for 2+1-resonance with $ 1\rangle$ as initial state.	161
Fig. 7.8(c)	Time evolution of ρ_{33} for 2+1-resonance with $ 1\rangle$ as initial state.	161
Fig. 7.8(d)	Time evolution of ρ_{11} for 2+1-resonance with $ 3\rangle$ as initial state.	161
Fig. 7.8(e)	Time evolution of ρ_{22} for 2+1-resonance with $ 3\rangle$ as initial state.	161
Fig. 7.8(f)	Time evolution of ρ_{33} for 2+1-resonance with $ 3\rangle$ as initial state.	161
Fig. 7.9	Effect of laser bandwidths on EIA resonance for data of Fig. 6.9(a).	163
Fig. 7.10	Effect of critical cross correlations on EIA resonance of Fig. 7.9.	164
Fig. 8.1	Quadrant diagram of $\varepsilon_r - \mu_r$.	166
Fig. 8.2(a)	Schematic diagram of model (a) for the study of negative refraction.	170
Fig. 8.2(b)	Schematic diagram of model (b) for the study of negative refraction.	170
Fig. 8.3(a)	$\text{Re}(\varepsilon_r)$ vs. Δ_p for $(\alpha_{rf}, \Delta_c, \Delta_{rf}) = (5\gamma, 0, 0)$, $\alpha_c = \gamma, 5\gamma, 10\gamma$.	176
Fig. 8.3(b)	$\text{Im}(\varepsilon_r)$ vs. Δ_p for $(\alpha_{rf}, \Delta_c, \Delta_{rf}) = (5\gamma, 0, 0)$, $\alpha_c = \gamma, 5\gamma, 10\gamma$.	176
Fig. 8.3(c)	$\text{Re}(\mu_r)$ vs. Δ_p for $(\alpha_{rf}, \Delta_c, \Delta_{rf}) = (5\gamma, 0, 0)$, $\alpha_c = \gamma, 5\gamma, 10\gamma$.	176
Fig. 8.3(d)	$\text{Im}(\mu_r)$ vs. Δ_p for $(\alpha_{rf}, \Delta_c, \Delta_{rf}) = (5\gamma, 0, 0)$, $\alpha_c = \gamma, 5\gamma, 10\gamma$.	176
Fig. 8.3(e)	n_r vs. Δ_p for $(\alpha_{rf}, \Delta_c, \Delta_{rf}) = (5\gamma, 0, 0)$, $\alpha_c = \gamma, 5\gamma, 10\gamma$.	176
Fig. 8.3(f)	A vs. Δ_p for $(\alpha_{rf}, \Delta_c, \Delta_{rf}) = (5\gamma, 0, 0)$, $\alpha_c = \gamma, 5\gamma, 10\gamma$.	176

Fig. 8.4	n_r vs. Δ_p for $\alpha_c = \alpha_{rf} = 10\gamma$, $(\Delta_c, \Delta_{rf}) = (0, 20\gamma), (20\gamma, 0)$.	178
Fig. 8.5(a)	n_r vs. Δ_p for $(\alpha_c, \Delta_c, \Delta_{rf}) = (10\gamma, 0, 0)$, $\alpha_{rf} = \gamma, 10\gamma$.	178
Fig. 8.5(b)	A vs. Δ_p for $(\alpha_c, \Delta_c, \Delta_{rf}) = (10\gamma, 0, 0)$, $\alpha_{rf} = \gamma, 10\gamma$.	178
Fig. 8.6(a)	$\text{Re}(\varepsilon_r)$ vs. Δ_p for $(\alpha_{rf}, \Delta_c, \Delta_{rf}) = (5\gamma, 0, 0)$, $\alpha_c = \gamma, 5\gamma, 10\gamma$.	182
Fig. 8.6(b)	$\text{Im}(\varepsilon_r)$ vs. Δ_p for $(\alpha_{rf}, \Delta_c, \Delta_{rf}) = (5\gamma, 0, 0)$, $\alpha_c = \gamma, 5\gamma, 10\gamma$.	182
Fig. 8.6(c)	$\text{Re}(\mu_r)$ vs. Δ_p for $(\alpha_{rf}, \Delta_c, \Delta_{rf}) = (5\gamma, 0, 0)$, $\alpha_c = \gamma, 5\gamma, 10\gamma$.	182
Fig. 8.6(d)	$\text{Im}(\mu_r)$ vs. Δ_p for $(\alpha_{rf}, \Delta_c, \Delta_{rf}) = (5\gamma, 0, 0)$, $\alpha_c = \gamma, 5\gamma, 10\gamma$.	182
Fig. 8.6(e)	n_r vs. Δ_p for $(\alpha_{rf}, \Delta_c, \Delta_{rf}) = (5\gamma, 0, 0)$, $\alpha_c = \gamma, 5\gamma, 10\gamma$.	182
Fig. 8.6(f)	A vs. Δ_p for $(\alpha_{rf}, \Delta_c, \Delta_{rf}) = (5\gamma, 0, 0)$, $\alpha_c = \gamma, 5\gamma, 10\gamma$.	182
Fig. 8.7	n_r vs. Δ_p for $\alpha_c = \alpha_{rf} = 10\gamma$, $(\Delta_c, \Delta_{rf}) = (0, 20\gamma), (20\gamma, 0)$.	183
Fig. 8.8(a)	n_r vs. Δ_p for $(\alpha_c, \Delta_c, \Delta_{rf}) = (5\gamma, 0, 0)$, $\alpha_{rf} = \gamma, 6\gamma, 10\gamma$.	184
Fig. 8.8(b)	A vs. Δ_p for $(\alpha_c, \Delta_c, \Delta_{rf}) = (5\gamma, 0, 0)$, $\alpha_{rf} = \gamma, 6\gamma, 10\gamma$.	184

LIST OF TABLES

		Page no.
Table-1	Energy and permanent dipole moment of selected levels in HCN \rightarrow HNC isomerization.	54
Table-2(a)	Energy, permanent dipole moment and lifetime of selected levels in ^7LiH molecule ($\mu_{13} < 0$).	65
Table-2(b)	Frank Condon factor and transition dipole moment of transitions associated with levels of Table-2(a).	66
Table-3(a)	Energy, permanent dipole moment and lifetime of selected levels in ^7LiH molecule ($\mu_{13} > 0$).	66
Table-3(b)	Frank Condon factor and transition dipole moment of transitions associated with levels of Table-3(a).	66
Table-4	Comparison of EIT positions and their linewidths in Λ , DDL and six-level configurations for $\Delta_1 = 0$.	85
Table-5	Dressed states of model A in N type system for $\Delta_1 = \Delta_2$.	122
Table-6	Dressed states of model B in N type system for $\Delta_2 = \Delta_3$.	124
Table-7	Dependence of $\alpha_c, \alpha_{rf}, \Delta_c, \Delta_{rf}$ on maximum value and range of negative refractive index in model (a).	179
Table-8	Dependence of $\alpha_c, \alpha_{rf}, \Delta_c, \Delta_{rf}$ on maximum value and range of negative refractive index in model (b).	184

CHAPTER 1

INTRODUCTION

Coherent control is one of the leading themes of quantum optics research that is rich in new and counter-intuitive phenomena. The control strategies here are derived from the phenomena of quantum coherence and interference established in multilevel atomic systems driven coherently by two or more electromagnetic fields. In particular, the control of optical response of an atomic/molecular medium and manipulation of light propagation through such a medium has received considerable attention [1-4]. Some of the best known examples of this research are Autler-Townes (AT) splitting [5-9], coherent population trapping (CPT) [10-13], electromagnetically induced transparency (EIT) [14-39], electromagnetically induced absorption (EIA) [40-52] and lasing without population inversion (LWI) [53-79]. These phenomena are characterized by ultra-narrow linewidths, and modified linear and nonlinear susceptibilities. While on one hand these phenomena help to understand the subtle quantum effects in laser-atom interactions, they on the other hand provide useful platform for development of quantum technologies, e.g., frequency stabilizer [80-82], miniaturized atomic clock [83-87], precision magnetometer

[88-91], laser cooling [92,93] and quantum information processing [94,95]. In very recent years the research in this area has expanded in several new and exotic directions which include for example, subluminal and superluminal light propagation [96-114] and search for systems exhibiting negative refractive index [115-131].

The main objective of this thesis is to investigate the phenomenon of quantum coherence and interference in optical processes with the objective of achieving control of the interaction between atomic or molecular systems and electromagnetic fields. This chapter discusses briefly the basic physics underlying these optical phenomena and provides a perspective of their applications. The discussion presented here forms the basis for research work presented in the subsequent chapters.

1.1 Coherence and Interference in Atom-Field Interaction

Coherence is fundamental to the quantum optical phenomena. An atomic system interacting with a coherent electromagnetic field retains a distinct phase relationship with the field as long as the incoherent processes, i.e., decays due to spontaneous emission or collisions, do not override the atom-field interaction dynamics. The problem then can be addressed in the framework of quantum mechanics, where superposition and interference play an important role. The essential features of this quantum description are usually discussed by considering a finite-level atom interacting with a classical electromagnetic field. Such idealized n -level systems can be realized experimentally by identifying suitable hyperfine levels or Zeeman sublevels in simple atoms, e.g., alkali atoms. Two- and three-level atomic systems are paradigm of these studies, although general n -level systems ($n > 3$) provide opportunities to study more complex quantum dynamics as we

see later. The energy levels and atom-field interaction parameters relevant for the discussion of two- and three-level atoms are schematically shown in Fig. 1.1 and 1.2 respectively.

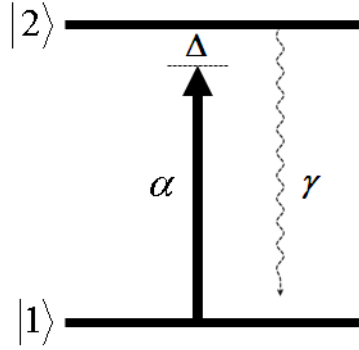


Fig. 1.1: Two-level atom coherently driven by a laser field of Rabi frequency α . Δ is the detuning of laser from atomic transition frequency. γ is the radiative decay rate associated with $|2\rangle \rightarrow |1\rangle$ transition.

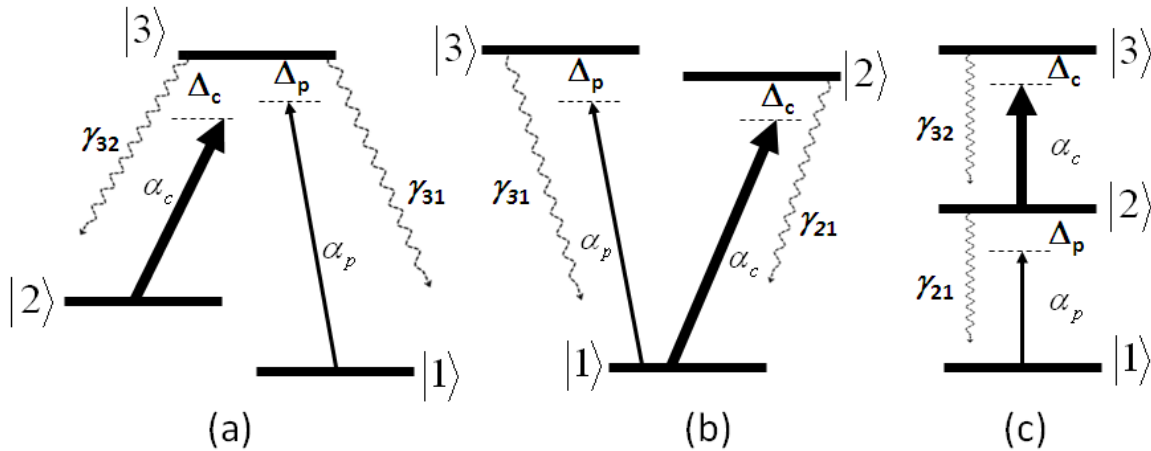


Fig. 1.2: Level scheme representation of (a) Λ (b) V and (c) Ξ systems. Here Δ_c (Δ_p) and $2\alpha_c$ ($2\alpha_p$) are respectively the detuning and Rabi frequency of the pump (probe) laser field and γ_{ij} is radiative decay rate associated with $|i\rangle \rightarrow |j\rangle$ transition.

The quantum mechanical framework necessary for description of finite-level systems interacting with two or more lasers and with vacuum of radiation field is explicitly developed in Chapter-2. In what follows, the essential results concerning coherence and interference in atomic media and pertaining to the scope of this thesis are reviewed.

1.1.1 Rabi Oscillations and Dressed States

For a two-level atom interacting with classical electromagnetic field, $E = E_0 \cos(\omega t)$, the atom-field dynamics is described by Hamiltonian,

$$H = H_o + V, \quad (1.1)$$

where H_o is the field-free Hamiltonian and $V = -d \cdot E$ is the interaction in electric dipole approximation. Here E and ω are respectively the electric field and frequency of radiation field, and d is the transition dipole moment associated with $|1\rangle \rightarrow |2\rangle$ transition. Atom-field dynamics is then determined by the Rabi frequency (2α) and detuning (Δ) defined as

$$2\alpha = d \cdot E / \hbar, \quad \Delta = \omega_{21} - \omega, \quad (1.2)$$

where ω_{21} is the atomic transition frequency. For a loss-less system, the ground and excited level populations exhibit out of phase oscillations, i.e., Rabi oscillations. The oscillation frequency is given by the generalized Rabi frequency defined as

$$\Omega_R = (4\alpha^2 + \Delta^2)^{1/2}. \quad (1.3)$$

Incoherent decay (2γ) results in damping of the Rabi oscillations, and for $\alpha > \gamma$ coherence can persist over several Rabi periods. The model of two-level atom interacting with monochromatic radiation field also permits to introduce the dressed states $|\psi_{\pm}\rangle$, i.e. the eigen states of the atom + field Hamiltonian H , of energies ε_{\pm} such that

$$|\psi_{\pm}\rangle = \sqrt{\frac{\Omega_R \mp \Delta}{2\Omega_R}} |1\rangle \mp \sqrt{\frac{\Omega_R \pm \Delta}{2\Omega_R}} |2\rangle, \quad \varepsilon_{\pm} = (\Delta \pm \Omega_R) / 2. \quad (1.4)$$

The dressed states can be observed using the techniques of coherent pump-probe spectroscopy. As a part of research work reported in this thesis, suitable experimental

techniques were developed to identify relevant dressed states corresponding to coherent interaction of a strong pump with hyperfine levels of D₂ transition in alkali atoms.

1.1.2 Autler-Townes Splitting

Autler-Townes (AT) splitting refers to the splitting of the absorption line due to dressing of an atom by a coherent radiation field [5]. Three-level systems as shown in Fig. 1.2 provide the requisite platform for observation of AT splitting. For example, in Fig. 1.2(a), transition $|2\rangle \rightarrow |3\rangle$ is dressed by a strong pump (control) laser of Rabi frequency $2\alpha_c$ and the resulting dressed states are interrogated by a weak probe laser that is scanned in the vicinity of $|1\rangle \rightarrow |3\rangle$ transition. Probe absorption spectrum is then a doublet corresponding to the dressed state transitions $|1\rangle \rightarrow |\psi_{\pm}\rangle$. Frequency separation between these two resonances is given by $\Omega_R = (\Delta_c^2 + 4\alpha_c^2)^{1/2}$ (cf. Eq. (1.4)) and their half widths are

$$\Gamma_{\pm} = \frac{\gamma_3 + D}{2} \left(1 \mp \frac{\Delta_c}{\Omega_R} \right), \quad (1.5)$$

where $\gamma_3 = \gamma_{31} + \gamma_{32}$ and D is a measure of Doppler width of the medium [6]. One thus observes that for $\Delta = 0$, both resonances have equal linewidth ($\Gamma_+ = \Gamma_-$), while for $|\Delta| \gg \alpha$ one of the resonances can be made of sub-Doppler or even sub-natural linewidth. AT splitting provides a useful way to obtain the properties of an atom/molecule interacting with near resonant radiation [1-6]. Recently AT doublet has also been studied in reference to high order nonlinear processes [7], quantum beats and quantum well structures [8] and in molecular systems [9]. The prospect of obtaining

ultra-narrow linewidth (*cf.* Eq. (1.5)) has been employed for development of tunable atomic frequency offset locking (AFOL) schemes [80-82].

1.1.3 Coherent Population Trapping

Susceptibility (χ) of a two-level atomic medium interacting with a monochromatic field is largely dominated by absorption, i.e., $\text{Im}(\chi)$ [1-4]. Thus this system is unsuitable for applications in nonlinear optics. A three-level system interacting with two coherent fields gives rise to a range of coherent phenomena including CPT and EIT which suppress the resonant absorption [10-39]. The result is a very large dispersive optical nonlinearity which can also be used to control the propagation of light through the medium. The difference between AT and CPT/EIT is closely connected with the difference in the behaviour of two- and three-level systems undergoing resonant excitations. While AT doublet is related only to the development of atomic coherence, EIT and CPT are the results of quantum interference between absorption pathways in a multilevel system [10-19]. It is therefore possible to discriminate AT and EIT on the basis of Fano type interference in the latter mechanism [20] and threshold coupling [21]. A significant feature of EIT and CPT is that they afford sub-natural resolution even in a Doppler broadened medium [22-32].

The basic principle of CPT lies in the use of laser-induced coherences to generate a dark state formed from the coherent superposition of two long lived bare atomic states [10-12]. Consider for example a three-level system in Λ configuration (*cf.* Fig. 1.2 (a)). When $\alpha_p \sim \alpha_c$, both the fields participate in the dressing of the medium and the

diagonalization of the total Hamiltonian results into the formation of a bright (coupled) state $|C\rangle$ and a dark (non-coupled) state $|NC\rangle$, i.e.,

$$|C\rangle = (\alpha_p / \alpha_T)|1\rangle + (\alpha_c / \alpha_T)|2\rangle, \quad (1.6a)$$

$$|NC\rangle = (\alpha_c / \alpha_T)|1\rangle - (\alpha_p / \alpha_T)|2\rangle, \quad (1.6b)$$

where $\alpha_T = (\alpha_c^2 + \alpha_p^2)^{1/2}$. The dark state is uncoupled from the excited state, i.e. $\langle 3|d \cdot E|NC\rangle \rightarrow 0$ and therefore after being pumped into this dark state, atoms cannot be excited by either of the laser fields. This optical pumping process removes all the population from $|C\rangle$ and traps it into $|NC\rangle$ eventually. This results in the formation of an ultra-narrow ‘dark’ resonance; where the word ‘dark’ is used to denote its non-absorptive nature. These dark resonances are of particular interest for several applications such as efficient nonlinear processes [13], amplification without inversion (AWI) [53-79], atomic frequency standards [80-91], laser cooling [92,93], quantum information processing [94,95] and control of light propagation within a medium [96-114].

1.1.4 Electromagnetically Induced Transparency

EIT is a special case of CPT where the probe field is much weaker compared to the pump field. It represents cancellation of linear susceptibility at the two-photon resonance condition ($\Delta_p = \Delta_c$) via destructive quantum interference; thus rendering an otherwise optically opaque medium transparent [14-18]. The classical analogy of EIT with coupled harmonic oscillators has been demonstrated by Alzar *et al.* [19]. EIT can be described in terms of two processes that work in tandem to create transparency in the

media: formation of two dressed states by the strong pump and destructive interference in the probe absorption to these states. For $\alpha_p \ll \alpha_c$, Eq. (1.6) can be simplified to obtain

$$|1\rangle = [\alpha_c |NC\rangle + \alpha_p |C\rangle] / \alpha_T \sim |NC\rangle, \quad (1.7)$$

implying that the ground state is decoupled from the excited state. Atoms prepared in this state do not interact with the probe field and hence its absorption in the media vanishes. Though EIT and CPT appear to be interrelated, there are some distinct differences between the two processes. CPT is associated with the change in populations only, while EIT depends on the optical response of the medium. Further EIT is an instantaneous process (time scale $\sim 1/\alpha_c$), while the response time of CPT is much slower i.e. of the order of several radiative lifetimes or optical pumping timescales [14-16].

In case of a Doppler broadened atomic medium, EIT may be thought of as arising from the AT doublets corresponding to atoms of velocity v which modifies the pump detuning Δ_c to $\Delta_c + k \cdot v$ due to Doppler shift where k is the wave vector. Consider for example the case when $\Delta_c = 0$. For zero velocity group of atoms, the AT doublet is symmetric with respect to $\Delta_p = 0$. For all other velocity groups due to Doppler shift one of the AT components is drawn arbitrarily close to the central frequency while the other one is pushed away. The averaging of all these AT doublet spectra results into an ultra-narrow transparency window at $\Delta_p = 0$, which corresponds to EIT resonance. This representation of EIT is convenient in arriving at the linewidth of EIT in a Doppler broadened atomic medium as given by Javan *et al.* [35-37].

For a three-level Λ system under weak saturation the half width of EIT is given by $\Gamma_{EIT} = \alpha_c [2\Gamma_{21}(1+s)/\gamma]^{1/2}$ with $\gamma = \gamma_{31} = \gamma_{32}$ and $s = \alpha_c^2 \gamma / 2\Gamma_{21} W_D^2$ where $2W_D$ is the

Doppler width of the medium [34-37]. Importance of Γ_{21} , which determines the coherence lifetime of the system, is clear from this expression. Note here that the Λ system has minimum coherence dephasing rate compared to V and Ξ systems, and as a consequence ultra-narrow linewidth EIT can be obtained in a Λ system compared to the other configurations [38,39]. Interest in EIT stems from its wide range of applications in enhancement of nonlinear processes [14-16], quantum information control [17], LWI [53-79], AFOL [80-82], time and frequency standards [83], laser cooling and trapping [93], Bose-Einstein condensate [93], super- and sub-radiance [95], slowing [96-98] and storage [99] of light, and realization of negative refraction [126-131].

1.1.5 Electromagnetically Induced Absorption

In contrast to EIT, EIA corresponds to the enhanced absorption of light around resonance due to constructive quantum interference between the excitation amplitudes [40-50]. There are two underlying physical mechanisms for EIA, transfer of coherence (TOC) and transfer of population (TOP) [41]. In a closed system when the pump and probe beams have different polarizations, TOC gives rise to EIA. Here EIA is associated with creation of light induced Zeeman coherences in the excited state and their transfer to ground state by spontaneous emission [40,41]. This happens in the absence of ground state population trapping under the condition that lasers couple two degenerate atomic levels and that the angular moment of the excited state is higher than that of the ground state [41]. EIA can also arise when TOP mediated by collisions from the ground state to a reservoir (a nearby level that does not interact with the pump) is greater than that from the excited state. Such EIA is observed in an open system, when the pump and probe

beams have same polarizations [42]. It is important to note that unlike EIT, EIA can only occur in systems which behave as open Λ systems and in the absence of population trapping [41-43]. Such systems can show both positive and negative dispersion. Further, absorption in these systems is reported to have a peak at the line centre accompanied with negative dispersion [43].

Most of the studies on EIA and conversion of EIT to EIA have been done using two-level degenerate systems and N- system [40-44]. In these contexts, the effect of Doppler broadening, coupling powers and temporal evolution of EIA have been studied both theoretically and experimentally [44-49]. EIA phenomenon has also been investigated to realize negative group velocity of light producing superluminal light pulses which may be helpful in storage of light [50-52].

1.2 Role of Incoherence

Incoherence in the laser-atom interaction dynamics is usually introduced by two distinct ways. First is the incoherent processes such as spontaneous emission and collisional decays associated with the medium, while the second is a fallout of intrinsic phase fluctuations associated with the driving field which gives it a finite bandwidth. Generally incoherence leads to destruction of atom-field phase relationship and adversely affects the quantum coherence and interference established in an atomic medium.

1.2.1 Collisional Relaxation

The collisional relaxation processes encountered in a typical vapour cell experiments are of two categories: phase changing and velocity changing collisions. As

the name suggests phase changing collisions cause change in the phase of atomic states thereby preventing the maintenance of coherent excitation. Therefore these collisions adversely affect EIT/CPT linewidths [132-136]. To counter this effect buffer gas and anti-relaxation coatings are used in the experiments. Buffer gas prevents relaxation by slowing down the diffusion of atoms thereby increasing their transit time across the laser beam. In contrast the velocity changing collisions can produce sharper EIT/CPT signals [136]. Velocity changing collisions are elastic collisions which can reduce/increase the velocity of atoms, thereby shuffling them between different velocity groups spanning over the Doppler profile. This increases the transit time and hence the Raman coherence lifetime. Further this causes more atoms to participate in coherence build up thereby aiding optical pumping. The narrowing of spectral lines by these collisions is termed as Dicke narrowing and is more pronounced when the mean free path between velocity collisions is smaller than the wavelength of light [137].

1.2.2 Spontaneously Generated Coherence

Spontaneous emission is a major limiting factor in the observation of coherent processes [1]. However a counter-intuitive phenomenon called spontaneously generated coherence (SGC) occurs in a degenerate or near degenerate level system where the interference between spontaneous emission channels from the same excited level to closely spaced ground levels or from two close lying excited levels to a ground level gives rise to an additional coherence in the medium [138]. SGC arises due to interaction of the closely spaced levels with the vacuum of electromagnetic field and has marked effect on the dynamics of a system. The essential conditions for obtaining SGC are

closely spaced level structure and non-orthogonal dipole matrix elements. SGC has been investigated in context of disappearance of dark state [138], spectral line narrowing and enhancement [139], dynamically controlled photonic band-gap structure [140], enhanced Kerr nonlinearity [141], charged quantum dots [142], AWI [143] etc.

1.2.3 Laser Phase Fluctuations

In coherent laser matter interaction the fields are idealized as monochromatic and pure sinusoid. However, in practice even the most stable laser is not truly monochromatic since random fluctuations in the field are a source of finite bandwidths. Considerable work has been reported in the literature on the effect of finite bandwidths of driving lasers on the coherent dynamics of two- and three-level systems [144-156]. In these works laser phase fluctuations are modeled as Gaussian white noise and theoretical models based on multiplicative stochastic processes have been developed to analyze the effect of bandwidths of lasers and any cross-correlation that may exist between the pump and probe fields [144-160].

For three-level systems it has been observed that the phase fluctuations in general broaden or destroy the coherence established in the medium [144-150]. The cross-correlation between the pump and probe fields can be effectively used to recover the coherent behavior, however, this recovery is dependent on the type of three-level configuration whether Λ , V or Ξ [146]. These studies point to the possibility of observing quantum coherence and interference based phenomena with finite bandwidth lasers provided the pump and probe beams are generated from the same laser source. Similar studies in the context of four-level configurations are scanty [157,158] and that

provides opportunities to investigate these issues in the context of complex quantum dynamics.

1.3 Scope and Perspectives

Quantum coherence and interference based phenomena have gone beyond the proof of principles. They have been increasingly employed in the development of quantum devices and also to explore newer frontiers of physics. A brief review of these areas pertinent to the present thesis is covered in this section.

1.3.1 Ultra-Precision Measurements

The narrow dark resonance generated in EIT and CPT provides a useful platform for ultra sensitive measurements which are of great interest in the field of metrology [83-91]. In the context of time and frequency standard, which is defined in terms of the separation between ground hyperfine levels of ^{133}Cs (9.192631770 GHz), ultra-narrow EIT/CPT resonances generated in room temperature Cs vapour cells provide an excellent reference frequency for the development of miniaturized atomic clock [85-87]. There exist two major advantages in using CPT/EIT for atomic clock development. Firstly, these clocks are passive frequency standards, i.e., they do not require microwave cavity for excitation of the ground hyperfine levels of ^{133}Cs , unlike the Cs vapour or even cold atom fountain clocks. This passive approach supports substantial miniaturization of the device. Secondly they afford significant reduction in the light shift under appropriate conditions of frequency modulation. EIT/CPT based clocks are compact and portable. Typical frequency stability reported for this type of clocks is $\sim 3 \times 10^{-11}$ (at 1 s of

integration time) [85], which make them useful in communication and in improved global positioning systems (GPS). Also a micro-fabricated atomic clock with a volume of 9.5 mm^3 , fractional frequency instability of $\sim 2.53 \times 10^{-10}$ (at 1 s of integration time) has been demonstrated by Knappe *et al.* [87].

The other application is ultra-sensitive magnetometers based on the measurement of Zeeman shifts in atomic spectra and correlation of these shifts with the local magnetic field [88-91]. The typical Zeeman shifts in alkali atoms is $\sim 4\text{-}6 \text{ Hz/nT}$. Experimental measurement of these Zeeman shifts using ultra-narrow dark resonances is central to the development of ultra-sensitive atomic magnetometer [88-91]. A chip scale Rb magnetometer with a sensor of 12 mm^3 , sensitivity of $50 \text{ pT/Hz}^{1/2}$ at 10 Hz bandwidth has been demonstrated by Schwindt *et al.* [90]. Theoretical limit of sensitivity of such magnetometers is $\sim 1 \text{ fT/Hz}^{1/2}$. Ultra sensitive magnetometers offer numerous applications in medical field, measurement of planetary magnetic field, earthquake detection, tests of the fundamental symmetries of nature and many more [91].

Yet another important application in the domain of frequency standard is atomic frequency offset locking (AFOL) where an ultra-narrow EIT/CPT resonance is generated using a pair of pump and probe lasers satisfying two-photon resonance condition in D_1 or D_2 transition of alkali atoms and the probe laser is then stabilized on the EIT/CPT resonance. This scheme establishes a fixed frequency offset between probe and pump lasers, and the value of the offset is exactly equal to the transition frequency between two ground levels of the Λ system for example. Frequency stability of EIT/CPT based AFOL schemes is much superior to that of the conventional master-slave laser systems [80-82].

1.3.2 Amplification without Inversion

The conventional population inversion condition for achieving lasing action arises from the equilibrium between stimulated absorption and stimulated emission processes. It is in general very difficult to achieve inversion condition at large frequencies, e.g. in extreme UV and X-ray regions, due to cubic dependence of spontaneous emission rate on frequency. The requirement of inversion can be circumvented by coherent preparation of atomic media and utilizing the non absorptive behaviour of EIT and CPT phenomena, and thereby making it possible to achieve AWI and LWI. AWI refers to observation of probe laser amplification in an atomic system where a coherent pump laser acting on one transition circumvents the population inversion condition for an adjoining transition connected by the weak probe [53-79]. LWI refers to the process of AWI plus an additional cavity to achieve lasing action. Interest in AWI and LWI stems from their potential application in generation of low threshold short wavelength lasers [53-59]. Further these radiation sources are expected to have interesting statistical properties such as narrower intrinsic linewidths and amplitude squeezing [60-65]. Also of interest are the issues that include LWI in quantum electrodynamics [66], nanostructures [67], and super- and sub-radiance [68].

Several schemes for the observation of AWI and LWI have been proposed [53-61] and successfully experimented [69-72]. It is widely accepted that inversionless gain in these systems is a consequence of many mechanisms [53-61]. The first one is related to recoil induced lasing where the asymmetry between shifts of stimulated emission and absorption is used to obtain frequency regions where the emission process dominates the absorption in the absence of population inversion. The second one is the inversion in the

dressed state or CPT basis [54-60]. The third mechanism is devoid of any hidden inversion and is a direct consequence of quantum interference. AWI in this situation arises due to the excitation of low frequency coherence in the medium. There exist many studies concerning the role of incoherent pumping [74-76] that compensates for the cavity and other losses, and the effect of homogenous as well as inhomogenous broadening [77-79] of the active medium in the achievement of the inversionless gain.

1.3.3 Slow, Fast and Stopped Light

Quantum interference phenomena give rise to steep change in dispersion of a medium, i.e, $\text{Re}(\chi)$ in the vicinity of the ensuing resonances. The unusual variations of the refractive index $n_r(\omega)$ of the medium then can be used to modify the group index (n_g) of the medium,

$$n_g = n_r(\omega) + \omega[dn_r(\omega)/d\omega], \quad (1.8)$$

so that the group velocity, $v_g = c/n_g$, can be manipulated to achieve fast, slow and stopped light [96-114]. Specifically at the EIT condition, the term $dn_r/d\omega$ can be made large and positive thereby giving rise to large group index and generate slowing of a pulse traveling in such a medium. A drastic reduction in speed of light has been demonstrated by Hau *et al.* [103]. Ultra slow light has promising applications in enhancing the efficiency of nonlinear processes, laser radars, telecommunications, and development of optical buffers and adjustable optical delays [103-107]. It is also possible to stop a light pulse completely when the group velocity is changing with time. In this case the information carried by the pulse is temporarily transferred to the medium

[108,109]. Pulses can then be “revived” with their original information intact [108-110]. Apart from its application in communications this phenomenon can also be used for storage of light [99], in quantum information and computing as ‘atomic memories’ [111]. The other promising applications of varying the group velocity are in amplification of ponderomotive dipole forces [106] and all optical switching [107].

On the other hand if the term $dn_r/d\omega$ is large and negative, for e.g. in an EIA media, the group index (n_g) can become negative [50-52]. This implies that the pulse propagation in the medium is much faster than the velocity of light, i.e., $v_g > c$. In other words, the anomalous dispersion region can be used for superluminal light propagation which may be helpful in communications and storage of light [111-114].

1.3.4 Negative Refraction

The fabrication of negative refractive index material, i.e., a medium exhibiting negative permittivity and permeability simultaneously, has attracted extensive attention in recent years [115-131]. These materials are also termed as left-handed materials (LHMs); the name derived from the fact that in such a medium the electric vector, the magnetic vector and the wave vector of a plane monochromatic wave form a left-handed coordinate frame. Since the pioneering work of Veselago [115,116], interest in these systems has grown enormously owing to the possibility of performing unusual and non-intuitive optics. Some of the exotic applications of LHMs are sub-wavelength imaging, reversed Doppler shift, reversed Snell’s law, obtuse angle for Cherenkov radiation, photon tunneling, electromagnetic cloaking and subluminal light propagation [115-121]. Most of the LHMs have been artificially realized in the microwave region by using

metallic split ring resonators and metallic wires, photonic crystals with periodicity much smaller than or of the order of the wavelength of the electromagnetic radiation [122,123].

Coherently driven multi-level atomic systems are promising and simpler candidates for realization of negative refractive index in the optical region [126-131]. With optimum choice of Rabi frequencies and detunings, it is possible to achieve large negative refractive index over a wide probe frequency band. EIT based systems are useful for cancelling the absorption in the medium [126-131]. Further the dispersion properties of such a medium can be used to control the group velocity of the probe beam from subluminal to superluminal [114].

1.3.5 Enhancement of Nonlinear Processes

The growing interest in enhancement of nonlinear processes stems from its several applications such as four-wave mixing, gigantic Kerr nonlinearities, generation of highly efficient optical parametric oscillator and quantum information processing [161-172]. It is interesting to note that while EIT is synonymous with the vanishing of linear susceptibility, the nonlinear susceptibility of the medium can undergo constructive interference which improves the conversion efficiency in four wave mixing [161,162]. The increased efficiency of nonlinear mixing processes is of interest in efficient frequency up-conversion, phase conjugation, control of phase matching and coherent Raman scattering [161-166]. It plays an important role in the generation of squeezed light when the intensity fluctuations in the probe are transferred to fluctuations in conjugate beam, resulting in a high intensity squeezed light [167,168]. It also concerns the area of ultra-cold atoms and Bose-Einstein condensates where standard quantum limit is an

important experimental factor [169,170]. An important nonlinear phenomenon is Kerr nonlinearity where the phase of an optical field is proportional to the intensity of another field. This is directly related to large cross phase modulation (XPM) [171,172]. Kerr nonlinearity offers numerous applications in information processing, generation of optical solitons, nondemolition measurements, quantum logic gates and generation of entangled states [164-166].

The major challenge in the observation of resonant nonlinear processes is that the nonlinear susceptibilities are much weaker than the linear susceptibilities. To this end the phenomena of EIT comes to help, since near the EIT resonance the linear susceptibility is completely cancelled. Consequently there is reduced resonant absorption, optimized phase matching condition due to zero dispersion and constructive interference for nonlinear susceptibility [161-166].

1.4 Organization of the Thesis

The present thesis deals with coherent dynamics of multi-level atomic/molecular systems and its manifestation in the observation of several of the above referred phenomena, i.e., EIT, EIA, AWI and negative refractive index, together with the issues connected with SGC, Kerr nonlinearity and the effect of finite bandwidths of driving fields. While major part of the thesis is concerned with theoretical studies, some work on experimental coherent pump-probe spectroscopy is also reported here. The investigations carried out in this thesis are organized in the following manner:

Chapter-2 provides the discussion on the master equation framework used for addressing the interaction of multi-level system with coherent multi-frequency

electromagnetic field. An explicit derivation of the semi-classical master equation in electric dipole and rotating wave approximations is discussed here for a three-level atomic system interacting with two external coherent fields and vacuum of radiation field. The treatment is generalized for four-level schemes of interest. Further generalization is achieved in the context of three-level molecular systems with permanent dipole moments for examining quantum coherence and interference in such systems.

Chapter-3 deals with coherent pump-probe spectroscopy of three-level molecular Λ system with permanent dipole moments. Motivation for these studies is provided by the very recent interest in EIT in the molecular domain. We explicitly show here the absence of amplification in 2+2-photon process for reversal in the signs of permanent moments, as reported earlier [173]. The effect of permanent dipole moments on the observation of EIT and its connection to the issue of subluminal and superluminal light propagation is analyzed. The role of virtual mechanism in 2+1-photon EIT is further examined. This chapter thus provides an integrated view of coherent pump-probe spectroscopy of a medium of dipolar molecules and its comparison with atomic case.

Chapter-4 presents detailed analysis of coherent pump-probe spectroscopy in Λ system with an additional adjacent excited level. The level scheme thus consists of two simultaneous Λ resonances with common ground levels and excited by the same pair of pump and probe fields, i.e., degenerate double lambda (DDL) resonance. Theoretical results are obtained for probe absorption spectrum and dispersion in the absence/presence of Doppler broadening to observe peculiar interference effects. These are illustrated using model schemes in D_1 and D_2 transitions of ^{85}Rb . The chapter is completed with experimental results on the dressed state spectroscopy in a Doppler broadened medium of

^{87}Rb atoms. The results of this chapter thus provide a realistic description of pump-probe spectroscopy of hyperfine transitions of alkali atoms.

Chapter-5 presents a detailed analysis and discussion on the phenomenon of AWI in the DDL system. It is shown here that a four-level DDL system under specific conditions can exhibit AWI without need of incoherent pumping. The dependence of AWI on atom-field interaction parameters, spontaneous emission rates, low-frequency coherence and Doppler velocity distribution is investigated. Approximate analytical expression for probe absorption is derived to corroborate the numerical results and to discuss the contrasting behavior, i.e., absorption *vs.* AWI, for the model DDL systems in D_1 and D_2 transitions of ^{87}Rb . The discussion on AWI is further augmented using quantum jump formalism, which provides useful insight into the underlying mechanism responsible for amplification.

Chapter-6 deals with theoretical analysis of interference effects in general four-level configurations, i.e., tripod system and N-resonance, driven by three coherent fields from the viewpoint of controlling of their coherent dynamics and its manifestations. Tripod system is studied to demonstrate the observation of ultra-narrow double dark resonances. Some specific issues addressed in context of N system include switching between EIT and EIA, role of SGC and enhancement of the Kerr nonlinearity. Also reported here are the experimental results on EIT in N system and its comparison with a Λ system in a medium of Doppler broadened ^{87}Rb atoms.

Chapter-7 deals with the investigations of laser phase fluctuations on the coherent dynamics of four-level systems with N-resonance as an example. The problem is formulated in the framework of master equation and multiplicative stochastic processes

and the effect of finite bandwidths of lasers and their cross-correlation on three-photon and 2+1-photon resonance is examined. It is observed that the phase fluctuations tend to broaden and destroy the sharp resonances, and dampen the Rabi oscillations; however the extent of this effect is critically dependent on the phase fluctuations and cross-correlations associated with the three fields. The effect of phase fluctuations on the EIT and EIA resonances is also reported here.

Chapter-8 is devoted to exploratory investigations on the observation of negative refractive index in four-level systems interacting with three coherent fields, a probe, a control and a *rf* field. In the framework of master equation and Classius-Mossotti relation, we obtain relative permittivity and permeability for a dense medium of such atoms to show the existence of probe frequency domains where permittivity and permeability can become simultaneously negative. The use of the dispersion property of the negative refractive index to control the group velocity of the probe beam from subluminal to superluminal is also discussed.

Finally the important conclusions of the present study and scope for future work are briefly summarized in Chapter-9.

CHAPTER 2

MASTER EQUATION APPROACH TO LASER- MATTER INTERACTION

2.1 Introduction

There exist several approaches to describe the interaction of a finite-level atom with radiation field. Conventional Schrodinger equation is valid only when the behaviour of interest occurs in time duration much shorter than the level life times. Another framework is Bloch equation approach where the relaxation processes are incorporated phenomenologically, i.e., longitudinal and transverse relaxations to describe population redistribution and damping of Rabi oscillations respectively. Master equation approach, which is followed throughout this thesis, treats the interaction of atom with external radiation field and the vacuum on the same footing thereby providing the first principle description of relaxation processes.

The master equation, also known as quantum Liouville equation (or Von-Neumann equation), describes the time evolution of a quantum system while taking into

account the effects of environment in terms of reduced density operator. The total system of atom and vacuum reservoir (bath) is described by a Hamiltonian in the second quantized form whereas the external fields are assumed to be classical. The technique of projection operators is used to eliminate the field modes and obtain the master equation for reduced atomic density operator. Reduced density operator corresponds to a subsystem of interest (here atomic system) of a larger system (atom + reservoir) obtained by tracing over the reservoir.

Master equation formulation is developed for a single atom within the space of some modest number of atomic states, i.e., essential state basis. The electromagnetic radiation field is considered classical and monochromatic. While a realistic source may have phase as well as amplitude fluctuations, we defer the discussion relating to incorporation of these effects to later chapters. The interaction of external radiation field with atoms is considered in the electric-dipole approximation and rotating wave approximation (RWA). Together with external field, the atomic system also interacts with the vacuum of radiation, i.e., the reservoir (bath). It is considered that reservoir is very large and its state is not affected by atomic coupling. Thus the reservoir density operator is time independent. Atoms and the reservoir are considered to be initially uncorrelated. This refers to adiabatic approximation; the consequence of which is that the state of the atomic system depends only on the instantaneous values of Hamiltonian matrix elements and not on the entire history of excitation. The analysis is performed in the Born approximation, i.e., assuming that the coupling between the atom and reservoir is weak and the relaxation time of the reservoir is much faster so that any correlation between the two is quickly lost. Thus the reservoir essentially does not change the state of

the atom but only produces a minor time dependent perturbation of initial population distribution. Finally the relaxation processes are considered to be Markovian, i.e., they have infinitesimally brief correlation times.

2.2 Derivation of the Master Equation for Three-level Systems

2.2.1 Hamiltonian

We consider a closed three-level atomic system in Λ configuration as shown in Fig. 1.2(a). Here two ground levels $|1\rangle$ and $|2\rangle$ are connected with an excited common level $|3\rangle$ by means of two near-resonant monochromatic radiation fields of frequencies Ω_1 and Ω_2 . The energy of level $|i\rangle$ is $\hbar\omega_i$ and $\omega_{ij} = \omega_i - \omega_j$ is the frequency of $|i\rangle \rightarrow |j\rangle$ transition. The total Hamiltonian of the system is given by

$$H = H_A + H_B + H_{AB} + H_{ext}(t) , \quad (2.1)$$

where H_A , H_B , H_{AB} and $H_{ext}(t)$ are the atomic, bath, atom-bath interaction and atom-field interaction Hamiltonians respectively given in atomic units ($e = \hbar = c = 1$) as

$$H_A = \sum_{i=1}^3 \omega_i A_{ii} , \quad H_B = \sum_k \omega_k b_k^+ b_k , \quad H_{AB} = -\vec{d} \cdot \vec{E} , \quad H_{ext} = -\vec{d} \cdot \vec{E}_{ext} . \quad (2.2)$$

Here $A_{ij} = |i\rangle\langle j|$ are the atomic operators with $\sum_{i=1}^3 A_{ii} = 1$. $|i\rangle$ is the eigenstate of atomic Hamiltonian H_A . The atomic operators satisfy the following commutation relation:

$$[A_{ij}, A_{pq}] = A_{iq} \delta_{jp} - A_{pj} \delta_{qi} . \quad (2.3)$$

Also the commutation relations of the boson operators b_k^+ and b_k are given as

$$[b_j, b_k^+] = \delta_{jk} , \quad [b_j, b_k] = [b_j^+, b_k^+] = 0 . \quad (2.4)$$

The dipole moment operator is defined as $\vec{d} = \sum_{i,j} \vec{d}_{ij} |i\rangle\langle j|$, where $\vec{d}_{ij} = \langle i | \vec{d} | j \rangle$ is the transition dipole moment of $|i\rangle \rightarrow |j\rangle$ transition. We choose \vec{d}_{ij} to be real. The reservoir and external fields are expressed as

$$\vec{E} = i \sum_k (2\pi k / V)^{1/2} \vec{\epsilon}_k \cdot \vec{b}_k \exp(i\vec{k} \cdot \vec{r}) + H.C, \quad (2.5)$$

$$\vec{E}_{ext} = \frac{1}{2} \vec{E}_1(t) \exp\{-i(\vec{k}_1 \cdot \vec{r} - \Omega_1 t)\} + \frac{1}{2} \vec{E}_2(t) \exp\{-i(\vec{k}_2 \cdot \vec{r} - \Omega_2 t)\} + H.C, \quad (2.6)$$

where $\vec{\epsilon}_k$ is polarization vector, V is quantization volume, $\vec{E}_j(t)$ is driving field amplitude, \vec{k} and \vec{k}_j are wave vectors, and $H.C$ stands for the hermitian conjugate.

Spatial variations of fields can be neglected under the dipole approximation to obtain

$$\vec{E} = i \sum_k (2\pi k / V)^{1/2} \vec{\epsilon}_k \cdot \vec{b}_k + H.C, \quad (2.7)$$

$$\vec{E}_{ext} = [\vec{E}_1(t) \exp(i\Omega_1 t) + \vec{E}_2(t) \exp(i\Omega_2 t) + H.C] / 2. \quad (2.8)$$

The atom-bath interaction Hamiltonian is given as

$$H_{AB} = \sum_k [g_{k1} (A_{13} + A_{31}) b_k + \sum_k g_{k2} (A_{23} + A_{32}) b_k + H.C], \quad (2.9)$$

$$g_{kj} = -i(2\pi k / V)^{1/2} \vec{\epsilon}_k \cdot \vec{d}_{j3}, \quad (j = 1, 2). \quad (2.10)$$

Similarly the atom-field interaction Hamiltonian can be obtained as

$$H_{ext} = -[\vec{d}_{13} \cdot \vec{E}_1(t) e^{i\Omega_1 t} (A_{13} + A_{31}) + \vec{d}_{23} \cdot \vec{E}_2(t) e^{i\Omega_2 t} (A_{23} + A_{32}) + H.C] / 2. \quad (2.11)$$

$H_A + H_{ext}$ expresses the behaviour of atom subjected to an analytically described semi-classical radiation field. The remaining part $H_B + H_{AB}$ describes uncontrollable random fluctuations in the Hamiltonian. H_{AB} may be simplified under RWA to obtain

$$H_{AB} = \sum_k g_{k1} A_{31} b_k + g_{k2} A_{32} b_k + g_{k1}^* b_k^+ A_{13} + g_{k2}^* b_k^+ A_{23}. \quad (2.12)$$

The physical meaning of RWA lies in neglecting energy non-conserving terms such as $A_{31}b_k^+$, $A_{13}b_k$ etc., i.e., terms involving simultaneous atomic excitation (decay) and photon creation (destruction). RWA on H_{ext} is done in the next subsection.

2.2.2 Time Evolution of the System

The statistical property of atom interacting with two fields is described by density operator $\rho_{A+B}(t)$ which satisfies the following quantum-Liouville equation

$$d\rho_{A+B}(t)/dt = -i[H, \rho_{A+B}(t)] = iL_{A+B}(t), \quad (2.13)$$

where L is the Hermitian operator called Liouville operator defined as

$$L..... = [H,.....] \quad \text{and} \quad L^\dagger = L. \quad (2.14)$$

For further analysis we divide the Hamiltonian into two parts: the first (H_1) is the unperturbed part with respect to interaction Hamiltonian $H_{AB} + H_{ext}$ and the second (H_2) is the unperturbed part with respect to atom-bath interaction Hamiltonian H_{AB} , i.e.

$$H_1 = H_A + H_B, \quad H_2 = H_A + H_B + H_{ext}(t). \quad (2.15)$$

We now introduce operators $\sigma_1(t)$ and $\sigma_2(t)$ defined as

$$\sigma_i(t) = U_i^\dagger(t,0) \rho_{A+B}(t) U_i(t,0), \quad (i = 1,2). \quad (2.16)$$

Here U_i is the time evolution operator defined as

$$U_i(t, \tau) = T \exp\left\{-\int_\tau^t dt' H_i(t')\right\}, \quad (i = 1,2), \quad (2.17)$$

where T is the Dyson time operator. The unitary transformations given by this time evolution operator lead to two interaction pictures. From Eq. (2.17) we have

$$U_1(t, \tau) = \exp[-iH_1(t - \tau)], \quad (2.18a)$$

$$U_2(t, \tau) = T \exp \left\{ -i \int_{\tau}^t dt' H_2(t') \right\}. \quad (2.18b)$$

Differentiating Eq. (2.18b), we obtain

$$dU_2(t, \tau) / dt = -i[H_1 + H_{ext}(t)]U_2(t, \tau). \quad (2.19)$$

We now define the operator $V(t, \tau)$ as

$$V(t, \tau) = \exp(iH_1 t) U_2(t, \tau) \exp(-iH_1 \tau), \quad (2.20)$$

which gives the following relation between U_1 and U_2 ,

$$U_2(t, \tau) = U_1(t, 0) V(t, \tau) U_1^+(\tau, 0). \quad (2.21)$$

Differentiating Eq. (2.20), we obtain

$$dV(t, \tau) / dt = -iH_{ext,1}(t)V(t, \tau), \quad (2.22)$$

$$H_{ext,1}(t) = U_1^+(t, 0) H_{ext}(t) U_1(t, 0). \quad (2.23)$$

The formal solution of the Eq. (2.22) can be obtained as

$$V(t, \tau) = T \exp \left\{ -i \int_{\tau}^t dt' H_{ext,1}(t') \right\}. \quad (2.24)$$

Using Eq. (2.16), (2.18) and (2.21) we obtain the relation between $\sigma_1(t)$ and $\sigma_2(t)$ as

$$\sigma_2(t) = V^+(t, 0) \sigma_1(t) V(t, 0). \quad (2.25)$$

Differentiating Eq. (2.25) we recover Liouville equation for $\sigma_2(t)$ as follows:

$$d\sigma_2(t) / dt - i[H_{AB2}(t), \sigma_2(t)] = -iL_{AB2}\sigma_2(t), \quad (2.26)$$

where

$$H_{AB2}(t) = U_2^+(t, 0) H_{AB}(t) U_2(t, 0). \quad (2.27)$$

The Liouville equation (2.26) contains variables of both the system of interest (atomic sub-system) as well as irrelevant reservoir part. For most statistical results full knowledge

of $\sigma_2(t)$ is not required. Further the reservoir is very large which can neither be controlled nor is accessible for direct measurements. Therefore we isolate the relevant atomic part $\sigma_{A2}(t)$ from the irrelevant part $\sigma_B(t)$ by taking trace of $\sigma_2(t)$ over reservoir variables. The decisive criteria to determine the relevant part is $\tau_{relevant} \gg \tau_{irrelevant}$, where τ are the relaxation times. The reduced density operator $\sigma_{A2}(t)$ corresponding to the atomic subsystem is given as

$$\sigma_{A2}(t) = Tr_B(\sigma_2(t)), \quad (2.28)$$

where Tr_B indicates the trace over reservoir variables. We now assume that the reservoir is initially at thermal equilibrium at temperature T_e . In this case the reservoir follows a Boltzmann distribution

$$\sigma_B(0) = \prod_j [1 - \exp(-\lambda_j)] \exp(-\lambda_j b_j^+ b_j), \quad (2.29)$$

where $\lambda_j = \omega_j / k_B T_e$ with k_B as the Boltzmann constant. It can be easily proved that

$$Tr_B(\sigma_B(0)) = 1. \quad (2.30)$$

Note that as $T_e \rightarrow 0$, the average number of photons, $\langle n_k \rangle = 1/[\exp(\lambda_k) - 1] \rightarrow 0$ for any mode. Therefore at $T_e \rightarrow 0$ it can be assumed that

$$\sigma_B(0) = |\{0\}\rangle\langle\{0\}|. \quad (2.31)$$

We further assume that the system and reservoir are initially uncorrelated so that

$$\sigma_2(0) = \sigma_{A2}(0)\sigma_B(0). \quad (2.32)$$

The formalism becomes more succinct by introducing two orthogonal projection operators P and Q defined as

$$P\dots = GTr_B\dots \quad (2.33)$$

where the basis states are included in P , and Q is represented by sum over the remaining states. The projection operators satisfy the following relations

$$P^2 = P, \quad Q^2 = Q, \quad PQ = QP = 0 \quad \text{and} \quad P + Q = 1. \quad (2.34)$$

The operator G satisfies $Tr_B(G) = 1$. Using Eq. (2.28) we have,

$$P\sigma_2(t) = GTr_B(\sigma_2(t)) = G\sigma_{A2}(t). \quad (2.35)$$

Thus at time $t = 0$ we can easily shown that,

$$P\sigma_2(0) = 0 \quad \text{and} \quad (1 - P)\sigma_2(0) = (\sigma_B(0) - G)\sigma_{A2}(0), \quad (2.36)$$

where we have used the fact that $\sigma_{A2}(0)$ and $\sigma_B(0)$ commute with each other. Choosing $G = \sigma_B(0)$ in Eq. (2.35) and (2.36) we get,

$$P\sigma_2(t) = \sigma_B(0)\sigma_{A2}(t), \quad (2.37)$$

$$(1 - P)\sigma_2(0) = Q\sigma_2(0) = 0. \quad (2.38)$$

From Eq. (2.26) we have,

$$dP\sigma_2(t) / dt = -i\{PH_{AB2}(t)(P + Q)\sigma_2(t) - P\sigma_2(t)H_{AB2}(t)\}. \quad (2.39)$$

Using the properties of projection operators (*cf.* Eq. (2.34)) we obtain the equation of motion for $P\sigma_2(t)$ as

$$dP\sigma_2(t) / dt = -iPL_{AB2}(t)P\sigma_2(t) - iPL_{AB2}(t)Q\sigma_2(t). \quad (2.40)$$

Similarly the equation of motion for $Q\sigma_2(t)$ can be derived as

$$dQ\sigma_2(t) / dt = -iQL_{AB2}(t)P\sigma_2(t) - iQL_{AB2}(t)Q\sigma_2(t). \quad (2.41)$$

The formal solution of Eq. (2.41) is given as

$$\begin{aligned} Q\sigma_2(t) = & T \exp(-i\int_0^t dt' QL_{AB2}(t')Q)Q\sigma_2(0) \\ & - i\int_0^t dt_1 T \exp\left\{-i\int_{t_1}^t dt' QL_{AB2}(t')Q\right\}QL_{AB2}(t_1)P\sigma_2(t_1). \end{aligned} \quad (2.42a)$$

Now since $Q\sigma_2(0)=0$, the above equation can be simplified to get

$$Q\sigma_2(t) = -i \int_0^t d\tau T \exp\left(-i \int_\tau^t dt' QL_{AB2}(t')Q\right) QL_{AB2}(\tau) P\sigma_2(\tau). \quad (2.42b)$$

Using the above expression of $Q\sigma_2(t)$ in Eq. (2.40), we obtain

$$dP\sigma_2(t)/dt + iPL_{AB2}(t)P\sigma_2(t) + PL_{AB2}(t) \int_0^t d\tau U(t,\tau) QL_{AB2}(\tau) P\sigma_2(\tau) = 0, \quad (2.43)$$

$$U(t,\tau) = T \exp\left(-i \int_\tau^t dt' QL_{AB2}(t')Q\right). \quad (2.44)$$

We now apply the Born approximation, i.e., $\tau_B \ll \tau_A$ where τ_B is the typical time during which correlation with bath subsystem exists and τ_A characterizes the evolution of operator $\rho_A(t)$ due to interaction with the reservoir

$$U(t,\tau) = 1. \quad (2.45)$$

Changing variables of integration in Eq. (2.43) and using Born approximation, we have

$$dP\sigma_2(t)/dt + iPL_{AB2}(t)P\sigma_2(t) + \int_0^t d\tau PL_{AB2}(t) QL_{AB2}(t-\tau) P\sigma_2(t-\tau) = 0. \quad (2.46)$$

Now using Eq. (2.25) and the fact that $[P, V(t,0)] = 0$ we obtain

$$P\sigma_1(t) = PV(t,0)\sigma_2(t)V^+(t,0) = V(t,0)P\sigma_2(t)V^+(t,0). \quad (2.47)$$

Differentiating Eq. (2.47), and making use of Eq. (2.22) and (2.46) we can show that

$$\begin{aligned} \frac{dP\sigma_1(t)}{dt} + i[H_{ext,1}(t), P\sigma_1(t)] + iPL_{AB1}(t)P\sigma_1(t) + \\ \left(\int_0^t d\tau PL_{AB1}(t) QL_{AB1}(t-\tau) P\sigma_1(t-\tau) \right) = 0. \end{aligned} \quad (2.48)$$

In the interaction picture Eq. (2.12) takes the form

$$H_{AB1}(t) = U_1^+(t,0) H_{AB} U_1(t,0), \quad U_1(t,0) = \exp(-iH_1 t). \quad (2.49)$$

We now list some mathematical identities which are needed for further analysis

$$(a) \quad \exp(-\lambda A)B \exp(\lambda A) = B + \lambda[A, B] + \frac{\lambda^2}{2!}[A, [A, B]] + \dots$$

$$(b) \quad Tr_B \{ \sigma_B(0) b_k^+ b_{k'} \} = \langle n_k \rangle \delta_{kk'}$$

$$(c) \quad Tr_B \{ \sigma_B(0) b_k b_{k'}^+ \} = (1 + \langle n_k \rangle) \delta_{kk'}$$

$$(d) \quad Tr_B \{ \sigma_B(0) b_k b_{k'} \} = Tr_B \{ \sigma_B(0) b_k^+ b_{k'}^+ \} = 0$$

Using Eq. (2.3), (2.4) and identity (a) we can easily show that

$$U_1^+(t, 0) g_{k1} A_{31} b_k U_1(t, 0) = g_{k1}(t) A_{31} b_k, \quad U_1^+(t, 0) g_{k2} A_{32} b_k U_1(t, 0) = g_{k2}(t) A_{32} b_k, \quad (2.50a)$$

$$U_1^+(t, 0) g_{k1}^* b_k^+ A_{13} U_1(t, 0) = g_{k1}^*(t) b_k^+ A_{13}, \quad U_1^+(t, 0) g_{k2}^* b_k^+ A_{23} U_1(t, 0) = g_{k2}^*(t) b_k^+ A_{23}, \quad (2.50b)$$

where

$$g_{k1}(t) = g_{k1} \exp[i(\omega_{31} - \omega_k)t], \quad g_{k2}(t) = g_{k2} \exp[i(\omega_{32} - \omega_k)t]. \quad (2.51)$$

Using Eq. (2.50) and (2.51) in Eq. (2.49) we obtain,

$$H_{AB1}(t) = \sum_k g_{k1}(t) A_{31} b_k + g_{k2}(t) A_{32} b_k + g_{k1}^*(t) b_k^+ A_{13} + g_{k2}^*(t) b_k^+ A_{23}. \quad (2.52)$$

Now since H_{AB1} is hermitian and $\langle \{0\} | b_k | \{0\} \rangle = \langle \{0\} | b_k^+ | \{0\} \rangle = 0$, it can be shown that

$$P L_{AB1}(t) P \sigma_1(t) = 0, \quad P \sigma_1(t) = \sigma_B(0) \sigma_{A1}(t). \quad (2.53)$$

Using Eq. (2.53) and $G = \sigma_B(0)$ in Eq. (2.48) we obtain

$$d\sigma_{A1}(t)/dt + i[H_{ext,1}, \sigma_{A1}(t)] + \int_0^t d\tau Tr_B \{ L_{AB1}(t) L_{AB1}(t-\tau) \sigma_B(0) \sigma_{A1}(t-\tau) \} = 0. \quad (2.54)$$

Using Eq. (2.14) we can expand the terms inside the integral of Eq. (2.54) as

$$\begin{aligned} & Tr_B \{ L_{AB1}(t) L_{AB1}(t-\tau) \sigma_B(0) \sigma_{A1}(t-\tau) \} \\ &= Tr_B [H_{AB1}(t), [H_{AB1}(t-\tau), \sigma_B(0) \sigma_{A1}(t-\tau)]] \\ &= Tr_B \{ H_{AB1}(t) H_{AB1}(t-\tau) \sigma_B(0) \sigma_{A1}(t-\tau) - H_{AB1}(t-\tau) \sigma_B(0) \sigma_{A1}(t-\tau) H_{AB1}(t) \\ &\quad - H_{AB1}(t) \sigma_B(0) \sigma_{A1}(t-\tau) H_{AB1}(t-\tau) + \sigma_B(0) \sigma_{A1}(t-\tau) H_{AB1}(t-\tau) H_{AB1}(t) \}. \end{aligned} \quad (2.55)$$

The four terms of Eq. (2.55) can be simplified using identities (b) – (e) as follows:

$$\begin{aligned}
 & Tr_B \{ H_{AB1}(t) H_{AB1}(t-\tau) \sigma_B(0) \sigma_{A1}(t-\tau) \} = \\
 & \left\{ \begin{aligned}
 & \sum_k |g_{k1}|^2 (1 + \langle n_k \rangle) e^{i(\omega_{31}-\omega_k)\tau} A_{31} A_{13} + |g_{k1}|^2 \langle n_k \rangle e^{-i(\omega_{31}-\omega_k)\tau} A_{13} A_{31} \\
 & + |g_{k2}|^2 (1 + \langle n_k \rangle) e^{i(\omega_{32}-\omega_k)\tau} A_{32} A_{23} + |g_{k2}|^2 \langle n_k \rangle e^{-i(\omega_{32}-\omega_k)\tau} A_{23} A_{32} \\
 & + g_{k1}^* g_{k2} \langle n_k \rangle e^{i\omega_k\tau} e^{-i\omega_{31}t} e^{i\omega_{32}(t-\tau)} A_{13} A_{32} \\
 & + g_{k2}^* g_{k1} \langle n_k \rangle e^{i\omega_k\tau} e^{-i\omega_{32}t} e^{i\omega_{31}(t-\tau)} A_{23} A_{31}
 \end{aligned} \right\} \sigma_{A1}(t-\tau), \quad (2.56a)
 \end{aligned}$$

$$\begin{aligned}
 & Tr_B \{ H_{AB1}(t-\tau) \sigma_B(0) \sigma_{A1}(t-\tau) H_{AB1}(t) \} \\
 & = \sum_k |g_{k1}|^2 (1 + \langle n_k \rangle) e^{i(\omega_{31}-\omega_k)\tau} A_{13} \sigma_{A1}(t-\tau) A_{31} + |g_{k1}|^2 \langle n_k \rangle e^{-i(\omega_{31}-\omega_k)\tau} A_{31} \sigma_{A1}(t-\tau) A_{13} \\
 & + |g_{k2}|^2 (1 + \langle n_k \rangle) e^{i(\omega_{32}-\omega_k)\tau} A_{23} \sigma_{A1}(t-\tau) A_{32} + |g_{k2}|^2 \langle n_k \rangle e^{-i(\omega_{32}-\omega_k)\tau} A_{32} \sigma_{A1}(t-\tau) A_{23} \quad (2.56b) \\
 & + g_{k1}^* g_{k2} (1 + \langle n_k \rangle) e^{-i\omega_k\tau} e^{i\omega_{32}t} e^{-i\omega_{31}(t-\tau)} A_{13} \sigma_{A1}(t-\tau) A_{32} \\
 & + g_{k2}^* g_{k1} (1 + \langle n_k \rangle) e^{-i\omega_k\tau} e^{i\omega_{31}t} e^{-i\omega_{32}(t-\tau)} A_{23} \sigma_{A1}(t-\tau) A_{31},
 \end{aligned}$$

$$\begin{aligned}
 & Tr_B \{ H_{AB1}(t) \sigma_B(0) \sigma_{A1}(t-\tau) H_{AB1}(t-\tau) \} \\
 & = \sum_k |g_{k1}|^2 (1 + \langle n_k \rangle) e^{-i(\omega_{31}-\omega_k)\tau} A_{13} \sigma_{A1}(t-\tau) A_{31} + |g_{k1}|^2 \langle n_k \rangle e^{i(\omega_{31}-\omega_k)\tau} A_{31} \sigma_{A1}(t-\tau) A_{13} \\
 & + |g_{k2}|^2 (1 + \langle n_k \rangle) e^{-i(\omega_{32}-\omega_k)\tau} A_{23} \sigma_{A1}(t-\tau) A_{32} + |g_{k2}|^2 \langle n_k \rangle e^{i(\omega_{32}-\omega_k)\tau} A_{32} \sigma_{A1}(t-\tau) A_{23} \quad (2.56c) \\
 & + g_{k1}^* g_{k2} (1 + \langle n_k \rangle) e^{i\omega_k\tau} e^{-i\omega_{31}t} e^{i\omega_{32}(t-\tau)} A_{13} \sigma_{A1}(t-\tau) A_{32} \\
 & + g_{k2}^* g_{k1} (1 + \langle n_k \rangle) e^{i\omega_k\tau} e^{-i\omega_{32}t} e^{i\omega_{31}(t-\tau)} A_{23} \sigma_{A1}(t-\tau) A_{31},
 \end{aligned}$$

$$\begin{aligned}
 & Tr_B \{ \sigma_B(0) \sigma_{A1}(t-\tau) H_{AB1}(t-\tau) H_{AB1}(t) \} \\
 & = \sigma_{A1}(t-\tau) \left\{ \begin{aligned}
 & \sum_k |g_{k1}|^2 (1 + \langle n_k \rangle) e^{-i(\omega_{31}-\omega_k)\tau} A_{31} A_{13} + |g_{k1}|^2 \langle n_k \rangle e^{i(\omega_{31}-\omega_k)\tau} A_{13} A_{31} \\
 & + |g_{k2}|^2 (1 + \langle n_k \rangle) e^{-i(\omega_{32}-\omega_k)\tau} A_{32} A_{23} + |g_{k2}|^2 \langle n_k \rangle e^{i(\omega_{32}-\omega_k)\tau} A_{23} A_{32} \\
 & + g_{k1}^* g_{k2} \langle n_k \rangle e^{-i\omega_k\tau} e^{i\omega_{32}t} e^{-i\omega_{31}(t-\tau)} A_{13} A_{32} \\
 & + g_{k2}^* g_{k1} \langle n_k \rangle e^{-i\omega_k\tau} e^{i\omega_{31}t} e^{-i\omega_{32}(t-\tau)} A_{23} A_{31}
 \end{aligned} \right\}. \quad (2.56d)
 \end{aligned}$$

It can be shown that as $T_e \rightarrow 0$, $\lambda_j \rightarrow \infty$ and $n_k \rightarrow 0$. Neglecting those terms in

Eq. (2.56) which oscillate as $\pm(\omega_{31} - \omega_{32})$ and substituting in Eq. (2.55), we obtain

$$\begin{aligned}
 & Tr_B \{ L_{AB1}(t) L_{AB1}(t-\tau) \sigma_B(0) \sigma_{A1}(t-\tau) \} \\
 & = \sum_k |g_{k1}|^2 (1 + \langle n_k \rangle) \left(e^{i(\omega_{31}-\omega_k)\tau} [A_{31}, A_{13} \sigma_{A1}(t-\tau)] + e^{-i(\omega_{31}-\omega_k)\tau} [\sigma_{A1}(t-\tau) A_{31}, A_{13}] \right) \\
 & + |g_{k1}|^2 \langle n_k \rangle \left(e^{i(\omega_{31}-\omega_k)\tau} [\sigma_{A1}(t-\tau) A_{13}, A_{31}] + e^{-i(\omega_{31}-\omega_k)\tau} [A_{13}, A_{31} \sigma_{A1}(t-\tau)] \right)
 \end{aligned}$$

$$\begin{aligned}
 & + |g_{k2}|^2 (1 + \langle n_k \rangle) \left(e^{i(\omega_{32} - \omega_k)\tau} [A_{32}, A_{23} \sigma_{A1}(t - \tau)] + e^{-i(\omega_{32} - \omega_k)\tau} [\sigma_{A1}(t - \tau) A_{32}, A_{23}] \right) \\
 & + |g_{k2}|^2 \langle n_k \rangle \left(e^{i(\omega_{32} - \omega_k)\tau} [\sigma_{A1}(t - \tau) A_{23}, A_{32}] + e^{-i(\omega_{32} - \omega_k)\tau} [A_{23}, A_{32} \sigma_{A1}(t - \tau)] \right).
 \end{aligned} \tag{2.57}$$

We now apply the Markov approximation by choosing time such that $\tau_B \ll t \ll \tau_A$ and $t \gg (1/\omega_{31}), (1/\omega_{32})$ so that we can substitute $t \rightarrow \infty$. Further in this approximation we can write $\sigma_{A1}(t - \tau) = \sigma_{A1}(t)$ inside the integral of Eq. (2.54). The integrals appearing in Eq. (2.54) are of the type

$$\int_0^{\infty} \exp(\pm ixt) dt = \pi \delta(x) \pm iP_r(1/x), \tag{2.58}$$

where P_r is the principal value. We now define the decay constants as

$$\gamma_{31} = \sum_k |g_{k1}|^2 (1 + \langle n_k \rangle) \pi \delta(\omega_{31} - \omega_k), \quad \gamma_{13} = \sum_k |g_{k1}|^2 \langle n_k \rangle \pi \delta(\omega_{31} - \omega_k), \tag{2.59a}$$

$$\gamma_{32} = \sum_k |g_{k2}|^2 (1 + \langle n_k \rangle) \pi \delta(\omega_{32} - \omega_k), \quad \gamma_{23} = \sum_k |g_{k2}|^2 \langle n_k \rangle \pi \delta(\omega_{32} - \omega_k), \tag{2.59b}$$

and frequency shifts as

$$\Omega_{31} = P_r \sum_k |g_{k1}|^2 \frac{1 + \langle n_k \rangle}{\omega_{31} - \omega_k}, \quad \Omega_{13} = P_r \sum_k |g_{k1}|^2 \frac{\langle n_k \rangle}{\omega_{31} - \omega_k}, \tag{2.60a}$$

$$\Omega_{32} = P_r \sum_k |g_{k2}|^2 \frac{1 + \langle n_k \rangle}{\omega_{32} - \omega_k}, \quad \Omega_{23} = P_r \sum_k |g_{k2}|^2 \frac{\langle n_k \rangle}{\omega_{32} - \omega_k}. \tag{2.60b}$$

Using Eq. (2.57) – (2.60) in Eq. (2.54), we obtain the equation of motion for $\sigma_{A1}(t)$ as

$$\begin{aligned}
 & d\sigma_{A1}(t)/dt + i[H_{ext,1}(t), \sigma_{A1}(t)] + \gamma_{31} \{ [A_{31}, A_{13} \sigma_{A1}(t)] + [\sigma_{A1}(t) A_{31}, A_{13}] \} \\
 & + \gamma_{13} \{ [\sigma_{A1}(t) A_{13}, A_{31}] + [A_{13}, A_{31} \sigma_{A1}(t)] \} + \gamma_{32} \{ [A_{32}, A_{23} \sigma_{A1}(t)] + [\sigma_{A1}(t) A_{32}, A_{23}] \} \\
 & + \gamma_{23} \{ [\sigma_{A1}(t) A_{23}, A_{32}] + [A_{23}, A_{32} \sigma_{A1}(t)] \} + i\Omega_{31} \{ [A_{31}, A_{13} \sigma_{A1}(t)] - [\sigma_{A1}(t) A_{31}, A_{13}] \} \\
 & + i\Omega_{13} \{ [\sigma_{A1}(t) A_{13}, A_{31}] - [A_{13}, A_{31} \sigma_{A1}(t)] \} + i\Omega_{32} \{ [A_{32}, A_{23} \sigma_{A1}(t)] - [\sigma_{A1}(t) A_{32}, A_{23}] \} \\
 & + i\Omega_{23} \{ [\sigma_{A1}(t) A_{23}, A_{32}] - [A_{23}, A_{32} \sigma_{A1}(t)] \} = 0.
 \end{aligned} \tag{2.61}$$

Now we revert back to the original representation, i.e.,

$$\rho_A(t) = U_1(t,0)\sigma_{A1}(t)U_1^+(t,0) = \exp(-iH_1t) \sigma_{A1}(t) \exp(iH_1t). \quad (2.62)$$

Thus it can easily shown that,

$$\begin{aligned} & d\rho_A(t)/dt + i[H_A, \rho_A(t)] + i[H_{ext}(t), \rho_A(t)] \\ & + \gamma_{31}(A_{33}\rho_A(t) - 2A_{13}\rho_A(t)A_{31} + \rho_A(t)A_{33}) + \gamma_{13}(A_{11}\rho_A(t) - 2A_{31}\rho_A(t)A_{13} + \rho_A(t)A_{11}) \\ & + \gamma_{32}(A_{33}\rho_A(t) - 2A_{23}\rho_A(t)A_{32} + \rho_A(t)A_{33}) + \gamma_{23}(A_{22}\rho_A(t) - 2A_{32}\rho_A(t)A_{23} + \rho_A(t)A_{22}) \\ & + i\Omega_{31}[A_{33}, \sigma_{A1}(t)] - i\Omega_{13}[A_{11}, \sigma_{A1}(t)] + i\Omega_{32}[A_{33}, \sigma_{A1}(t)] - i\Omega_{23}[A_{22}, \sigma_{A1}(t)] = 0. \end{aligned} \quad (2.63)$$

The last four terms of Eq. (2.63) contribute to the first order dispersion force between two atoms and hence can be neglected. Thus the master equation of the system is

$$\begin{aligned} & d\rho_A(t)/dt + i[H_A + H_{ext}(t), \rho_A(t)] \\ & + \gamma_{ij}\{A_{ii}\rho_A(t) - 2A_{ji}\rho_A(t)A_{ij} + \rho_A(t)A_{ii}\} = 0; \quad (ij = 31, 13, 32, 23). \end{aligned} \quad (2.64)$$

Further the decay terms γ_{13} and γ_{23} correspond to non-radiative high energy collisions which are unlikely in our domain of study. The low energy non-radiative decays Γ_{12} and Γ_{21} , which correspond to damping between the two dipole forbidden ground states, can be added similar to γ_{ij} . Thus we finally obtain,

$$\begin{aligned} & d\rho_A(t)/dt + i\omega_1[A_{11}, \rho_A(t)] + i\omega_2[A_{22}, \rho_A(t)] + i\omega_3[A_{33}, \rho_A(t)] + i[H_{ext}(t), \rho_A(t)] \\ & + \gamma_{ij}(A_{ii}\rho_A(t) - 2A_{ji}\rho_A(t)A_{ij} + \rho_A(t)A_{ii}) \\ & + \Gamma_{ij}(A_{ii}\rho_A(t) - 2A_{ji}\rho_A(t)A_{ij} + \rho_A(t)A_{ii}) = 0. \end{aligned} \quad (2.65)$$

We now apply the transformation,

$$\rho(t) = \exp(-ilt)\rho_A(t)\exp(ilt), \quad (2.66)$$

$$\ell = \Omega_1 A_{11} + \Omega_2 A_{22} = \Omega_1 + (\Omega_2 - \Omega_1)A_{22} - \Omega_1 A_{33}, \quad (2.67)$$

to obtain the following equation of motion

$$d\rho(t)/dt = -i(\Delta_p - \Delta_c)[A_{22}, \rho(t)] - i\Delta_p[A_{44}, \rho(t)] - i[H_{ext2}(t), \rho_A(t)] - \text{decay terms} \quad (2.68)$$

where

$$H_{ext2}(t) = \exp(-i\ell t)H_{ext}(t)\exp(i\ell t). \quad (2.69)$$

The detunings of the probe and control fields from the respective atomic transitions are

$$\Delta_p = \omega_{31} - \Omega_1, \quad \Delta_c = \omega_{32} - \Omega_2. \quad (2.70)$$

From the definition of external field Hamiltonian in Eq. (2.11) we have

$$H_{ext2}(t) = -\frac{1}{2} \{ \vec{d}_{13} [e^{-i\Omega_1 t} A_{13} + e^{i\Omega_1 t} A_{31}] + \vec{d}_{23} [e^{-i\Omega_2 t} A_{23} + e^{i\Omega_2 t} A_{32}] \} \\ \{ \vec{E}_1(t)e^{i\Omega_1 t} + \vec{E}_2(t)e^{i\Omega_2 t} + \vec{E}_1^*(t)e^{-i\Omega_1 t} + \vec{E}_2^*(t)e^{-i\Omega_2 t} \}, \quad (2.71)$$

Here $E_j(t) = E_j \exp(-i\varphi_j t)$ where φ_j is the phase of the EM field. For now we choose $E_j(t)$ to be real with no fluctuations i.e. $\varphi_j = 0$. The effect of phase fluctuations is discussed separately in Chapter-7.

Applying RWA in Eq. (2.71) to neglect the rapidly oscillating terms of the form $\exp(\pm 2\Omega_1 t)$, $\exp(\pm 2\Omega_2 t)$, $\exp(\pm(\Omega_1 \pm \Omega_2)t)$ etc. to obtain

$$H_{ext2}(t) = -\alpha_p (A_{13} + A_{31}) - \alpha_c (A_{23} + A_{32}). \quad (2.72)$$

Here $2\alpha_p$ and $2\alpha_c$ are the Rabi frequencies of pump and control fields defined as

$$\alpha_p = \vec{d}_{13} \cdot \vec{E}_1 / 2, \quad \alpha_c = \vec{d}_{23} \cdot \vec{E}_2 / 2. \quad (2.73)$$

2.2.3 Master Equation for Λ , V and Ξ Systems

The detailed analysis presented in Sec 2.2.2 can now be used to arrive at the final form of the master equation for a three-level Λ system. Substituting Eq. (2.72) in Eq. (2.68) we obtain the relevant master equation as

$$d\rho/dt = -i[H_o, \rho] - \gamma_{31}(A_{33}\rho - 2A_{13}\rho A_{31} + \rho A_{33}) - \gamma_{32}(A_{33}\rho - 2A_{23}\rho A_{32} + \rho A_{33}) \\ - \Gamma_{21}(A_{22}\rho - 2A_{12}\rho A_{21} + \rho A_{22}) - \Gamma_{12}(A_{11}\rho - 2A_{21}\rho A_{12} + \rho A_{11}). \quad (2.74)$$

where H_o is the semi-classical Hamiltonian of the system under RWA given as

$$H_o = -\alpha_p(A_{13} + A_{31}) - \alpha_c(A_{23} + A_{32}) + (\Delta_p - \Delta_c)A_{22} + \Delta_p A_{33}. \quad (2.75)$$

The procedure can be generalized to obtain master equation relevant for V system (cf. Fig. 1.2(b)) as

$$d\rho/dt = -i[H_o, \rho] - \gamma_{21}(A_{22}\rho - 2A_{12}\rho A_{21} + \rho A_{22}) - \gamma_{31}(A_{33}\rho - 2A_{13}\rho A_{31} + \rho A_{33}) - \Gamma_{23}(A_{22}\rho - 2A_{32}\rho A_{23} + \rho A_{22}) - \Gamma_{32}(A_{33}\rho - 2A_{23}\rho A_{32} + \rho A_{33}). \quad (2.76)$$

The semi-classical Hamiltonian of V system is

$$H_o = -\alpha_p(A_{13} + A_{31}) - \alpha_c(A_{12} + A_{21}) + \Delta_c A_{22} + \Delta_p A_{33}, \quad (2.77)$$

with Rabi frequencies and detunings defined as follows:

$$\alpha_p = \vec{d}_{13} \cdot \vec{E}_1 / 2, \quad \alpha_c = \vec{d}_{12} \cdot \vec{E}_2 / 2, \quad \Delta_p = \omega_{31} - \Omega_1, \quad \Delta_c = \omega_{21} - \Omega_2. \quad (2.78)$$

Similarly the master equation for cascade (Ξ) system (cf. Fig. 1.2(c)) can be obtained as

$$d\rho/dt = -i[H_o, \rho] - \gamma_{21}(A_{22}\rho - 2A_{12}\rho A_{21} + \rho A_{22}) - \gamma_{32}(A_{33}\rho - 2A_{23}\rho A_{32} + \rho A_{33}). \quad (2.79)$$

The semi-classical Hamiltonian of the system is

$$H_o = -\alpha_p(A_{12} + A_{21}) - \alpha_c(A_{23} + A_{32}) + (\Delta_p + \Delta_c)A_{33} + \Delta_p A_{22}, \quad (2.80)$$

with Rabi frequencies and detunings defined as

$$\alpha_p = \vec{d}_{12} \cdot \vec{E}_1 / 2, \quad \alpha_c = \vec{d}_{23} \cdot \vec{E}_2 / 2, \quad \Delta_p = \omega_{21} - \Omega_1, \quad \Delta_c = \omega_{32} - \Omega_2. \quad (2.81)$$

2.3 Master Equation for Four-Level Systems

Fig. 2.1 shows the schematic representation of four-level systems, i.e., degenerate double lambda (DDL), tripod and N type configurations, investigated in subsequent chapters. Master equations relevant for the discussion of atom-field dynamics in these cases are given below:

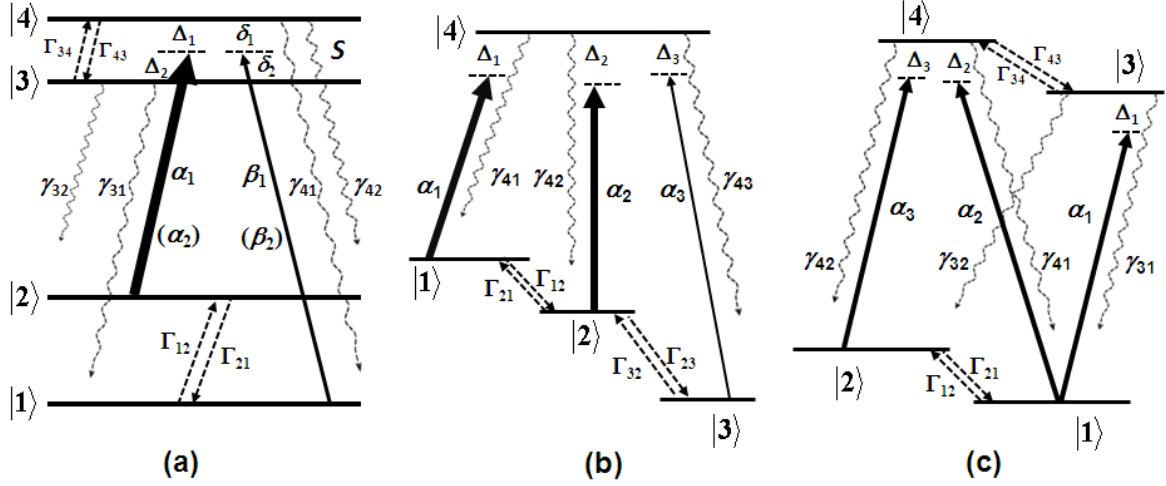


Fig. 2.1: Schematic representation of four-level system in (a) DDL, (b) tripod and (c) N configuration. Here γ_{ij} and Γ_{ij} respectively represent radiative and non-radiative decay rates associated with transition $|i\rangle \rightarrow |j\rangle$. The Rabi frequencies are in general denoted by $2\alpha_i$ and $2\beta_i$, and detunings are denoted by Δ_i and δ_i depending on the system. See text for details.

2.3.1 Degenerate Double Lambda System

Level configuration for this system is given in Fig. 2.1(a). The system consists of a pair of ground levels $|1\rangle, |2\rangle$ and a pair of excited levels $|3\rangle, |4\rangle$ that are driven by a common pair of pump and probe lasers. The separation between excited levels is specified by S . For a given pump (probe) laser intensity there exist two pump (probe) Rabi frequencies $2\alpha_1$ ($2\beta_1$) and $2\alpha_2$ ($2\beta_2$). The master equation for the system is

$$\begin{aligned}
 d\rho/dt = & -i[H_o, \rho] - \gamma_{31}(A_{33}\rho - 2A_{13}\rho A_{31} + \rho A_{33}) - \gamma_{41}(A_{44}\rho - 2A_{14}\rho A_{41} + \rho A_{44}) \\
 & - \gamma_{32}(A_{33}\rho - 2A_{23}\rho A_{32} + \rho A_{33}) - \gamma_{42}(A_{44}\rho - 2A_{24}\rho A_{42} + \rho A_{44}) \\
 & - \Gamma_{21}(A_{22}\rho - 2A_{12}\rho A_{21} + \rho A_{22}) - \Gamma_{12}(A_{11}\rho - 2A_{21}\rho A_{12} + \rho A_{11}) \\
 & - \Gamma_{43}(A_{44}\rho - 2A_{34}\rho A_{43} + \rho A_{44}) - \Gamma_{34}(A_{33}\rho - 2A_{43}\rho A_{34} + \rho A_{33}).
 \end{aligned} \tag{2.82}$$

The semi-classical Hamiltonian of the system under RWA is given as

$$\begin{aligned}
 H_o = & -\alpha_1(A_{24} + A_{42}) - \beta_1(A_{14} + A_{41}) - \alpha_2(A_{23} + A_{32}) - \beta_2(A_{13} + A_{31}) \\
 & + (\delta_1 - \Delta_1)A_{22} + \delta_2 A_{33} + \delta_1 A_{44},
 \end{aligned} \tag{2.83}$$

with Rabi frequencies and detunings defined as

$$\alpha_1 = \vec{d}_{24} \cdot \vec{E}_c / 2, \quad \beta_1 = \vec{d}_{14} \cdot \vec{E}_p / 2, \quad \alpha_2 = \vec{d}_{23} \cdot \vec{E}_c / 2, \quad \beta_2 = \vec{d}_{13} \cdot \vec{E}_p / 2, \quad (2.84)$$

$$\delta_1 = \omega_{41} - \omega_p, \quad \Delta_1 = \omega_{42} - \omega_c, \quad \delta_2 = \omega_{31} - \omega_p, \quad \Delta_2 = \omega_{32} - \omega_c. \quad (2.85)$$

2.3.2 Tripod System

Level configuration for this system is given in Fig. 2.1(b). The system consists of triplet ground state and an excited state interacting with a coherent trichromatic field. The Rabi frequencies (detunings) of pump, control and probe beams are $2\alpha_1(\Delta_1)$, $2\alpha_2(\Delta_1)$ and $2\alpha_3(\Delta_3)$ respectively. The master equation for the system has the form

$$\begin{aligned} d\rho/dt = & -i[H_o, \rho] - \gamma_{41}(A_{44}\rho - 2A_{14}\rho A_{41} + \rho A_{44}) - \gamma_{42}(A_{44}\rho - 2A_{24}\rho A_{42} + \rho A_{44}) \\ & - \gamma_{43}(A_{44}\rho - 2A_{34}\rho A_{43} + \rho A_{44}) - \Gamma_{12}(A_{11}\rho - 2A_{21}\rho A_{12} + \rho A_{11}) \\ & - \Gamma_{13}(A_{11}\rho - 2A_{31}\rho A_{13} + \rho A_{11}) - \Gamma_{21}(A_{22}\rho - 2A_{12}\rho A_{21} + \rho A_{22}) \\ & - \Gamma_{23}(A_{22}\rho - 2A_{32}\rho A_{23} + \rho A_{22}) - \Gamma_{31}(A_{33}\rho - 2A_{13}\rho A_{31} + \rho A_{33}) \\ & - \Gamma_{32}(A_{33}\rho - 2A_{23}\rho A_{32} + \rho A_{33}). \end{aligned} \quad (2.86)$$

The semi classical Hamiltonian of the system under RWA is given as

$$\begin{aligned} H_o = & -\alpha_1(A_{14} + A_{41}) - \alpha_2(A_{24} + A_{42}) - \alpha_3(A_{34} + A_{43}) \\ & + (\Delta_1 - \Delta_2)A_{22} + (\Delta_1 - \Delta_3)A_{33} + \Delta_1 A_{44}, \end{aligned} \quad (2.87)$$

with Rabi frequencies and detunings defined as

$$\alpha_1 = \vec{d}_{14} \cdot \vec{E}_1 / 2, \quad \alpha_2 = \vec{d}_{24} \cdot \vec{E}_2 / 2, \quad \alpha_3 = \vec{d}_{34} \cdot \vec{E}_3 / 2, \quad (2.88)$$

$$\Delta_1 = \omega_{41} - \Omega_1, \quad \Delta_2 = \omega_{42} - \Omega_2, \quad \Delta_3 = \omega_{43} - \Omega_3. \quad (2.89)$$

2.3.3 N- Resonance System

Level configuration of the system is given in Fig. 2.1(c). Transitions $|1\rangle \rightarrow |3\rangle$, $|1\rangle \rightarrow |4\rangle$ and $|2\rangle \rightarrow |4\rangle$ are excited by three laser fields of Rabi frequencies (detunings) $2\alpha_1(\Delta_1)$, $2\alpha_2(\Delta_2)$ and $2\alpha_3(\Delta_3)$. The master equation for the system is

$$\begin{aligned}
 d\rho/dt = & -i[H_o, \rho] - \gamma_{31}(A_{33}\rho - 2A_{13}\rho A_{31} + \rho A_{33}) - \gamma_{41}(A_{44}\rho - 2A_{14}\rho A_{41} + \rho A_{44}) \\
 & - \gamma_{32}(A_{33}\rho - 2A_{23}\rho A_{32} + \rho A_{33}) - \gamma_{42}(A_{44}\rho - 2A_{24}\rho A_{42} + \rho A_{44}) \\
 & - \Gamma_{21}(A_{22}\rho - 2A_{12}\rho A_{21} + \rho A_{22}) - \Gamma_{12}(A_{11}\rho - 2A_{21}\rho A_{12} + \rho A_{11}) \\
 & - \Gamma_{43}(A_{44}\rho - 2A_{34}\rho A_{43} + \rho A_{44}) - \Gamma_{34}(A_{33}\rho - 2A_{43}\rho A_{34} + \rho A_{33}).
 \end{aligned} \tag{2.90}$$

The semi classical Hamiltonian of the system under RWA is given as

$$H_o = -\alpha_1(A_{13} + A_{31}) - \alpha_2(A_{14} + A_{41}) - \alpha_3(A_{24} + A_{42}) + (\Delta_2 - \Delta_3)A_{22} + \Delta_1 A_{33} + \Delta_2 A_{44}, \tag{2.91}$$

with Rabi frequencies and detunings defined as

$$\alpha_1 = \vec{d}_{13} \cdot \vec{E}_1 / 2, \quad \alpha_2 = \vec{d}_{14} \cdot \vec{E}_2 / 2, \quad \alpha_3 = \vec{d}_{24} \cdot \vec{E}_3 / 2, \tag{2.92}$$

$$\Delta_1 = \omega_{31} - \Omega_1, \quad \Delta_2 = \omega_{41} - \Omega_2, \quad \Delta_3 = \omega_{42} - \Omega_3. \tag{2.93}$$

The master equation applicable to pertinent level scheme is used as a starting point for analysis of steady state as well as time dependent behaviour of these quantum systems and the associated interference effects.

2.4 Master Equation for Dipolar Molecular Systems

For a dipolar molecule, quantum coherence and interference can be substantially modified by the permanent dipole moments associated with molecular levels. Permanent dipole moments provide additional pathways for multi-photon transitions and consequently their inclusion in the master equation is of paramount importance while dealing with coherent pump-probe spectroscopy of molecular systems [173-180]. In this context, we develop and discuss the necessary master equation framework for a three-level molecular Λ system with permanent dipole moments and undergoing m – and n – photon transitions on pump and probe resonances. Here the time independent RWA Hamiltonian for interaction of external field with molecular systems cannot be obtained

as straight forwardly as in the atomic case. The theoretical techniques to treat the permanent dipole moments in laser-molecule interaction problems are well established by Meath and his coworkers [181-189].

We begin by considering a three-level Λ system (*cf.* Fig. 1.2(a)) relevant in the context of dipolar molecules so that $d_{ii} = \langle i|d|i\rangle \neq 0$, i.e., non-vanishing diagonal dipole matrix elements. The time evolution of state amplitudes $a(t)|_k = a_k(t)$ in the Schrodinger representation and under the dipole approximation can be written as

$$da(t)/dt = -i[E - \mu \cdot E_{ext}]a(t), \quad (2.94)$$

where the wave function of the system is $\psi(t) = \sum_{k=1}^3 a_k(t)|k\rangle$, and

$$a(t) = \begin{pmatrix} a_1(t) \\ a_2(t) \\ a_3(t) \end{pmatrix}, \quad E = \begin{pmatrix} \omega_1 & 0 & 0 \\ 0 & \omega_2 & 0 \\ 0 & 0 & \omega_3 \end{pmatrix}, \quad \mu = \begin{pmatrix} d_{11} & 0 & d_{13} \\ 0 & d_{22} & d_{23} \\ d_{31} & d_{32} & d_{33} \end{pmatrix}. \quad (2.95)$$

Here d_{ii} (d_{ij}) are the permanent (transition) dipole moments. We assume that the external field strength is given as

$$E_{ext}(t) = \hat{e}_p \varepsilon_p \cos(\omega_p t + \varphi_p) + \hat{e}_c \varepsilon_c \cos(\omega_c t + \varphi_c), \quad (2.96)$$

where $\varepsilon_p, \omega_p, \hat{e}_p, \varphi_p$ ($\varepsilon_c, \omega_c, \hat{e}_c, \varphi_c$) are the strengths, frequencies, polarizations and phases of the probe (control) field respectively. As is reported in earlier works [181-189] Eq. (2.94) is transformed into an interaction representation by an operator X such that,

$$a(t) = Xb(t), \quad (2.97)$$

$$X_{jk} = \delta_{jk} \exp[-i(\omega_k - \mathcal{G}_k)t] \exp(i\nu_{kk})b(t), \quad \nu_{kk} = d_{kk} \int_0^t E_{ext}(t') dt', \quad (2.98)$$

where \mathcal{G}_k , ($k=1,2,3$) are arbitrary phase factors.

The Schrodinger equation in the transformed representation thus takes the form

$$db(t)/dt = -iH^b(t)b(t), \quad (2.99)$$

$$H_{ij}^b = -d_{ij}E_{ext} \exp[i(\omega_i - \omega_j + \mathcal{G}_j - \mathcal{G}_i)t] \exp[i(\nu_{jj} - \nu_{ii})] \text{ and } H_{ii}^b = \mathcal{G}_i. \quad (2.100)$$

We assume that control transition involves coupling of m control photons and zero probe photons while probe transition involves coupling of n control probe photons and zero control photons. Applying RWA we neglect far off resonant terms to obtain

$$H^b(t) = \begin{pmatrix} \mathcal{G}_1 & 0 & -C_p \exp(i\Delta_{31}t) \\ 0 & \mathcal{G}_2 & -C_c \exp(i\Delta_{32}t) \\ -C_p \exp(-i\Delta_{31}t) & -C_c \exp(-i\Delta_{32}t) & \mathcal{G}_3 \end{pmatrix}. \quad (2.101)$$

$$C_p = n d_{13} \hat{e}_p \mathcal{E}_p (J_n(z_{13}^{(p)})/z_{13}^{(p)}) \exp[-i(z_{13}^{(p)} \sin \varphi_p - n\varphi_p)], \quad (2.102)$$

$$C_c = m d_{23} \hat{e}_c \mathcal{E}_c (J_m(z_{23}^{(c)})/z_{23}^{(c)}) \exp[-i(z_{23}^{(c)} \sin \varphi_c - m\varphi_c)], \quad (2.103)$$

$$z_{13}^{(p)} = \mu_{13} \cdot \hat{e}_p \mathcal{E}_p / \omega_p, \quad z_{23}^{(c)} = \mu_{23} \cdot \hat{e}_c \mathcal{E}_c / \omega_c, \quad (2.104)$$

$$\Delta_{31} = (\mathcal{G}_3 - \mathcal{G}_1 - \omega_{31}) + n\omega_p, \quad \Delta_{32} = (\mathcal{G}_3 - \mathcal{G}_2 - \omega_{32}) + m\omega_c, \quad (2.105)$$

$$\mu_{ij} = d_{jj} - d_{ii}, \quad \omega_{ij} = \omega_i - \omega_j. \quad (2.106)$$

An important point to be noted here is that the dynamics is dependent on the difference in the permanent moments (μ_{ij}) associated with the problem. We now define the arbitrary phase factors as $\mathcal{G}_1 = 0$, $\mathcal{G}_3 = \omega_{31} - n\omega_p$ and $\mathcal{G}_2 = \mathcal{G}_3 - \omega_{32} + m\omega_c$ to remove the time dependence of the Hamiltonian. Thus the effective Hamiltonian that describes the field-molecule interaction for a molecular Λ system under RWA can be obtained as

$$H = \begin{pmatrix} 0 & 0 & -\Omega_{pn} \\ 0 & \Delta_p - \Delta_c & -\Omega_{cm} \\ -\Omega_{pn}^* & -\Omega_{cm}^* & \Delta_p \end{pmatrix}. \quad (2.107)$$

The field-molecule couplings (Ω) are given in terms of the Bessel functions $J_k(z)$ as

$$\Omega_{pn} = 2n\alpha_p \frac{J_n(z_{13}^{(p)})}{z_{13}^{(p)}} \exp[-i(z_{13}^{(p)} \sin \varphi_p - n\varphi_p)], \quad (2.108)$$

$$\Omega_{cm} = 2m\alpha_c \frac{J_m(z_{23}^{(c)})}{z_{23}^{(c)}} \exp[-i(z_{23}^{(c)} \sin \varphi_c - m\varphi_c)], \quad (2.109)$$

where $2\alpha_p$ and $2\alpha_c$ are the Rabi frequencies as defined in atomic problem, i.e.,

$$\alpha_p = d_{13} \cdot \hat{e}_p \varepsilon_p / 2\hbar, \quad \alpha_c = d_{23} \cdot \hat{e}_c \varepsilon_c / 2\hbar. \quad (2.110)$$

The generalized n – and m – photon detunings for probe and control fields are given by

$$\Delta_p = \omega_{31} - n\omega_p, \quad \Delta_c = \omega_{32} - m\omega_c. \quad (2.111)$$

The connection to the atomic system ($m = n = 1$) can be established by putting $\mu_{ij} = 0$ in Eq. (2.104), (2.108) and (2.109) to obtain $\Omega_{pn} = \alpha_p$ and $\Omega_{cm} = \alpha_c$. Thus Ω_{cm} and Ω_{pn} are the generalized m – and n – photon molecular analogues of pump and probe Rabi frequencies of the atomic problem. The role of the factors $J_n(z_{13}^{(p)})/z_{13}^{(p)}$ and $J_m(z_{23}^{(c)})/z_{23}^{(c)}$ is in damping of the laser-molecule coupling [180].

We now introduce the molecular operators $A_{ij} = |i\rangle\langle j|$, ($i, j = 1, 2, 3$) similar to atomic operators where A_{ij} satisfy the relation in Eq. (2.3). Thus we can express H as

$$H = -\Omega_{pn} A_{13} - \Omega_{pn}^* A_{31} - \Omega_{cm} A_{23} - \Omega_{cm}^* A_{23} + (\Delta_p - \Delta_c) A_{22} + \Delta_p A_{33}. \quad (2.112)$$

The time evolution of the system is therefore given by the master equation

$$\begin{aligned} d\rho/dt = & -i[H, \rho] - \gamma_{31}(A_{33}\rho - 2A_{13}\rho A_{31} + \rho A_{33}) - \gamma_{32}(A_{33}\rho - 2A_{23}\rho A_{32} + \rho A_{33}) \\ & - \Gamma_{21}(A_{22}\rho - 2A_{12}\rho A_{21} + \rho A_{22}) - \Gamma_{12}(A_{11}\rho - 2A_{21}\rho A_{12} + \rho A_{11}). \end{aligned} \quad (2.113)$$

Eq. (2.112) and (2.113) thus provide the description of field-molecule interaction dynamics in case of dipolar molecules.

CHAPTER 3

COHERENCE AND INTERFERENCE IN THREE-LEVEL DIPOLAR MOLECULE

3.1 Introduction

Theoretical and experimental investigations of quantum coherence and interference are dominated by atomic systems, and in particular by alkali atoms where a suitable three-level scheme can be conveniently constructed using the hyperfine manifold of D_1 or D_2 transitions. In comparison the research in EIT in molecular domain has picked up only in more recent years [173-180]. The major difficulties in this research include relatively small magnitudes of the transition dipole moments and the existence of several decay channels that may prevent establishment of pump induced coherence in a molecular medium [175,176]. The later problem, i.e., EIT in open system, has been well studied in the atomic domain [37] and the conclusions drawn there are applicable to molecular systems as well.

A particular issue that is unique for molecules is the existence of diagonal or permanent dipole moments. The role of permanent dipole moments on laser-molecule interactions has been explored extensively by Meath and his group [181-189]. These works show that the permanent moments significantly modify the laser-molecule coupling leading to several interesting multi-photon and non-linear optical effects. For EIT in molecular domain, it is therefore interesting to explore the role of permanent moments on the development of coherence and ensuing interference in coherently driven molecular systems. Recently Zhou *et al.* [173] have addressed this problem theoretically in the context of a molecular Λ system undergoing $m + n$ photon transition by pump and probe fields. Their analysis however considers a medium of stationary molecules and therefore is not applicable to typical EIT experiments that are carried out in gas cells where the effect of Doppler broadening is of important concern. The authors have also reported the observation of gain without inversion in 2+2-photon excitation for change in the sign of the difference of the permanent moments of the excited and ground levels. This observation requires further investigation in the light of discussions on Λ system in atomic domain. Intimately connected with this is the issue of subluminal and superluminal light propagation in the medium of dipolar molecules.

In this chapter we discuss coherent pump-probe spectroscopy of molecular Λ system with permanent dipole moments, and provide analytical results for pump induced coherence in such a medium and its manifestation on the observation of EIT. The analysis of EIT and related phenomena in molecular systems has been done on the backdrop of coherent spectroscopy in the atomic domain [34-37]. The model considered here is a three-level Λ system undergoing permanent dipole moment assisted $m -$ and

n -photon transitions by pump and probe lasers respectively. We first consider the molecular medium consisting of stationary molecules and further generalize the results to a Doppler broadened medium. The analytical results are supplemented by numerical calculations. While the work presented here clarifies erroneous observations made in Ref. [173], it further establishes a connection between EIT and other related phenomena in atomic and molecular media. The importance of virtual mechanism in the treatment of multi-photon absorption based EIT phenomenon is discussed by taking an example of 2+1-photon EIT in dipolar molecules. The discussion presented in this chapter, thus, provides an integrated view of coherent pump-probe spectroscopy of a medium of dipolar molecules and its comparison with atomic case.

3.2 Theoretical Formulation

We consider a dilute gaseous medium of dipolar molecules that are idealized as three-level Λ system as shown in Fig. 3.1.

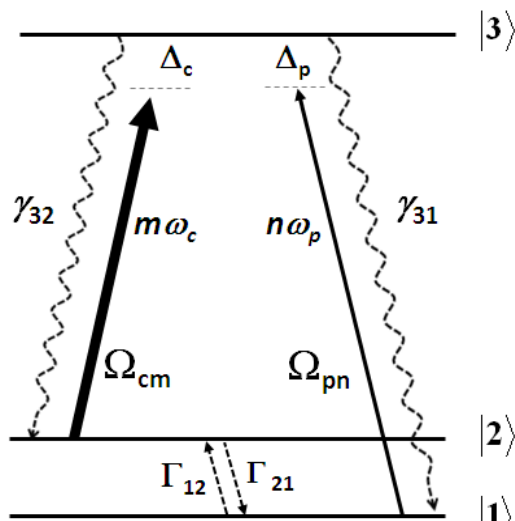


Fig. 3.1: Schematic representation of three-level Λ system. Transitions $|2\rangle \rightarrow |3\rangle$ and $|1\rangle \rightarrow |3\rangle$ are driven by pump and probe lasers of frequencies ω_c and ω_p respectively. The laser-molecule couplings and detunings of the pump (probe) fields are Ω_{cm} (Ω_{pn}) and Δ_c (Δ_p) respectively. Here m and n represent the number of photons associated with the pump and probe transitions respectively. Radiative and non-radiative decay rates associated with $|i\rangle \rightarrow |j\rangle$ transition are denoted by γ_{ij} and Γ_{ij} respectively.

A strong pump (control) laser of electric field $E_c(t) = \hat{e}_c \mathcal{E}_c \cos(\omega_c t + \varphi_c)$ is used to drive the transition $|2\rangle \rightarrow |3\rangle$ and a weak probe laser of electric field $E_p(t) = \hat{e}_p \mathcal{E}_p \cos(\omega_p t + \varphi_p)$ is scanned across $|1\rangle \rightarrow |3\rangle$ transition. Due to the presence of permanent dipole moments (d_{ii}), control and probe field can induce in general m -photon and n -photon transitions respectively on $|2\rangle \rightarrow |3\rangle$ and $|1\rangle \rightarrow |3\rangle$, where $m, n > 1$. The generalized m - and n -photon Rabi frequencies (detunings) of pump and probe fields are $\Omega_{cm} (\Delta_c)$ and $\Omega_{pn} (\Delta_p)$ respectively as defined in Eq. (2.108) – (2.111). For now we consider the multi-photon transitions are mediated only by the permanent dipole mechanism. The complexity arising from virtual mechanism is discussed in Sec. 3.5.

The time evolution of this system is governed by the master equation (2.113). This equation can be cast in a c-number representation to obtain the following equations for $\rho_{ij} = \langle i | \rho | j \rangle = \rho_{ji}^*$, ($i, j = 1, 2, 3$).

$$d\rho_{11} / dt = -2\Gamma_{12}\rho_{11} + 2\Gamma_{21}\rho_{22} + 2\gamma_{31}\rho_{33} - i\Omega_{pn}^* \rho_{13} + i\Omega_{pn} \rho_{31}, \quad (3.1a)$$

$$d\rho_{22} / dt = 2\Gamma_{12}\rho_{11} - 2\Gamma_{21}\rho_{22} + 2\gamma_{32}\rho_{33} - i\Omega_{cm}^* \rho_{23} + i\Omega_{cm} \rho_{32}, \quad (3.1b)$$

$$d\rho_{33} / dt = -2(\gamma_{31} + \gamma_{32})\rho_{33} + i\Omega_{pn}^* \rho_{13} - i\Omega_{pn} \rho_{31} + i\Omega_{cm}^* \rho_{23} - i\Omega_{cm} \rho_{32}, \quad (3.1c)$$

$$d\rho_{21} / dt = -[(\Gamma_{12} + \Gamma_{21}) + i(\Delta_p - \Delta_c)]\rho_{21} - i\Omega_{pn}^* \rho_{23} + i\Omega_{cm} \rho_{31}, \quad (3.1d)$$

$$d\rho_{31} / dt = -[(\gamma_{32} + \gamma_{31} + \Gamma_{12}) + i\Delta_p]\rho_{31} - i\Omega_{pn}^* (\rho_{33} - \rho_{11}) + i\Omega_{cm}^* \rho_{21}, \quad (3.1e)$$

$$d\rho_{32} / dt = -[(\gamma_{32} + \gamma_{31} + \Gamma_{21}) + i\Delta_c]\rho_{32} - i\Omega_{cm}^* (\rho_{33} - \rho_{22}) + i\Omega_{pn}^* \rho_{12}. \quad (3.1f)$$

Of interest in pump-probe spectroscopy is the appropriate steady state polarization, imaginary and real parts of which are related to the probe absorption and

dispersion respectively. While in general recourse may be taken to numerical solutions, steady state solutions of ρ_{ij} can be obtained perturbatively up to the first order of Ω_{pn} .

We first note that the closed system is constrained by the condition $\dot{\rho}_{11} + \dot{\rho}_{22} + \dot{\rho}_{33} = 0$, i.e. $\rho_{11} + \rho_{22} + \rho_{33} = 1$. Substituting Ω_{pn} by $\tilde{\kappa}\Omega_{pn}$ and $\rho_{ij} = \rho_{ij}^{(0)} + \tilde{\kappa}\rho_{ij}^{(1)}$ in Eq. (3.1a-f) where $\rho_{ij}^{(n)}$ is the n^{th} order coherence and $\tilde{\kappa}$ is the perturbation parameter, we obtain the relevant n^{th} order terms as

$$\rho_{11}^{(0)} = [2\gamma_3\Gamma_{21}a + |\Omega_{cm}|^2(\Gamma_{12} + \gamma_{31})]/y, \quad (3.2a)$$

$$\rho_{22}^{(0)} = [2\gamma_3\Gamma_{12}a + |\Omega_{cm}|^2\Gamma_{12}]/y, \quad (3.2b)$$

$$\rho_{33}^{(0)} = |\Omega_{cm}|^2\Gamma_{12}/y, \quad (3.2c)$$

$$\rho_{23}^{(0)} = -i\Omega_{cm}(\rho_{22}^{(0)} - \rho_{33}^{(0)})/[(\gamma_3 + \Gamma_{21}) - i\Delta_c], \quad (3.2d)$$

$$\rho_{31}^{(1)} = -i\Omega_{pn}^* [b(\rho_{33}^{(0)} - \rho_{11}^{(0)}) + i\Omega_{cm}^*\rho_{23}^{(0)}] / [bc + |\Omega_{cm}|^2], \quad (3.2e)$$

where

$$\gamma_3 = \gamma_{31} + \gamma_{32}, \quad (3.3a)$$

$$a = [(\gamma_3 + \Gamma_{21})^2 + \Delta_c^2] / 2(\gamma_3 + \Gamma_{21}), \quad (3.3b)$$

$$b = \Gamma_{12} + \Gamma_{21} + i(\Delta_p - \Delta_c), \quad (3.3c)$$

$$c = \gamma_3 + \Gamma_{12} + i\Delta_p, \quad (3.3d)$$

$$y = 2\gamma_3(\Gamma_{12} + \Gamma_{21})a + |\Omega_{cm}|^2(\gamma_{31} + 2\Gamma_{12} + \Gamma_{21}). \quad (3.3e)$$

For weak probe field the Bessel function $J_n(z_{13}^{(p)})$ in Eq. (2.108) can be approximated as

$$J_n(z_{13}^{(p)}) = \sum_{k=0}^{\infty} \frac{(-1)^k}{k!(n+k)!} (z_{13}^{(p)}/2)^{2k+n} \approx \frac{(z_{13}^{(p)}/2)^n}{n!}, \quad (3.4)$$

so that the probe field-molecule coupling Ω_{pn} takes the form

$$\Omega_{pn} = \frac{\alpha_p (z_{13}^{(p)})^{n-1}}{2^{n-1} (n-1)!} \exp[-i(z_{13}^{(p)} \sin \varphi_p - n\varphi_p)]. \quad (3.5)$$

Note here that phases φ_p and φ_c in Eq. (2.108) and (2.109) are explicitly retained in the formulation of the problem. In what follows, we assume $\varphi_p = \varphi_c = 0$ as in the work of Zhou *et al.* [173]. The equations governing the atomic EIT can be obtained by putting $\mu_{ij} = 0$ in Eq. (3.1) – (3.2).

The model developed here and used further for discussion of absorption spectrum and dispersion is for general $m + n$ photon transition in a three-level Λ system. However the practical values of m and n that are relevant for experiments are ≤ 2 , owing to the difficulties associated with the multi-photon processes of orders > 2 .

3.3 Absorption Spectrum and Dispersion

The susceptibility (χ) of the medium is related to pump induced polarization ρ_{31} .

Following the treatment for atomic pump-probe spectroscopy [34-37] we define

$$\chi = \xi \left(\frac{\rho_{31}^{(1)}(k\nu)}{\Omega_{pn}} \right), \quad \xi = \left(\frac{3}{8\pi} \right) N \gamma_{31} \lambda^3, \quad (3.6)$$

where N is the molecular density, $k = 2\pi/\lambda$ is the wave vector, λ is the transition wavelength and ν is the velocity of molecules. Unlike Zhou *et al.* [173] we have used the form of Eq. (3.6) for susceptibility, the consequences of which will be clear in what follows. Absorption (A) and refractive index (η) of the weak probe is given as

$$A = \text{Im}(\chi), \quad \eta = \text{Re}(\chi). \quad (3.7)$$

We first focus on stationary molecules as in Ref. [173]. From Eq. (3.2) we may note that

$\rho_{11}^{(0)} \approx 1$ and $\rho_{22}^{(0)} \approx \rho_{33}^{(0)} \approx 0$. Eq. (3.2e) then simplifies to

$$\rho_{31}^{(1)} = -\frac{\alpha_p (z_{13}^{(p)})^{n-1} [\Delta_p - \Delta_c - i(\Gamma_{12} + \Gamma_{21})]}{2^{n-1} (n-1)! [(\Gamma_{12} + \Gamma_{21}) + i(\Delta_p - \Delta_c)] (\gamma_3 + \Gamma_{12} + i\Delta_p) + \Omega_{cm}^2}, \quad (3.8)$$

where we have explicitly used the form of Eq. (3.5) for Ω_{pm} valid at low probe intensities. A and η experienced by the weak probe then is calculated by using Eq. (3.6) – (3.8). The pole structure of Eq. (3.8) reveals that it consists of two resonances whose energy (frequency) positions ($\Delta_p = \Delta_{\pm}$) and half-widths (Γ_{\pm}) are given as

$$\Delta_{\pm} = (\Delta_c \pm \sqrt{\Delta_c^2 + 4\Omega_{cm}^2})/2, \quad (3.9a)$$

$$\Gamma_{\pm} = \frac{\gamma_3}{2} \left[1 \mp \frac{\Delta_c}{\sqrt{\Delta_c^2 + 4\Omega_{cm}^2}} \right] + \frac{\Gamma_{21}}{2} \left[1 \pm \frac{\Delta_c}{\sqrt{\Delta_c^2 + 4\Omega_{cm}^2}} \right] + \Gamma_{12}. \quad (3.9b)$$

Eq. (3.9) gives the expression for Autler-Townes (AT) doublet [6] for the molecular problem generalized for m -photon transition induced by the pump field. The transparency between these two resonances is an EIT, albeit for a medium of stationary molecules. When the control field is at m -photon resonance with $|2\rangle \rightarrow |3\rangle$ transition, i.e., $\Delta_c = 0$, the doublet is symmetric with respect to $\Delta_p = 0$ and both resonances have equal half-widths that is essentially governed by the decay rates associated with the problem. Further under the conditions $\gamma_{31}, \gamma_{32}, |\Omega_{cm}| \gg \Gamma_{12}, \Gamma_{21}$ and $\Omega_{cm}^2 \gg \gamma_3 \Gamma_{12}, \gamma_3 \Gamma_{21}$ the absorption of the probe beam for $\Delta_c = 0$ is given by

$$A \approx \frac{\xi [(\Gamma_{12} + \Gamma_{21})(\Omega_{cm}^2 - \Delta_p^2) + \Delta_p^2 \gamma_3]}{(\Omega_{cm}^2 - \Delta_p^2)^2 + \Delta_p^2 \gamma_3^2}. \quad (3.10)$$

The maximum probe absorption is obtained at the energy of the AT resonance i.e. at $\Delta_p = \pm |\Omega_{cm}|$, which implies $A|_{\max} \approx \xi / \gamma_3$. The EIT half-width (Γ_{EIT}) corresponds to the half-width of transmission window between the AT doublets i.e.,

$$A(\Delta_p = \Gamma_{EIT}) = \xi / 2\gamma_3, \quad (3.11)$$

which gives the following equation for Δ_p ,

$$\Delta_p^4 - (2\Omega_{cm}^2 + \gamma_3^2)\Delta_p^2 + \Omega_{cm}^4 = 0. \quad (3.12)$$

The solution of Eq. (3.12) can easily be obtained as

$$\Delta_p^2 = \frac{\gamma_3^2}{2} \left[2s_1 + 1 \pm \sqrt{4s_1 + 1} \right], \quad s_1 = \Omega_{cm}^2 / \gamma_3^2. \quad (3.13)$$

Therefore, the half-width of EIT for a stationary atom is given by

$$\Gamma_{EIT} = |\Omega_{cm}| - \gamma_3 / 2 \quad \text{for } |\Omega_{cm}| \gg \gamma_3 \quad (s_1 \gg 1), \quad (3.14a)$$

$$= \Omega_{cm}^2 / \gamma_3 \quad \text{for } |\Omega_{cm}| \ll \gamma_3 \quad (s_1 \ll 1). \quad (3.14b)$$

Zhou *et al.* [173] have studied the doublet and the transparency window between the components of the doublet given by Eq. (3.9) and (3.14). Note here that from Eq. (3.5) – (3.8), the doublet spectrum is independent of the permanent dipole moments associated with the probe transition $|1\rangle \rightarrow |3\rangle$. Therefore the sign of the absorption spectrum cannot be reversed in any n -photon probe absorption spectrum by changing the sign of μ_{13} ($= d_{33} - d_{11}$). Hence for any given Λ system the probe will always be absorbed and not amplified irrespective of the sign of μ_{13} . We thus show here that the observation of Zhou *et al.* [173] regarding the amplification of the probe ($A < 0$) for $\mu_{13} < 0$ in the 2+2-photon EIT is erroneous. One may also provide a simple physical argument to refute the

observation of gain in 2+2-photon EIT. Consider for example a situation where $\Omega_{cm} \approx 0$, which may be obtained near the zero of the Bessel function $J_2(z_{23}^{(c)}) = 0$. In this case probe laser sees the unperturbed transition $|1\rangle \rightarrow |3\rangle$ and it gives rise to an absorption profile of linewidth $\gamma_3 + \Gamma_{12}$ at $\Delta_p = 0$ (*cf.* Eq. (3.8)). As per Zhou *et al.*, this absorption profile will reverse its sign for the change of sign of μ_{13} (Eq. (19) of Ref. [173]). This is unacceptable since transition $|2\rangle \rightarrow |3\rangle$ is not at all dressed by the pump laser, and therefore probe absorption spectrum must correspond to normal two-photon absorption.

The reason for this erroneous result may be traced to the choice of Ω_{peff} made by Zhou *et al.* [173]. For 1+1-photon EIT, they use $\Omega_{peff} = d_{13}\epsilon_p$ while for 2+2-photon EIT the form used is $\Omega_{peff} = [d_{12}d_{23}/(2\omega_{21} - \omega_{31})]\epsilon_p^2$. The later form of Ω_{peff} is from the work of J.C. Petch *et al.* [161] who have obtained it for a three-level atomic system. Since atoms do not have permanent dipole moments, two-photon transition can take place only by the virtual level mechanism. Consider now a three-level scheme of Fig. 3.1 for atoms, where the probe laser of frequency $\omega_p = \omega_{31}/2$ induces a two-photon transition $|1\rangle \rightarrow |3\rangle$ and $|2\rangle$ acts as a virtual level. The amplitude for this process is proportional to $[d_{12}d_{23}/(2\omega_{21} - \omega_{31})]\epsilon_p^2$, which is essentially the form of Ω_{peff} for two-photon transition. On the contrary for molecules with $\mu_{13} \neq 0$, the two-photon transition $|1\rangle \rightarrow |3\rangle$ takes place by permanent dipole mechanism, wherein the excited level may be viewed as the virtual level of dipole moment μ_{13} . Consequently the two-photon amplitude in this case is proportional to $\mu_{13}d_{13}\epsilon_p^2/\omega_p$, which is the correct form of Ω_{peff} for two-photon

process in the present case. With this form of Ω_{peff} it may be seen that μ_{13} cancels identically in the expression of probe absorption spectrum. In general for any n -photon transition mediated only by the permanent dipole mechanism, the correct form of Ω_{peff} is given by Ω_{pn} as may be seen from Eq. (3.5). The effect of μ_{13} on probe absorption spectrum therefore vanishes for any $m+n$ photon EIT. The corollary of this result is that the general behaviour of $m+n$ photon EIT is governed only by m . Also note here that in the true spirit of a Λ system, we must ideally have $d_{12}=0$. In this situation Ω_{peff} used by Zhou *et al.* [173] becomes zero and that leads to infinite absorption which is unphysical. The requirement of $d_{12}=0$ for the observation of EIT arises from the considerations outlined in the next section.

The effect of permanent moments on the widths of Autler-Townes doublet (Γ_{\pm}) and EIT (Γ_{EIT}) may be discussed using Eq. (3.9b) and (3.14). For 1+1-photon EIT the effect of permanent dipole moments is to damp the laser-molecule coupling and that results in decrease in the separation between the Autler-Townes doublet and in narrowing of EIT resonance. Thus for a given pump intensity, the EIT resonance in dipolar molecules is expected to be narrower than its atomic counterpart provided the radiative decay rates are the same. Similarly the progressive decrease in Γ_{EIT} with increase in the order of the m -photon process is evident from Eq. (3.14). These general features are seen in Fig. 3.2(a), where we have shown the comparison of absorption profiles for $m=1$ ($z_{23}^{(c)}=0$ and $z_{23}^{(c)}\neq 0$) and $m=2$ ($z_{23}^{(c)}\neq 0$). The corresponding dispersion profiles are plotted in Fig. 3.2(b). The data chosen for these calculations is similar to that used in Ref. [173], i.e., for HCN \rightarrow HNC isomerization [190] as summarized in Table-1 except that

we have used $\Gamma_{12} = \Gamma_{21} \neq 0$. The transition dipole moments for the pump and probe transitions are considered as 0.01 a.u. [173]. For simplicity we scale the parameters of Rabi frequencies and detunings in terms of $\gamma = \gamma_{31} = \gamma_{32}$.

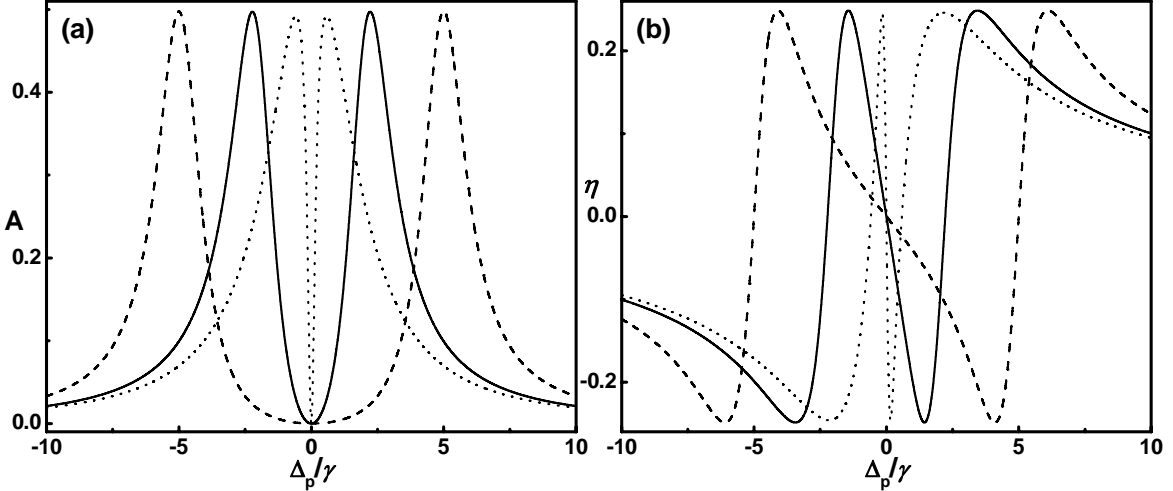


Fig. 3.2: (a) Probe absorption (A) and (b) dispersion (η) as a function of probe detuning (Δ_p) for $\alpha_c = 5\gamma$, $\Delta_c = 0$ and $\Gamma_{12} = \Gamma_{21} = 10^{-3}\gamma$. The dashed curve is for one-photon ($m=1$) atomic case ($z_{23}^{(c)} = 0$) while the solid curve is its molecular analogue with $z_{23}^{(c)} = 2.37$. The dotted curve is for two-photon ($m=2$) molecular case with $z_{23}^{(c)} = 4.74$. The medium is assumed to consist of stationary molecules and A is in the units of ξ . The spectra are independent of n .

Table 1: Energy and permanent dipole moment for HCN \rightarrow HNC isomerization [190]

	Molecular state (ν_1, ν_2, ν_3)	Energy (cm^{-1})	d_{ii} (a.u.)
$ 1\rangle$	(0,0,0) of HCN	0	1.17
$ 2\rangle$	(0,0,0) of HNC	5023.15	-1.17
$ 3\rangle$	(3,1,0) of HCN	10323.7	1.18

Of particular importance in Fig. 3.2(b) is the slope of the dispersion profile, i.e., $d\eta/d\omega_p = -d\eta/d\Delta_p$ in the EIT region, since it is related to the group velocity index

[35-37], i.e. $n_g = n_r + \omega_p (dn_r / d\omega_p)$ where $n_r = \sqrt{1+\eta}$ is the refractive index. For $m=1$, we find that $d\eta/d\omega_p$ is higher for $z_{23}^{(c)} \neq 0$ in comparison to that for $z_{23}^{(c)} = 0$. Further the slope becomes steeper for $m=2$, thereby exhibiting higher group velocity index. We may therefore conclude that the permanent moments lead to two identifiable effects, i.e., narrowing of the EIT linewidth and increase in the group velocity index.

3.4 Doppler Averaging

Thermal motion of molecules modify the detunings Δ_c and Δ_p as $\Delta_c = \Delta_c + k \cdot v$ and $\Delta_p = \Delta_p + k \cdot v$. Therefore in order to obtain EIT in the Doppler broadened molecular medium, Eq. (3.6) is integrated over the Maxwell-Boltzmann distribution of molecular velocities [6].

$$G(v) = \frac{1}{\sqrt{2\pi D^2}} \exp[-(\omega - \omega_0)^2 / 2D^2], \quad (3.15)$$

where D is a measure of the Doppler width of the medium.

Fig. 3.3 compares the effect of Doppler broadening on 1+1-probe absorption spectra in atomic and molecular case. Doppler averaging causes broadening of the AT resonances creating a narrow EIT resonance at the two-photon resonance condition $\Delta_p = \Delta_c$. It is clear from Fig. 3.3 that the presence of permanent dipole moments results in narrower EIT resonance and steeper dispersion which corresponds to larger group velocity index. These effects are further enhanced for multi-photon EIT ($m > 1$) as is discussed in the next subsection.

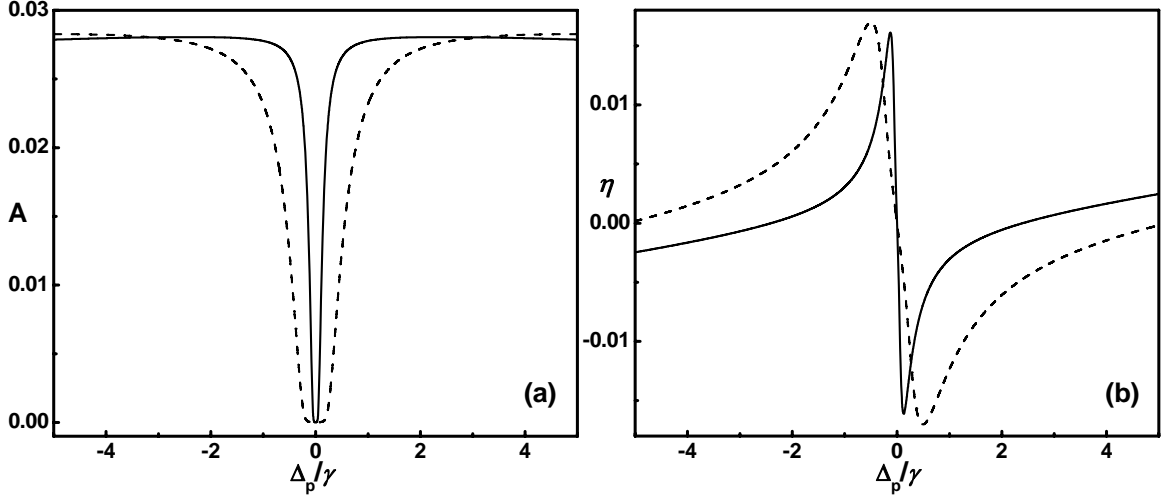


Fig. 3.3: Effect of Doppler averaging on the probe absorption and dispersion spectra for the data of Fig. 3.2. The Doppler width (FWHM) is $2W_D = 100\gamma$. Here the dashed curve is for one-photon ($m = 1$) atomic case while the solid curve is its molecular analogue with $z_{23}^{(c)} = 2.37$.

3.4.1 Linewidth of EIT in a Doppler Broadened Medium

The effect of Doppler averaging on atomic EIT has been discussed in details by Javan *et al.* [35-37]. They have developed a useful analytical procedure for obtaining approximate form of EIT linewidth for case of resonant pump beam. This procedure can be applied identically to the molecular problem for $\Delta_c = 0$. The underlying assumptions are $W_D \gg \gamma$, $\Omega_{cm} \gg \Gamma_{12} = \Gamma_{21}$ and $\Omega_{cm}^2 \gg \gamma\Gamma_{21}$ where W_D is the Doppler half-width ($2W_D = 2.35D$). Following Javan *et al.* [35-37], Gaussian velocity distribution in Eq. (3.15) may be replaced by Lorentzian velocity distribution $f(kv)$ such that

$$f(kv) = \frac{W_D / \pi}{W_D^2 + (kv)^2}. \quad (3.16)$$

Eq. (3.16) is justified by the fact that the central distributions of Lorentzian and Gaussian distributions are similar when the former distribution is multiplied by a factor of $\sqrt{\pi \ln 2}$.

The susceptibility of Doppler broadened medium is therefore given as

$$\chi = \int \xi f(kv) \left(\frac{\rho_{31}^{(1)}(kv)}{\Omega_{pn}} \right) d(kv). \quad (3.17)$$

For this analysis we do not consider $\rho_{11}^{(0)} \approx 1$ but use exact form of Eq. (3.2e) to obtain

$$\rho_{31}^{(1)} = \frac{i\Omega_{pn}}{bc + \Omega_{cm}^2} \frac{1}{y} \left[b(2\gamma\mathcal{I}_{21}x + \Omega_{cm}^2\gamma_{31}) - \frac{2\Omega_{cm}^2\gamma\mathcal{I}_{21}x}{(\gamma + \Gamma_{21} - i\Delta_c)} \right]. \quad (3.18a)$$

Replacing $\Delta_c \rightarrow \Delta_c + k \cdot v$ and $\Delta_p \rightarrow \Delta_p + k \cdot v$, and for $\Delta_c = 0$, we have

$$\rho_{31}^{(1)}(kv) = \frac{i\Omega_{pn}}{G} \frac{1}{y} \left[(2\Gamma_{21} + i\Delta_p)(2\gamma\mathcal{I}_{21}x + \Omega_{cm}^2\gamma_{31}) - \frac{2\Omega_{cm}^2\gamma\mathcal{I}_{21}x}{(\gamma + \Gamma_{21} - ikv)} \right], \quad (3.18b)$$

$$G = bc + \Omega_{cm}^2 = (2\Gamma_{21} + i\Delta_p)(\gamma + \Gamma_{21} + i\Delta_p + ikv) + \Omega_{cm}^2, \quad (3.18c)$$

$$x = \frac{(\gamma + \Gamma_{21})^2 + (kv)^2}{2(\gamma + \Gamma_{21})} \approx \frac{\gamma^2 + (kv)^2}{2\gamma}. \quad (3.18d)$$

Eq. (3.17) can be considered as a contour integration in the complex plane. There are five poles of this expression. In the upper half plane there are three poles located at $kv = [\Delta_p(\Omega_{cm}^2 - \Gamma_{21}^2 - \Delta_p^2) + i(\Delta_p^2\gamma + \Gamma_{21}^2\gamma + \Gamma_{21}\Omega_{cm}^2)]/(\Gamma_{21}^2 + \Delta_p^2)$ (from G), $kv = iW_D$ (from $f(kv)$) and $kv = i(\Omega_{cm}^2\gamma/2\Gamma_{21})^{1/2}$ (from y). In the lower half plane there are two poles, $kv = -iW_D$ (from $f(kv)$) and $kv = -i(\Omega_{cm}^2\gamma/2\Gamma_{21})^{1/2}$ (from y). We consider the contour in the lower half plane and define the susceptibility as

$$\chi = \chi_1 + \chi_2, \quad (3.19a)$$

$$\chi_1 = -2\pi i \text{Residue}(kv = -iW_D), \quad \chi_2 = -2\pi i \text{Residue}(kv = -i\sqrt{\Omega_{cm}^2\gamma/2\Gamma_{21}}). \quad (3.19b)$$

For the pole at $kv = -iW_D$ we obtain

$$\chi_1 = -\frac{i\xi}{2l_1l_2} [(l_3 - \Delta_p^2) - i\Delta_p W_D](l_4 - i\Delta_p l_5) \quad (3.20)$$

where

$$l_1 = -2\Gamma_{21}W_D^2 + \Omega_{cm}^2\gamma, \quad l_2 = (2W_D\Gamma_{21} + \Omega_{cm}^2 - \Delta_p^2)^2 + \Delta_p^2W_D^2, \quad (3.21a)$$

$$l_3 = 2\Gamma_{21}W_D + \Omega_{cm}^2, \quad l_4 = 2\Gamma_{21}W_D(2\Gamma_{21}W_D + \Omega_{cm}^2\gamma) - 4\Gamma_{21}\Omega_{cm}^2\gamma, \quad (3.21b)$$

$$l_5 = -2\Gamma_{21}W_D^2 + 2\Omega_{cm}^2\gamma. \quad (3.21c)$$

Similarly for the pole at $kv = -i\sqrt{\Omega_{cm}^2\gamma/2\Gamma_{21}} = -im_1$ we have,

$$\chi_2 = \frac{i\xi\Omega_{cm}^2\gamma W_D}{2l_1m_1m_2}[(m_3 - \Delta_p^2) - i\Delta_p m_1](m_4 - i\Delta_p) \quad (3.22)$$

where

$$m_1 = \sqrt{\Omega_{cm}^2\gamma/2\Gamma_{21}}, \quad m_2 = (2m_1\Gamma_{21} + \Omega_{cm}^2 - \Delta_p^2)^2 + \Delta_p^2m_1^2, \quad (3.23a)$$

$$m_3 = 2m_1\Gamma_{21} + \Omega_{cm}^2, \quad m_4 = -2\Gamma_{21} + \Omega_{cm}^2/m_1. \quad (3.23b)$$

The imaginary parts of χ_1 and χ_2 can therefore be obtained as

$$\chi_1'' = -\frac{\xi}{2l_1l_2}[(l_3 - \Delta_p^2)l_4 - \Delta_p^2W_Dl_5], \quad (3.24a)$$

$$\chi_2'' = \frac{\xi\Omega_{cm}^2\gamma W_D}{2l_1l_2m_1}[(m_3 - \Delta_p^2)m_4 - \Delta_p^2m_1]. \quad (3.24b)$$

Since probe absorption is maximum at $\Delta_p = \pm|\Omega_{cm}|$, $\chi_1''|_{\max} = -(\xi/l_1W_D)(\Gamma_{21}W_D^2 - \Omega_{cm}^2\gamma)$

and $\chi_2''|_{\max} = -\xi\Gamma_{21}W_D/l_1$. This implies $A|_{\max} = \chi''|_{\max} = \xi/W_D$. The EIT width therefore

corresponds to the condition

$$A(\Delta_p = \Gamma_{EIT}) = \xi/2W_D. \quad (3.25)$$

Under assumptions $m_1 \gg \gamma, \Gamma_{21}, \Omega_{cm}$ and replacing $\Omega_{cm}^2 - \Delta_p^2 \rightarrow \Omega_{cm}^2$ in l_2 and m_2 we get

$$\Delta_p^4 - \frac{\Omega_{cm}^2}{\gamma} \frac{(2\Gamma_{21}W_D^2 + \Omega_{cm}^2\gamma)}{W_D^2} \Delta_p^2 - \frac{2\Gamma_{21}\Omega_{cm}^6}{\gamma W_D^2} = 0. \quad (3.26)$$

The final expression for the half-width of EIT in a Doppler broadened molecular medium is therefore given as

$$\Gamma_{EIT} = \left[\frac{\Gamma_{21}}{\gamma} \Omega_{cm}^2 (1+s) \left[1 + \left(1 + \frac{4s}{(1+s)^2} \right)^{1/2} \right] \right]^{1/2} \approx \left[\frac{2\Gamma_{21}}{\gamma} \Omega_{cm}^2 (1+s) \right]^{1/2}, \quad (3.27)$$

$$s = \frac{\gamma |\Omega_{cm}|^2}{2\Gamma_{21} W_D^2}. \quad (3.28)$$

The expressions (3.27) – (3.28) are identical to the atomic EIT [35,36] with a difference; the atomic Rabi frequency (α_c) is replaced by its molecular analogue (Ω_{cm}). The parameter s defined in Eq. (3.28) is the saturation parameter and it exhibits dependence on μ_{23} again through Ω_{cm} . The permanent moments thus result in reduction in the saturation parameter. For $s \ll 1$, Eq. (3.27) leads to $\Gamma_{EIT} \approx |\Omega_{cm}| \sqrt{2\Gamma_{21}/\gamma}$, i.e., a linear dependence on laser-molecule coupling. The damping effect of Bessel functions [188,189] is then evident in narrowing of the EIT linewidth.

We have tested the validity of Eq. (3.27) by comparing its predictions with exact numerical calculations. In these calculations we take the general form of ρ_{31} as given by Eq. (3.8) and integrate it numerically over the given Doppler velocity distribution (*cf.* Eq. (3.15)). We chose $2\alpha_c = 10\gamma$ and $2W_D = 100\gamma$ for these calculations, which is consistent with the molecular EIT experiments [175,176]. The results are shown in Fig. 3.4 for $n = 1$ and $m = 1, 2$. We see in Fig. 3.4 that the analytical result of Eq. (3.27) is in excellent agreement with the numerical calculations. Note here that at the zeroes of the Bessel functions, Ω_{cm} vanishes and consequently the medium is not dressed resulting in the absence of EIT. We have therefore evaluated numerically Γ_{EIT} in their neighborhood.

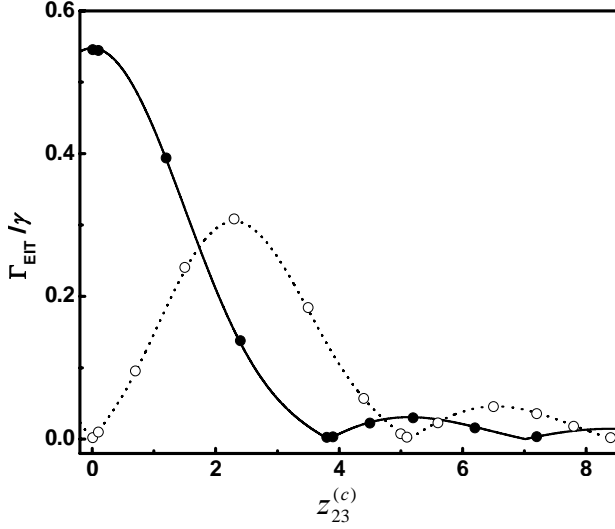


Fig. 3.4: Γ_{EIT} as a function of $z_{23}^{(c)}$ in a Doppler broadened molecular medium for $\alpha_c = 5\gamma$, $\Delta_c = 0$, $\Gamma_{12} = \Gamma_{21} = 10^{-3}\gamma$ and $2W_D = 100\gamma$. The solid and dotted curves correspond to Γ_{EIT} as calculated using Eq. (3.27) for $m=1$ and 2 respectively. Numerically calculated values of Γ_{EIT} are shown by solid ($m=1$) and hollow ($m=2$) circles. The behavior is symmetric for $z_{23}^{(c)} \rightarrow -z_{23}^{(c)}$.

The general observation from Eq. (3.27) and Fig. 3.4 is that the permanent moments damp the Rabi frequency α_c and that results in a sharper EIT in molecular case. Further for a fixed pump laser intensity EIT gets sharper as the order of the multi-photon process is increased. It is pertinent to discuss here the role of decay rate in the formation of EIT and in its linewidth. From Eq. (3.27) it is clear that for weaker Γ_{21} a sharper EIT can be obtained in the Doppler broadened medium. In essence Γ_{21}^{-1} is the Raman coherence time in a Λ system, which is very essential for the observation of EIT. This necessarily means that $|2\rangle$ is not strongly coupled to $|1\rangle$ by radiative transition and Γ_{12} , Γ_{21} are essentially contributed by collisions in the medium.

3.4.2 Dispersion at EIT Resonance

We now obtain the slope of the dispersion profile at the peak of the EIT resonance ($\Delta_p = 0$) in a Doppler broadened medium. Using Eq. (3.20) – (3.23) the real parts of χ_1 and χ_2 can be obtained as

$$\chi'_1 = -\frac{\xi\Delta_p}{2l_1l_2}[(l_3 - \Delta_p^2)l_5 + W_D l_4], \quad (3.29a)$$

$$\chi'_2 = \frac{\xi\Omega_{cm}^2\gamma W_D}{2l_1m_1m_2}\Delta_p[(m_3 - \Delta_p^2) + m_1m_4]. \quad (3.29b)$$

The derivatives of the above Eq. (3.29) at resonance ($\Delta_p = 0$) are given as

$$\left. \frac{d\chi'_1}{d\Delta_p} \right|_{\Delta_p=0} = -\frac{\xi\gamma}{l_1}, \quad \left. \frac{d\chi'_2}{d\Delta_p} \right|_{\Delta_p=0} = \frac{\xi\sqrt{4\gamma\Gamma_{21}W_D^2/\Omega_{cm}^2}}{l_1}, \quad (3.30)$$

where the approximations used are $2W_D\Gamma_{21}, 2m_1\Gamma_{21} < \Omega_{cm}^2$. The dispersion of the medium

is given by $\eta = \chi'_1 + \chi'_2$. Therefore we finally obtain the slope of EIT at resonance as

$$\begin{aligned} \frac{d\eta}{d\omega_p} &= -\frac{d\eta}{d\Delta_p} = \frac{\xi}{\Omega_{cm}^2} \frac{\sqrt{s}}{\sqrt{s+1}} \\ &\approx \frac{\xi}{\Omega_{cm}^2} \quad \text{for } s \gg 1, \\ &\approx \frac{\xi}{|\Omega_{cm}W_D|} \sqrt{\frac{\gamma}{2\Gamma_{21}}} \quad \text{for } s \ll 1. \end{aligned} \quad (3.31)$$

We have examined the validity of Eq. (3.31) by comparing the analytical results with numerical calculations as shown in Fig. 3.5.

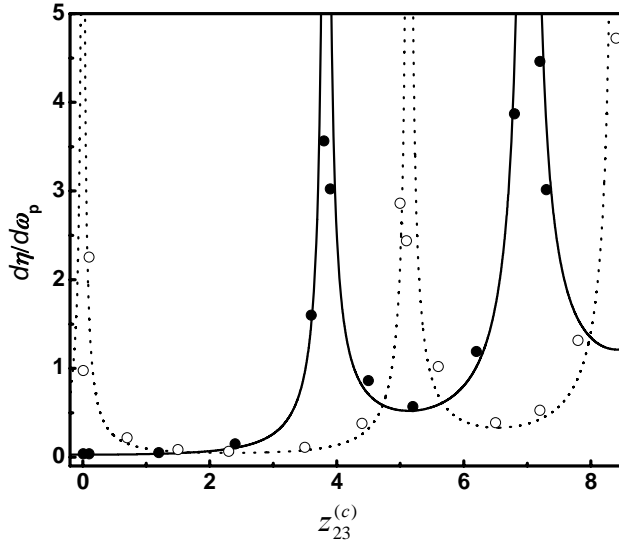


Fig. 3.5: Slope of the dispersion profile ($d\eta/d\omega_p$) at the peak of EIT resonance ($\Delta_p = 0$). Other details are same as in Fig. 3.4.

Note here in Fig. 3.5 that in the vicinity of zeros of the Bessel functions, slope of the dispersion profile rises steeply and in this region large group index can be achieved. This region therefore can be of potential interest for achieving slow light propagation. At the zeros of the Bessel function, however, the molecular medium is not dressed. This situation corresponds to return of the medium back to its original dispersion properties.

3.5. Role of Virtual Mechanism

It is well known that in a dipolar molecule a general m -photon transition is supported by both permanent dipole moment and virtual mechanism. Inclusion of virtual mechanism in two-photon transitions provides two competing pathways connecting the initial and final levels, and that leads to observable effects in two-photon spectroscopy [187-189]. It is therefore important to consider the virtual mechanism for multi-photon transition along with the permanent dipole mechanism in the context of EIT in dipolar molecules. Since for a general $m+n$ photon EIT the theoretical analysis is too complex, we have examined here the case of 2+1-photon EIT, where the pump field dresses $|2\rangle \rightarrow |3\rangle$ transition by two-photon excitation, while the weak probe is near one-photon resonance with $|1\rangle \rightarrow |3\rangle$ transition (*cf.* Fig. 3.1). In order to include the effect of virtual mechanism we assume a set of levels $|k\rangle$ of energy E_k , which act as virtual levels for two-photon transition. Since the probe field is considered weak, two-photon transition via virtual mechanism is assumed to take place only due to the strong pump.

Following the treatment of Meath and Jagatap [189], the Hamiltonian ($H^{(3+q)}$) describing the interaction of pump and probe fields with a three-level Λ system together

with additional levels $|k\rangle$, $k=4,5,\dots,q$ is given by

$$H^{(3+q)} = \begin{pmatrix} H & B \\ B^+ & C \end{pmatrix}. \quad (3.32)$$

Here H is the Hamiltonian of three-level Λ system as given by Eq. (2.112), B is a $3 \times q$ matrix consisting of laser-molecule couplings corresponding to the virtual levels $|k\rangle$, B^+ is the adjoint of B and C is a $q \times q$ diagonal matrix such that

$$B_{ik} = -\Omega_{ik}(1 - \delta_{i1}), \quad (i = 1, 2, 3) \quad (3.33a)$$

$$C_{kk} = \Delta_k + \Delta_p - \Delta_c, \quad (3.33b)$$

where the field-molecule couplings and detunings follows from Eq. (2.108) – (2.111) as

$$\Omega_{ik} = 2\alpha_{ik} \frac{J_i(z_{ik}^{(c)})}{z_{ik}^{(c)}} \exp[-i(z_{ik}^{(c)} \sin \varphi_c - \varphi_c)], \quad (3.34a)$$

$$\alpha_{ik}^{(c)} = d_{ik} \cdot \hat{e}_c \varepsilon_c / 2, \quad \Delta_k = \omega_{k2} - \omega_c. \quad (3.34b)$$

In obtaining equations (3.32) – (3.34), it is assumed that the pump field acts only on $|2\rangle \rightarrow |3\rangle$ transition and induces two-photon absorption ($\Delta_c = \omega_{32} - 2\omega_c$) via permanent dipole as well as virtual mechanisms, while the probe field acting on $|1\rangle \rightarrow |3\rangle$ transition induces one-photon transition ($\Delta_p = \omega_{31} - \omega_p$). The effective Hamiltonian (H^{eff}) is therefore given as

$$\begin{aligned} H^{eff} &= H - BC^{-1}B^+ = \begin{pmatrix} 0 & 0 & -\Omega_{p1} \\ 0 & \Delta'_p - \Delta'_c & -\Omega'_{c2} \\ -\Omega_{p1}^* & -\Omega_{c2}^* & \Delta'_p \end{pmatrix} \\ &= -\Omega_{p1} A_{13} - \Omega_{p1}^* A_{31} - \Omega'_{c2} A_{23} - \Omega_{c2}^* A_{32} + (\Delta'_p - \Delta'_c) A_{22} + \Delta'_p A_{33}, \end{aligned} \quad (3.35)$$

where

$$\Omega'_{c2} = \Omega_{c2} + \sum_k \frac{\Omega_{2k}\Omega_{k3}}{C_{kk}}, \quad (3.36a)$$

$$\Delta'_p = \Delta_p - \varpi_1, \quad \Delta'_c = \Delta_c + \varpi_2 - \varpi_1, \quad (3.36b)$$

$$\varpi_1 = \sum_k \frac{|\Omega_{3k}|^2}{C_{kk}}, \quad \varpi_2 = \sum_k \frac{|\Omega_{2k}|^2}{C_{kk}}, \quad (3.36c)$$

and $\Omega_{p1}(\Omega_{c2})$ are the probe (pump)-molecule coupling with $n=1$ ($m=2$). Time evolution of the system is then given by Eq. (2.113) with H replaced by H^{eff} .

Comparing Eq. (2.112) with Eq. (3.35), we observe that the inclusion of the virtual mechanism can modify the EIT dynamics in a significant way. Firstly the pump-molecule coupling Ω'_{c2} is a sum of the contributions of both permanent dipole and virtual mechanisms involving pertinent dipole matrix elements d_{ij} and μ_{ij} associated with $|2\rangle$, $|3\rangle$ and $|k\rangle$. For large dipolar molecules Ω'_{c2} can be significantly different from Ω_{c2} [187-189] and that has considerable effect on the observed EIT linewidth (*cf.* Eq. (3.14) and (3.27)) as well as on the group velocity index (*cf.* Eq. (3.31)). Secondly the inclusion of virtual levels results in the shifts (ϖ_1 and ϖ_2) in molecular resonance frequencies [189], which reflect in the frequency position of the EIT resonance. Note here that ϖ_1 is the energy shift of level $|3\rangle$ so that $\omega'_3 = \omega_3 - \varpi_1$ and the modified probe detuning is $\Delta'_p = \omega'_3 - \omega_1 - \omega_p = \Delta_p - \varpi_1$. In a similar manner the level $|2\rangle$ is also shifted to $\omega'_2 = \omega_2 - \varpi_2$ so that the modified pump detuning becomes $\Delta'_c = \omega'_{32} - 2\omega_c = \Delta_c - \varpi_1 + \varpi_2$. In the absence of virtual levels the EIT condition is $\Delta_p = \Delta_c$, which is now given by $\Delta'_p = \Delta'_c$ and that implies the frequency shift in the EIT resonance due to the

presence of virtual levels is ϖ_2 . The origin of this shift is in the coherent coupling of the virtual levels with Λ system and its magnitude is dependent on μ_{ik} , d_{ik} and Δ_k . It may be mentioned here that analogous shifts in the EIT position of Λ system due to the presence of a few additional adjacent levels are reported in the atomic domain [191]. Thus the inclusion of virtual mechanism leads to modification of the laser-molecule coupling which has a bearing on Γ_{EIT} and $d\eta/d\omega_p$ and results in the frequency shift of EIT resonance also.

3.6 Configuring a Three-level Molecular System

In the preceding sections, we have used molecular data pertinent to $\text{HCN} \rightarrow \text{HNC}$ isomerization to discuss a three-level dipolar molecular system. In order to help experimentalists to explore various issues concerning coherence and interference in three-level dipolar molecules, we have identified suitable schemes with $\mu_{13} < 0$ and $\mu_{13} > 0$. These level schemes are given in Tables-2 and -3 respectively.

Case 1: $\mu_{13} < 0$

Table-2(a): Energy, permanent dipole moment and lifetime of selected levels in ${}^7\text{LiH}$ molecule [192-195].

	Molecular state	Energy (cm^{-1})	d_{ii} (a.u.)	Lifetime (s)
1⟩	$X^1\Sigma_+ v'' = 0 J'' = 0$	0	2.314	∞
2⟩	$X^1\Sigma_+ v'' = 1 J'' = 0$	1359.71	2.357	21.77×10^{-3}
3⟩	$A^1\Sigma_+ v' = 4 J' = 1$	27252.91	-0.211	30.00×10^{-9}

Table-2(b): Frank Condon factor and transition dipole moment of transitions associated with levels of Table-2(a) [196]

Transition	Frank Condon factor	d_{ij} (a.u.)
$ 1\rangle \leftrightarrow 3\rangle$	0.0570	0.1378
$ 2\rangle \leftrightarrow 3\rangle$	0.1030	0.1997

Case 2: $\mu_{13} > 0$

Table-3(a): Energy, permanent dipole moment and lifetime of selected levels in ${}^7\text{LiH}$ molecule [192-195]

Molecular state	Energy (cm^{-1})	d_{ii} (a.u.)	Lifetime (s)
$ 1\rangle \quad X^1\Sigma_+ \nu'' = 21 \quad J'' = 0$	0	1.2645	4.49×10^{-3}
$ 2\rangle \quad X^1\Sigma_+ \nu'' = 22 \quad J'' = 0$	237.71	0.7063	7.98×10^{-3}
$ 3\rangle \quad A^1\Sigma_+ \nu' = 14 \quad J' = 1$	11852.61	1.4130	35.60×10^{-9}

Table-3(b): Frank Condon factor and transition dipole moment of transitions associated with levels of Table-3(a) [196]

Transition	Frank Condon factor	d_{ij} (a.u.)
$ 1\rangle \leftrightarrow 3\rangle$	0.0911	0.4130
$ 2\rangle \leftrightarrow 3\rangle$	0.0624	0.3277

The level configurations of Tables-2 and -3 can be used to explore experimentally the coherence and interference in dipolar molecules.

CHAPTER 4

COHERENCE IN DEGENERATE DOUBLE Λ SYSTEM

4.1 Introduction

Alkali vapors are well suited for atomic coherence and interference experiments. These atoms have appropriate cross-sections, high vapor pressures at room temperature to allow significant absorption and a simple level structure with transitions between ground and excited states lying in visible and near infrared regions. Further single mode lasers are commercially available to drive their resonance transitions. In particular three-level Λ or V schemes can be conveniently constructed using D_1 and D_2 transitions of alkali atoms. The supremacy of Λ scheme for preserving coherence in atom-field interaction makes it a preferred platform for realizing ultra-narrow CPT/EIT signal. In actual practice, however, the experimental situation becomes complicated owing to close spacing of excited hyperfine levels in D_1 or D_2 transition and consequently the dynamics of a chosen Λ system can be altered significantly by the presence of adjacent levels. This

issue has been recognized and discussed in some works. Earliest among these is the work by Schlossberg and Javan [197], which deals with the modifications of nonlinear gain characteristics of coherently prepared system due to closely spaced level structure. Xia *et al.* [198] have theoretically investigated EIT in a Λ system with close lying hyperfine levels. They observed that the extra off-resonance level only slightly modifies the EIT system and an EIT corresponding to pure Λ system can be obtained by tuning the laser fields to the centre of gravity of relevant hyperfine levels. Mazets *et al.* [199] have calculated the correction to propagation of normal mode of EIT in a Λ system arising due to the presence of additional excited level. Ye and Zibrov [200] have attributed the distorted shape of EIT resonance in experiments with Λ system in D_2 transition of ^{87}Rb atoms to the asymmetry of the AT doublet originating from detuned hyperfine level. Similar asymmetry in EIT line profile has been reported by Kale *et al.* [201]. Wong *et al.* [202] have shown that presence of an additional excited hyperfine level in a Λ system gives rise to several non-linear processes, which result in a very rich structure of resonances in the pump-probe spectroscopy of D_1 transition of sodium. Recently Chen *et al.* [191] have investigated numerically a six-level system in D_2 transition of ^{87}Rb to show that the multi-level coupling results in frequency shift of the EIT line centre. These observations point to the need of a detailed analysis of the problem concerning the role of adjacent levels in development of coherence and interference in a multilevel atomic system, and in particular in a Λ system.

In this chapter we investigate coherent pump-probe spectroscopy of a three-level Λ system with a close lying excited level particularly in the context of EIT and related phenomena. The level scheme thus consists of a pair of ground levels connected to a pair

of excited levels by pump and probe lasers. We describe this level configuration as ‘degenerate’ double lambda (DDL) resonance to contrast with double Λ resonance that involves four lasers. Recently such a system has been studied in context of phase dependent fluorescence spectrum [203] and effect of SGC on quantum interference effects [139]. The work presented here provides a realistic description of pump-probe spectroscopy of hyperfine transitions of alkali atoms.

4.2 Theoretical Formulation

We consider a typical situation encountered in the pump-probe spectroscopy of Λ system as depicted in Fig. 4.1 for D_2 transition of ^{85}Rb atom. A strong pump laser excites the hyperfine transitions $5s_{1/2}F = 3 \rightarrow 5p_{3/2}F' = 2,3$ and the probe laser accesses the transitions $5s_{1/2}F = 2 \rightarrow 5p_{3/2}F' = 2,3$.

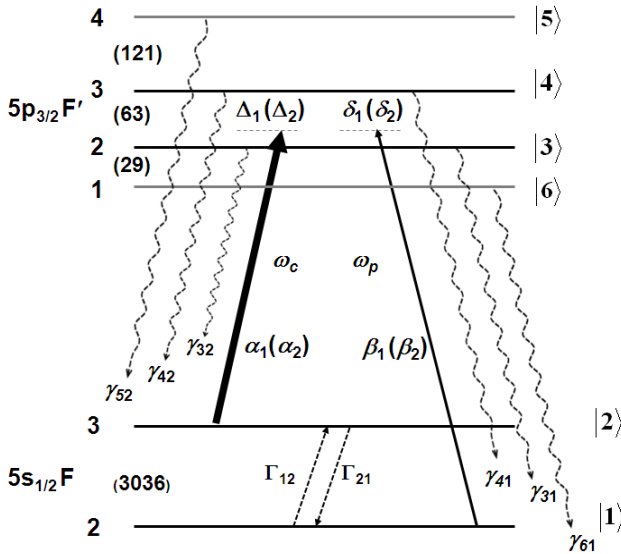


Fig. 4.1: Schematic representation of DDL system formed in the hyperfine manifold of D_2 transition of ^{85}Rb atom. The bracketed entries represent the separation between adjacent hyperfine levels in MHz. The four-level subset forming the DDL scheme are $|1\rangle$, $|2\rangle$, $|3\rangle$ and $|4\rangle$.

The problem of adjacent additional close lying excited level is clear in Fig. 4.1. The four-level subset that is relevant for discussion here consists of the levels $|1\rangle \equiv |F=2\rangle$, $|2\rangle \equiv |F=3\rangle$, $|3\rangle \equiv |F'=2\rangle$ and $|4\rangle \equiv |F'=3\rangle$ such that only non-vanishing

dipole matrix elements are $d_{13} = \sqrt{7/18}\mu_{D_2}$, $d_{14} = \sqrt{14/45}\mu_{D_2}$, $d_{23} = \sqrt{5/63}\mu_{D_2}$, $d_{24} = \sqrt{5/18}\mu_{D_2}$, where μ_{D_2} is the dipole moment for D_2 transition of ^{85}Rb [204]. The excitation scheme is thus a DDL system, i.e, consisting of two simultaneously excited Λ resonances, $\Lambda^{(1)}$ and $\Lambda^{(2)}$ constituted by levels $|1\rangle, |2\rangle, |4\rangle$ and $|1\rangle, |2\rangle, |3\rangle$ respectively. The frequency separation between the excited levels is $S = \omega_{43} = \omega_4 - \omega_3$ and $S = 63.4$ MHz for ^{85}Rb D_2 transition [204]. The Rabi frequencies (detunings) of pump and probe lasers for each three-level system $\Lambda^{(i)}$ are denoted by $\alpha_i(\Delta_i)$ and $\beta_i(\delta_i)$ as defined in Eq. (2.84) – (2.85). Since $\Lambda^{(1)}$ and $\Lambda^{(2)}$ are driven by same pair of pump and probe fields, the detunings satisfy the relation

$$\delta_1 - \delta_2 = \Delta_1 - \Delta_2 = S. \quad (4.1)$$

The master equation of the system given by Eq. (2.82) is cast in a c-number representation to obtain the following equations for $\rho_{ij} = \rho_{ji}^*$,

$$d\rho_{11}/dt = -2\Gamma_{12}\rho_{11} - i\beta_1(\rho_{14} - \rho_{41}) - i\beta_2(\rho_{13} - \rho_{31}) + 2\Gamma_{21}\rho_{22} + 2\gamma_{31}\rho_{33} + 2\gamma_{41}\rho_{44}, \quad (4.2a)$$

$$d\rho_{21}/dt = -\kappa_1\rho_{21} + i\alpha_1\rho_{41} + i\alpha_2\rho_{31} - i\beta_1\rho_{24} - i\beta_2\rho_{23}, \quad (4.2b)$$

$$d\rho_{31}/dt = i\alpha_2\rho_{21} - i\beta_1\rho_{34} + i\beta_2(\rho_{11} - \rho_{33}) - \kappa_2\rho_{31}, \quad (4.2c)$$

$$d\rho_{41}/dt = i\alpha_1\rho_{21} + i\beta_1(\rho_{11} - \rho_{44}) - i\beta_2\rho_{43} - \kappa_3\rho_{41}, \quad (4.2d)$$

$$d\rho_{22}/dt = 2\Gamma_{12}\rho_{11} - 2\Gamma_{21}\rho_{22} - i\alpha_1(\rho_{24} - \rho_{42}) - i\alpha_2(\rho_{23} - \rho_{32}) + 2\gamma_{32}\rho_{33} + 2\gamma_{42}\rho_{44}, \quad (4.2e)$$

$$d\rho_{32}/dt = i\alpha_2(\rho_{22} - \rho_{33}) + i\beta_2\rho_{12} - \kappa_4\rho_{32} - i\alpha_1\rho_{34}, \quad (4.2f)$$

$$d\rho_{42}/dt = i\alpha_1(\rho_{22} - \rho_{44}) + i\beta_1\rho_{12} - \kappa_5\rho_{42} - i\alpha_2\rho_{43}, \quad (4.2g)$$

$$d\rho_{33}/dt = i\alpha_2(\rho_{23} - \rho_{32}) + i\beta_2(\rho_{13} - \rho_{31}) - 2\gamma_3\rho_{33} + 2\Gamma_{43}\rho_{44}, \quad (4.2h)$$

$$d\rho_{43}/dt = i\alpha_1\rho_{23} - i\alpha_2\rho_{42} + i\beta_1\rho_{13} - i\beta_2\rho_{41} - \kappa_6\rho_{43}, \quad (4.2i)$$

$$d\rho_{44}/dt = i\alpha_1(\rho_{24} - \rho_{42}) + i\beta_1(\rho_{14} - \rho_{41}) - 2\gamma_4\rho_{44} + 2\Gamma_{34}\rho_{33}, \quad (4.2j)$$

where the coefficients κ_i , ($i=1,2\dots 6$) are defined as follows:

$$\kappa_1 = \Gamma_{12} + \Gamma_{21} + i(\delta_1 - \Delta_1), \quad \kappa_2 = \gamma_3 + \Gamma_{12} + i\delta_2, \quad \kappa_3 = \gamma_4 + \Gamma_{12} + i\delta_1, \quad (4.3a)$$

$$\kappa_4 = \gamma_3 + \Gamma_{21} + i\Delta_2, \quad \kappa_5 = \gamma_4 + \Gamma_{21} + i\Delta_1, \quad \kappa_6 = \gamma_3 + \gamma_4 + iS, \quad (4.3b)$$

$$\gamma_3 = \gamma_{31} + \gamma_{32} + \Gamma_{34}, \quad \gamma_4 = \gamma_{41} + \gamma_{42} + \Gamma_{43}. \quad (4.4)$$

Absorption (A) and dispersion (η) of the weak probe can be obtained as

$$A = \text{Im}(\tilde{P}), \quad \eta = \text{Re}(\tilde{P}), \quad (4.5)$$

where the polarization \tilde{P} is defined as

$$\tilde{P} = (\rho_{41}\gamma_{41}/\beta_1) + (\rho_{31}\gamma_{31}/\beta_2). \quad (4.6)$$

Here ρ_{31} and ρ_{41} are the induced polarizations on $|1\rangle \rightarrow |3\rangle$ and $|1\rangle \rightarrow |4\rangle$ transitions respectively. Note here that all Rabi frequencies and detunings (*cf.* Eq. (2.84) and (4.1)) are not independent. Consequently A and η are studied in terms of the laser-atom interaction parameters of subsystem $\Lambda^{(1)}$, i.e., β_1 , α_1 , δ_1 and Δ_1 .

4.3 Perturbative Analysis and Dressed States

Eq. (4.2a) – (4.2j) can be solved numerically using standard techniques. However for a weak probe laser, steady-state solutions for ρ_{ij} can be obtained perturbatively up to first order in β_1 and β_2 . The relevant coherences are given as follows:

$$\rho_{21}^{(1)} = [-\alpha_2\beta_2\kappa_3(\rho_{11}^{(0)} - \rho_{33}^{(0)}) - \alpha_1\beta_1\kappa_2(\rho_{11}^{(0)} - \rho_{44}^{(0)}) + \alpha_1\beta_2\kappa_2\rho_{43}^{(0)} + \alpha_2\beta_1\kappa_3\rho_{34}^{(0)} - i\kappa_2\kappa_3(\beta_1\rho_{24}^{(0)} + \beta_2\rho_{23}^{(0)})]/C, \quad (4.7a)$$

$$\rho_{31}^{(1)} = [\alpha_2\kappa_3(\beta_2\rho_{23}^{(0)} + \beta_1\rho_{24}^{(0)}) + i[\beta_2(\kappa_1\kappa_3 + \alpha_1^2)(\rho_{11}^{(0)} - \rho_{33}^{(0)}) - \beta_1\alpha_1\alpha_2(\rho_{11}^{(0)} - \rho_{44}^{(0)})]$$

$$+ \beta_2 \alpha_1 \alpha_2 \rho_{43}^{(0)} - \beta_1 (\kappa_1 \kappa_3 + \alpha_1^2) \rho_{34}^{(0)}] / C, \quad (4.7b)$$

$$\rho_{41}^{(1)} = [\alpha_1 \kappa_2 (\beta_2 \rho_{23}^{(0)} + \beta_1 \rho_{24}^{(0)}) + i[\beta_1 (\kappa_1 \kappa_2 + \alpha_2^2) (\rho_{11}^{(0)} - \rho_{44}^{(0)}) - \beta_2 \alpha_1 \alpha_2 (\rho_{11}^{(0)} - \rho_{33}^{(0)}) + \beta_1 \alpha_1 \alpha_2 \rho_{34}^{(0)} - \beta_2 (\kappa_1 \kappa_2 + \alpha_2^2) \rho_{43}^{(0)}] / C, \quad (4.7c)$$

$$C = \kappa_1 \kappa_2 \kappa_3 + \alpha_1^2 \kappa_2 + \alpha_2^2 \kappa_3. \quad (4.8)$$

The zero order terms are given in *Appendix-1*. For the purpose of discussion related to this section, we equate $\rho_{11}^{(0)} \approx 1$ and $\rho_{ij}^{(0)} \approx 0$ in Eq. (4.6) – (4.7) and obtain

$$\begin{aligned} \tilde{P} = & -\{(\delta_1 - \Delta_1)[\delta_1 \gamma_{31} + \delta_2 \gamma_{41} - i\gamma_{31}(\gamma_4 + \Gamma_{12}) - i\gamma_{41}(\gamma_3 + \Gamma_{12})] \\ & + (\alpha_1 \alpha_2 / \beta_1 \beta_2)(\beta_1^2 \gamma_{31} + \beta_2^2 \gamma_{41}) - \alpha_1^2 \gamma_{31} - \alpha_2^2 \gamma_{41} - (\Gamma_{12} + \Gamma_{21})[\gamma_{31}(\gamma_4 + \Gamma_{12}) \\ & + \gamma_{41}(\gamma_3 + \Gamma_{12})] - i(\Gamma_{12} + \Gamma_{21})(\delta_1 \gamma_{31} + \delta_2 \gamma_{41})\} / C, \end{aligned} \quad (4.9)$$

$$\begin{aligned} C = & (\delta_1 - \Delta_1)[(\gamma_3 + \Gamma_{12})(\gamma_4 + \Gamma_{12}) - \delta_1 \delta_2 + i\delta_1(\gamma_3 + \Gamma_{12}) + i\delta_2(\gamma_4 + \Gamma_{12})] \\ & + (\Gamma_{12} + \Gamma_{21})[\delta_1(\gamma_3 + \Gamma_{12}) + \delta_2(\gamma_4 + \Gamma_{12})] + \alpha_1^2 \delta_2 + \alpha_2^2 \delta_1 \\ & - i\{\alpha_1^2(\gamma_3 + \Gamma_{12}) + \alpha_2^2(\gamma_4 + \Gamma_{12}) + (\Gamma_{12} + \Gamma_{21})[(\gamma_3 + \Gamma_{12})(\gamma_4 + \Gamma_{12}) - \delta_1 \delta_2]\}. \end{aligned} \quad (4.10)$$

For DDL configuration, the pump field dresses the levels $|2\rangle$, $|3\rangle$ and $|4\rangle$, and as a consequence probe absorption spectrum consists of three resonances corresponding to the transitions $|1\rangle \rightarrow \psi_i$, where ψ_i , ($i=1,2,3$) are the dressed states of the problem. Dressed state energies (ε_i) and linewidths (Γ_i) of the corresponding resonances can be obtained from the zeroes of Eq. (4.10). Now expressing δ_2 and Δ_2 by δ_1 and Δ_1 respectively (*cf.* Eq. (4.1)) in Eq. (4.10), we seek the roots $\lambda_k = \varepsilon_k + i\Gamma_k$, ($k=1, 2, 3$) of the cubic equation

$$\delta_1^3 + p_c \delta_1^2 + q_c \delta_1 + r_c = 0; \quad (4.11)$$

$$\begin{aligned} r_c = & S[\alpha_1^2 + (\Gamma_{12} + \Gamma_{12})(\gamma_4 + \Gamma_{12})] + \Delta_1(\gamma_4 + \Gamma_{12})[(\gamma_3 + \Gamma_{12}) - iS] + i\alpha_1^2(\gamma_3 + \Gamma_{12}) \\ & + i\alpha_2^2(\gamma_4 + \Gamma_{12}) + i(\Gamma_{12} + \Gamma_{21})(\gamma_3 + \Gamma_{12})(\gamma_4 + \Gamma_{12}), \end{aligned} \quad (4.12)$$

$$\begin{aligned} q_c = & -[\alpha_1^2 + \alpha_2^2 + (\gamma_3 + \Gamma_{12})(\gamma_4 + \Gamma_{12}) + (\Gamma_{12} + \Gamma_{21})(\gamma_3 + \gamma_4 + 2\Gamma_{12}) - \Delta_1 S] \\ & + i[\Delta_1(\gamma_3 + \gamma_4 + 2\Gamma_{12}) + S(\gamma_4 + 2\Gamma_{12} + \Gamma_{21})], \end{aligned} \quad (4.13)$$

$$p_c = -[S + \Delta_1 + i(\gamma_3 + \gamma_4 + 3\Gamma_{12} + \Gamma_{21})]. \quad (4.14)$$

It is difficult to obtain simplified closed form analytical solution of Eq. (4.11). Therefore we obtain approximate ε_i and Γ_i under some limiting conditions. In the discussion that follows, dressed states are arranged such that $\varepsilon_1 > \varepsilon_2 > \varepsilon_3$. The first obvious limiting case is $\alpha_2 \sim 0$, i.e., when the pump field essentially dresses $|2\rangle \rightarrow |4\rangle$ transition. The dressed state energies $\varepsilon_i^{(0)}$ and the half-widths of resonances $\Gamma_i^{(0)}$ are given as

$$\varepsilon_1^{(0)} = (\Delta_1 - \xi_1)/2, \quad \Gamma_1^{(0)} = [(\Gamma_{12} + \Gamma_{21})(1 - \Delta_1/\xi_1) + (\gamma_4 + \Gamma_{12})(1 + \Delta_1/\xi_1)]/2 \quad (4.15a)$$

$$\varepsilon_2^{(0)} = (\Delta_1 + \xi_1)/2, \quad \Gamma_2^{(0)} = [(\Gamma_{12} + \Gamma_{21})(1 + \Delta_1/\xi_1) + (\gamma_4 + \Gamma_{12})(1 - \Delta_1/\xi_1)]/2 \quad (4.15b)$$

$$\varepsilon_3^{(0)} = S, \quad \Gamma_3^{(0)} = (\gamma_3 + \Gamma_{12}) \quad (4.15c)$$

$$\xi_1 = \sqrt{\Delta_1^2 + 4\alpha_1^2}. \quad (4.16)$$

Here $\varepsilon_{1,2}^{(0)}$ are the energies of the dressed states $\psi_{1,2}^{(0)}$ of the two-level system $|2\rangle \rightarrow |4\rangle$ and $\varepsilon_3^{(0)}$ coincides with $|3\rangle$. Eq. (4.15a) – (4.15b) thus correspond to the AT doublet of $|2\rangle \rightarrow |4\rangle$. Note here that Eq. (4.15) provides approximate analytical expressions for ε_i and Γ_i for $\Delta_1 \leq 0$. It is straightforward to see that for $|\Delta_1| \gg 0$ probe absorption spectrum consists of a sub-natural linewidth resonance at $\delta_1 \approx \Delta_1$ and two resonances of natural linewidth at $\delta_1 \approx 0$ and $\delta_1 = S$. The second limiting case is $\alpha_1 \sim 0$, i.e., preferential dressing of $|2\rangle \rightarrow |3\rangle$ transition. In this case $\varepsilon_i^{(S)}$ and $\Gamma_i^{(S)}$ are given as

$$\varepsilon_1^{(S)} = 0, \quad \Gamma_1^{(S)} = (\gamma_4 + \Gamma_{12}) \quad (4.17a)$$

$$\varepsilon_2^{(S)} = S + (\Delta_2 - \xi_2)/2, \quad \Gamma_2^{(S)} = [(\Gamma_{12} + \Gamma_{21})(1 - \Delta_2/\xi_2) + (\gamma_3 + \Gamma_{12})(1 + \Delta_2/\xi_2)]/2 \quad (4.17b)$$

$$\varepsilon_3^{(S)} = S + (\Delta_2 + \xi_2)/2, \quad \Gamma_3^{(S)} = [(\Gamma_{12} + \Gamma_{21})(1 + \Delta_2/\xi_2) + (\gamma_3 + \Gamma_{12})(1 - \Delta_2/\xi_2)]/2 \quad (4.17c)$$

$$\xi_2 = \sqrt{\Delta_2^2 + 4\alpha_2^2}. \quad (4.18)$$

Here $\varepsilon_{1,2}^{(S)}$ are the energies of the dressed states $\psi_{1,2}^{(S)}$ of the two-level system $|2\rangle \rightarrow |3\rangle$. Eq. (4.17a) – (4.17c) serve as approximate expressions for ε_i and Γ_i when $\Delta_1 \geq S$ and for $|\Delta_1| \geq S$, the resonance at $\delta_1 \approx \Delta_1$ has sub-natural linewidth. Eq. (4.17b) – (4.17c) correspond to the AT doublet of $|2\rangle \rightarrow |3\rangle$.

The region of interest from experimental point of view is $0 \leq \Delta_1 \leq S$, i.e., when pump field dresses the transitions $|2\rangle \rightarrow |3\rangle, |4\rangle$ simultaneously. In this domain of pump detuning, approximate analytical expressions for ε_i and Γ_i can be obtained when $\alpha_1^2 \Delta_2 + \alpha_2^2 \Delta_1 = 0$. This case corresponds to the situation where pump detunings for respective transitions are adjusted in accordance with their Rabi frequencies. In this case dressed state energies ε_i and widths Γ_i are

$$\varepsilon_1 = [S - \sqrt{S^2 + 4\alpha^2}] / 2, \quad \Gamma_1 = \gamma_d + \Gamma_{12}, \quad (4.19a)$$

$$\varepsilon_2 = \Delta_1, \quad \Gamma_2 \sim \left[\frac{\alpha^2(\gamma_d + \Gamma_{12}) + (\Gamma_{12} + \Gamma_{21})\{(\gamma_d + \Gamma_{12})^2 - \Delta_1\Delta_2\}}{\alpha^2 + (\gamma_d + \Gamma_{12})^2 + 2(\gamma_d + \Gamma_{12})(\Gamma_{12} + \Gamma_{21}) - \Delta_1\Delta_2} \right], \quad (4.19b)$$

$$\varepsilon_3 = [S + \sqrt{S^2 + 4\alpha^2}] / 2, \quad \Gamma_3 = (\gamma_d + \Gamma_{12}). \quad (4.19c)$$

where $\alpha^2 = \alpha_1^2 + \alpha_2^2$ and we have assumed $\gamma_3 = \gamma_4 = \gamma_d$ for simplicity. Note here that none of the dressed state energies corresponds to the energies of bare atomic states owing to simultaneous dressing of $|2\rangle \rightarrow |3\rangle, |4\rangle$ transitions and that the dressed state resonance at $\delta_1 \approx \Delta_1$ has sub-natural linewidth. Thus in the region $0 \leq \Delta_1 \leq S$ the problem amounts to the three-level generalization of two-level AT splitting. In general for a DDL system the resonance appearing at $\delta_1 \approx \Delta_1$ has sub-natural linewidth. In DDL system $\delta_1 \approx \Delta_1$ also implies $\delta_2 \approx \Delta_2$ (cf. Eq. (4.1)), i.e., the probe detuning at which Raman resonance

condition is approximately satisfied for $\Lambda^{(1)}$ and $\Lambda^{(2)}$ simultaneously. Fig. 4.2 shows the variation of ε_i and Γ_i as a function of Δ_1 obtained from the numerical solution of Eq. (4.11) for the model DDL system of ^{85}Rb . The correlation of ε_i with $\varepsilon_i^{(0)}$ and $\varepsilon_i^{(S)}$ is explicitly shown in Fig. 4.2(a). It is interesting to note that in the region $0 \leq \Delta_1 \leq S$ all dressed state resonances can have sub-natural linewidths (*cf.* fig. 4.2(b)). Fig. 4.2 is compared with their analogous plots of AT doublets for $\Lambda^{(1)}$ and $\Lambda^{(2)}$ systems in Fig. 4.3.

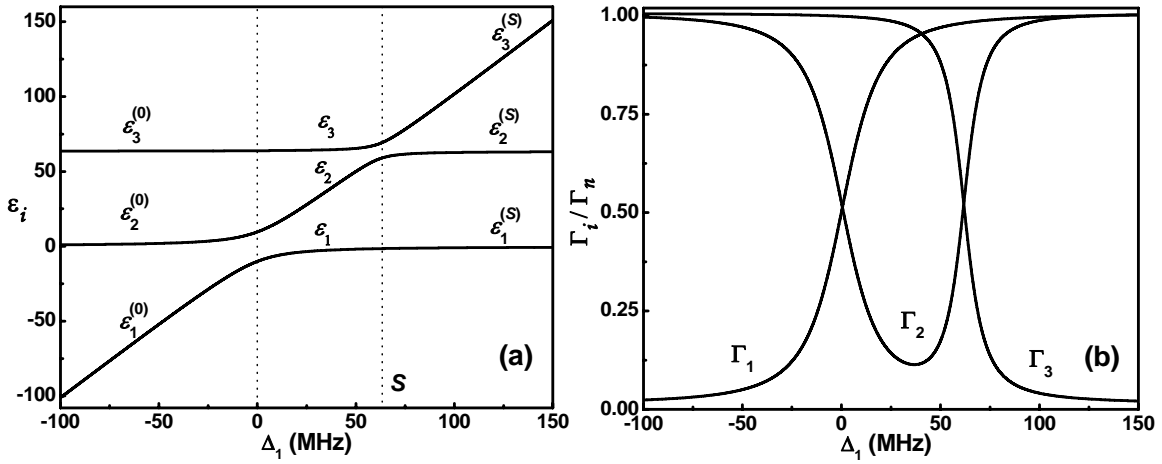


Fig. 4.2: Variation of (a) dressed state energies and (b) widths of dressed level transitions with pump detuning (Δ_1) for $\alpha_1 = 10$ MHz. All γ_{ij} are assumed to be equal and they add to natural linewidth $2\Gamma_n = 6.067$ MHz. The incoherent decay rates are $\Gamma_{12} = \Gamma_{21} = \Gamma_{34} = \Gamma_{43} = 0.02$ MHz.

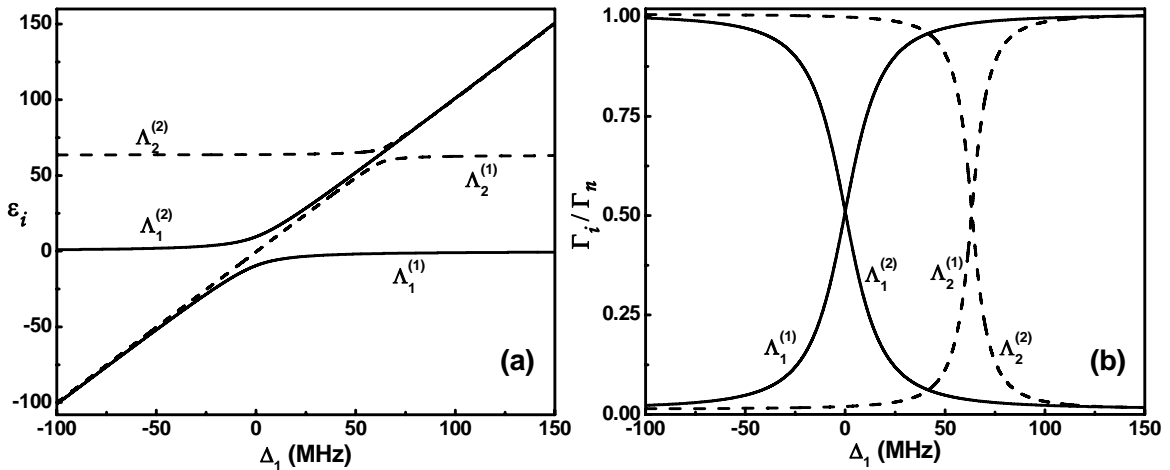


Fig. 4.3: Variation of (a) energies and (b) widths of AT doublet with pump detuning for $\Lambda^{(1)}$ (solid lines) and $\Lambda^{(2)}$ (dashed lines) systems. The data is same as in Fig. 4.2.

Typical probe absorption (dispersion) spectra, $A(\eta)$ vs. δ_1 for DDL system are shown in Fig. 4.4. We may observe that the dressed state resonance at $\delta_1 \approx \Delta_1$ is always of sub-natural linewidth, as has been explicitly shown by considering the special cases.

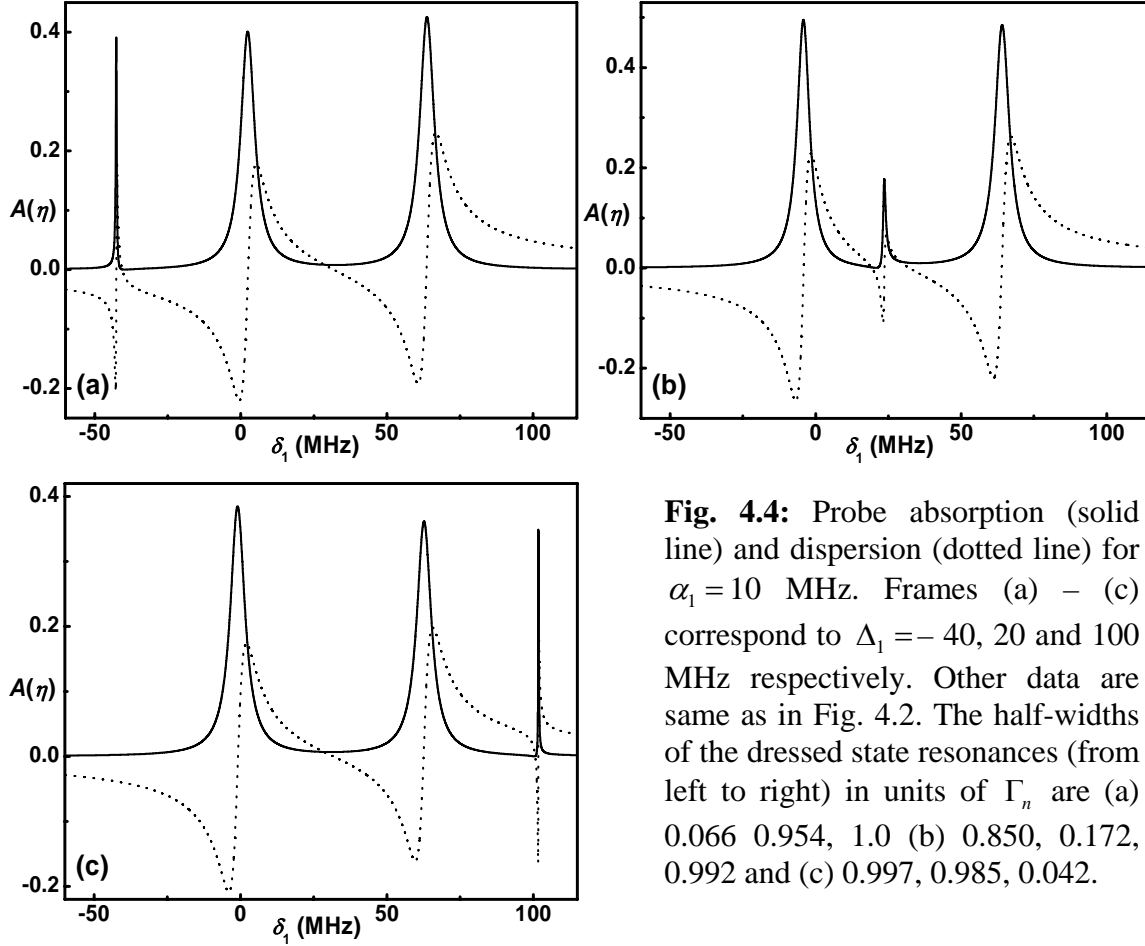


Fig. 4.4: Probe absorption (solid line) and dispersion (dotted line) for $\alpha_1 = 10$ MHz. Frames (a) – (c) correspond to $\Delta_1 = -40, 20$ and 100 MHz respectively. Other data are same as in Fig. 4.2. The half-widths of the dressed state resonances (from left to right) in units of Γ_n are (a) 0.066, 0.954, 1.0 (b) 0.850, 0.172, 0.992 and (c) 0.997, 0.985, 0.042.

4.4 Suppression of Subnatural Resonance

An interesting observation in a DDL system is suppression and reappearance of sub-natural resonance (at $\delta_1 \approx \Delta_1$) for a combination of Δ_1 and α_1 . Fig. 4.5 shows a representative behaviour of dressed state resonances and dispersion profiles. Vanishing of sub-natural resonance (*cf.* Fig. 4.5(b)) and its reappearance is clearly seen in this figure.

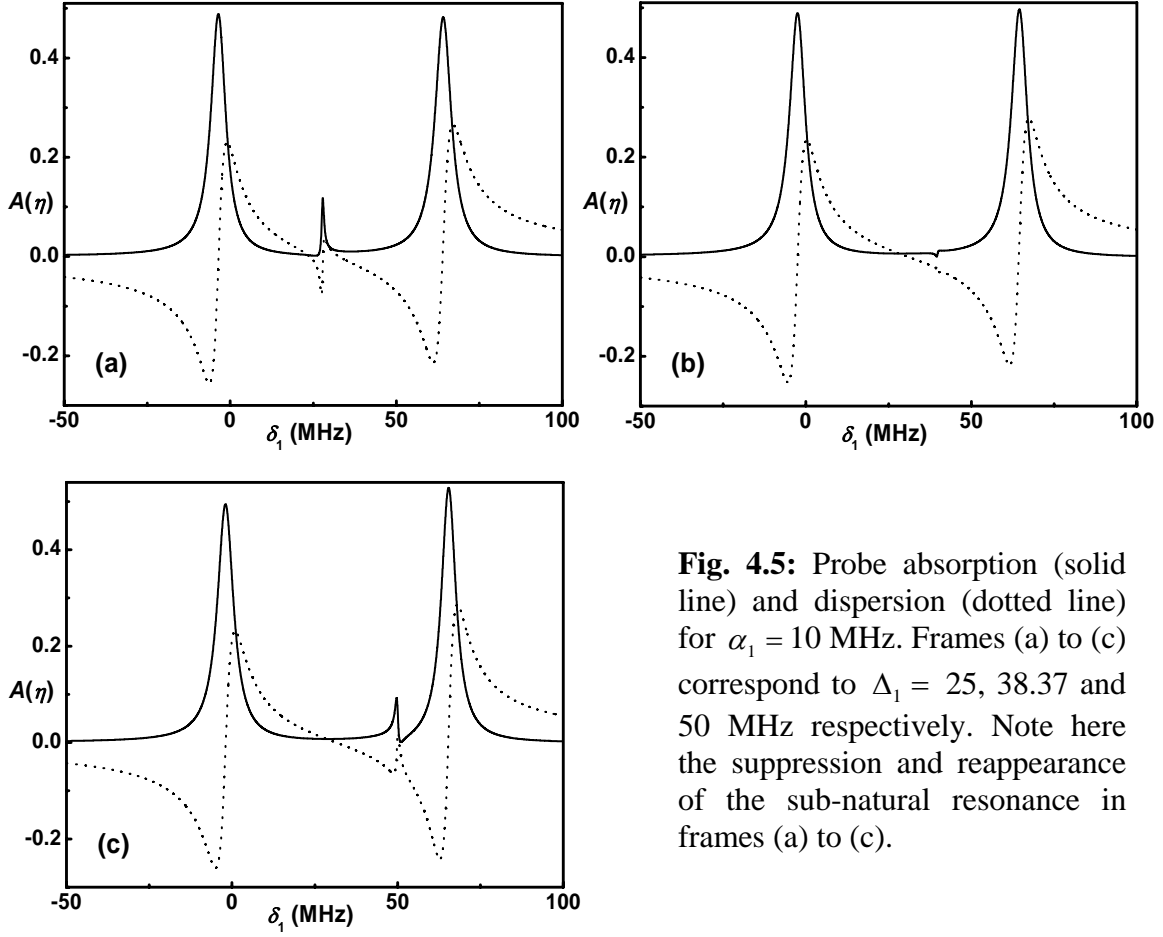


Fig. 4.5: Probe absorption (solid line) and dispersion (dotted line) for $\alpha_1 = 10$ MHz. Frames (a) to (c) correspond to $\Delta_1 = 25, 38.37$ and 50 MHz respectively. Note here the suppression and reappearance of the sub-natural resonance in frames (a) to (c).

Note here that the resonance at $\delta_1 \approx \Delta_1$ corresponds to the excitation $|1\rangle \rightarrow \psi_2$.

Now expressing $\psi_2 = \sum_{i=2}^4 c_i |i\rangle$, where c_i are appropriate mixing coefficients, we may

obtain the dipole moment for the transition $|1\rangle \rightarrow \psi_2$ as

$$d(1, \psi_2) = \langle 1 | d | \psi_2 \rangle = c_3 d_{13} + c_4 d_{14}, \quad (4.20)$$

where c_i are obtained by diagonalizing the Hamiltonian of Eq. (2.83) with $\beta_1 = \beta_2 = 0$.

While this is difficult in general, we make use of the correlation of two-level and three-level dressed states to develop the physical idea underlying the suppression of the sub-

natural resonance. Since ψ_2 correlates with $\psi_2^{(S)} = \sum_{i=2,3} c_i^{(S)} |i\rangle$ and $\psi_2^{(0)} = \sum_{i=2,4} c_i^{(0)} |i\rangle$, we

may approximate c_3 and c_4 by $c_3^{(S)}$ and $c_4^{(0)}$ respectively and obtain

$$d(1, \psi_2) \approx d_{13} \sqrt{(\xi_2 + \Delta_2)/2\xi_2} - d_{14} \sqrt{(\xi_1 - \Delta_1)/2\xi_1}. \quad (4.21)$$

Eq. (4.21) suggests that $d(1, \psi_2)$ can be made vanishingly small over a range of Δ_1 for a given α_1 , since $\Delta_2(\xi_2)$ is related to $\Delta_1(\xi_1)$. This vanishing of the dipole moment $d(1, \psi_2)$ is therefore responsible for suppression of the subnatural resonance. In order to test this premise, we have numerically obtained the dressed states $|\psi_i\rangle$ and evaluated the dipole matrix elements $d(1, \psi_i)$, ($i=1, 2, 3$) in DDL system of ^{85}Rb for $\alpha_1 = 10$ MHz. The results of these calculations as a function of Δ_1 are plotted in Fig. 4.6.

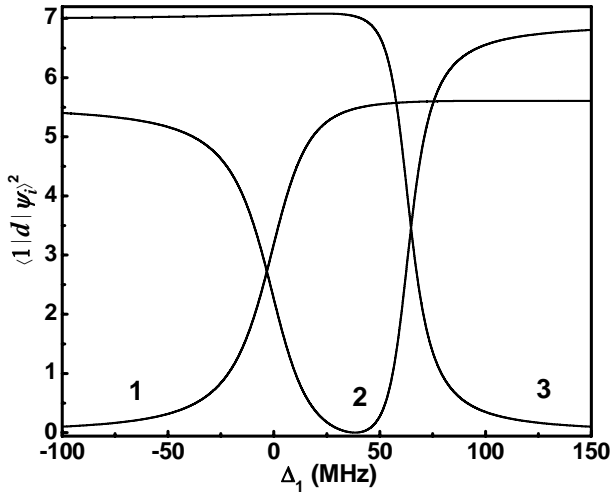


Fig. 4.6: Variation of square of the dipole matrix element $\langle 1|d|\psi_i\rangle$ calculated for $\alpha_1 = 10$ MHz. Curves 1, 2 and 3 correspond to the dressed states $|\psi_1\rangle$, $|\psi_2\rangle$ and $|\psi_3\rangle$ respectively.

Note in Fig. 4.6 that in the neighborhood of $\Delta_1 = 38.37$ MHz, $d(1, \psi_2) \rightarrow 0$ and it is in this region that we observe suppression of the subnatural resonance in Fig. 4.5. Interestingly for $\alpha_1 = 10$ MHz, Eq. (4.21) predicts that minimum of $d(1, \psi_2)$ to occur at $\Delta_1 \approx 39.41$ MHz, which is close to the value of Δ_1 observed in Fig. 4.5. Suppression of sub-natural resonance may therefore be viewed as a result of coherence and interference developed in simultaneous excitation of $|2\rangle \rightarrow |3\rangle, |4\rangle$ transitions.

4.5 Electromagnetically Induced Transparency

An analysis of EIT linewidth similar to that by Javan *et al.* [35-37] is too unwieldy for a DDL system. Consequently we numerically evaluate A and η using Eq. (4.5) – (4.6), and average them over Maxwell-Boltzmann velocity distribution. In these calculations we do not assume $\rho_{11}^{(0)} = 1$ and $\rho_{ij}^{(0)} = 0$ in Eq. (4.7), but develop and use necessary equations for all $\rho_{ij}^{(0)}$ (*cf. Appendix-1*). For $\Lambda^{(1)}$ subsystem in Fig. 4.1, susceptibility of the medium vanishes identically at $\delta_1 = \Delta_1$ which gives rise to a sharp EIT resonance in the absorption spectrum. Note here that in DDL system $\delta_1 = \Delta_1$ corresponds to $\delta_2 = \Delta_2$, which means that the Raman resonance condition is satisfied simultaneously for both $\Lambda^{(1)}$ and $\Lambda^{(2)}$. The resultant EIT, therefore, is a superposition of two EIT resonances depending on the coherence established in the medium.

We first examine the situation when the pump laser is at exact resonance with $F = 3 \rightarrow F' = 2$ so that $\Delta_1 = S = 63.401$ MHz. Doppler averaged absorption spectrum in this case for $\alpha_1 = 10$ MHz is shown in Fig. 4.7, which consists of a sub-natural EIT resonance at $\delta_1 = \Delta_1$, but it differs from the EIT in a three-level Λ system in some ways. An inspection of Eq. (4.9) shows that $\tilde{P} \approx 0$, but not exactly zero at $\delta_1 = \Delta_1$ as in a three-level Λ system. The susceptibility of DDL system remains finite though small at $\delta_1 = \Delta_1$ and as a consequence A does not go to zero at $\delta_1 \approx \Delta_1$ (*cf. Appendix-2*). The minimum of the transparency window is also shifted away from $\delta_1 = \Delta_1$. Such frequency shift has been observed in earlier works [191]. In Fig. 4.7 this shift is 0.296 MHz. This effect is more pronounced for small S since $A \sim \delta_1^{-2}$ at two-photon resonance.

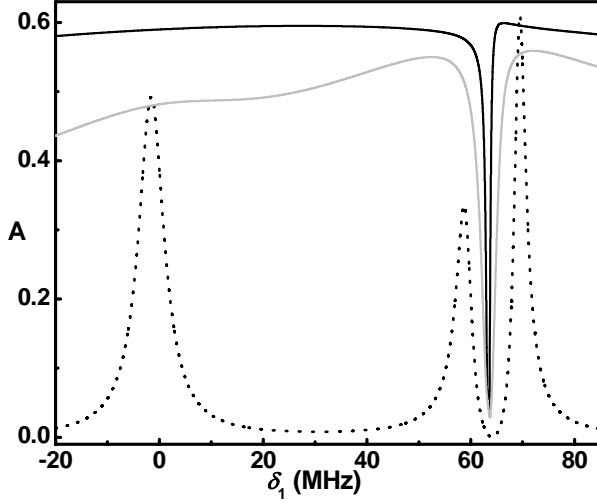


Fig. 4.7: Doppler averaged probe absorption spectrum (solid line) for $\alpha_1 = 10$ MHz, $\Delta_1 = S$ ($=63.401$ MHz), $\Gamma_{12} = \Gamma_{21} = 0$ and $2W_D = 515$ MHz. The dotted curve is the corresponding spectrum for a stationary atom. The gray curve is the Doppler averaged absorption spectrum for $\Gamma_{12} = \Gamma_{21} = 0.02$ MHz.

Another point that may be noted from Fig. 4.7 is that EIT line shape is asymmetric as has been reported experimentally [200,201]. For $\delta_1 = \Delta_1 = S$, $\Lambda^{(2)}$ sub-system is at exact Raman resonance ($\delta_2 = \Delta_2 = 0$) while $\Lambda^{(1)}$ sub-system is at detuned Raman resonance. EIT in Fig. 4.7 may therefore be considered as an EIT of $\Lambda^{(2)}$ system which is perturbed by the EIT of $\Lambda^{(1)}$ sub-system. The extent of such asymmetry is dependent on $\alpha_1/\alpha_2 = d_{24}/d_{23}$ and S . In the present case $d_{24}/d_{23} = \sqrt{7/2}$ and as a consequence there exists observable distortion in the shape of the resultant EIT. Inclusion of collisional decay (Γ_{12}) tends to reduce the asymmetry of the EIT profile, albeit with increase in its linewidth. Consider now the situation corresponding to suppression of stationary state absorption. Doppler averaged absorption spectrum for a representative case is shown in Fig. 4.8. Formation of an EIT resonance at $\delta_1 \approx \Delta_1$ is evident in this figure. As expected the Doppler averaged refractive index undergoes sharp change in the region of EIT resonance as is evident in Fig. 4.8.

We now study the dependence of linewidth of EIT (Γ_{EIT}) on pump intensity. In this context, we consider $\Delta_1 = 0$, and obtain Γ_{EIT} and $\Gamma_{EIT}^{(1)}$ corresponding to DDL and

$\Lambda^{(1)}$ systems. For $\Delta_1 = 0$, $\Lambda^{(1)}$ is at exact resonance while $\Lambda^{(2)}$ is detuned ($\Delta_2 = -S$) with respect to pump frequency. These results are shown in Fig. 4.9. Note here that for $\alpha_1 > 10$ MHz, $\Gamma_{EIT} > \Gamma_{EIT}^{(1)}$, whereas for $\alpha_1 < 10$ MHz, $\Gamma_{EIT} < \Gamma_{EIT}^{(1)}$ for the data chosen in Fig. 4.9.

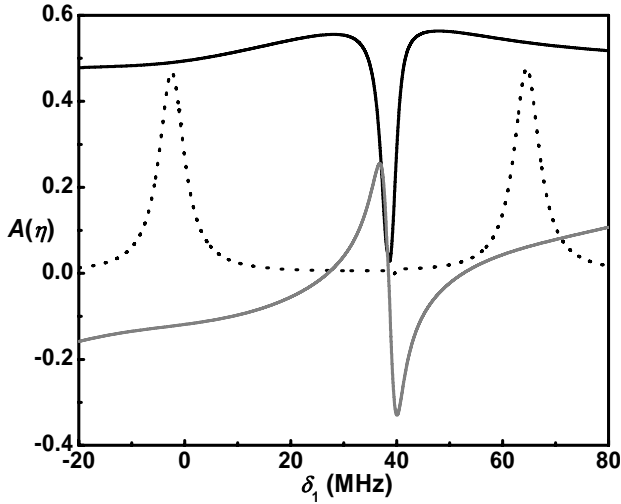


Fig. 4.8: Effect of Doppler broadening on the probe absorption (black line) and dispersion (gray line) for the case where the sub-natural resonance in the absorption spectrum of a stationary atom (dotted line) is suppressed. Here $\alpha_1 = 10$ MHz, $\Delta_1 = 38.37$ MHz, $\Gamma_{12} = \Gamma_{21} = 0.02$ MHz and $2W_D = 515$ MHz.

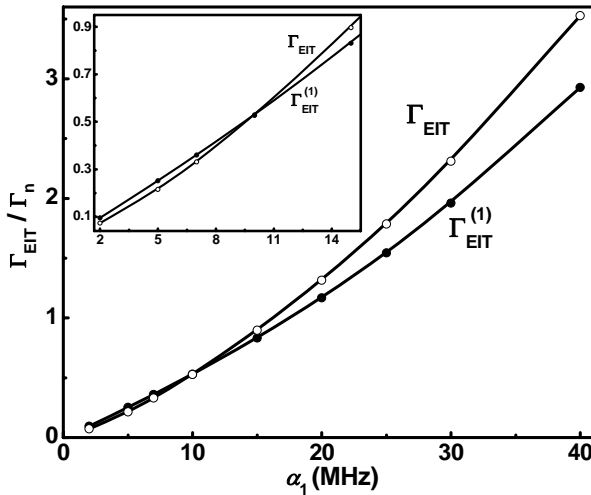


Fig. 4.9: EIT linewidth (measured in terms of the natural linewidth) as a function of pump Rabi frequency (α_1) when $\Delta_1 = 0$, $\Gamma_{12} = \Gamma_{21} = 0.02$ MHz and $2W_D = 515$ MHz. The solid and hollow circles represent results for $\Lambda^{(1)}$ and DDL systems respectively. Inset highlights the region of low pump saturation.

In the absence of analytical results for Γ_{EIT} , we seek the explanation of the observed behaviour on the backdrop of EIT in a Λ system. Javan *et al.* [35-37] and Ye *et al.* [200] have shown that for a Λ system EIT is a consequence of competition between coherent optical pumping rate (R) and collisional relaxation rate (Γ_{21}) between dipole forbidden ground levels and the EIT condition is given by $R > \Gamma_{21}$. Applying the analysis

of three-level $\Lambda^{(1)}$ system (cf. Eq. (3.27)), one observes that for low pump saturation $\Gamma_{EIT}^{(1)} = 2\alpha_1\sqrt{\Gamma_{21}/\Gamma_n}$ whereas for high pump saturation $\Gamma_{EIT}^{(1)} = \alpha_1^2/W_D$. For DDL system one needs to take into account the optical pumping rates $R^{(1)}$ and $R^{(2)}$ for sub-systems $\Lambda^{(1)}$ and $\Lambda^{(2)}$ respectively. Considering these two sub-systems independent, we may write $R^{(1)} \sim \alpha_1^2/\Gamma_n$ and $R^{(2)} \sim \alpha_2^2\Gamma_n/\Gamma_n^2 + S^2$, when $\Delta_1 = 0$. The total optical pumping rate R for DDL system then may be given as $R = R^{(1)}(1 + \Xi)$, where Ξ is the incremental addition to $R^{(1)}$ due to simultaneous excitation of $\Lambda^{(2)}$. Note here that $R \neq R^{(1)} + R^{(2)}$, due to interference effects arising from the concurrent excitation of two Λ systems. Therefore for low pump saturation we may write the linewidth of EIT in DDL system as $\Gamma_{EIT} = \Gamma_{EIT}^{(1)}[1 + \Xi]^{-1/2}$. We thus see that $\Gamma_{EIT} < \Gamma_{EIT}^{(1)}$, which is consistent with the observations in Fig. 4.9. On the other hand for high pump saturation, drawing parallel with Λ system, we may write $\Gamma_{EIT} \sim (\alpha_1^2 + \alpha_2^2)/W_D \sim \Gamma_{EIT}^{(1)}(1 + d_{23}^2/d_{24}^2)$. Consequently $\Gamma_{EIT} > \Gamma_{EIT}^{(1)}$ for large α_1 , as is observed in Fig. 4.9. Although the discussion provided here is qualitative, it suffices to provide a physical insight in the observations of Fig. 4.9. In Fig. 4.10 we show the behavior of Γ_{EIT} and $\Gamma_{EIT}^{(1)}$ as a function of Δ_1 .

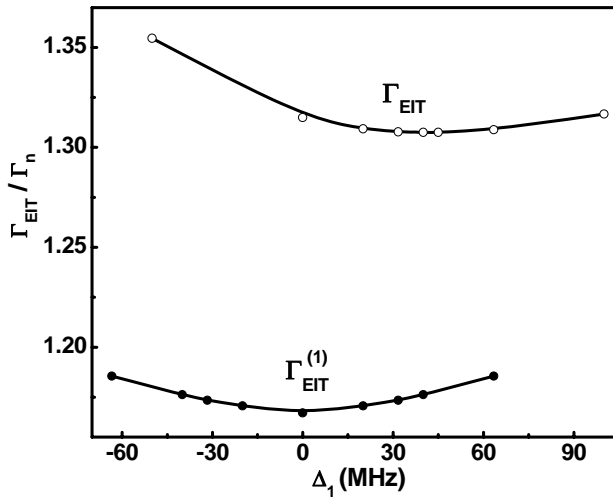


Fig. 4.10: EIT linewidth for $\Lambda^{(1)}$ (solid circles) and DDL system (hollow circles) as a function of pump detuning Δ_1 . Other data are $\alpha_1 = 20$ MHz, $\Gamma_{12} = \Gamma_{21} = 0.02$ MHz and $2W_D = 515$ MHz.

It is seen that $\Gamma_{ETT}^{(1)}$ assumes minimum value at $\Delta_1 = 0$ as expected. However Γ_{ETT} is minimized at Δ_1 that is somewhat close to the centre of gravity of the excited levels. We may add that Γ_{ETT} is studied here at the backdrop of three level model [35,36], where the collisional decay of population is accounted by Γ_{12} and Γ_{21} . Such a description of the ground state relaxation mechanism for a Λ or a DDL system holds true for a rarefied alkali vapour medium (10^{-6} mbar) without any buffer gas. We have simply assumed $\Gamma_{12} = \Gamma_{21} = 20$ kHz, which is also representative of the time of flight of atoms in a typical pump-probe spectroscopy experiment [200,201]. The situation is changed dramatically when buffer gas is introduced in the vapour cell. Figueroa *et al.* [134] have considered pure dephasing kind of ground state relaxation in such a collision rich environment. Theoretical results presented here are therefore more likely to be replicated in a low pressure alkali vapour medium.

It is worthwhile to comment here on the non-radiative decay rates associated with the excited levels. Since for dilute alkali vapours without buffer gas, $\Gamma_{34}, \Gamma_{43} \ll \gamma_3, \gamma_4$ [202], we find that these nonradiative decays have negligible effect on the outcome of the pump-probe spectroscopy. The result of the coherent pump probe spectroscopy is thus primarily dependent on the Raman coherence time, which is governed by non-radiative decay rates associated with the ground levels.

4.6 Coherent Spectroscopy in Six-Level Configuration

In the model calculations presented above, we considered only two excited levels ($F' = 2, 3$) of the hyperfine manifold of $5p_{3/2}$ since only these levels are simultaneously

connected to the ground levels ($F = 2, 3$) owing to the dipole selection rule. It may be of interest to discuss here the effect of additional levels $|5\rangle = |F' = 4\rangle$ and $|6\rangle = |F' = 1\rangle$ on the coherent pump-probe dynamics. In such a six-level model (*cf.* Fig. 4.1), level $|6\rangle$ is not expected to participate in the development of pump-induced coherence since $d_{26} = 0$. Pump laser however can dress $|2\rangle \rightarrow |3\rangle, |4\rangle, |5\rangle$ transitions simultaneously and that may lead to some observable effects although $d_{15} = 0$. The two additional non-vanishing dipole matrix elements in this case are $d_{25} = \sqrt{9/14}\mu_{D2}$ and $d_{16} = \sqrt{3/10}\mu_{D2}$. Probe absorption in this situation is a quadruplet spectra corresponding to dressing of $|2\rangle \rightarrow |3\rangle, |4\rangle, |5\rangle$ transition. In the presence of Doppler broadening EIT resonance appears at two-photon resonance condition similar to DDL system. We have investigated the six-level scheme numerically to find no effect of additional levels on the vanishing of the sub-natural resonance (*cf.* Fig. 4.5). This is consequence of the fact that $d(1, \psi_2)$ retains the form of the type given by Eq. (4.21) owing to $d_{15} = 0$. Doppler averaging of six-level model, however, shows some visible effects on the EIT resonance. The noticeable effects are shift of EIT resonance and increase in Γ_{EIT} when additional levels $|5\rangle$ and $|6\rangle$ are included in the four-level model. This increase can again be attributed to the effect of additional levels on coherent optical pumping. In the six-level model, pump laser dresses $|2\rangle \rightarrow |3\rangle, |4\rangle, |5\rangle$ transitions simultaneously, however since $d_{15} = 0$, effective optical pumping rate decreases and that causes increase in Γ_{EIT} compared to the four-level model. This increase in EIT width becomes more pronounced at higher pump

intensities. The effect of additional levels on EIT positions and their linewidths is summarized in Table-4.

Table-4: Comparison of EIT positions and widths in Λ , DDL and six level configurations for $\Delta_1 = 0$

α_1	EIT position (MHz)			Γ_{EIT} / Γ_n		
	$\Lambda^{(1)}$	DDL	6-level model	$\Lambda^{(1)}$	DDL	6-level model
5	0	0.123	0.43	0.252	0.215	0.246
10	0	0.331	1.48	0.528	0.526	0.775
15	0	0.607	2.25	0.830	0.896	1.490
20	0	0.965	3.36	1.167	1.315	2.507
25	0	1.402	4.8	1.543	1.785	3.631
30	0	1.918	6.53	1.960	2.310	4.908

4.7 Experimental Realization of Simultaneous Dressing

In order to provide a flavor of the coherent pump-probe spectroscopy for precision measurements we report here our experimental results on dressed state spectroscopy in ^{87}Rb [205] where $S=156.95$ MHz. The four level scheme forming the DDL system comprises of $|1\rangle \equiv |5s_{1/2} F=1\rangle$, $|2\rangle \equiv |5s_{1/2} F=2\rangle$, $|3\rangle \equiv |5p_{3/2} F'=1\rangle$ and $|4\rangle \equiv |5p_{3/2} F'=2\rangle$.

4.7.1 Experimental Scheme

A schematic of experimental set up is shown in Fig. 4.11. Two commercial Sacher Lasertechnik external cavity diode lasers (ECDL 1 and 2) with maximum output powers of 105 mW and 45 mW are used as control and probe lasers. Both lasers operate

near ^{87}Rb D_2 transition (780 nm) and have a linewidth ~ 1 MHz. The two beams have a typical diameter of 0.36 mm. Optical isolators are used to avoid optical feedback. A weak part ($\sim 100 \mu\text{W}$) of ECDL1 beam is used for saturation absorption spectroscopy (SAS).

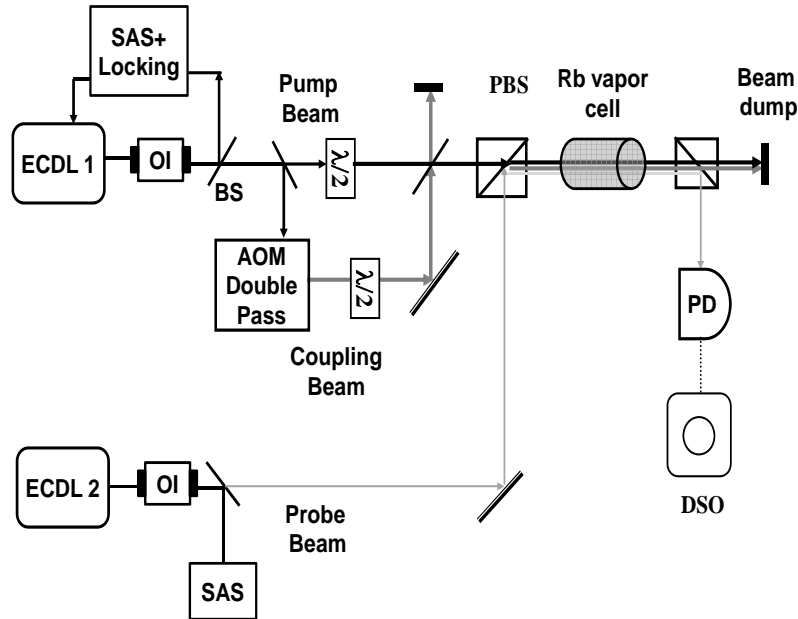


Fig. 4.11: Schematic of experimental set up for coherent pump-probe spectroscopy. Here ECDL: external cavity diode laser, SAS: saturation absorption spectroscopy, OI: optical isolator, BS: beam splitter, $\lambda/2$: half wave plate, AOM: acousto optic modulator, PBS: polarizing cubic beam splitter, PD: photodiode and DSO: digital storage oscilloscope. The pump, coupling and probe beams are shown by black, dark gray and light gray lines respectively. For the present experiment the coupling beam is turned off.

SAS is used for subsequent stabilization and calibration of control laser frequency. To convert the SAS signal to suitable frequency discriminator we modulate the laser current by applying a very small sinusoidal voltage and demodulate the photodiode signal through a lock-in amplifier (LIA). This gives first derivative spectrum of the SAS signal and the laser is locked on the zero point of first derivative signal by electronic feedback to the piezo actuator (PZT) of the ECDL. Very small current modulation does not affect the linewidth of the control laser, hence causing minimum effect on the experimental outcome. The remaining beam of the control laser is split into

two parts, a part is used as pump beam and the other part is passed through an acousto optic modulator (AOM) for optical frequency conversion thus generating a coupling beam of desired detuning. AOM is used in a double pass configuration to avoid the problem of physical displacement of beam while tuning its frequency as well as in providing flexibility to control the coupling laser detuning. AOM frequency is tuned by applying external voltage to the voltage control oscillator (VCO) of the driver unit. For the present experiment in a Λ system coupling beam is turned off. This beam is used for N-system experiments as discussed in Chapter-6.

A small part of ECDL2 is also used to generate SAS for frequency calibration and the remaining part is used as the probe beam. Pump beam is locked at a specified detuning Δ_1 and its intensity is varied to obtain Rabi frequency α_1 in the range of 5 - 50 MHz. Probe beam is further split into two unequal parts, one weak ($\sim 110 \mu\text{W}$) and the other strong ($\sim 180 \mu\text{W}$). Pump beam and weaker part of the probe beam are passed co-propagating through a Rb vapour cell of 2 cm diameter and 5 cm length in orthogonal linear polarization configuration. The vapour cell is kept at room temperature and is wrapped with a μ - metal shield to reduce the effect of stray magnetic field. The stronger part of probe beam is sent counter-propagating through the cell. These three beams overlap over a length of ~ 1.5 cm in the sample cell.

In this arrangement, the co-propagating probe and coupling beams participate in the dressed state spectroscopy, while the counter-propagating part of the probe beam helps to eliminate the first order Doppler effect as seen by the weaker part of the probe beam. This technique is similar to SAS and is used here to reduce Doppler background which improves the signal to noise ratio (contrast) of the dressed level spectrum. After

the exit of the beams from the vapour cell, probe beam is separated using a polarizing beam splitter (PBS) and detected on a photodiode. The dressed state resonances are obtained using amplitude modulation technique. This experimental arrangement extracts weak signals and provides nearly Doppler-free probe absorption signals, albeit with somewhat broader linewidths.

4.7.2 Results and Discussion

Pump laser is locked at different hyperfine and crossover components of ^{87}Rb $5s_{1/2}F = 2 \rightarrow 5p_{3/2}F' = 1, 2, 3$ manifold by a frequency stabilized servo loop and the weak probe is scanned across $5s_{1/2}F = 1 \rightarrow 5p_{3/2}F' = 0, 1, 2$. The probe spectrum is recorded on a 1 GHz digital storage oscilloscope. The powers of pump and probe beams are 1.9 W/cm^2 and 0.08 W/cm^2 respectively. The control beam detuning (Δ_1) varies from -557 MHz to 265 MHz . However with shift from the central frequency, the power of control beam decreases and reduces to as low as $870 \mu\text{W}$ at the detuning of -557 MHz .

An important technique employed in this experiment is the phase sensitive detection of probe absorption. Pump beam is modulated at 30 kHz using AOM and modulation transfer to the probe beam is measured using phase sensitive detection technique. The modulation frequency of the pump laser is set as the reference signal for lock in amplifier (LIA). This indirect modulation transfer to probe beam is strongly dependent on pump-probe interaction which is directly related to susceptibility. Therefore the demodulated output appears only at those frequencies where both beams interact. If the pump beam is locked in a highly off-resonant condition the modulation depth is weak hence the signal strength reduces. Hence the probe beam is kept at a high power of 110

μW which can take modulation even at such low frequencies. This technique not only extracts weak signal from large background noise but also provides a clean and nearly Doppler free probe spectrum. However the disadvantage here is that the demodulated spectrum has broader linewidths compared to the unmodulated probe signal. A typical probe absorption spectrum for red detuned pump field is shown in Fig. 4.12. Here the pump laser is locked at $5s_{1/2}F = 2 \rightarrow 5p_{3/2}F' = 2$ transition. The fixed frequency of the pump laser, as locked above is further shifted appropriately using AOM so that the effect of pump detuning on the dressed levels can be studied in details. In Fig. 4.12 this shift is 108 MHz which implies $\Delta_1 = 265$ MHz. The absorption spectrum exhibits a triplet, which is a signature of dressing of $5s_{1/2}F = 2 \rightarrow 5p_{3/2}F' = 1, 2$ by the pump laser. This result thus emphasizes the importance of taking into account nearby resonant level in dressed state spectroscopy.

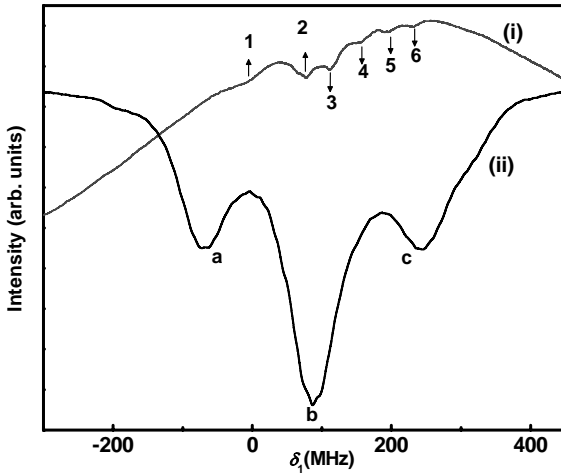


Fig. 4.12: Dressed state spectroscopy of ^{87}Rb D_2 transition. (i) Probe saturation absorption spectrum where the various resonances are marked as (1): $F = 1 \rightarrow F' = 2$, (2): crossover between $F = 1 \rightarrow F' = 1, 2$, (3): crossover between $F = 1 \rightarrow F' = 0, 2$, (4): $F = 1 \rightarrow F' = 1$, (5): crossover between $F = 1 \rightarrow F' = 0, 1$ and (6): $F = 1 \rightarrow F' = 0$. (ii) Probe intensity ($-A$) in the presence of pump laser of intensity of $\sim 1.9\text{W}/\text{cm}^2$ and $\Delta_1 \approx 265$ MHz. The resonances a, b and c are at $\delta_1 = -86$, 89 and 263 MHz respectively.

For red detuned pump field, level $|5\rangle$ ($5p_{3/2}F' = 3$) is far off-resonant and does not participate in dressing of the medium. However for large blue detuned pump, the system corresponds to six-level Λ type system as was discussed in the Sec. 4.6. A

representative behaviour of this situation is shown in Fig. 4.13. Here the pump beam is locked at $5s_{1/2}F = 2 \rightarrow 5p_{3/2}F' = 3$ and is further up-shifted by 200 MHz using AOM ($\Delta_1 \approx -467$ MHz). The dressed state spectrum in this case consists of more than three resonances due to dressing of $5s_{1/2}F = 2 \rightarrow 5p_{3/2}F' = 1, 2, 3$ transition by the pump beam.

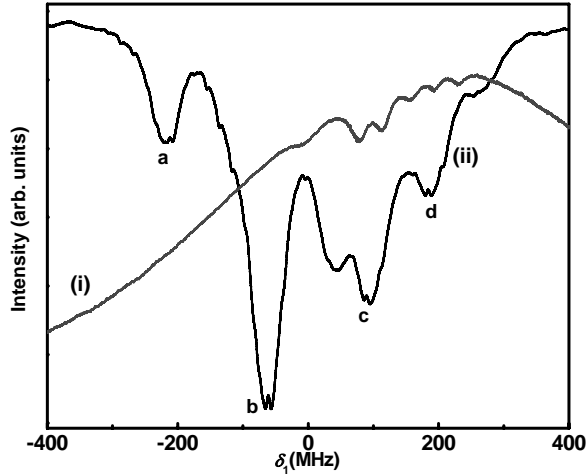


Fig. 4.13: Dressed state spectroscopy of D_2 transition of ^{87}Rb for $\Delta_1 \approx -467$ MHz. (i) Probe saturation absorption spectrum and (ii) probe intensity ($-A$) in the presence of pump laser of intensity of $\sim 1.9\text{W}/\text{cm}^2$. The resonances a, b, c and d correspond to $\delta_1 \sim -212, -52, 95$ and 195 MHz respectively.

As discussed in theoretical treatment of Sec. 4.3 we observe that the separation and line widths of the dressed resonances are critically dependent on α_1 . While an increase in α_1 tends to increase the separation between the resonances, it also increases their widths and that results in the smearing of the absorption spectrum. Though our experimental results qualitatively agree with the theoretical modeling the quantitative comparison is complicated due to various experimental restrictions, for e.g. there is an uncertainty in determining the effective pumping Rabi frequency which depends on the focusing of pump beam, change in pump intensity along the cell and its spatial shape in the radial direction. The stability of pump laser locking and uncertainty in exact matching of pump and probe lasers also affect the observed spectrum. Further the large probe power and modulation transfer detection technique contribute to the increased linewidths of the dressed resonances as compared to that expected from the theoretical analysis.

CHAPTER 5

AMPLIFICATION WITHOUT INVERSION IN DEGENERATE DOUBLE Λ SYSTEM

5.1 Introduction

Quantum coherence and interference in driven multi-level atomic systems are central to a number of interesting and counter intuitive phenomena that are important in the understanding of subtle effects in coherent photon-atom interactions and also in several practical applications [1-17]. One such phenomenon that has attracted much attention is amplification without inversion (AWI) or lasing without inversion (LWI) [53-79]. The underlying physics and extra-ordinary interest pertaining to AWI and LWI are discussed in Chapter-1.

In this chapter we investigate AWI in a degenerate double lambda (DDL) system of Chapter-4. Hyperfine manifold of D_1 transition of ^{87}Rb is used as a model system to discuss the effect of pump induced coherence on the absorption of the weak probe beam. The system is observed to exhibit AWI very close to two-photon resonance as a result of

interference between two simultaneously excited lambda resonances. AWI is found to be critically dependent on pump detuning and low frequency coherence established between the pair of ground levels. Approximate analytical expression for probe absorption is derived to corroborate the numerical results and to discuss the contrasting behavior, i.e., absorption instead of AWI for the model DDL system in D_2 transition of ^{87}Rb . This distinctive behavior is further enhanced on inclusion of Doppler broadening.

5.2. Model and Numerical Results

We consider a DDL system (*cf.* Fig. 2.1(a)) formed by the hyperfine manifold of D_1 transition of ^{87}Rb . The four-level subset that forms the DDL scheme is $|1\rangle \equiv |5s_{1/2} F=1\rangle$, $|2\rangle \equiv |5s_{1/2} F=2\rangle$, $|3\rangle \equiv |5p_{1/2} F'=1\rangle$ and $|4\rangle \equiv |5p_{1/2} F'=2\rangle$ such that the only non-vanishing dipole matrix elements are $d_{13} = \mu_{D_1}/\sqrt{6}$, $d_{14} = \mu_{D_1}\sqrt{5/6}$ and $d_{23} = d_{24} = \mu_{D_1}/\sqrt{2}$, where μ_{D_1} is the transition matrix element associated with D_1 transition [204]. Pump laser is used to dress the hyperfine transitions $5s_{1/2}F=2 \rightarrow 5p_{1/2}F'=1,2$ and probe is scanned across $5s_{1/2}F=1 \rightarrow 5p_{1/2}F'=1,2$ transition. For D_1 transition of ^{87}Rb , $S = 814.5$ MHz and the natural linewidth ($2\Gamma_n$) of the transition is 5.75 MHz [204].

We consider dilute atomic vapour medium so that $\Gamma_{12}, \Gamma_{21}, \Gamma_{34}, \Gamma_{43} \ll \Gamma_n$.

Absorption (A) and dispersion (η) of the weak probe are defined in Eq. (4.5). Clearly $A > 0$ represents probe absorption while $A < 0$ corresponds to amplification of the probe beam by the coherently prepared atomic system. Fig. 5.1 shows the steady state probe absorption spectrum for a situation where the strong pump ($\alpha_1 = 20$ MHz) is

detuned ($\Delta_1 = 430$ MHz) in such a way that its frequency lies midway between levels $|3\rangle$ and $|4\rangle$, and a weak probe ($\beta_1 = 0.1$ MHz) is tuned across $|1\rangle \rightarrow |3\rangle, |4\rangle$ transition. We observe that at $\delta_1 = 0$ and S the probe beam is absorbed while close to two-photon resonance, $\delta_1 = \Delta_1$, it is amplified. In particular in Fig. 5.1, amplification occurs at $\delta_1 = 429.89$ MHz. This small deviation ($< 5\%$) from exact two-photon resonance is observed in all calculations, especially when $\alpha_1 > \Gamma_n$. As was discussed in Chapter-4, the two-photon resonance condition is simultaneously satisfied for both $\Lambda^{(1)}$ and $\Lambda^{(2)}$ at $\delta_1 = \Delta_1$, albeit approximately.

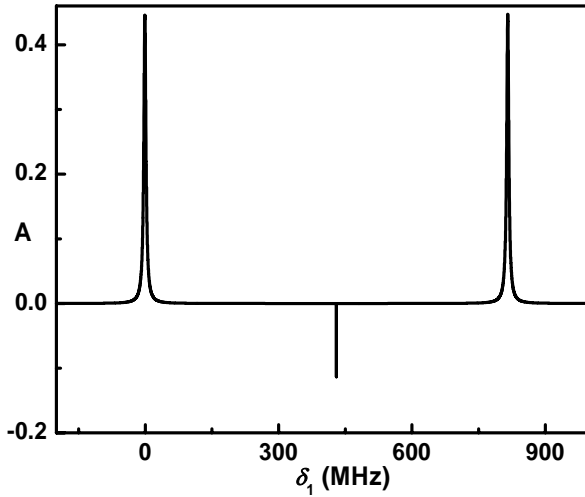


Fig. 5.1: Steady state probe absorption spectrum calculated for $\alpha_1 = 20$ MHz, $\beta_1 = 0.1$ MHz and $\Delta_1 = 430$ MHz. This data corresponds to $\alpha_2 = 20$ MHz, $\beta_2 = 0.045$ MHz and $\Delta_2 = -384.5$ MHz. All γ_{ij} are assumed to be equal and they add to natural linewidth $2\Gamma_n = 5.75$ MHz. The incoherent decay rates are $\Gamma_{12} = \Gamma_{21} = 1$ kHz.

For the same set of parameters, steady state populations in the bare atomic levels ($\rho_{ii}, i = 1-4$) are plotted in Fig. 5.2. It is observed that $\rho_{11} \gg \rho_{33}, \rho_{44}$ implying that there is no population inversion in the bare states and therefore the observation of gain at two-photon resonance is indeed AWI. We further obtain the dressed states, $|\psi_i\rangle, (i = 1, 2, 3)$, formed by the coherent coupling of $|2\rangle \rightarrow |3\rangle, |4\rangle$ transitions and compare their populations (ρ_{ψ_i}) with ρ_{11} . While this data is not explicitly shown here,

we observe that the behavior is very similar to that in Fig. 5.2 indicating absence of inversion in the dressed states.

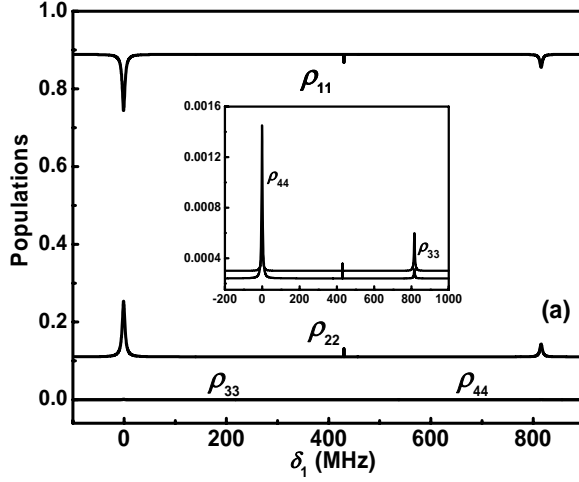


Fig. 5.2: Steady state populations in the bare atomic levels for the data used in Fig. 5.1. Inset shows the expanded view of ρ_{33} and ρ_{44} .

Further clarity to the origin of AWI is brought by studying the amplification as a function of pump detuning Δ_1 . For variation of Δ_1 in the range $0 < \Delta_1 < S$, the amplification observed near two-photon resonance ($\delta_1 \approx \Delta_1$) is plotted in Fig. 5.3. We see that the gain is maximized at $\Delta_1^{\max} = 407.25$ MHz, i.e., $\Delta_1 = S/2$, and it decreases on either side of Δ_1^{\max} to become zero as Δ_1 approaches 0 and S . Note here that for $\Delta_1 = 0$ and S , the pump laser is at exact resonance with $|1\rangle \rightarrow |4\rangle$ and $|1\rangle \rightarrow |3\rangle$ transitions respectively. The results of Fig. 5.3 indicate that the observed AWI is a result of interference between two competing Λ resonances. For $\Delta_1 \approx 0$, the $\Lambda^{(1)}$ resonance is expected to be significantly stronger than the far detuned $\Lambda^{(2)}$ resonance ($\Delta_2 = -S$). On the other hand for $\Delta_1 \approx S$, $\Lambda^{(1)}$ resonance weakens substantially in comparison to $\Lambda^{(2)}$ resonance ($\Delta_2 = 0$). At intermediate detuning, $\Delta_1 \approx S/2$, both the Λ resonances are of equal strength and that leads to maximization of the observed AWI. There however exists a range of Δ_1 (250 to 550 MHz in Fig. 5.3) for which the interference between two Λ

resonances results in probe amplification. Fig. 5.4 shows dependence of pump intensity (α_1) on AWI. For $0 < \alpha_1 < 20$ MHz, AWI exhibits close to quadratic dependence and thereafter saturation behaviour.

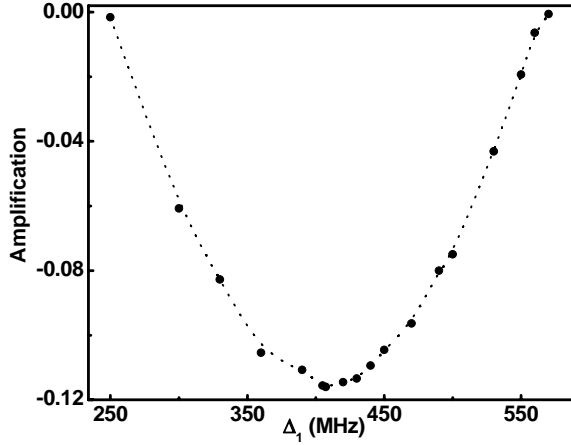


Fig. 5.3: Effect of pump detuning on AWI. Other data are same as in Fig. 5.1. The dotted line is only indicative of the trend.

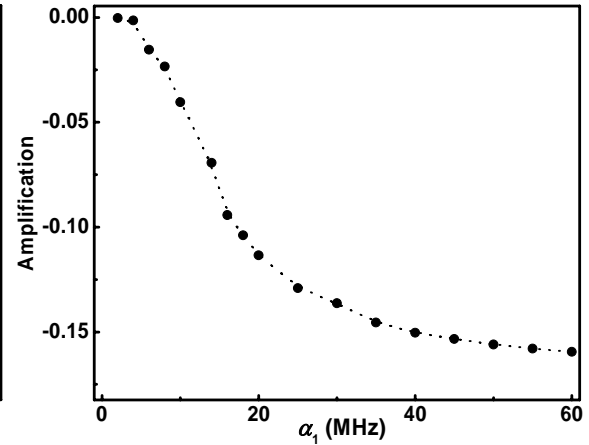


Fig. 5.4: Dependence of AWI on pump Rabi frequency. Other data are same as in Fig. 5.1.

The importance of coherence between dipole forbidden levels in the observation of AWI may be seen from Fig. 5.5 where the gain is plotted as a function of incoherent decay rates $\Gamma_{12}(= \Gamma_{21})$ and $\Gamma_{34}(= \Gamma_{43})$. AWI decreases rapidly to zero as Γ_{12} is increased, while it is relatively insensitive to Γ_{34} . The low frequency coherence established in the ground hyperfine levels is thus an important factor in the observation of AWI.

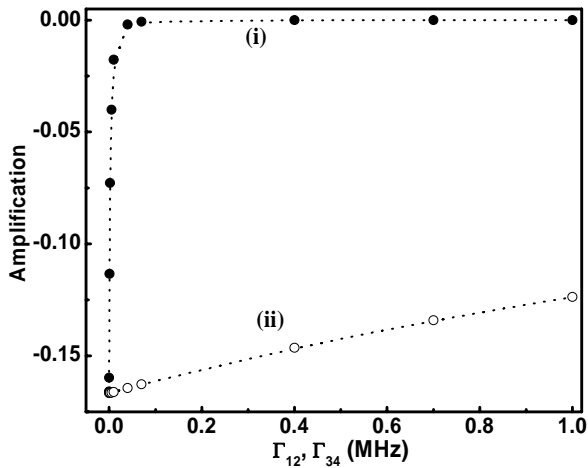


Fig. 5.5: Variation of AWI with the incoherent decay rate (i): $\Gamma_{12}(= \Gamma_{21})$ and (ii): $\Gamma_{34}(= \Gamma_{43})$. For curve (i) $\Gamma_{34}(= \Gamma_{43}) = 0$ and for curve (ii) $\Gamma_{12}(= \Gamma_{21}) = 0$. Other data are same as in Fig. 5.1.

5.3 Perturbative Analysis

Probe absorption and dispersion in a DDL system under weak probe limit has been discussed in Chapter-4. Here we look for the atom-field parameters contributing to AWI in this limit. Perturbative analysis of Eq. (4.2), when substituted in Eq. (4.6) yields

$$\tilde{P} = i(\chi_1 + \chi_2 + \chi_3), \quad (5.1)$$

$$\chi_1 = (\gamma_{31}/\kappa_2)(\rho_{11}^{(0)} - \rho_{33}^{(0)}) + (\gamma_{41}/\kappa_3)(\rho_{11}^{(0)} - \rho_{44}^{(0)}), \quad (5.2)$$

$$\chi_2 = \rho_{21}^{(1)}\zeta, \quad (5.3)$$

$$\chi_3 = -[(\beta_1\gamma_{31}/\beta_2\kappa_2)\rho_{34}^{(0)} + (\beta_2\gamma_{41}/\beta_1\kappa_3)\rho_{43}^{(0)}], \quad (5.4)$$

$$\zeta = (\alpha_2\gamma_{31}/\beta_2\kappa_2) + (\alpha_1\gamma_{41}/\beta_1\kappa_3). \quad (5.5)$$

The form of Eq. (5.1) suggests that we need to consider only $\text{Re}(\chi_1)$, $\text{Re}(\chi_2)$ and $\text{Re}(\chi_3)$, since $A = \text{Im}(P)$. Relative contribution of these terms is shown in Fig. 5.6, where we observe that $\text{Re}(\chi_2)$ essentially contributes at $\delta_1 = \Delta_1$.

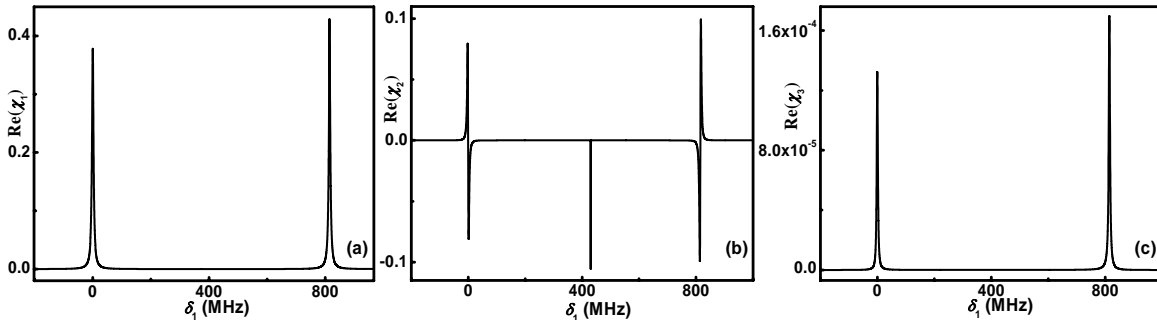


Fig. 5.6: Variation of $\text{Re}(\chi_1)$, $\text{Re}(\chi_2)$ and $\text{Re}(\chi_3)$ with probe detuning for the parameters of Fig. 5.1.

The behavior observed in Fig. 5.6 can be explained based on the steady state polarizations and populations in zeroth and first order given in Chapter-4 and *Appendix-1*. These may be used to obtain the general expression for A that is valid for arbitrary

values of laser-atom interaction parameters, albeit at weak probe intensity. These expressions are explicitly provided in *Appendix-2*. To obtain physical insight into the problem, we consider here the region of pump detuning that maximizes AWI, i.e., the region where $|\Delta_1|, |\Delta_2| \gg \alpha_1, \alpha_2, \gamma_{ij}$. This restriction also implies $|\delta_1|, |\delta_2| \gg \alpha_1, \alpha_2, \gamma_{ij}$, since AWI is observed to occur close to two-photon resonance. At such large detunings, the excitation is weak and that corresponds to the situation where $\rho_{11}^{(0)} \approx 1$ and $\rho_{22}^{(0)} = \rho_{33}^{(0)} = \rho_{44}^{(0)} \approx 0$ (cf. Fig. 5.2). In this domain of interest, an inspection of Eq. (5.2) shows that the contribution of $\text{Re}(\chi_1)$ is sum of two Lorentzians peaked at $\delta_1 = 0$ and S , and its contribution to A is negligible near two-photon resonance ($\delta_1 = \Delta_1$). Also the contribution of χ_3 can be neglected since $\rho_{34}^{(0)} = f(\rho_{22}^{(0)}, \rho_{33}^{(0)}, \rho_{44}^{(0)})$. The probe absorption thus assumes a simpler form,

$$A = \text{Re}(\chi_2) = \text{Re}(\rho_{21}^{(1)})\text{Re}(\zeta) - \text{Im}(\rho_{21}^{(1)})\text{Im}(\zeta). \quad (5.6)$$

It may be further seen from Eq. (5.5) that $\text{Re}(\zeta) \propto \Delta_1^{-2}$ whereas $\text{Im}(\zeta) \propto \Delta_1^{-1}$, and as a consequence for large pump detuning, we may write

$$A = -\text{Im}(\rho_{21}^{(1)})\text{Im}(\zeta), \quad (5.7)$$

where $\text{Im}(\rho_{21}^{(1)})$ is given by Eq. (A3.3) in *Appendix-3* and

$$\text{Im}(\zeta) = -\frac{\alpha_1}{\beta_1} \gamma_{41} \frac{\delta_1}{(\gamma_4 + \Gamma_{12})^2 + \delta_1^2} - \frac{\alpha_2}{\beta_2} \gamma_{31} \frac{\delta_2}{(\gamma_3 + \Gamma_{12})^2 + \delta_2^2}. \quad (5.8)$$

The two terms of Eq. (5.8) correspond respectively to $\Lambda^{(1)}$ and $\Lambda^{(2)}$ resonances. Without loss of generality, we may assume $\Gamma_{34} = \Gamma_{43}$, $\Gamma_{12} = \Gamma_{21}$ and $\gamma_3 = \gamma_4 = \gamma_d$ so that $\gamma_3 + \gamma_4 = 2(\Gamma_n + \Gamma_{34})$ and simplify Eq. (5.7) under the condition of two-photon resonance, i.e., $\delta_1 - \Delta_1 = \delta_2 - \Delta_2 = 0$. Note also from the numerical results of Sec. 5.2 that AWI is

maximized when $\Delta_1 = S/2$, which also implies that $\Delta_2 = -S/2$. Under these approximations, we finally obtain the following expression for absorption at $\delta_1 = \Delta_1$,

$$A(\delta_1 \approx \Delta_1 \approx S/2) = \Gamma_n \alpha_1^2 M_1 M_2 \frac{Z}{Z^2 + S^2 (\alpha_2^2 - \alpha_1^2)^2}, \quad (5.9)$$

$$Z = \Gamma_{12} S^2 + 2(\Gamma_n + \Gamma_{12} + \Gamma_{34})(\alpha_1^2 + \alpha_2^2), \quad (5.10)$$

$$M_1 = (d_{23}/d_{24}) - (d_{13}/d_{14}), \quad (5.11)$$

$$M_2 = (d_{23}/d_{24}) - (d_{14}/d_{13}). \quad (5.12)$$

We have thus expressed the competition between two simultaneously excited Λ resonances in terms of the relevant dipole matrix elements. Since all other quantities except M_1 and M_2 are positive definite, the sign of A is governed by the relative magnitudes of dipole moments. Specifically, for amplification to occur the relevant dipole moments need to be such that M_1 and M_2 have opposite signs. For D_1 transition of ^{87}Rb [204], $M_1 = 0.553$ and $M_2 = -1.236$, and as a consequence $A < 0$ at $\delta_1 \approx \Delta_1$, as is seen in the numerical calculations. The dependence of AWI on α_1 (*cf.* Fig. 5.4) is closely predicted by Eq. (5.9). For low pump intensities, i.e., $(\alpha_1^2 + \alpha_2^2) < \Gamma_{12} S^2 / 2(\Gamma_n + \Gamma_{12} + \Gamma_{34})$, Eq. (5.9) predicts that $A \propto \alpha_1^2$ whereas at high pump intensities the term $2(\Gamma_n + \Gamma_{12} + \Gamma_{34})(\alpha_1^2 + \alpha_2^2)$ begins to contribute and leads to the saturation of AWI. It may also be seen from Eq. (5.9) that AWI is very sensitive to Γ_{12} since $A \propto \Gamma_{12}^{-1}$. In comparison the effect of Γ_{34} comes into play only at high pump intensities and even there the effect is marginal since $\Gamma_{34} < \Gamma_n$. This analysis is consistent with the behaviour observed in Fig. 5.5. Low frequency coherence associated with the ground levels is thus

more important compared to that in the excited levels.

On the contrary from Eq. (5.9) one observes that if $M_1 M_2 > 0$, then $A > 0$, and that corresponds to the situation where the probe is absorbed at $\delta_1 \approx \Delta_1$. This prospect prompts us to employ it to a model DDL system in D_2 transition of ^{87}Rb , $5s_{1/2} F = 1, 2 \rightarrow 5p_{3/2} F' = 0, 1, 2, 3$. The relevant electric dipole allowed transitions which simultaneously connect the ground hyperfine levels to upper hyperfine levels are $5s_{1/2} F = 1, 2 \rightarrow 5p_{3/2} F' = 1, 2$. We therefore consider $|1\rangle \equiv |F = 1\rangle$, $|2\rangle \equiv |F = 2\rangle$, $|3\rangle \equiv |F' = 1\rangle$ and $|4\rangle \equiv |F' = 2\rangle$. Here $S = 156.95$ MHz and the relevant dipole moments are $d_{13} = d_{14} = \mu_{D_2} \sqrt{5/12}$, $d_{23} = \mu_{D_2} / \sqrt{20}$ and $d_{24} = \mu_{D_2} / 2$, where μ_{D_2} is the transition matrix element of D_2 transition [204]. We observe here that $M_1 = M_2 = -0.553$, which as a consequence must yield $A > 0$. In Fig. 5.7 we have plotted the numerically calculated absorption spectrum for the DDL system in D_2 transition, where we indeed see that, the probe is absorbed instead of being amplified at two-photon resonance condition $\delta_1 \approx \Delta_1$.

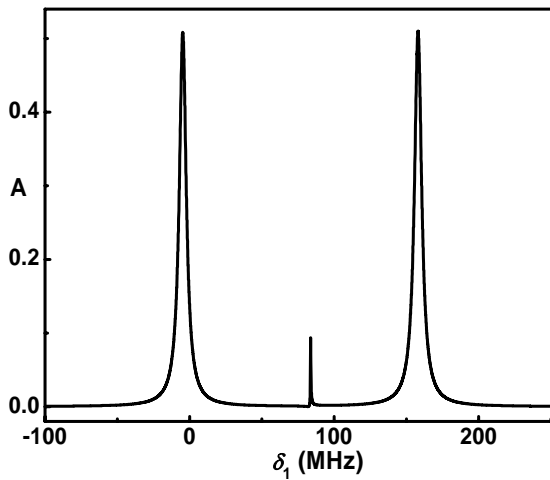


Fig. 5.7: Probe absorption spectrum for DDL system formed in D_2 transition of ^{87}Rb . Here $S = 156.95$ MHz, $\alpha_1 = 20$ MHz, $\beta_1 = 0.1$ MHz and $\Delta_1 = 80$ MHz, which corresponds to $\alpha_2 = 8.94$ MHz, $\beta_2 = 0.1$ MHz and $\Delta_2 = -76.95$ MHz. All γ_{ij} are assumed to be equal and they all add to $2\Gamma_n = 6.066$ MHz, and $\Gamma_{12} = \Gamma_{21} = 0.001$ MHz.

We may mention here that the DDL system in ^{87}Rb is merely a representative case. DDL system can be formed in other alkali atoms also, where the separation between

excited levels is much smaller, for e.g., (361.58, 63.401) MHz in (D_1 , D_2) transitions of ^{85}Rb and (26.1, 1.507) MHz in (D_1 , D_2) transitions of ^6Li . In these systems the contrast behaviour of amplification and absorption observed for D_1 and D_2 transitions respectively is expected to be more pronounced. In order to ascertain the S^{-2} dependence of AWI, we show in Fig. 5.8 the probe absorption in case of a model DDL system in D_1 transition of ^6Li . We indeed observe enhanced AWI at $\delta_1 \approx \Delta_1 \approx S/2$.

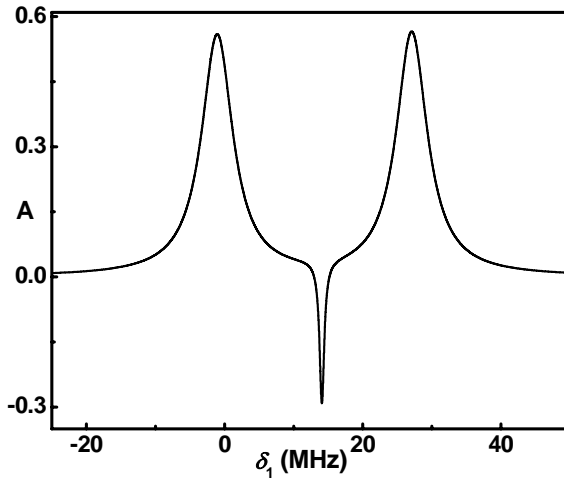


Fig. 5.8: AWI in D_1 transition of ^6Li for $(\alpha_1, \alpha_2, \beta_1, \beta_2, S, \Delta_1, 2\Gamma_n) = (4, 3.58, 0.01, 0.003, 26.1, 14, 5.87)$ MHz. The incoherent decay rates are $\Gamma_{12} = \Gamma_{21} = 0.001$ MHz.

At this juncture it is important to comment on the frequency position at which the amplification is observed. This information may be obtained from the dressed state energies of the system. While the dressed state energies are obtained in Sec. 4.3 for some specific cases, e.g. $\alpha_1^2 \Delta_2 + \alpha_2^2 \Delta_1 = 0$, we observe that for $0 < \Delta_1 < S$ and $\alpha_1, \alpha_2 \ll S$, the approximate energies are given as

$$\delta_1 \approx \frac{S\alpha_1^2 + \Delta_1\gamma_3\gamma_4}{\alpha_1^2 + \alpha_2^2 - \Delta_1 S + \gamma_3\gamma_4}, \Delta_1 + \frac{\alpha_1^2 \Delta_2 + \alpha_2^2 \Delta_1}{\Delta_1 \Delta_2 - \alpha_1^2 - \alpha_2^2 - \gamma_3\gamma_4}, S + \frac{-S\alpha_2^2 + \Delta_2\gamma_3\gamma_4}{\alpha_1^2 + \alpha_2^2 + \Delta_2 S + \gamma_3\gamma_4}. \quad (5.13)$$

As discussed in Chapter-4, the first and third roots in Eq. (5.13) correspond to the resonances appearing in the proximity of atomic resonances $|1\rangle \rightarrow |4\rangle$ and $|1\rangle \rightarrow |3\rangle$

respectively, whereas the second root corresponds to the frequency where amplification is observed (*cf.* Fig. 5.1). The amplification thus does not occur exactly at exact two-photon resonance, i.e., $\delta_1 = \Delta_1$, but is shifted depending on the strength of the Rabi frequencies. For $\Delta_2 = 430$ MHz and $\alpha_2 = 20$ MHz the correction to the exact two-photon resonance is -0.11 MHz, which is consistent with the observations in Fig. 5.1.

5.4. Doppler Averaging

We now consider the atomic motion to include the Doppler effect on the observed AWI. To this end, we integrate the probe absorption spectrum over the Maxwell-Boltzmann distribution of atomic velocities. Further we consider co-propagating pump and probe, and Rb vapor with Doppler width of 250 MHz and 500 MHz. These Doppler widths correspond to vapour temperature of 75 K and 298 K respectively. The effect of Doppler broadening on the probe absorption spectrum of Fig. 5.1 is shown in Fig. 5.9.

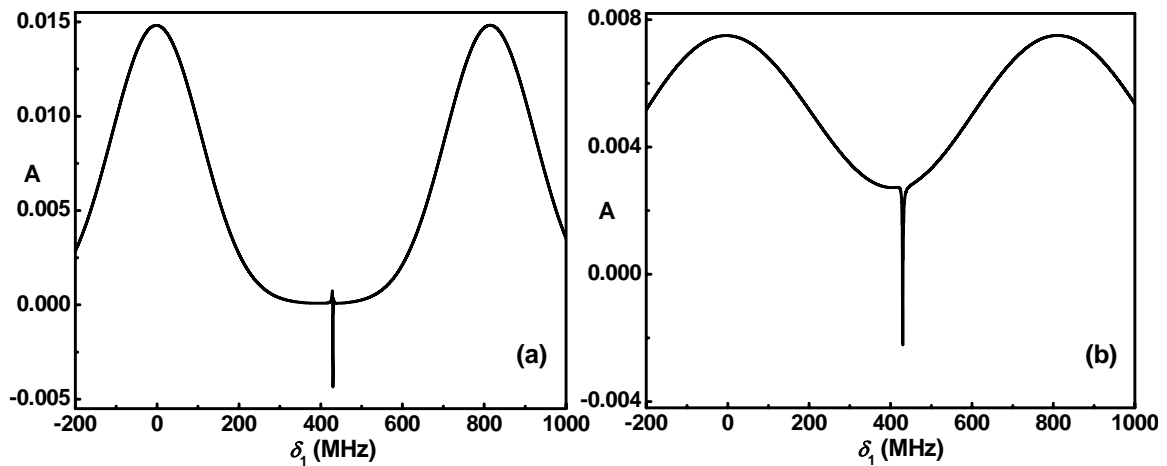


Fig. 5.9: Effect of Doppler broadening on the probe absorption spectrum of Fig. 5.1. $2W_D = 250$ MHz and 500 MHz for frames (a) and (b) respectively.

Note here in Fig. 5.9 that with increase in the temperature of the medium, the bare atomic resonances at $\delta_1 = 0$ and $\delta_1 = S$ broaden and they begin to contribute steadily to

the probe absorption near $\delta_1 \approx \Delta_1$. The increase in the baseline absorption therefore results in steady decrease in AWI. The progressive decrease in the height of the amplification peak with increase in Doppler width is shown in Fig. 5.10. Nevertheless, even at room temperature we observe noticeable AWI in the calculations.

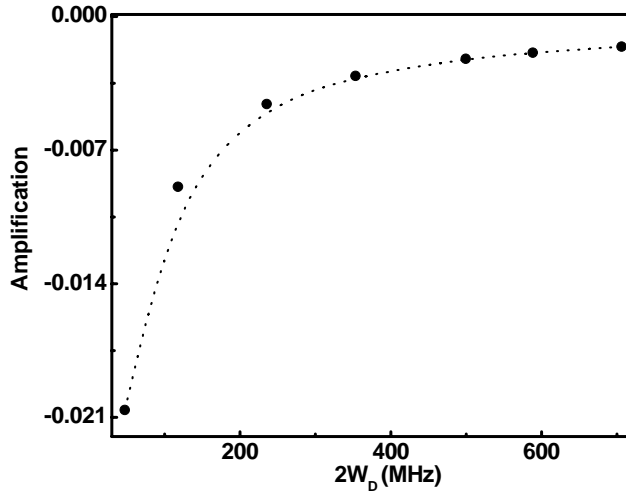


Fig. 5.10: Variation of amplification with Doppler width. Other data are same as in Fig. 5.1.

In order to contrast the behavior of the DDL system of D_1 transition with that of D_2 transition under Doppler averaging, we show in Fig. 5.11 the effect of Doppler broadening on the absorption spectrum of Fig. 5.7. Absorption spectrum here is a familiar profile that corresponds to the EIT resonance as was studied in Chapter-4. These observations highlight the remarkable features of a coherently driven DDL system.

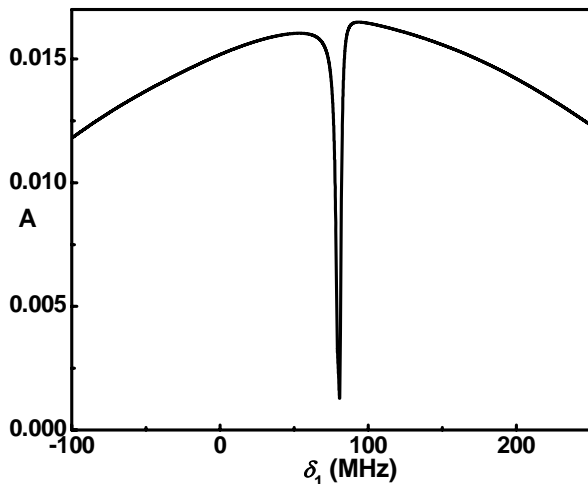


Fig. 5.11: Effect of Doppler broadening ($2W_D = 510$ MHz) on the probe absorption spectrum for the data of Fig. 5.7.

AWI resonance under Doppler averaging (*cf.* Fig. 5.9) exhibits finite linewidth (Γ_{AWI}), which is a strong function of the pump intensity as may be seen from Fig. 5.12.

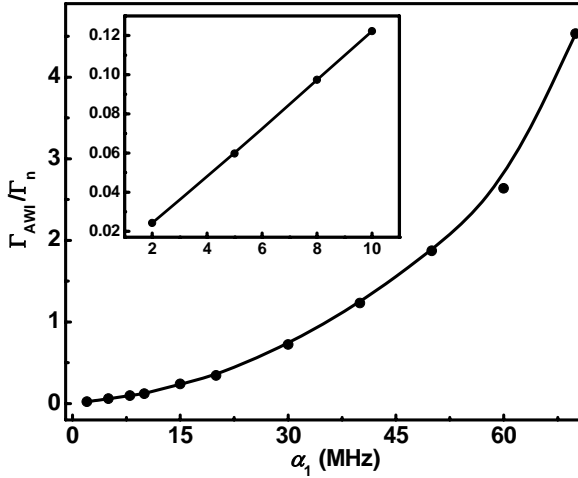


Fig. 5.12: Variation of the width of Doppler averaged AWI resonance with pump intensity (α_1). Here $2W_D = 500$ MHz and other data are same as in Fig. 5.1. Inset shows the linear behaviour of Γ_{AWI} at low pump intensities.

While the complexities involved in the four-level system do not permit us to obtain a closed form solution for AWI half-width (Γ_{AWI}), it may be interesting to compare the observed behavior of Γ_{AWI} with that of the linewidth of an EIT spectrum. For a three-level Λ system, the linewidth of EIT follows Eq. (3.27). Analogous behaviour is observed in Fig. 5.12 for Γ_{AWI} . For $\alpha_1 < 10$ MHz, Γ_{AWI} varies linearly with respect to α_1 , while for $\alpha_1 > 10$ MHz, the dependence is quadratic.

5.5. Quantum Jump Approach to AWI

Physical insight into the problem may be obtained by employing the quantum jump approach proposed by Cohen Tannoudji [206]. This approach has been used in several works to identify the processes responsible for amplification of the medium [206-208], and also in the studies of absorption mechanism in a four-level N system [209] and dissipative dynamics in quantum optics [210].

For the system under consideration we define the manifold $\zeta(N_1, N_2)$ of atom + laser system such that

$$\zeta(N_1, N_2) = \{ | \{3,4\}, N_1, N_2 \rangle, | 2, N_1, N_2 + 1 \rangle, | 1, N_1 + 1, N_2 \rangle \}, \quad (5.14)$$

where N_1 and N_2 refer to the number of photons associated with the probe and pump fields, and notation $\{3,4\}$ is used to denote simultaneous excitation of $|3\rangle$ and $|4\rangle$ by both pump and probe fields. Time evolution of the atomic system is viewed as coherent evolution within a manifold as determined by four Rabi frequencies and detunings, and quantum jumps to a neighboring manifold is governed by the dissipative processes. Different manifolds $\zeta(N_1, N_2)$ relevant for the present discussion are shown in Fig. 5.13.

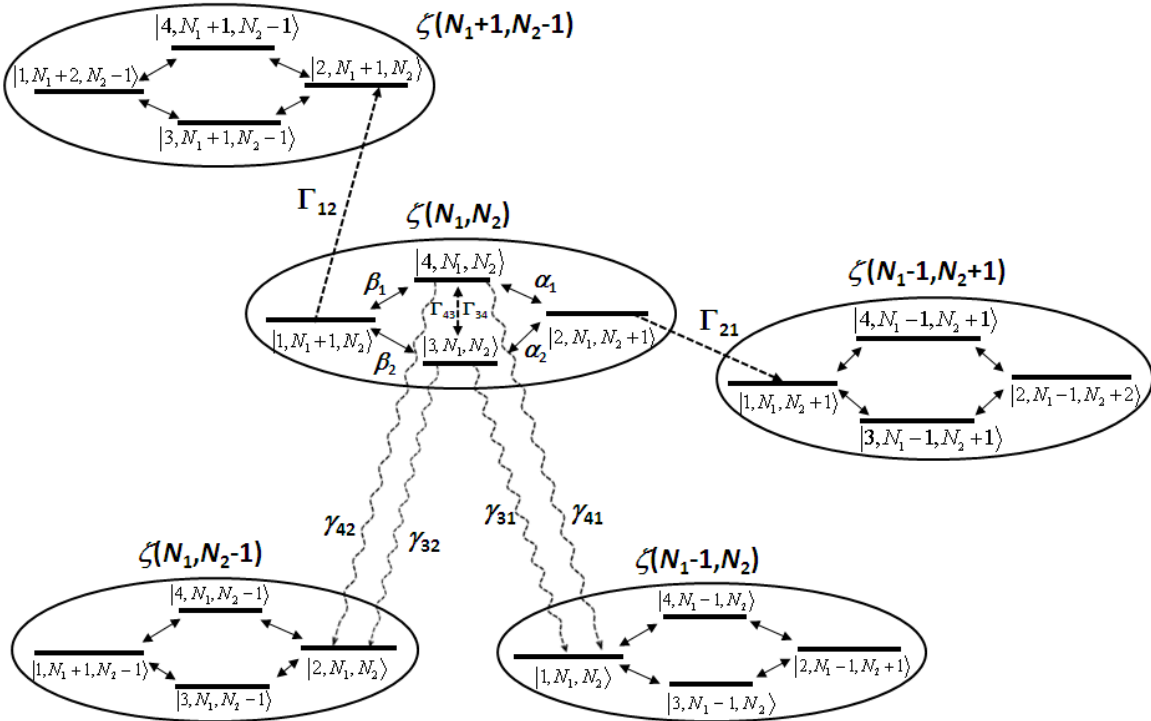


Fig. 5.13: Different manifolds of atom + photon system for a DDL scheme. Coherent coupling between the states within a manifold is characterized by Rabi frequencies as shown by solid arrows. Quantum jumps are governed by incoherent processes which cause jump of the system from one manifold to other. These radiative and non-radiative dissipative processes are shown by wavy and dashed lines respectively.

Spontaneous emissions from $\{3,4\}$ to $|1\rangle$ and $|2\rangle$ make the system to jump from the manifold $\zeta(N_1, N_2)$ to the manifolds $\zeta(N_1 - 1, N_2)$ and $\zeta(N_1, N_2 - 1)$ respectively, while the collisional decay processes characterized by rates Γ_{12} and Γ_{21} bring it to the manifolds $\zeta(N_1 + 1, N_2 - 1)$ and $\zeta(N_1 - 1, N_2 + 1)$ respectively. The incoherent decay rates Γ_{34}, Γ_{43} do not change the manifold of the system.

We now define the coherent period (i, j) in a given manifold $\zeta(N_1, N_2)$ such that the system enters the manifold in the state $|i\rangle$ and leaves it from state $|j\rangle$ by quantum jumps. Of the 9 periods involved in the present problem, only four periods, i.e., (1,2), (2,1), (1, {3,4}) and ({3,4},1) contribute to the change in N_1 . Here the periods (1,2) and (2,1) correspond respectively to stimulated Raman loss and gain processes respectively, while (1,{3,4}) and ({3,4},1) correspond to probe absorption and stimulated emission processes respectively. The mean change in the number of probe and pump photons is related to the probability $P(i, j)$ of observing a coherent period (i, j) such that

$$P(i, j) = P(j)P(j|i), \quad (5.15)$$

where $P(j|i)$ is the conditional probability that given the period has started in $|i\rangle$, it ends in $|j\rangle$ and $P(i)$ is the probability that a randomly chosen period starts in $|i\rangle$, i.e.,

$$P(i) = \sum_j P(j)Q(i_{start} | j_{start}). \quad (5.16)$$

Here $Q(i_{start} / j_{start})$ is the conditional probability of starting a period in $|i\rangle$ given that the previous period has started in $|j\rangle$ and $\sum_j P(j) = 1$. The conditional probability is given by

$$Q(i_{start} | j_{start}) = \sum_k P(k | j) \Xi_{ki}, \quad (5.17)$$

where $\sum_i Q(i_{start} | j_{start}) = 1$ for all j_{start} and Ξ_{ki} is the jump probability, i.e., probability that the quantum jump starts from $|k\rangle$ of a given manifold and ends in $|i\rangle$ of a neighboring manifold. From Fig. 5.13 it is clear that

$$\begin{aligned}\Xi_{1i} &= \delta_{2i}, & \Xi_{2i} &= \delta_{1i}, \\ \Xi_{3i} &= \delta_{1i} \frac{\gamma_{31}}{\gamma_3} + \delta_{2i} \frac{\gamma_{32}}{\gamma_3}, & \Xi_{4i} &= \delta_{1i} \frac{\gamma_{41}}{\gamma_4} + \delta_{2i} \frac{\gamma_{42}}{\gamma_4}.\end{aligned}\quad (5.18)$$

Using Eq. (5.17) – (5.18) it is easy to show that $Q(\{3,4\} | j_{start}) = 0$ for all j . Consequently $P(\{3,4\}) = 0$ and $P(\{3,4\}, 1) = 0$. Now denoting by $\langle \Delta N_1 \rangle$ the mean change (decrease) in the number of photons, we find

$$\langle \Delta N_1 \rangle = P(1, 2) - P(2, 1) + P(1, \{3, 4\}). \quad (5.19)$$

The conditional probability $P(j/i)$ required for evaluation of $\langle \Delta N_1 \rangle$ is given by

$$P(j/i) = G_j \int_0^\infty |c_{ij}(\tau)|^2 d\tau, \quad (5.20)$$

where G_j is the total departure rate from $|j\rangle$ via a quantum jump, i.e., $G_1 = 2\Gamma_{12}$, $G_2 = 2\Gamma_{21}$, $G_3 = 2\gamma_3$ and $G_4 = 2\gamma_4$, and $c_{ij}(\tau)$ is the probability amplitude of finding an atom in $|j\rangle$ at time $t + \tau$ when it started its coherent evolution in $|i\rangle$ at time t , i.e., $c_{ij}(\tau) = \langle j | \exp(-iH_{eff}\tau) | i \rangle$. The effective non-Hermitian Hamiltonian [211] relevant to the atomic system of Fig. 5.13 is given as

$$H_{eff} = \begin{pmatrix} -i\Gamma_{12} & 0 & -\beta_2 & -\beta_1 \\ 0 & (\delta_1 - \Delta_1) - i\Gamma_{21} & -\alpha_2 & -\alpha_1 \\ -\beta_2 & -\alpha_2 & \delta_2 - i\gamma_3 & 0 \\ -\beta_1 & -\alpha_1 & 0 & \delta_1 - i\gamma_4 \end{pmatrix}. \quad (5.21)$$

The equations of motion for $c_{ij}(\tau)$ can therefore be obtained as,

$$\dot{C}_{i1}(\tau) = -\Gamma_{12}C_{i1} + i\beta_2C_{i3} + i\beta_1C_{i4}, \quad (5.22a)$$

$$\dot{C}_{i2}(\tau) = -[\Gamma_{21} + i(\delta_1 - \Delta_1)]C_{i2} + i\alpha_2C_{i3} + i\alpha_1C_{i4}, \quad (5.22b)$$

$$\dot{C}_{i3}(\tau) = i\beta_2C_{i1} + i\alpha_2C_{i2} - (\gamma_3 + i\delta_2)C_{i3}, \quad (5.22c)$$

$$\dot{C}_{i4}(\tau) = i\beta_1C_{i1} + i\alpha_1C_{i2} - (\gamma_4 + i\delta_1)C_{i4}, \quad (5.22d)$$

These equations are solved with initial conditions $C_{ij}(\tau=0) = \delta_{ij}$. We use adiabatic elimination technique to obtain C_{ij} (cf. Appendix-4), which are then used to calculate $P(j/i)$ and $P(i,j)$. Without the loss of generality we take $G_3 = G_4 = G_{34}$ and write $P(1, \{3,4\})$ as

$$P(1, \{3,4\}) = G_{34}P(1) \int_0^\infty |c_{13}(\tau) + c_{14}(\tau)|^2 d\tau = P(1,3) + P(1,4) + P_{\text{interference}}, \quad (5.23)$$

where $P_{\text{interference}}$ is the interference term arising from the simultaneous absorption processes $|1\rangle \rightarrow |3\rangle, |4\rangle$ and is defined as

$$P_{\text{interference}} = 2G_{34}P(1) \int_0^\infty \text{Re}(c_{13}^*(\tau)c_{14}(\tau))d\tau. \quad (5.24)$$

Eq. (5.19) then takes the form

$$\langle \Delta N_1 \rangle = P(1,2) - P(2,1) + P(1,3) + P(1,4) + P_{\text{interference}}. \quad (5.25)$$

and the probe absorption is given by $A \propto \langle \Delta N_1 \rangle$. AWI therefore corresponds to the situation where $\langle \Delta N_1 \rangle < 0$. In Fig. 5.14 we show explicitly the relative contributions of the terms on the right side of Eq. (5.25) in the spectral region where AWI is observed. We see here that while $P(1,2), P(2,1), P(1,3), P(1,4)$ are positive, $P_{\text{interference}}$ is negative and

this particular contribution is responsible for the observation of AWI in the DDL system. As a counter example, we show in Fig. 5.15 the behavior of the various terms contributing to $\langle \Delta N_1 \rangle$ for a DDL system of ^{87}Rb D_2 transition.

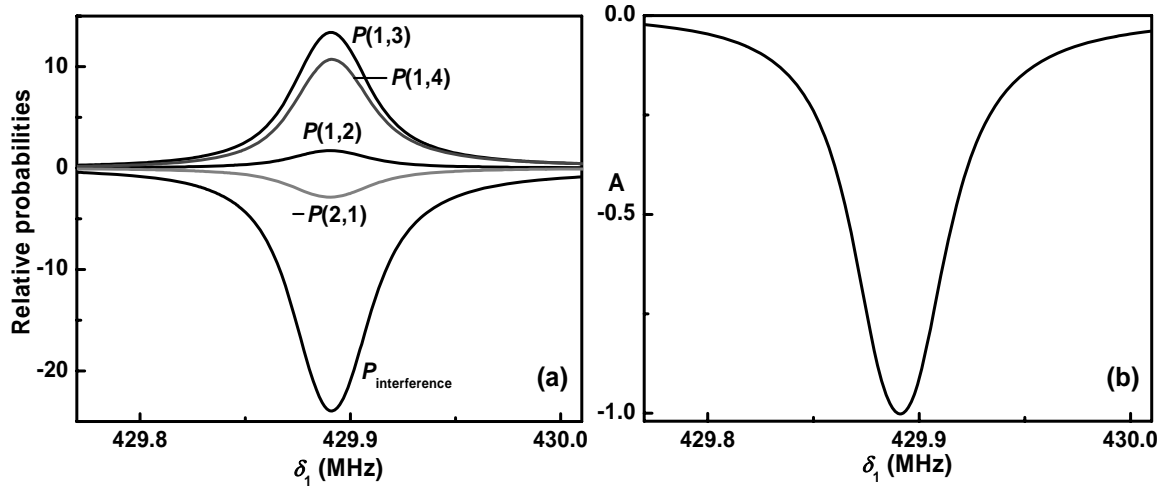


Fig. 5.14: (a): Relative probabilities of coherent periods and (b) relative absorption (in terms of $\langle \Delta N_1 \rangle$) at $\delta_1 = \Delta_1$ for the data of Fig. 5.1.

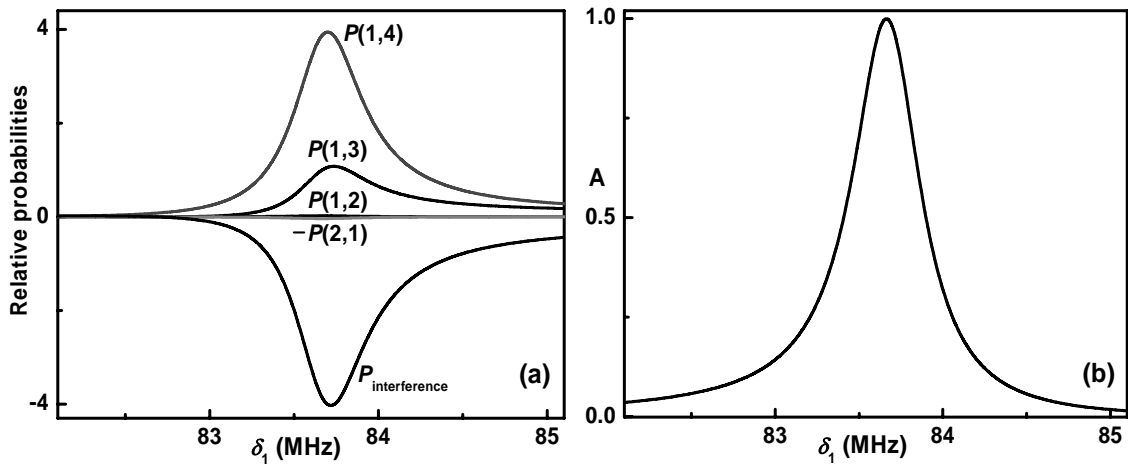


Fig. 5.15: (a): Relative probabilities of coherent periods and (b) relative absorption (in terms of $\langle \Delta N_1 \rangle$) at $\delta_1 = \Delta_1$ for the data of Fig. 5.7.

We observe in Fig. 5.15 that $|P_{\text{interference}}| < P(1,3) + P(1,4)$ at $\delta_1 = \Delta_1$, which results in absorption instead of AWI. It is thus clear that the interference in one-photon absorption processes is primarily responsible for the observation of AWI.

CHAPTER 6

COHERENCE AND INTERFERENCE IN DOUBLE DARK RESONANT SYSTEMS

6.1 Introduction

Coherent pump-probe spectroscopy of double dark resonant systems has received considerable attention in recent times. Some of the interesting four-level configurations discussed in the literature are N-resonance, Y type, K type and tripod systems [26-31]. The presence of additional atomic states and extra control fields has marked effect on the coherent dynamics of such systems and pose an advantage of control over more physical variables. These systems are associated with the observation of ultra-narrow ‘double dark’ resonances, i.e. splitting of dark state resonance associated with EIT. Double dark resonant systems have been studied in contexts of sub-Doppler and sub-natural narrowing [26-31], coherent hole burnings [212,213], optical switching [214-217], slow and fast light [218-220], enhanced cross phase modulation and Kerr nonlinearity [219-222], squeezed vacuum survival [223], AWI [224] and numerous other applications [225-227].

A tripod system is an extension of a three-level Λ system where an additional transition from a nearby ground level is driven by a third control field [28-30]. The main issue examined here is the demonstration of double dark resonances i.e. two EIT windows in this system and control of their linewidths. The other system studied in this chapter is a four level system in N-configuration. Three-photon resonance in this system is reported as a promising alternative to CPT resonance for atomic frequency standards [227]. An interesting feature of N system is that it can show EIA, EIT and AWI depending on the tri-chromatic field parameters [40-43]. We study the effect of driving fields on the optical response of this system, particularly in the context of inversion in dressed states, observation of more than one transparency window and switching between EIT and EIA. The effect of spontaneously generated coherence (SGC) on the linear and nonlinear response of N system is also investigated. The chapter is concluded with an experimental study of EIT in N system and its comparison with Λ system.

6.2 Double Control EIT Resonances in Tripod System

6.2.1 Model and Basic Formulation

We consider a tripod system (*cf.* Fig. 2.1(b)) where levels $|1\rangle$, $|3\rangle$ and $|4\rangle$ form the usual Λ system such that a pump laser of frequency Ω_1 excites $|1\rangle \rightarrow |4\rangle$ transition and a probe laser of frequency Ω_3 is tuned across $|3\rangle \rightarrow |4\rangle$ resonance. Level $|2\rangle$ is an additional ground level that is connected to the excited level $|4\rangle$ by a control laser of frequency Ω_2 . Such a system can be realized within the Zeeman manifold of alkali atoms placed in magnetic field and using appropriate polarizations of the excitation fields. The

Rabi frequencies of pump, control and probe beams are $2\alpha_1$, $2\alpha_2$ and $2\alpha_3$ respectively (cf. Eq. (2.88)) and the relevant detunings are defined in Eq. (2.89). The system is characterized by radiative decay rates $2\gamma_{41}$, $2\gamma_{42}$ and $2\gamma_{43}$. There exist additional non-radiative decay rates, $2\Gamma_{ij}$, ($i, j = 1, 2, 3$), i.e., those involving the three ground levels. The time evolution of this system is governed by the master Eq. (2.86). The elements of density operator satisfy the following equations:

$$d\rho_{11}/dt = -2\Gamma_1\rho_{11} - i\alpha_1(\rho_{14} - \rho_{41}) + 2\Gamma_{21}\rho_{22} + 2\Gamma_{31}\rho_{33} + 2\gamma_{41}\rho_{44}, \quad (6.1a)$$

$$d\rho_{12}/dt = -b_1\rho_{12} - i\alpha_2\rho_{14} + i\alpha_1\rho_{42}, \quad (6.1b)$$

$$d\rho_{13}/dt = -b_2\rho_{13} - i\alpha_3\rho_{14} + i\alpha_1\rho_{43}, \quad (6.1c)$$

$$d\rho_{14}/dt = -i\alpha_1(\rho_{11} - \rho_{44}) - i\alpha_2\rho_{12} - i\alpha_3\rho_{13} - b_3\rho_{14}, \quad (6.1d)$$

$$d\rho_{22}/dt = 2\Gamma_{12}\rho_{11} - 2\Gamma_2\rho_{22} - i\alpha_2(\rho_{24} - \rho_{42}) + 2\Gamma_{32}\rho_{33} + 2\gamma_{42}\rho_{44}, \quad (6.1e)$$

$$d\rho_{23}/dt = -b_4\rho_{23} - i\alpha_3\rho_{24} + i\alpha_2\rho_{43}, \quad (6.1f)$$

$$d\rho_{24}/dt = -i\alpha_1\rho_{21} - i\alpha_2(\rho_{22} - \rho_{44}) - i\alpha_3\rho_{23} - b_5\rho_{24}, \quad (6.1g)$$

$$d\rho_{33}/dt = 2\Gamma_{13}\rho_{11} + 2\Gamma_{23}\rho_{22} - 2\Gamma_3\rho_{33} - i\alpha_3(\rho_{34} - \rho_{43}) + 2\gamma_{43}\rho_{44}, \quad (6.1h)$$

$$d\rho_{34}/dt = -i\alpha_1\rho_{31} - i\alpha_2\rho_{32} - i\alpha_3(\rho_{33} - \rho_{44}) - b_6\rho_{34}, \quad (6.1i)$$

$$d\rho_{44}/dt = -i\alpha_1(\rho_{41} - \rho_{14}) - i\alpha_2(\rho_{42} - \rho_{24}) - i\alpha_3(\rho_{43} - \rho_{34}) - 2\gamma_4\rho_{44}, \quad (6.1j)$$

where various coefficients b_i , ($i = 1, 2 \dots 6$) are defined as

$$\begin{aligned} b_1 &= \Gamma_1 + \Gamma_2 - i(\Delta_1 - \Delta_2), & b_2 &= \Gamma_1 + \Gamma_2 - i(\Delta_1 - \Delta_3), & b_3 &= \Gamma_1 + \gamma_4 - i\Delta_1, \\ b_4 &= \Gamma_2 + \Gamma_3 - i(\Delta_2 - \Delta_3), & b_5 &= \Gamma_2 + \gamma_4 - i\Delta_2, & b_6 &= \Gamma_3 + \Gamma_4 - i\Delta_3, \end{aligned} \quad (6.2)$$

$$\Gamma_1 = \Gamma_{12} + \Gamma_{13}, \quad \Gamma_2 = \Gamma_{21} + \Gamma_{23}, \quad \Gamma_3 = \Gamma_{31} + \Gamma_{32}, \quad \gamma_4 = \gamma_{41} + \gamma_{42} + \gamma_{43}. \quad (6.3)$$

In what follows we are interested in steady state absorption of the weak probe field

$A = \text{Im}(\rho_{43}\gamma_{43} / \alpha_3)$, where ρ_{43} is the induced polarization on $|4\rangle \rightarrow |3\rangle$ transition. For weak probe field, i.e. $\alpha_3 \ll \alpha_1, \alpha_2$, analytical solution for ρ_{43} can be obtained as

$$\rho_{43}^{(1)} = \frac{\alpha_3[\alpha_2 b_2 \rho_{24}^{(0)} + \alpha_1 b_4 \rho_{14}^{(0)} + i b_2 b_4 (\rho_{33}^{(0)} - \rho_{44}^{(0)})]}{b_2 b_4 b_6^* + \alpha_1^2 b_4 + \alpha_2^2 b_2}, \quad (6.4a)$$

$$\rho_{24}^{(0)} = \frac{i\alpha_2[(b_1^* b_3^* + \alpha_2^2)(\rho_{44}^{(0)} - \rho_{22}^{(0)}) + \alpha_1^2(\rho_{11}^{(0)} - \rho_{44}^{(0)})]}{b_5 b_1^* b_3^* + \alpha_1^2 b_3^* + \alpha_2^2 b_5}, \quad (6.4b)$$

$$\rho_{14}^{(0)} = \frac{i\alpha_1[(b_1 b_5^* + \alpha_1^2)(\rho_{44}^{(0)} - \rho_{11}^{(0)}) + \alpha_2^2(\rho_{22}^{(0)} - \rho_{44}^{(0)})]}{b_5 b_1^* b_3^* + \alpha_1^2 b_3^* + \alpha_2^2 b_5}. \quad (6.4c)$$

The steady state populations of the system are given in *Appendix-5*. Detailed analysis shows that $\rho_{33}^{(0)} \approx 1$, $\rho_{ij}^{(0)} \approx 0$, ($i, j \neq 3$) and hence

$$\rho_{43}^{(1)} = \alpha_3(p_T - iq_T)/(r_T - is_T), \quad (6.5)$$

$$p_T = (\Gamma_1 + \Gamma_3)(\Gamma_2 + \Gamma_3) - (\Delta_1 - \Delta_3)(\Delta_2 - \Delta_3), \quad (6.6a)$$

$$q_T = (\Gamma_1 + \Gamma_3)(\Delta_2 - \Delta_3) + (\Gamma_2 + \Gamma_3)(\Delta_1 - \Delta_3), \quad (6.6b)$$

$$r_T = \Delta_3(p_T + \alpha^2) - \alpha_1^2 \Delta_2 - \alpha_2^2 \Delta_1 - (\Gamma_3 + \gamma_4)q_T, \quad (6.6c)$$

$$s_T = (\Gamma_3 + \gamma_4)p_T + \alpha_1^2(\Gamma_2 + \Gamma_3) + \alpha_2^2(\Gamma_1 + \Gamma_2) + \Delta_3 q_T, \quad (6.6d)$$

where $\alpha^2 = \alpha_1^2 + \alpha_2^2$. For coherent spectroscopy in vapour cells containing dilute atomic gas, collisional relaxation rates are negligible, therefore Γ_{ij} can be neglected to obtain,

$$\rho_{43}^{(1)} = \frac{\alpha_3(\Delta_1 - \Delta_3)(\Delta_2 - \Delta_3)}{\alpha_2^2 \Delta_1 + \alpha_1^2 \Delta_2 - \Delta_3(\alpha_1^2 + \alpha_2^2) + (\Delta_1 - \Delta_3)(\Delta_2 - \Delta_3)(\Delta_3 - i\gamma_4)}. \quad (6.7)$$

Further in the absence of control laser ($\alpha_2 = \Delta_2 = 0$), Eq. (6.7) gives the familiar result for a three-level Λ system [6], i.e.

$$\rho_{43}^{(1)} = \alpha_3(\Delta_1 - \Delta_3)/[\alpha_1^2 - i(\gamma_4 + i\Delta_3)(\Delta_1 - \Delta_3)]. \quad (6.8)$$

The dressed state resonances for a tripod system in the absence of Doppler broadening, thus, appear at $\Delta_3 = \varepsilon_{T1}, \varepsilon_{T2}$ and ε_{T3} which are the roots of following equation

$$\Delta_3^3 - \Delta_3^2(\Delta_1 + \Delta_2) + \Delta_3(\Delta_1\Delta_2 - \alpha_1^2 - \alpha_2^2) + \alpha_2^2\Delta_1 + \alpha_1^2\Delta_2 = 0. \quad (6.9)$$

For a Λ system (*cf.* Eq. (6.8)), there exist two dressed state resonances located at

$$\Delta_3 = (\Delta_1 \pm \sqrt{\Delta_1^2 + 4\alpha_1^2})/2. \quad (6.10)$$

Note that for a tripod system the susceptibility vanishes identically at $\Delta_3 = \Delta_1$ and $\Delta_3 = \Delta_2$ (*cf.* Eq. (6.7)), and these correspond to the positions of two EIT resonances.

6.2.2 Results and Discussion

We calculate the probe absorption spectrum for Λ and tripod systems for a range of Rabi frequencies and detunings using the radiative data of D_2 transition of ^{87}Rb atoms. Non-radiative decay rates are taken to be 1 kHz corresponding to the transit time in typical experiments conducted in vapour cells without buffer gas. Typical results for representative atom-field interaction data are shown in Fig. 6.1. For Λ system, there appear two dressed state resonances at Δ_3 given by Eq. (6.10), and an EIT resonance at $\Delta_3 = \Delta_1$. For tripod system, there exist three dressed state resonances at $\varepsilon_{T1,T2} = (\Delta_1 \pm \sqrt{\Delta_1^2 + 4\alpha_1^2})/2$ and $\varepsilon_{T3} \sim \Delta_2$ when $\alpha_2 < \alpha_1$. Further the system exhibits two EIT resonances at $\Delta_3 = \Delta_1$ and $\Delta_3 = \Delta_2$ (*cf.* Fig. 6.1(b)). A special case of the tripod system corresponds to the equal detuning of the pump and control lasers, i.e., $\Delta_1 = \Delta_2$. In this case one observes two dressed state resonances at $(\Delta_1 \pm \sqrt{\Delta_1^2 + 4\alpha^2})/2$, and a single EIT at $\Delta_3 = \Delta_1$.

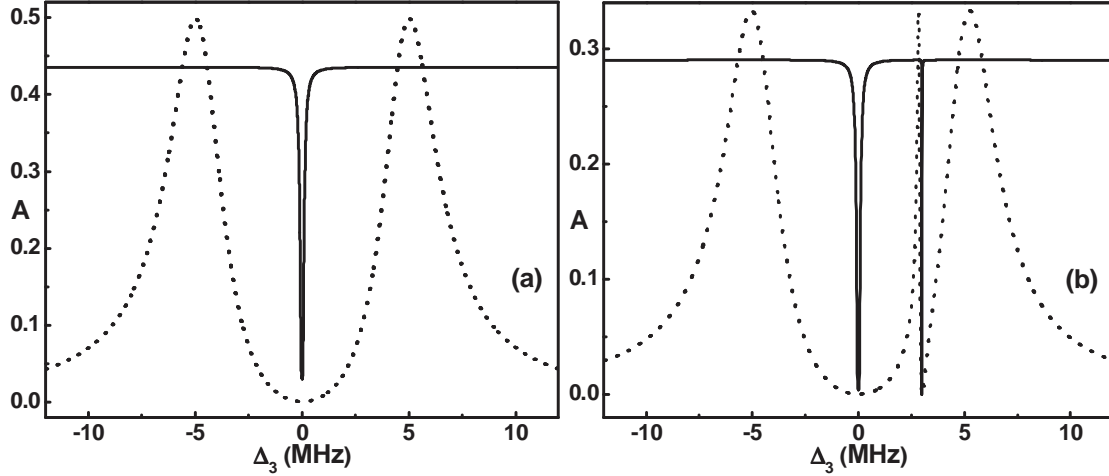


Fig. 6.1: Probe absorption spectrum for (a) Λ system with $(\alpha_1, \Delta_1) = (5, 0)$ MHz, and (b) tripod system with $(\alpha_1, \Delta_1, \alpha_2, \Delta_2) = (5, 0, 1, 3)$ MHz. The dotted and solid curves (scaled up by 50) in each frame correspond to spectra in the absence ($2W_D = 0$) and presence ($2W_D = 510$ MHz) of Doppler broadening.

We now focus on the quantity of interest which is the linewidth (Γ_{EIT}) of EIT resonance. In Fig. 6.1, the EIT resonance in the Λ system has $\Gamma_{EIT} \sim 0.034\Gamma_n$, whereas the linewidths of two EIT resonances in the tripod system, i.e., $\Gamma_{EIT}(\Delta_3 = \Delta_1)$ and $\Gamma_{EIT}(\Delta_3 = \Delta_2)$, are $\sim 0.032\Gamma_n$ (nearly equal to that for Λ system) and $\sim 10^{-3}\Gamma_n$ respectively. The possibility of observing an ultra-narrow EIT profile by use of a control laser field makes the tripod system interesting in applications related to metrology. For $\Delta_1 = \Delta_2$, a single EIT resonance of width $\sim 0.034\Gamma_n$ appears at $\Delta_3 = \Delta_1 = \Delta_2$ similar to that in a Λ system (*cf.* Fig. 6.1(a)). It is thus possible to manipulate the probe response of a Λ system by inclusion of an additional control field. The control laser Rabi frequency has a dramatic effect on the EIT resonances in a tripod system. Fig. 6.2 shows the behaviour of EIT resonances as a function of α_2 . It is seen in Fig. 6.2 that $\Gamma_{EIT}(\Delta_3 = \Delta_1)$ and $\Gamma_{EIT}(\Delta_3 = \Delta_2)$ are both of sub-natural linewidth at low strengths of pump and control fields, and their linewidths are proportional to respective field strengths. On increasing

the control field strength, both EIT resonances broaden, however, $\Gamma_{EIT}(\Delta_3 = \Delta_2)$ increases at a much faster rate compared to $\Gamma_{EIT}(\Delta_3 = \Delta_1)$. The broadening in both resonances is asymmetric with respect to their line centers, particularly at large α_2 . It is interesting to note from Fig. 6.2 that while both the EIT resonances broaden, they do not overlap even at large α_2 and there always exists a narrow absorption window in between two EIT resonances. Interestingly linewidth of this absorption window can be made sub-natural or even ultra-narrow by increasing the control field strength (*cf.* Fig. 6.2(d)).

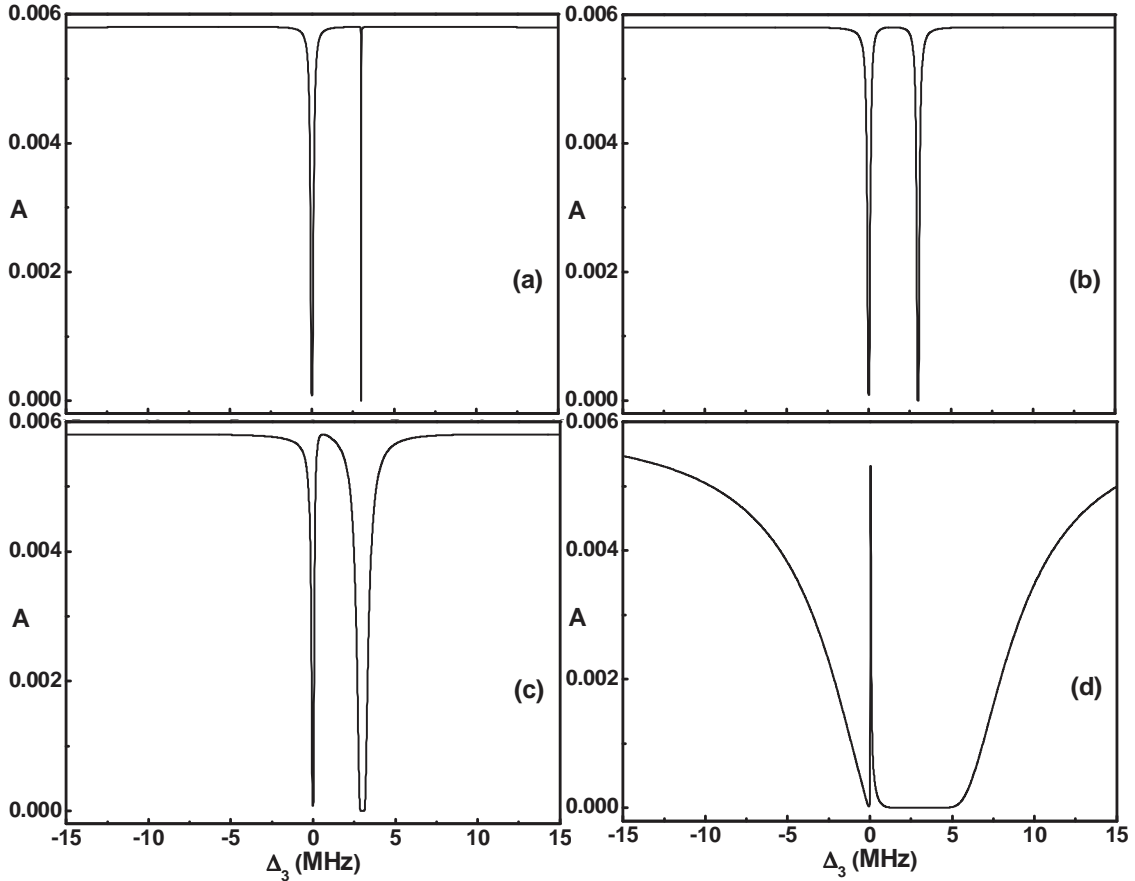


Fig. 6.2: EIT in a tripod system as a function of control field strength α_2 . Here $(\alpha_1, \Delta_1, \Delta_2) = (5, 0, 3)$ MHz. $2W_D = 510$ MHz, $\gamma_{41} = \gamma_{42} = \gamma_{43} = 1.017$ MHz. $\alpha_2 = 1, 5, 10$ and 40 MHz for frames (a) to (d) respectively.

We now examine the behaviour of EIT linewidth for tripod system in the light of three-level Λ system. Fig. 6.3(a) and 6.4(a) show the variation of EIT linewidths with

control Rabi frequency (α_2) for fixed $\alpha_1, \alpha_3, \Delta_1$ and Δ_2 . We observe that $\Gamma_{EIT}(\Delta_3 = \Delta_1)$ is a much weaker function of control intensities compared to $\Gamma_{EIT}(\Delta_3 = \Delta_2)$.

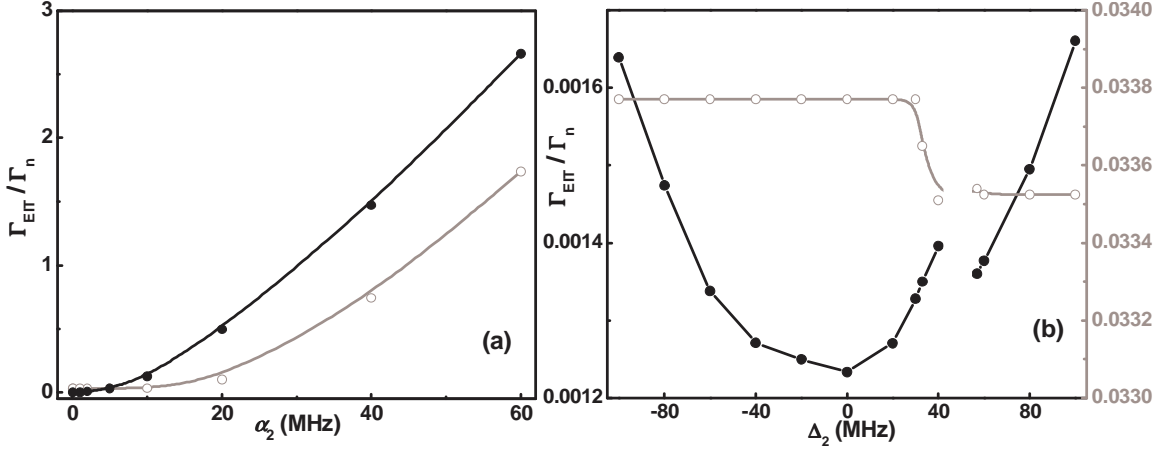


Fig. 6.3: EIT widths as a function of (a) control Rabi frequency and (b) control field detuning. Here $\alpha_1 = 5$ MHz. For frame (a) $(\Delta_1, \Delta_2) = (0, 3)$ MHz and for frame (b) $(\alpha_2, \Delta_1) = (1, 50)$ MHz. The gray and black curves represent EIT at $\Delta_3 = \Delta_1$ and $\Delta_3 = \Delta_2$ respectively. Note the scale for $\Gamma_{EIT}(\Delta_3 = \Delta_1)$ on the right hand side of frame (b).

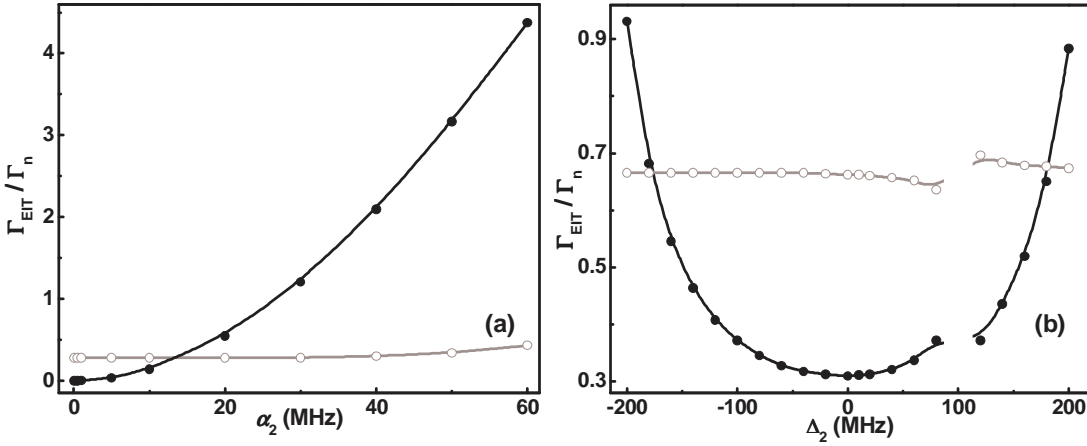


Fig. 6.4: EIT widths as a function of (a) control Rabi frequency and (b) control field detuning. Here $\alpha_1 = 20$ MHz. For frame (a) $(\Delta_1, \Delta_2) = (0, 20)$ MHz and for frame (b) $(\alpha_2, \Delta_1) = (15, 100)$ MHz. The gray and black curves represent EIT at $\Delta_3 = \Delta_1$ and $\Delta_3 = \Delta_2$ respectively.

At lower intensities of control laser, $\Gamma_{EIT}(\Delta_3 = \Delta_1)$ remains almost constant. This implies that at lower α_2 , $\Gamma_{EIT}(\Delta_3 = \Delta_1)$ is a function of pump strength α_1 only. At higher

α_2 , both the strong fields contribute to its width. This behaviour is more evident in Fig. 6.4(a) where $\alpha_1 > \alpha_2$. Contrarily $\Gamma_{EIT}(\Delta_3 = \Delta_2)$ closely follows the behaviour predicted in a Λ system. For low pump intensity, i.e., $\alpha_2 \ll \alpha_s$, $\Gamma_{EIT}(\Delta_3 = \Delta_2) \propto \alpha_2 \sqrt{\Gamma_{13}/\Gamma_n}$, which gives a linear dependence on α_2 . On the other hand when $\alpha_2 \gg \alpha_s$, $\Gamma_{EIT}(\Delta_3 = \Delta_2) \propto \alpha_2^2$ and that corresponds to the region where the optical pumping rate α_2^2/Γ_n starts to exceed Γ_{13} and the susceptibility of the atomic medium exhibits square dependence on α_2 , where $\alpha_s \sim W_D \sqrt{\Gamma_{13}/\Gamma_n}$ is the saturation intensity. The crossover between the two curves in Fig. 6.3(a) and 6.4(a) represent the case when control and pump fields are of equal strengths which causes $\Gamma_{EIT}(\Delta_3 = \Delta_1) = \Gamma_{EIT}(\Delta_3 = \Delta_2)$. Until this crossover $\Gamma_{EIT}(\Delta_3 = \Delta_1)$ is constant and after this point both α_1 and α_2 contribute to its width. When $\alpha_2 \gg \alpha_1$ $\Gamma_{EIT}(\Delta_3 = \Delta_1)$ increases much faster, almost parallel with $\Gamma_{EIT}(\Delta_3 = \Delta_2)$ i.e., the stronger field α_2 has the major contribution to its width.

Fig. 6.3(b) and 6.4(b) shows the dependence of control field detuning (Δ_2) on the width of the two EIT windows for fixed α_1 , α_2 , α_3 and Δ_1 . It is seen that $\Gamma_{EIT}(\Delta_3 = \Delta_2)$ exhibits a stronger dependence on Δ_2 compared to $\Gamma_{EIT}(\Delta_3 = \Delta_1)$. Note here that in Fig. 6.3(b), $\Gamma_{EIT}(\Delta_3 = \Delta_2) < \Gamma_{EIT}(\Delta_3 = \Delta_1)$ since $\alpha_2 < \alpha_1$. While $\Gamma_{EIT}(\Delta_3 = \Delta_1)$ remains fairly constant, $\Gamma_{EIT}(\Delta_3 = \Delta_2)$ is minimum at $\Delta_3 = \Delta_2$ and shows quadratic dependence on Δ_2 . Further both the EIT resonances exhibit minimum width at the respective two-photon resonance conditions. Interestingly in the vicinity of $\Delta_1 = \Delta_2$ both EIT widths undergo rapid changes resulting in a discontinuous behaviour at $\Delta_1 = \Delta_2$. As discussed before, at

$\Delta_1 = \Delta_2$, the two EIT resonances become degenerate and that results in $\Gamma_{EIT}(\Delta_3 = \Delta_1) = \Gamma_{EIT}(\Delta_3 = \Delta_2)$. In Fig. 6.3(b) and 6.4(b) this condition is satisfied at $\Delta_2 = 50$ and 100 MHz respectively and consequently the behaviour of EIT at these points are not shown.

6.3 Pump-Probe Spectroscopy of N-Resonance System

6.3.1 Variants of N System

We consider here a typical example of N system formed by D_2 transition of ^{87}Rb as shown in Fig 2.1(c). The four level subset forming the N scheme are $|1\rangle \equiv |5s_{1/2} F=1\rangle$, $|2\rangle \equiv |5s_{1/2} F=2\rangle$, $|3\rangle \equiv |5p_{3/2} F'=1\rangle$ and $|4\rangle \equiv |5p_{3/2} F'=2\rangle$. Depending on choice of probe field three completely different configurations can be realized within the manifold.

Model A: In this configuration field E_3 is used as the probe. The scheme can be identified as an ideal three-level Λ system for EIT comprising of $|1\rangle \rightarrow |4\rangle$ and $|2\rangle \rightarrow |4\rangle$ transitions driven by strong pump E_2 and a weak probe E_3 respectively. This system is perturbed by an additional strong field E_1 coupling $|1\rangle \rightarrow |3\rangle$ transition.

Model B: In this scheme the field E_1 is used as the probe. Here a V system formed by transitions $|1\rangle \rightarrow |3\rangle$ and $|1\rangle \rightarrow |4\rangle$ is driven by an additional field E_3 .

Model C: Here two strong fields E_1 and E_3 dress the transitions $|1\rangle \rightarrow |3\rangle$ and $|2\rangle \rightarrow |4\rangle$ respectively. The resulting dressed states are probed by a weak probe laser E_2 scanned across $|1\rangle \rightarrow |4\rangle$ transition. The scheme can be thought of as two quasi-independent ‘two-level systems’ $|1\rangle \rightarrow |3\rangle$ and $|2\rangle \rightarrow |4\rangle$ being coupled by the weak probe.

Note that in models A and B the probe field shares a common level with one of the strong fields E_2 which results in the observation of EIT or EIA at the two-photon resonance conditions $\Delta_3 = \Delta_2$ and $\Delta_1 = \Delta_2$ respectively, whereas in model C probe field shares a common level with both the strong fields which yields interesting characteristics in the absorption and dispersion profiles.

6.3.2 Theoretical Formulation

Master equation of the system is given by Eq. (2.90) which is cast in c-number representation to obtain the following equations:

$$d\rho_{11}/dt = -a_1\rho_{11} - i\alpha_1(\rho_{13} - \rho_{31}) - i\alpha_2(\rho_{14} - \rho_{41}) + 2\Gamma_{21}\rho_{22} + 2\gamma_{31}\rho_{33} + 2\gamma_{41}\rho_{44} \quad (6.11a)$$

$$d\rho_{12}/dt = -a_2\rho_{12} - i\alpha_3\rho_{14} + i\alpha_1\rho_{32} + i\alpha_2\rho_{42}, \quad (6.11b)$$

$$d\rho_{13}/dt = -i\alpha_1(\rho_{11} - \rho_{33}) - a_3\rho_{13} + i\alpha_2\rho_{43}, \quad (6.11c)$$

$$d\rho_{14}/dt = -i\alpha_2(\rho_{11} - \rho_{44}) - i\alpha_3\rho_{12} - a_4\rho_{14} + i\alpha_1\rho_{34}, \quad (6.11d)$$

$$d\rho_{22}/dt = 2\Gamma_{12}\rho_{11} - a_6\rho_{22} - i\alpha_3(\rho_{24} - \rho_{42}) + 2\gamma_{32}\rho_{33} + 2\gamma_{42}\rho_{44}, \quad (6.11e)$$

$$d\rho_{23}/dt = -i\alpha_1\rho_{21} - a_7\rho_{23} + i\alpha_3\rho_{43}, \quad (6.11f)$$

$$d\rho_{24}/dt = -i\alpha_2\rho_{21} - i\alpha_3(\rho_{22} - \rho_{44}) - a_8\rho_{24}, \quad (6.11g)$$

$$d\rho_{33}/dt = i\alpha_1(\rho_{13} - \rho_{31}) - a_{11}\rho_{33} + 2\Gamma_{43}\rho_{44}, \quad (6.11h)$$

$$d\rho_{34}/dt = i\alpha_1\rho_{14} - i\alpha_2\rho_{31} - i\alpha_3\rho_{32} - a_{12}\rho_{34}, \quad (6.11i)$$

$$d\rho_{44}/dt = i\alpha_2(\rho_{14} - \rho_{41}) + i\alpha_3(\rho_{24} - \rho_{42}) + 2\Gamma_{34}\rho_{33} - a_{16}\rho_{44}. \quad (6.11j)$$

where the Rabi frequencies (α_i) and detunings (Δ_i) are defined in Eq. (2.92) and (2.93),

and the coefficients a_i are defined as follows:

$$\begin{aligned}
 a_1 &= 2\Gamma_{12}, & a_2 &= \Gamma_{12} + \Gamma_{21} + i(\Delta_3 - \Delta_2) = a_5^*, & a_3 &= \Gamma_{12} + \Gamma_3 - i\Delta_1 = a_9^*, \\
 a_4 &= \Gamma_{12} + \Gamma_4 - i\Delta_2 = a_{13}^*, & a_6 &= 2\Gamma_{21}, & a_7 &= \Gamma_{21} + \Gamma_3 - i(\Delta_3 - \Delta_2 + \Delta_1) = a_{10}^*, \\
 a_8 &= \Gamma_{21} + \Gamma_4 - i\Delta_3 = a_{14}^*, & a_{11} &= 2\Gamma_3, & a_{12} &= \Gamma_3 + \Gamma_4 + i(\Delta_1 - \Delta_2) = a_{15}^*, \\
 a_{16} &= 2\Gamma_4, & \Gamma_3 &= \gamma_{31} + \gamma_{32} + \Gamma_{34}, & \Gamma_4 &= \gamma_{41} + \gamma_{42} + \Gamma_{43}. \quad (6.12)
 \end{aligned}$$

Under the weak probe approximation the relevant coherences of the medium for the three model schemes are obtained as follows:

(a) Model A

$$\rho_{42}^{(1)} = \alpha_3 [a_{10}\alpha_2\rho_{14}^{(0)} + i\{(\alpha_1^2 + a_2a_{10})(\rho_{22}^{(0)} - \rho_{44}^{(0)}) + \alpha_1\alpha_2\rho_{34}^{(0)}\}] / A_{N1}, \quad (6.13a)$$

$$\rho_{14}^{(0)} = -i\alpha_2 [(a_9a_{12} + \alpha_2^2)(\rho_{11}^{(0)} - \rho_{44}^{(0)}) - \alpha_1^2(\rho_{11}^{(0)} - \rho_{33}^{(0)})] / A_{N2}, \quad (6.13b)$$

$$\rho_{34}^{(0)} = \alpha_1\alpha_2 [a_4(\rho_{11}^{(0)} - \rho_{33}^{(0)}) + a_9(\rho_{11}^{(0)} - \rho_{44}^{(0)})] / A_{N2}, \quad (6.13c)$$

$$A_{N1} = a_2a_{10}a_{14} + \alpha_1^2a_{14} + \alpha_2^2a_{10}, \quad A_{N2} = a_4a_9a_{12} + \alpha_1^2a_9 + \alpha_2^2a_4. \quad (6.13d)$$

(b) Model B

$$\rho_{31}^{(1)} = \alpha_1 [a_{10}\alpha_2\rho_{14}^{(0)} + i\{(\alpha_3^2 + a_{10}a_{12})(\rho_{11}^{(0)} - \rho_{33}^{(0)}) - \alpha_2\alpha_3\rho_{12}^{(0)}\}] / B_{N1}, \quad (6.14a)$$

$$\rho_{12}^{(0)} = -\alpha_2\alpha_3 [a_{14}(\rho_{11}^{(0)} - \rho_{44}^{(0)}) + a_4(\rho_{22}^{(0)} - \rho_{44}^{(0)})] / B_{N2}, \quad (6.14b)$$

$$\rho_{14}^{(0)} = -i\alpha_2 [(a_2a_{14} + \alpha_2^2)(\rho_{11}^{(0)} - \rho_{44}^{(0)}) + \alpha_3^2(\rho_{44}^{(0)} - \rho_{22}^{(0)})] / B_{N2}, \quad (6.14c)$$

$$B_{N1} = a_9a_{10}a_{12} + \alpha_2^2a_{10} + \alpha_3^2a_9, \quad B_{N2} = a_2a_4a_{14} + \alpha_2^2a_4 + \alpha_3^2a_{14}. \quad (6.14d)$$

(c) Model C

$$\begin{aligned}
 \rho_{41}^{(1)} &= \alpha_2 [(\alpha_1^2 - \alpha_3^2)(\alpha_1\rho_{13}^{(0)} - \alpha_3\rho_{24}^{(0)}) + a_7(a_5\alpha_1\rho_{13}^{(0)} + a_{15}\alpha_3\rho_{24}^{(0)}) \\
 &\quad + i\{(a_5a_7a_{15} + \alpha_1^2a_{15} + \alpha_3^2a_5)(\rho_{11}^{(0)} - \rho_{44}^{(0)})\}] / C_N, \quad (6.15a)
 \end{aligned}$$

$$\rho_{13}^{(0)} = -i\alpha_1(\rho_{11}^{(0)} - \rho_{33}^{(0)}) / a_3, \quad \rho_{24}^{(0)} = -i\alpha_3(\rho_{22}^{(0)} - \rho_{44}^{(0)}) / a_8, \quad (6.15b)$$

$$C_N = a_5a_7a_{13}a_{15} + \alpha_1^4 + \alpha_3^4 - 2\alpha_1^2\alpha_3^2 + \alpha_1^2(a_5a_7 + a_{13}a_{15}) + \alpha_3^2(a_5a_{13} + a_7a_{15}). \quad (6.15c)$$

Populations for the three models are given in *Appendix-6*. Absorption A and refractive index η of the weak probe are given by $A = \text{Im}(\tilde{P})$, $\eta = \text{Re}(\tilde{P})$ where $\tilde{P} = (\rho_{42}^{(1)}\gamma_{42}/\alpha_3)$, $(\rho_{31}^{(1)}\gamma_{41}/\alpha_1)$ and $(\rho_{41}^{(1)}\gamma_{41}/\alpha_2)$ for models (A), (B) and (C) respectively.

6.3.3 Absorption Spectra

(a) Absorption in Model A

Fig. 6.5 shows the calculated probe absorption spectra in absence and presence of inhomogeneous broadening for a few representative values of field strengths. Steady state spectra is characterized by three dressed states formed by the coherent coupling of $|1\rangle \rightarrow |3\rangle$ and $|1\rangle \rightarrow |4\rangle$ transitions by two strong fields E_1 and E_2 . These dressed states can therefore be obtained from the eigenstates of V system formed by levels $|1\rangle$, $|3\rangle$ and $|4\rangle$. For $\Delta_1 = \Delta_2$, these dressed states are given in Table-5. Here dressed state ψ_1 at $\Delta_3 = \Delta_2 (= \Delta_1)$ corresponds to resonant bright resonance.

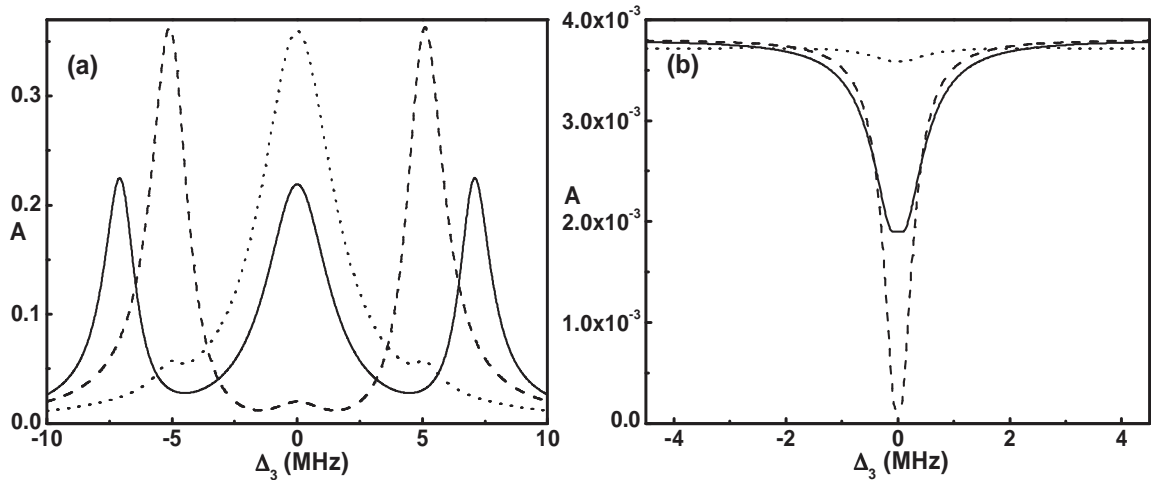


Fig. 6.5: Probe absorption spectrum for model A. Here $\Delta_1 = \Delta_2 = 0$, $(\alpha_1, \alpha_2) = (5, 5)$, $(1, 5)$ and $(5, 1)$ MHz for solid, dashed and dotted lines respectively. The decay rates are $\gamma_{31} = \gamma_{41} = 1.115$ MHz, $\gamma_{32} = 0.134$ MHz, $\gamma_{42} = 0.669$ MHz and $\Gamma_{12} = \Gamma_{12} = \Gamma_{34} = \Gamma_{34} = 1$ kHz. Frames (a) and (b) correspond to the spectra in the absence ($2W_D = 0$) and presence ($2W_D = 510$ MHz) of inhomogeneous broadening.

Table-5: Dressed states of model A for $\Delta_1 = \Delta_2$

Dressed state energy	Dressed state eigen vector
Δ_2	$\psi_1 = \frac{\alpha_2 3\rangle - \alpha_1 4\rangle}{\sqrt{\alpha_1^2 + \alpha_2^2}}$
$(\Delta_2 \mp \xi_1)/2$	$\psi_{2,3} = \sqrt{\frac{\xi_1 \pm \Delta_2}{2\xi_1}} 1\rangle \pm \alpha_1 \sqrt{\frac{2}{\xi_1(\xi_1 \pm \Delta_2)}} 3\rangle \pm \alpha_2 \sqrt{\frac{2}{\xi_1(\xi_1 \pm \Delta_2)}} 4\rangle$
$\xi_1 = \sqrt{\Delta_2^2 + 4(\alpha_1^2 + \alpha_2^2)}$	

From Table-5 it is clear that relative amplitudes of the three dressed resonances depends on the ratio of field strengths α_1 and α_2 , and the transition dipole moment of excited states to the probe ground state $|2\rangle$. Since for ^{87}Rb $d_{23} \ll d_{24}$, amplitude of the state ψ_1 is directly related to α_1 whereas that of the other two dressed resonances are related to α_2 . This is in agreement with the observed change in heights of the dressed resonances with change in field strengths as shown in Fig. 6.5(a). Fig. 6.6 shows the effect of Δ_1 and Δ_2 on the probe absorption spectra when $\alpha_1 = \alpha_2$.

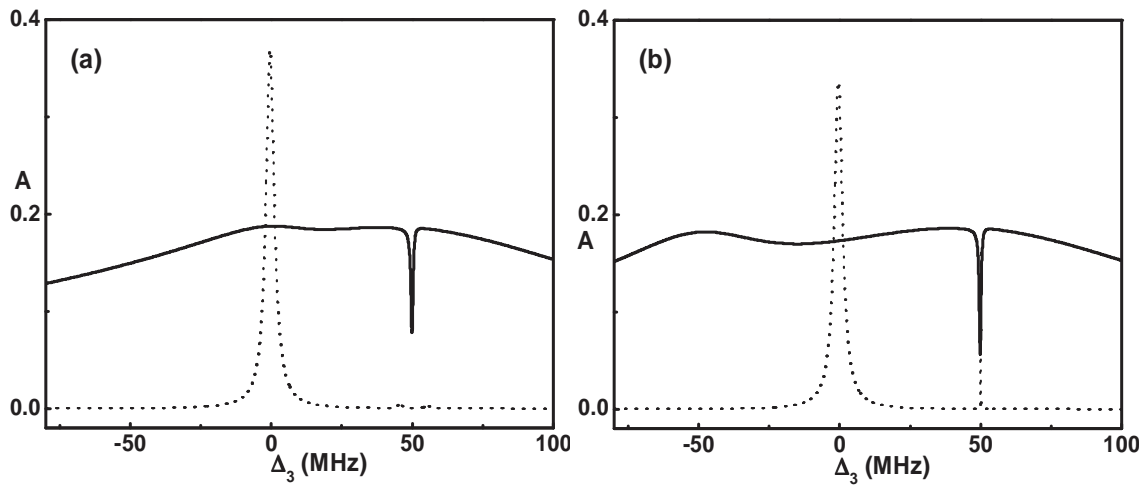


Fig. 6.6: Absorption in absence (dotted line) and presence (solid line) of Doppler broadening. Here $(\alpha_1, \alpha_2) = (5, 5)$ MHz and $(\Delta_1, \Delta_2) = (0, 50)$ and $(-50, 50)$ for frames (a) and (b) respectively. The solid curves are scaled up by 50. Other data are same as in Fig. 6.5.

In the steady state nearly all the population is transferred to the probe ground level $|2\rangle$. This fulfills the prerequisite for EIT and hence in a thermal broadened media one observes a narrow EIT at $\Delta_3 = \Delta_2$. The effect of field E_1 on the Λ system ($|1\rangle, |3\rangle, |4\rangle$) becomes significant when $\alpha_1 > \alpha_2$ as may be seen the dotted curve in Fig. 6.5(b). Here EIT is retained but with much smaller amplitude and a larger width. Further it is observed that EIT always appears at $\Delta_3 = \Delta_2$ irrespective of the detuning Δ_1 (cf. Fig. 6.6).

(b) Absorption in Model B

In the absence of inhomogeneous broadening absorption spectra exhibits a triplet formed by dressing of $|1\rangle \rightarrow |4\rangle$ and $|2\rangle \rightarrow |4\rangle$ transitions by two strong fields E_2 and E_3 . Representative probe absorption spectra for $\Delta_2 \neq \Delta_3$ are shown in Fig. 6.7.

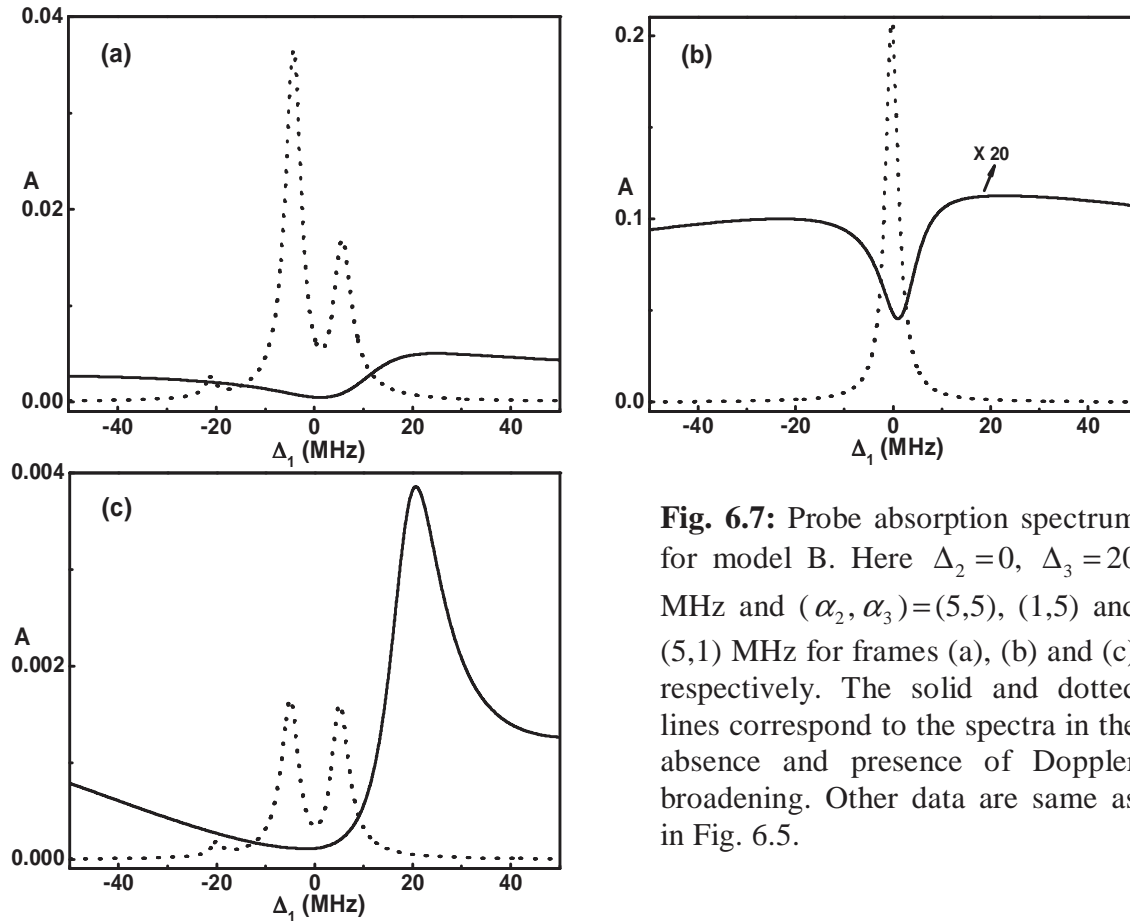


Fig. 6.7: Probe absorption spectrum for model B. Here $\Delta_2 = 0$, $\Delta_3 = 20$ MHz and $(\alpha_2, \alpha_3) = (5, 5)$, $(1, 5)$ and $(5, 1)$ MHz for frames (a), (b) and (c) respectively. The solid and dotted lines correspond to the spectra in the absence and presence of Doppler broadening. Other data are same as in Fig. 6.5.

Though the analytical dressed states for $\Delta_2 \neq \Delta_3$ are difficult to obtain, it can be argued that for $\alpha_2 > \alpha_3$ there is preferential dressing of two-level system $|1\rangle \leftrightarrow |4\rangle$. Hence the dressed spectrum constitutes an AT doublet $\Delta_1 = (\Delta_2 \pm \sqrt{\Delta_2^2 + 4\alpha_2^2})/2$ (cf. dotted curves in Fig. 6.7(a) and (c)). The third dressed resonance appears at the three-photon resonance condition $\Delta_1 = \Delta_2 - \Delta_3$ [227]. Analytical form of dressed states can be obtained under the condition $\Delta_2 = \Delta_3$ and are given in Table-6. The dressed state ψ'_1 at $\Delta_1 = \Delta_2 (= \Delta_3)$ is called dark resonance.

Table -6: Dressed states for model B for $\Delta_2 = \Delta_3$

Dressed state energy	Dressed state eigen vector
Δ_2	$\psi'_1 = \frac{\alpha_3 1\rangle - \alpha_2 2\rangle}{\sqrt{\alpha_2^2 + \alpha_3^2}}$
$(\Delta_2 \mp \xi_2)/2$	$\psi'_{2,3} = \pm \alpha_2 \sqrt{\frac{2}{\xi_2(\xi_2 \pm \Delta_2)}} 1\rangle \pm \alpha_3 \sqrt{\frac{2}{\xi_2(\xi_2 \pm \Delta_2)}} 2\rangle - \sqrt{\frac{\xi_2 \pm \Delta_2}{2\xi_2}} 4\rangle$
$\xi_2 = \sqrt{\Delta_2^2 + 4(\alpha_2^2 + \alpha_3^2)}$	

In the presence of Doppler broadening observation of transparency or absorption resonance in the medium depends on relative strengths of the two strong fields. While α_2 increases the absorption, α_3 tends to make the medium transparent. Hence for $\alpha_2 = \alpha_3$ and $\Delta_2 = \Delta_3$ the Doppler averaged spectra do not show any characteristics of EIT or EIA. When $\alpha_2 < \alpha_3$, an EIT resonance is obtained at the two-photon resonance condition $\Delta_1 \approx \Delta_2$ (cf. in Fig. 6.7(b)). When $\alpha_2 > \alpha_3$, an EIA resonance appears at $\Delta_1 \approx \Delta_3$ (cf. Fig. 6.7(c)). Further unlike the previous model, steady state population in this case is not trapped in the probe ground state, but is shared between levels $|1\rangle$ and $|2\rangle$.

(c) Absorption in Model C

We now concentrate on model C which is most interesting of the three configurations. In the absence of inhomogeneous broadening probe absorption spectra is a quadruplet formed by dressing of the four bare states. In general two pairs of dressed states are formed by dressing of two-level systems $|1\rangle \leftrightarrow |3\rangle$ by E_1 and $|2\rangle \leftrightarrow |4\rangle$ by E_3 . The corresponding dressed states are $S_{1,2} = (\Delta_1 \pm \sqrt{\Delta_1^2 + 4\alpha_1^2})/2$ and $S_{3,4} = (\Delta_3 \pm \sqrt{\Delta_3^2 + 4\alpha_3^2})/2$. These four dressed states are probed by field E_2 resulting in absorption at $\Delta_2 = S_3 - S_1, S_3 - S_2, S_4 - S_1$ and $S_4 - S_2$. Fig. 6.8 shows probe absorption spectra for fixed detunings and varying field strengths. Note here that the scheme under consideration is a combination of a Λ ($|1\rangle, |2\rangle, |4\rangle$) and a V ($|1\rangle, |3\rangle, |4\rangle$) system, each driven by its own strong control field but having a common probe field.

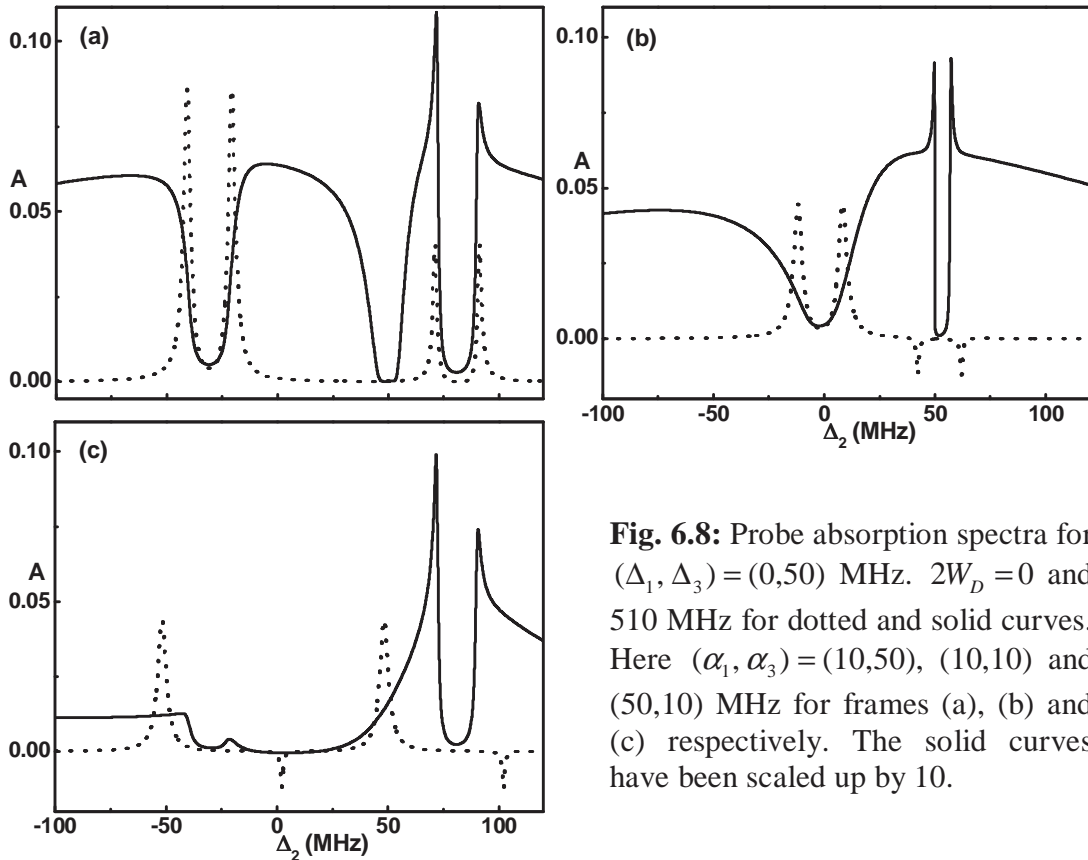


Fig. 6.8: Probe absorption spectra for $(\Delta_1, \Delta_3) = (0, 50)$ MHz. $2W_D = 0$ and 510 MHz for dotted and solid curves. Here $(\alpha_1, \alpha_3) = (10, 50), (10, 10)$ and $(50, 10)$ MHz for frames (a), (b) and (c) respectively. The solid curves have been scaled up by 10.

When $\alpha_1 < \alpha_3$, Λ system is stronger and nearly all the steady state population is distributed in the probe ground state $|1\rangle$ and excited state $|3\rangle$ ($\rho_{11} \approx 0.43$ and $\rho_{33} \approx 0.42$). In this condition one observes four absorptive resonances in the absence of inhomogeneous broadening as shown in Fig. 6.8(a). When $\alpha_1 \geq \alpha_3$, the resonant V system is relatively stronger and the maximum population is transferred to level $|2\rangle$ ($\rho_{22} \approx 0.6$). Thus there is inversion between state $|1\rangle$ and one of the dressed resonances arising from coherent coupling of $|2\rangle \leftrightarrow |4\rangle$ transition by control field E_3 . This results in the amplification as observed in Fig. 6.8(b) – (c). The effect of thermal averaging is to fill in the transparency region between the four dressed states resulting into the formation of three EIT resonances as shown in Fig. 6.8(a). It may be noted here that the inversion in the dressed states is not retained in the Doppler averaged spectrum.

6.3.4 Switching Between EIA and EIT in Model C

Depending on relative strengths of the two strong fields one observes both EIA and EIT in this configuration as shown in Fig. 6.9. This provides an interesting prospect of controlling light propagation from subluminal to superluminal in the medium. When $\alpha_1 = \alpha_3$ and $\Delta_1 = \Delta_3$, the inherent Λ and V systems are at equal footing. In this case a narrow EIA resonance flanked by two transparency regions is obtained at $\Delta_2 = \Delta_3 = \Delta_1$ as shown in Fig. 6.9(a). As α_3 is increased, the dominating Λ system creates a narrow transparency window within the EIA resonance while increasing the amplitude of the adjacent transparency windows as is shown in Fig. 6.9(b). For $\alpha_3 \gg \alpha_1$ three EIT

resonances are obtained (*cf.* Fig. 6.9(c)) as was discussed in the previous subsection. The creation of EIA is due to the buildup of low frequency coherence between the excited states and its transfer to the ground state by spontaneous emission. Switching between EIA to EIT can therefore be attributed to TOC [40-43] in the medium. Similar to EIT linewidth, EIA linewidth decreases with increase in W_D as shown in Fig. 6.10.

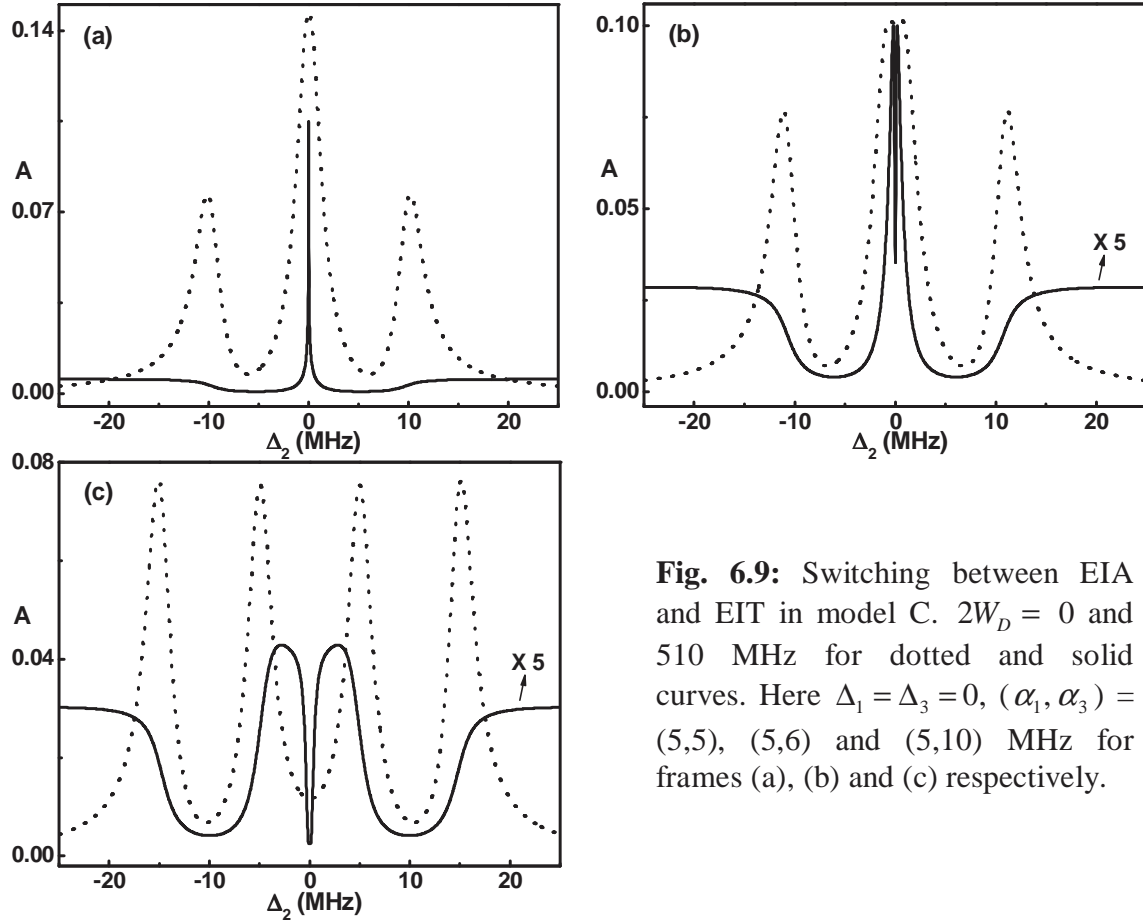


Fig. 6.9: Switching between EIA and EIT in model C. $2W_D = 0$ and 510 MHz for dotted and solid curves. Here $\Delta_1 = \Delta_3 = 0$, $(\alpha_1, \alpha_3) = (5, 5)$, $(5, 6)$ and $(5, 10)$ MHz for frames (a), (b) and (c) respectively.

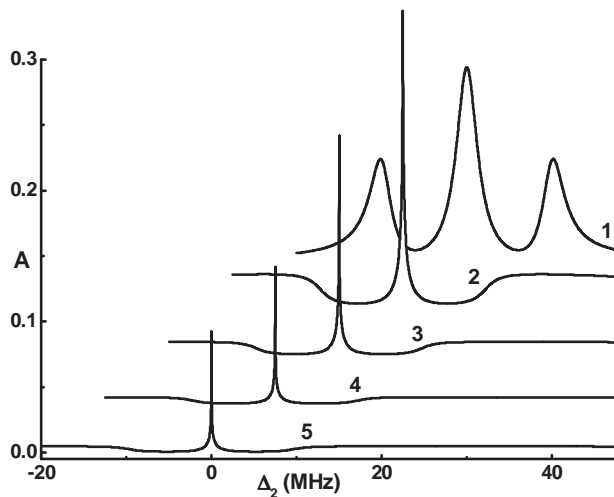


Fig. 6.10: Narrowing of EIA resonance with increase in Doppler width. Here $\Delta_1 = \Delta_3 = 0$, $\alpha_1 = \alpha_3 = 5$ MHz. $2W_D = 0, 100, 250, 500$ and 600 MHz for curves 1, 2, 3, 4 and 5 respectively.

6.4 Spontaneously Generated Coherence in N system

6.4.1 Theoretical Formulation

We consider an experimental situation of closed N system in configuration C for the present study. When the levels $|1\rangle$ and $|2\rangle$ are closely spaced, the two spontaneous decay channels $(\gamma_{31}, \gamma_{32})$ and $(\gamma_{41}, \gamma_{42})$ give rise to coherent superposition of the two ground states resulting in establishment of SGC in the medium. Since electric dipole moments (d_{31}, d_{32}) and (d_{41}, d_{42}) need not be orthogonal, the angles θ_1 and θ_2 between the two pairs of induced dipole moments play the deciding role in SGC. The alignment of dipole moments is defined in terms of parameters $\Phi_1 = (\vec{d}_{31} \cdot \vec{d}_{32}) / |\vec{d}_{31}| |\vec{d}_{32}| = \cos\theta_1$ and $\Phi_2 = (\vec{d}_{41} \cdot \vec{d}_{42}) / |\vec{d}_{41}| |\vec{d}_{42}| = \cos\theta_2$. In such a case $\Phi_1 \sqrt{\gamma_{31}\gamma_{32}}$ and $\Phi_2 \sqrt{\gamma_{41}\gamma_{42}}$ are the SGC parameters which represent the quantum interference effects resulting from the cross coupling between spontaneous emissions channels ($|3\rangle \rightarrow |1\rangle, |3\rangle \rightarrow |2\rangle$) and ($|4\rangle \rightarrow |1\rangle, |4\rangle \rightarrow |2\rangle$) respectively. Under the condition that each field drives only one transition, the Rabi frequencies of the driving fields are related to the alignment of dipole moments as $\alpha_1^s = \alpha_1 \sin\theta_1 = \alpha_1 \sqrt{1 - \Phi_1^2}$ and $\alpha_{2(3)}^s = \alpha_{2(3)} \sin\theta_2 = \alpha_{2(3)} \sqrt{1 - \Phi_2^2}$. It may be noted that when the dipole moments $(d_{31}, d_{32}), (d_{41}, d_{42})$ are near parallel, $\Phi_1 = \Phi_2 \approx 1$ representing the maximum SGC effect. However for large energy spacing of the ground states, the oscillatory terms average out to zero, $\Phi_1 = \Phi_2 = 0$ and SGC effect vanishes. The presence of two SGC channels modify the master equation of system (*cf.* Eq. 2.90) as

$$\begin{aligned} d\rho/dt = & -i[H_o, \rho] - \text{decay terms} + 2\Phi_1 \sqrt{\gamma_{31}\gamma_{32}} (A_{13}\rho A_{32} + A_{23}\rho A_{31}) \\ & + 2\Phi_2 \sqrt{\gamma_{41}\gamma_{42}} (A_{14}\rho A_{42} + A_{24}\rho A_{41}). \end{aligned} \quad (6.16)$$

The difference between Eq. (2.90) and Eq. (6.16) is the inclusion of last two SGC terms.

The elements of density operator satisfy the same equations 6.11(a) – (j) with $\alpha_i \rightarrow \alpha_i^S$,

except the ground state coherence equation 6.11(b) which is modified as follows:

$$\frac{d\rho_{12}}{dt} = -a_2\rho_{12} - i\alpha_3^S\rho_{14} + i\alpha_1^S\rho_{32} + i\alpha_2^S\rho_{42} + 2\Phi_1\sqrt{\gamma_{31}\gamma_{32}}\rho_{33} + 2\Phi_2\sqrt{\gamma_{41}\gamma_{42}}\rho_{44}. \quad (6.17)$$

6.4.2 Perturbative Analysis

Steady-state solutions for ρ_{ij} can be obtained perturbatively up to third order in probe field strength α_2^S to obtain relevant atomic coherences as

$$\rho_{21}^{(0)}C_N = X_N^{(0)}\{a_7a_{13}a_{15} + a_7(\alpha_1^S)^2 + a_{13}(\alpha_3^S)^2\}, \quad \rho_{31}^{(0)} = i\alpha_1^S(\rho_{11}^{(0)} - \rho_{33}^{(0)})/a_9, \quad (6.18a)$$

$$\rho_{41}^{(0)}C_N = iX_N^{(0)}\alpha_3^S\{a_7a_{15} - (\alpha_1^S)^2 + (\alpha_3^S)^2\}, \quad \rho_{42}^{(0)} = i\alpha_3^S(\rho_{22}^{(0)} - \rho_{44}^{(0)})/a_{14}, \quad (6.18b)$$

$$\rho_{23}^{(0)}C_N = iX_N^{(0)}\alpha_1^S\{a_{13}a_{15} + (\alpha_1^S)^2 - (\alpha_3^S)^2\}, \quad \rho_{43}^{(0)}C_N = X_N^{(0)}\alpha_1^S\alpha_3^S(a_7 + a_{13}), \quad (6.18c)$$

$$\begin{aligned} \rho_{21}^{(j)}C_N &= \alpha_2^S\alpha_3^S(\rho_{44}^{(j-1)} - \rho_{11}^{(j-1)})\{a_7a_{15} - (\alpha_1^S)^2 + (\alpha_3^S)^2\} \\ &\quad + X_N^{(j)}\{a_7a_{13}a_{15} + a_7(\alpha_1^S)^2 + a_{13}(\alpha_3^S)^2\} \\ &\quad + i\alpha_2^S[\rho_{13}^{(j-1)}(a_7 + a_{13})\alpha_1^S\alpha_3^S - \rho_{24}^{(j-1)}\{a_7(\alpha_1^S)^2 + a_{13}(\alpha_3^S)^2 + a_7a_{13}a_{15}\}], \end{aligned} \quad (6.19)$$

$$\rho_{31}^{(j)} = i[\alpha_1^S(\rho_{11}^{(j-1)} - \rho_{33}^{(j-1)}) - \alpha_2^S\rho_{34}^{(j-1)}]/a_9, \quad (6.20)$$

$$\rho_{42}^{(j)} = i[\alpha_3^S(\rho_{22}^{(j-1)} - \rho_{44}^{(j-1)}) + \alpha_2^S\rho_{12}^{(j-1)}]/a_{14}, \quad (6.21)$$

$$\begin{aligned} \rho_{43}^{(j)}C_N &= \alpha_1^S\alpha_2^S(\rho_{11}^{(j-1)} - \rho_{44}^{(j-1)})\{(\alpha_1^S)^2 - (\alpha_3^S)^2 + a_5a_7\} + X_N^{(j)}\alpha_1^S\alpha_3^S(a_7 + a_{13}) \\ &\quad + i\alpha_2^S[\rho_{13}^{(j-1)}\{a_{13}(\alpha_1^S)^2 + a_7(\alpha_3^S)^2 + a_5a_7a_{13}\} - \alpha_1^S\alpha_3^S\rho_{24}^{(j-1)}(a_7 + a_{13})], \end{aligned} \quad (6.22)$$

$$\begin{aligned} \rho_{41}^{(j)}C_N &= \alpha_2^S\{(\alpha_1^S)^2 - (\alpha_3^S)^2\}(\alpha_1^S\rho_{13}^{(j-1)} - \alpha_3^S\rho_{24}^{(j-1)}) + \alpha_2^S a_7(a_5\alpha_1^S\rho_{13}^{(j-1)} \\ &\quad + a_{15}\alpha_3^S\rho_{24}^{(j-1)}) + i[\alpha_2^S(\rho_{11}^{(j-1)} - \rho_{44}^{(j-1)})\{a_5a_7a_{15} + (\alpha_1^S)^2 a_{15} \\ &\quad + (\alpha_3^S)^2 a_5\} + X_N^{(j)}\alpha_3^S\{a_7a_{15} - (\alpha_1^S)^2 + (\alpha_3^S)^2\}], \end{aligned} \quad (6.23)$$

$$X_N^{(j)} = 2\Phi_1\sqrt{\gamma_{31}\gamma_{32}}\rho_{33}^{(j)} + 2\Phi_2\sqrt{\gamma_{41}\gamma_{42}}\rho_{44}^{(j)}. \quad (6.24)$$

The relevant zero and higher order populations are same as in the case without SGC (*cf.* Appendix 6) with $\alpha_i \rightarrow \alpha_i^S$.

The response of the atomic medium to the probe field is governed by the polarization $P = \epsilon_o \chi E_2(t)$ where $E_2(t) = [E_2 \exp(-i\Omega_2 t) + E_2^* \exp(i\Omega_2 t)]/2$ and $\chi = \chi^{(1)} + 3E_2^2 \chi^{(3)}$. For an ensemble of N_a atoms we may write the polarization of the medium as $P = N_a [d_{14} \rho_{14} \exp(i\Omega_2 t) + d_{41} \rho_{41} \exp(-i\Omega_2 t)]$, where $d_{14} = d_{41}$. The first and third order susceptibilities of the atomic medium can therefore be obtained as [220]

$$\chi^{(1)} = \frac{N_a |d_{14}|^2 \rho_{41}^{(1)}}{\epsilon_o \hbar \alpha_2^S}, \quad \chi^{(3)} = \frac{-N_a |d_{14}|^4 \rho_{41}^{(3)}}{12 \epsilon_o \hbar^3 (\alpha_2^S)^3}. \quad (6.25)$$

Here $\text{Re}(\chi^{(1)})$ and $\text{Im}(\chi^{(1)})$ represent the linear absorption and dispersion of the weak probe field. $\text{Re}(\chi^{(3)})$ corresponds to Kerr index of the medium whereas $\text{Im}(\chi^{(3)})$ accounts for the nonlinear absorption coefficient of probe field.

6.4.3 Results and Discussion

We now examine the effect of SGC on probe absorption and relate its consequences to the Kerr nonlinearity of the medium. We first focus on the case when $\alpha_1 = \alpha_3$ and $\Delta_1 = \Delta_3 = 0$. Fig. 6.11 shows the effect of SGC on the linear probe absorption spectra for a representative situation. Fig. 6.11(a) shows the triplet dressed states and EIA resonance in the absence of SGC (*cf.* Sec. 6.3.4). The inclusion of two SGC channels has a marked effect on it. If $\Phi_1 \neq \Phi_2$ or only one SGC channel is taken into account, the probe field sees different strengths of the two control fields, hence the medium exhibits four dressed resonances in the absence of inhomogeneous broadening

with a considerable decrease in absorption (*cf.* Fig. 6.11(b)). Further EIA observed in the Doppler broadened medium is transformed into three EIT resonances, out of which the EIT resonance at $\Delta_2 = \Delta_1 = \Delta_3 = 0$ is much sharper which manifests into an enhanced change in susceptibility of the medium. For $\Phi_1 = \Phi_2$, $\alpha_1^S = \alpha_3^S$ and this results in triplet absorption spectra in the absence and an EIA resonance in the presence of Doppler broadening as is shown in Fig. 6.11(c). However the presence of SGC results in reduced absorption as compared the case without SGC. Fig. 6.12 shows the effect of SGC channels on $\chi^{(1)}$ and $\chi^{(3)}$ of the medium for the data of Fig. 6.11. It is observed that Kerr nonlinearity gradually increases along with a decrease in linear/nonlinear absorption with the increase in SGC parameters Φ_1 and Φ_2 . Kerr nonlinearity for maximum SGC becomes almost double to the case without SGC.

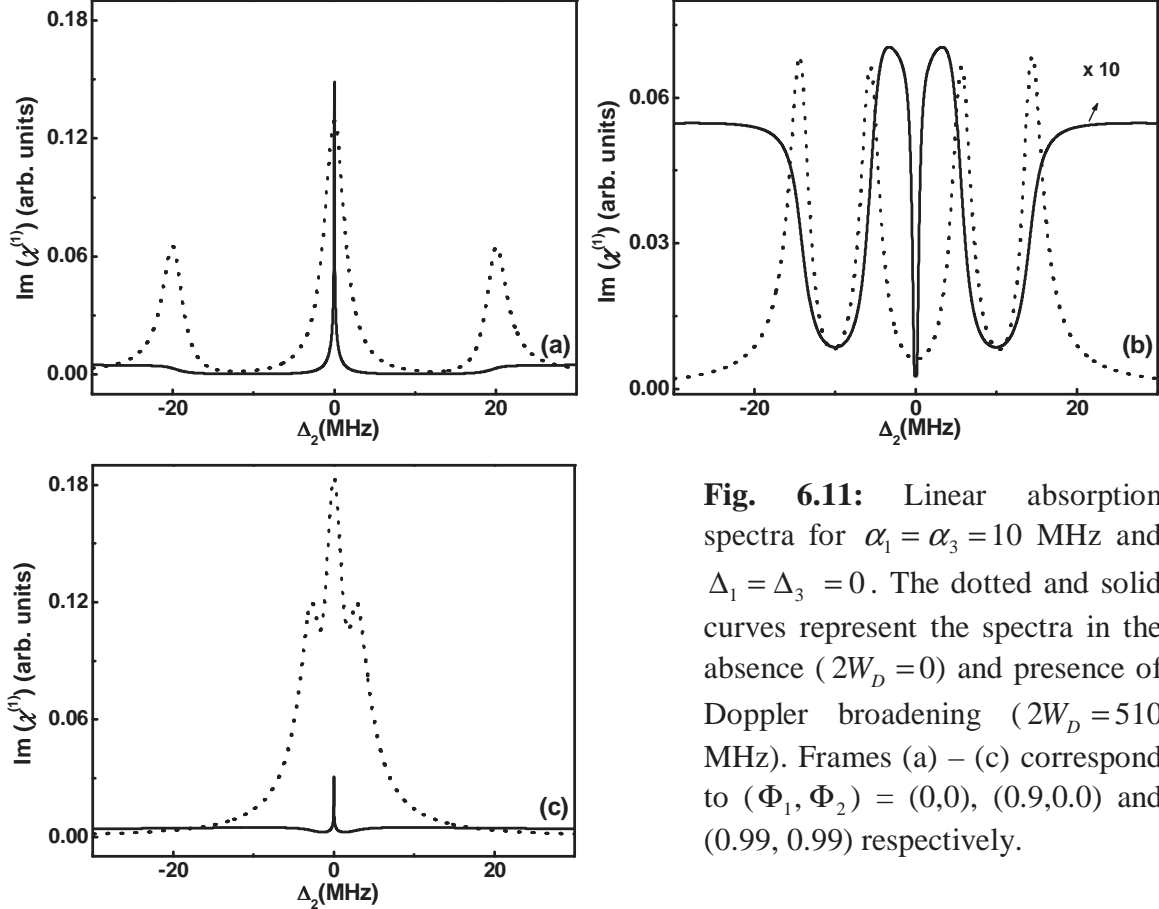


Fig. 6.11: Linear absorption spectra for $\alpha_1 = \alpha_3 = 10$ MHz and $\Delta_1 = \Delta_3 = 0$. The dotted and solid curves represent the spectra in the absence ($2W_D = 0$) and presence of Doppler broadening ($2W_D = 510$ MHz). Frames (a) – (c) correspond to $(\Phi_1, \Phi_2) = (0, 0)$, $(0.9, 0.0)$ and $(0.99, 0.99)$ respectively.

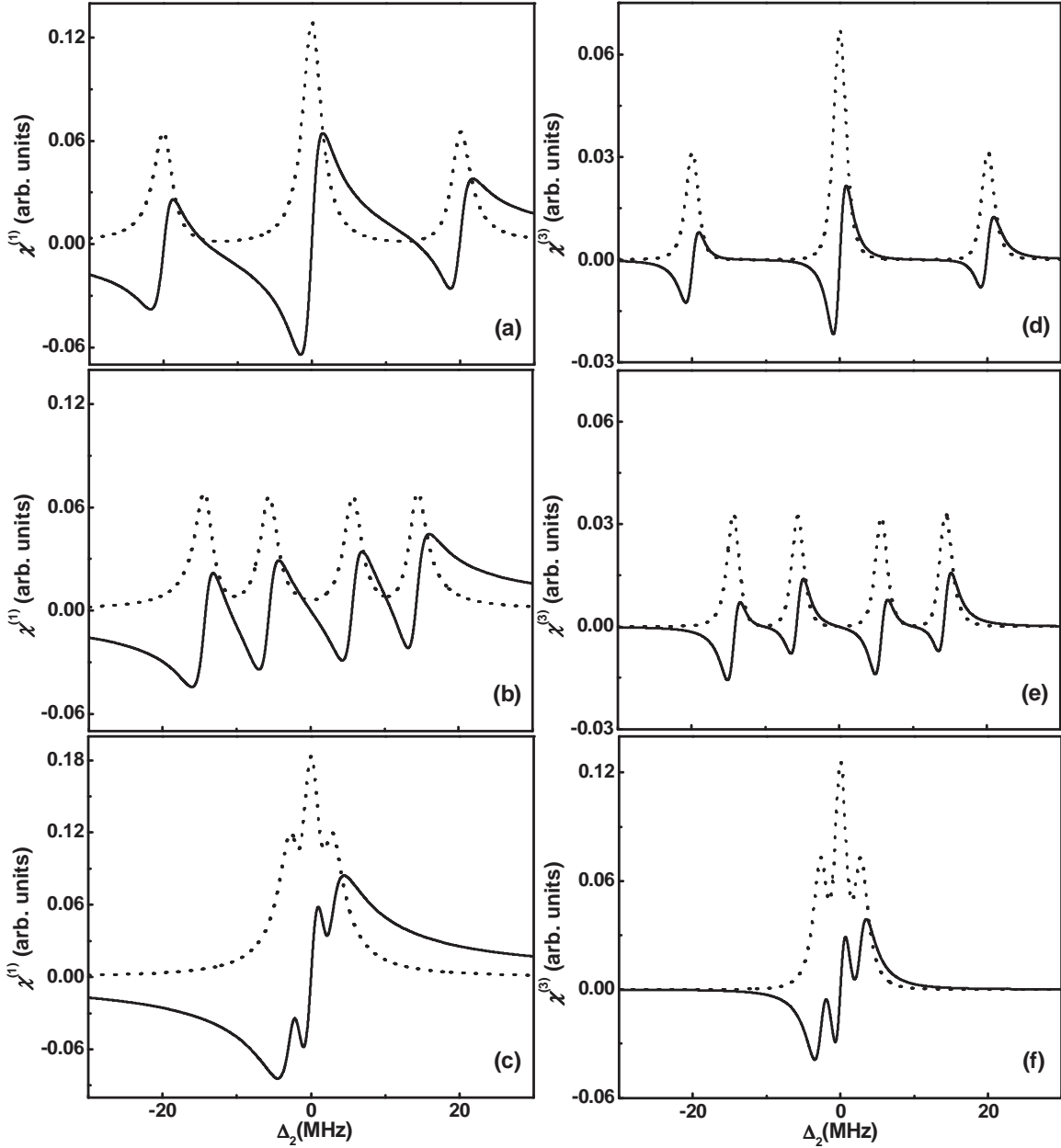


Fig. 6.12: Linear absorption $\text{Im}(\chi^{(1)})$ and dispersion $\text{Re}(\chi^{(1)})$ vs. Δ_2 are shown by dotted and solid curves respectively in frames (a) – (c). Nonlinear absorption $\text{Im}(\chi^{(3)})$ and Kerr nonlinearity $\text{Re}(\chi^{(3)})$ vs. Δ_2 are shown by dotted and solid curves respectively in frames (d) – (f). $(\Phi_1, \Phi_2) = (0, 0)$ for frames (a), (d); $(0.9, 0.0)$ for frames (b), (e) and $(0.99, 0.99)$ for frames (c), (f). Other data are same as in Fig. 6.11.

An important point to note from Fig. 6.12 is that the enhancement of Kerr nonlinearity is same whether $(p_1, p_2) = (0.9, 0.0)$ or $(p_1, p_2) = (0.99, 0.99)$. When $p_1 < p_2$

or when only one SGC channel ($p_1 \neq 0$) is taken into account the enhanced Kerr nonlinearity is accompanied with a decrease in linear/nonlinear absorption (*cf.* Fig. 6.12 (b), (e)). However for maximum SGC in both the channels ($p_1 = p_2 = 0.99$) the linear and nonlinear absorption increases in the region of enhancement as compared to the case without SGC. Hence when control fields are of equal strengths, one can obtain suppression of absorption and large enhancement of Kerr nonlinearity with the increase in the cross coupling between radiative decay channels ($|3\rangle \rightarrow |1\rangle, |3\rangle \rightarrow |2\rangle$).

When $\alpha_1 = \alpha_3$ the maximum steady population is distributed in levels $|1\rangle$ and $|3\rangle$. However when $\alpha_1 < \alpha_3$, i.e. the inherent V system is weaker, maximum population is transferred to the probe ground state $|1\rangle$. This population trapping causes makes the medium transparent. Further in this case the Kerr nonlinearity is increased by a factor of 10 as is shown in Fig. 6.13. The enhanced Kerr nonlinearity enters the nonlinear transparency window with increase in SGC parameters. Thus one can attain enhanced Kerr nonlinearity with almost no absorption by controlling the field and SGC parameters.

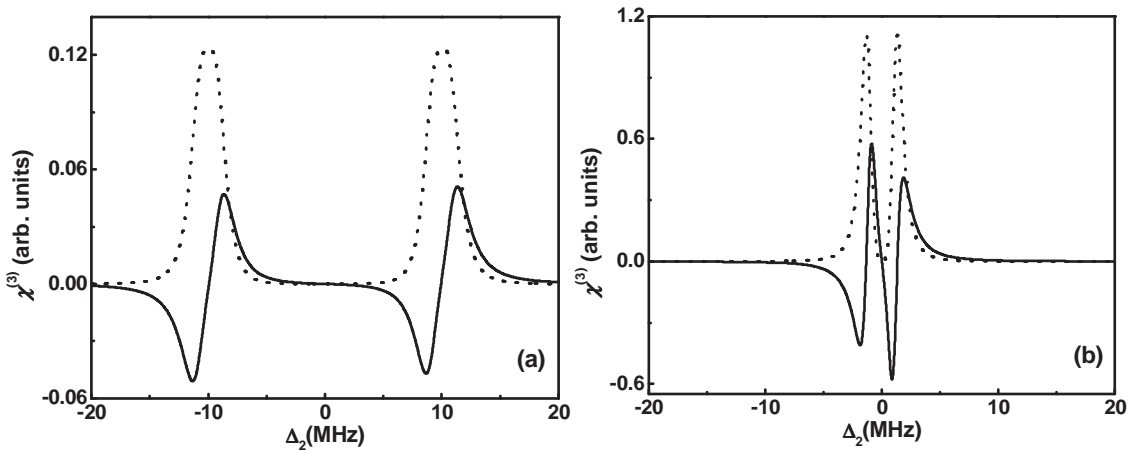


Fig. 6.13: $\text{Im}(\chi^{(3)})$ (dotted curve) and $\text{Re}(\chi^{(3)})$ (solid curve) vs. Δ_2 for $\alpha_1 = 1$ MHz. $(\Phi_1, \Phi_2) = (0, 0)$ and $(0.99, 0.99)$ for frames (a) and (b) respectively. Other data are same as in Fig. 6.11.

Fig. 6.14 shows the effect of SGC on $\chi^{(1)}$ and $\chi^{(3)}$ for $\alpha_1 < \alpha_3$ and off-resonant control field. In this case the Kerr nonlinearity is enhanced by almost 75 times for maximum SGC; however it is accompanied with an increase in absorption. In this case, SGC helps in obtaining narrow EIT resonances in the presence of Doppler broadening.

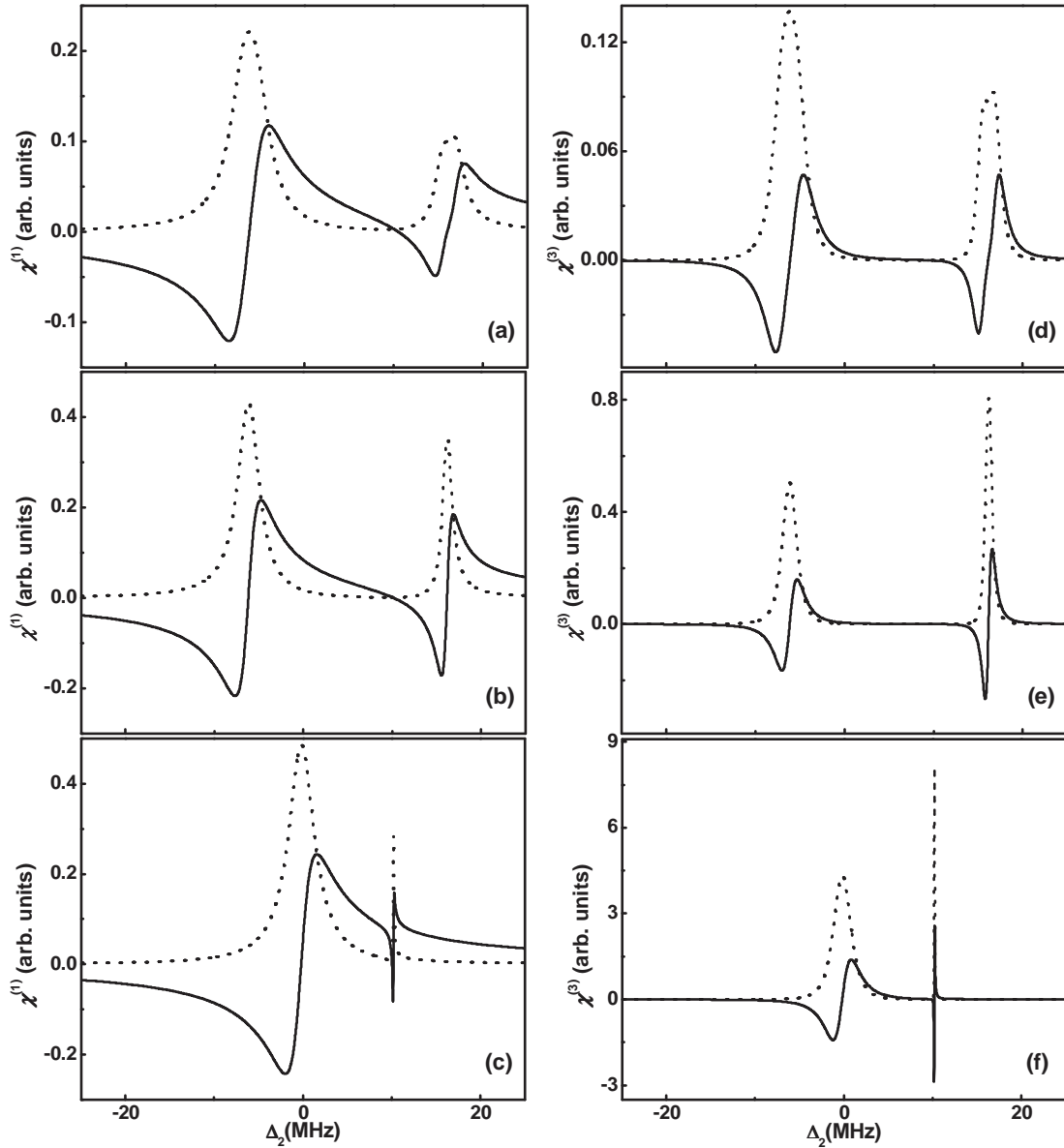


Fig. 6.14: $\text{Im}(\chi^{(1)})$ and $\text{Re}(\chi^{(1)})$ vs. Δ_2 are shown by dotted and solid curves respectively in frames (a) – (c). $\text{Im}(\chi^{(3)})$ and $\text{Re}(\chi^{(3)})$ vs. Δ_2 are shown by dotted and solid curves respectively in frames (d) – (f). Here $(\alpha_1, \alpha_3) = (1, 10)$ MHz and $(\Delta_1, \Delta_3) = (0, 10)$ MHz. $(\Phi_1, \Phi_2) = (0, 0)$ for frames (a),(d); $(0.9, 0.0)$ for frames (b),(e) and $(0.99, 0.99)$ for frames (c),(f).

From Eq. (6.18) – (6.23) it is clear that the coherences $\rho_{12}^{(0)}, \rho_{14}^{(0)}, \rho_{23}^{(0)}, \rho_{34}^{(0)}$ and hence $\rho_{ii}^{(1)}, \rho_{13}^{(1)}, \rho_{24}^{(1)}, \rho_{12}^{(2)}, \rho_{14}^{(2)}, \rho_{34}^{(2)}, \rho_{ii}^{(3)}$ ($i=1-4$) are zero in the absence of SGC ($X_N^{(j)} = 0$) but become finite in its presence. These coherences then modify the first and third order probe polarizations $\rho_{41}^{(1)}$ and $\rho_{41}^{(3)}$. A closer inspection of these terms reveals that the major contribution to the response of the atomic media is the buildup of low frequency coherence term $\rho_{21}^{(2)}$. Thus the change in optical response of the medium and enhancement of Kerr nonlinearity can be attributed to the two SGC channels and the interference between them which causes generation of extra coherences in the medium.

6.5 EIT in Λ and N System: Experimental

We now discuss our experimental results on EIT in Λ and N configurations. We consider here the N system of model A, i.e. where E_3 is the probe, E_2 is the pump and E_1 is the coupling (control) beam. The level scheme used in the present experiment correspond to D₂ transition of ⁸⁷Rb as shown in Fig. 6.15. The experimental set-up is same as that shown in Fig. 4.11. For EIT experiments, we avoid the additional counter-propagating probe beam which was used in the dressed state spectroscopy (*cf.* Sec. 4.7) and measure the probe absorption signal directly to obtain EIT. This helps in obtaining a narrower EIT linewidth as compared to the dressed state spectroscopy signal.

In case of the Λ system formed by levels $|1\rangle$, $|2\rangle$ and $|4\rangle$, we first obtain EIT signal at exact pump resonance and in the absence of the coupling beam. A typical EIT scan is shown in Fig. 6.16. Here the pump laser is stabilized on $5s_{1/2}F = 2 \rightarrow 5p_{3/2}F' = 1$

hyperfine transition i.e. $\Delta_2 = 0$. In this configuration, when the probe laser is scanned across the excited hyperfine manifold, a transparency window appears at $\Delta_3 \approx 0$. This narrow ‘dark’ resonance is flanked by two velocity selective resonances. The velocity selective resonances appear due to non-resonant excitation of different velocity group of atoms by the pump beam. The observed width of the EIT resonance is ~ 3 MHz, which is substantially lower than the natural line width (6.1 MHz) of ^{87}Rb D_2 transition. Under optimized experimental conditions the line width of the ‘dark’ resonance can be further narrowed to ~ 1 MHz. This type of ultra-narrow resonance can act as an ideal frequency discriminator in the field of metrology.

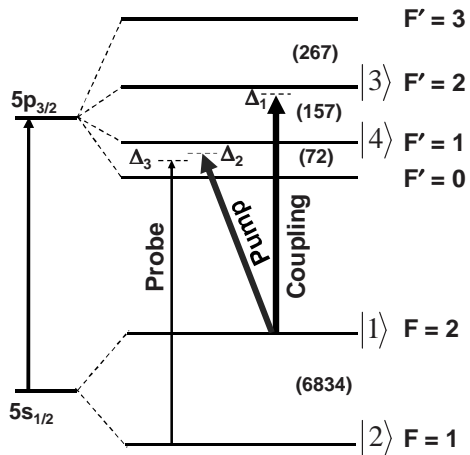


Fig. 6.15: Energy-level diagram for EIT experiment in ^{87}Rb D_2 line. The bracketed entries represent the separation (in MHz) between adjacent levels. The Λ system is formed with probe and pump lasers tuned to $F = 1 \rightarrow F' = 1$ and $F = 2 \rightarrow F' = 1$ transitions. For realization of N system an additional coupling field is tuned to $F = 2 \rightarrow F' = 2$ transitions. The detunings of the coupling, pump and probe lasers are Δ_1 , Δ_2 and Δ_3 respectively.

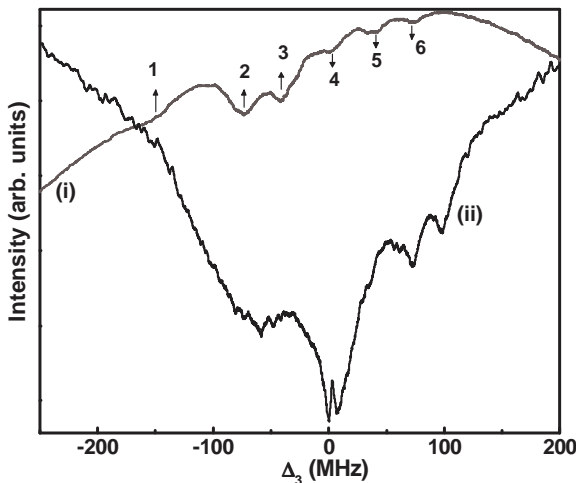


Fig 6.16: EIT in Λ configuration of D_2 transition of ^{87}Rb where pump is exactly resonant with $5s_{1/2} F = 2 \rightarrow 5p_{3/2} F' = 1$ transition. (i) Probe saturation absorption spectrum of $5s_{1/2} F = 1 \rightarrow 5p_{3/2} F'$ transition, where the resonances are as marked in Fig. 4.15. (ii) Probe intensity in the presence of the pump laser with $\Delta_2 = 0$ and Rabi $\alpha_2 \sim 17$ MHz. The EIT signal at $\Delta_3 \approx 0$ has a linewidth (FWHM) of ~ 3 MHz (obtained by Lorentz fitting).

For EIT in N system the coupling beam is turned on. Here the pump and coupling beams are derived from the same diode laser using an AOM. Pump beam is locked at crossover resonance between $5s_{1/2}F=2 \rightarrow 5p_{3/2}F'=1,2$ transitions using frequency modulation spectroscopy (FMS) and the coupling beam is 78 MHz up-shifted through AOM, which implies $\Delta_1 \approx 0$ and $\Delta_2 \approx -78.5$ MHz. EIT is recorded in Λ and N systems together by scanning the probe laser over appropriate hyperfine transitions. The powers of pump, coupling and probe beams are 1 mW, 2.5 mW and 70 μ W respectively. It may be noted here that this configuration gives rise to EIT in Λ system under non-resonant condition ($\Delta_2 \neq 0$). It is well known that the width of EIT in Λ system with $\Delta_2 \neq 0$ is expected to be substantially higher than that for $\Delta_2 = 0$ [14-16]. This however is not a limitation since we can compare the EIT signal in both these systems under identical experimental conditions to draw inference on the general features. A representative result is shown in Fig. 6.17. It is clear from Fig. 6.17 that EIT in Λ system occurs at the two photon resonance condition $\Delta_3 = \Delta_2$, while for N system it is observed at three-photon resonance condition $\Delta_3 = \Delta_2 - \Delta_1$, which reduces to 2+1-photon resonance for $\Delta_1 = 0$ [227]. This is satisfied for $\Delta_3 = -78.5$ MHz (*cf.* Fig. 6.17). We may observe here that the width of EIT in N system (~ 5 MHz) is significantly narrower than that in Λ system (~ 16 MHz). This agrees with the general observation that the EIT in N resonance is superior to that in Λ system and that makes it more attractive for applications relating to time and frequency standards.

The amplitude of the EIT resonance depends on the experimental parameters such as the field strengths and the density of the atoms. For achieving the largest absorption

reduction, the power of the coupling, pump and probe beams needs to be carefully monitored, and the probe beam is taken to be sufficiently weak to eliminate the saturation of atoms while maintaining appropriate signal to noise ratio. It is also important to note that while the pump and coupling strengths affect the frequency positions of dressed states, they do not change the EIT resonance frequency.

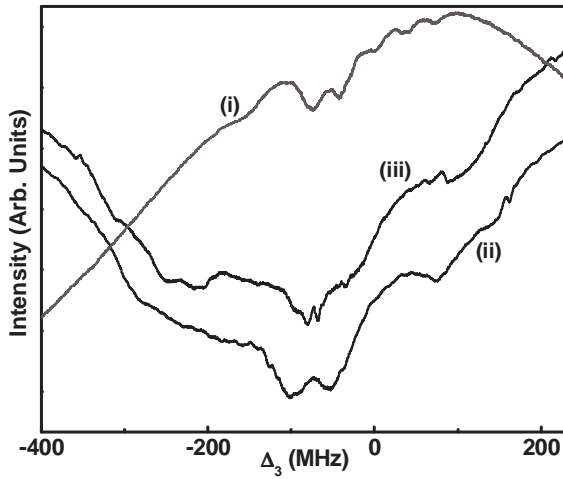


Fig 6.17: Comparison of EIT in three- and four-level systems. (i) Probe saturation absorption spectrum (ii) probe intensity in the presence of pump laser for Λ system and (iii) in the presence of pump and coupling lasers for N system. The widths of EIT for Λ and N system are 16 and 5 MHz respectively. See text for details.

We expect that improved optimization of the beam size and shape, laser focus, alignment, and intensity; and automated digital frequency locking of pump and coupling lasers can help in further narrowing the EIT resonance while increasing its amplitude. This ultra narrow EIT resonance can prove useful in frequency offset locking where one can stabilize the probe laser on the peak position of the EIT signal. This is done by locking the probe laser on the first derivative spectrum of EIT resonance. This atomic frequency offset locking (AFOL) technique provides better frequency stability than saturation absorption spectroscopy [82]. Further it eliminates the need of direct modulation of laser frequency and the spectral resolution is limited only by the linewidths of the laser systems.

CHAPTER 7

PHASE FLUCTUATIONS IN COHERENT DYNAMICS OF N-RESONANCE

7.1 Introduction

In coherent pump-probe spectroscopy experiments several techniques are used to generate the requisite multi-frequency fields, e.g., independent lasers [80-82], independent but phase locked lasers [83] and sidebands of a single laser [101] etc. An important problem that has a direct bearing on the experimental outcome is how the finite bandwidths of driving lasers and their cross-correlations affect the coherent dynamics of multi-level systems. The laser bandwidth is related to stochastic correlations of each frequency fluctuation with itself and cross-correlation between two fluctuating fields depends on the experimental techniques used for their generation.

It is well known from the study of two-level systems that the phase fluctuations in laser fields are a major cause of deterioration of the coherent optical processes. The effect of excitation bandwidths on resonance fluorescence [144] and Autler-Townes doublet

[145] was studied by Agarwal *et al.* Dalton and Knight [146] have reported a detailed analysis of the effects of laser bandwidths and cross-correlations on the coherences of a three-level system driven by two coherent fields. This work shows that whether atomic coherences are dephased or not depends on the laser bandwidths and correlations, and also on the atomic level configurations, i.e., Λ , V and Ξ . The same group has analyzed the effect of unequal phase fluctuating laser fields on CPT in ladder and Λ schemes [147]. They have reported that uncorrelated laser fields destroy CPT and damp the narrow coherence hole in the fluorescent intensity. However if the fields are critically cross-correlated atomic coherences are much less affected and a significant degree of re-trapping occurs [147]. The effect of finite bandwidths on optical double resonance (ODR) spectra and second-order intensity correlation functions was studied numerically and analytically by Lawande and co-workers [148,149]. There also exist studies on the effect of phase fluctuations on EIT, LWI, refractive index enhancement and entanglement generation [150-156]. While numerous papers have analyzed the effect of laser phase fluctuations on the optical response of three-level systems [144-156], relatively little work is reported on multilevel systems [157,158]. Fleischhauer *et al.* [157] have shown that in a double- Λ non inversion laser, pump-field phase diffusion leads to a fluctuating oscillation frequency of coherence and hence reduces the laser gain. A general condition for population trapping has been obtained in a four level system by Osman [158]. In particular no such work has been reported on N system, probably due to the complex configuration of the levels and coupling fields.

In this chapter we examine the effect of phase fluctuations on the response of three- and 2+1-photon resonance in terms of steady state and time dependent populations

as well as EIT/ EIA resonance in a N system. The framework of multiplicative stochastic processes [159,160] is used to obtain master equation for the phase averaged density matrix. Phase fluctuations are modeled as Wiener-Levy diffusion processes i.e. phase noise is assumed to be the integral of white frequency noise. The distinctive features of steady state and time dependent behavior of the system under three-photon and 2+1-photon resonance conditions and for fluctuating fields are explicitly discussed. The results are illustrated using the N system of $^{40}\text{Ca}^+$ ion (or ^{87}Sr atom) as discussed in Ref. [227]. Further the effect of phase fluctuations on EIT/EIA resonance is discussed in reference with model C of Chapter-6.

7.2 Theoretical Formulation

We consider a four-level system (*cf.* Fig. 2.1(c)) in N-configuration interacting with three monochromatic laser fields which are near resonant with respective atomic transitions. The coherent dynamics of the system is described by the master equation (2.83a). The Rabi frequencies of the three fields are $\alpha_1 = d_{13}E_{1o}/2$, $\alpha_2 = d_{14}E_{2o}/2$ and $\alpha_3 = d_{24}E_{3o}/2$. We assume that the driving fields $E_j(t)$, ($j=1,2,3$) arise from the stochastic nature of phases and are described by

$$E_j(t) = E_{j_o} \exp(-i\varphi_j t), \quad \varphi_j(0) = \varphi_{j_o}, \quad (7.1)$$

where non-stochastic amplitudes E_{j_o} are positive real numbers, φ_{j_o} are uniformly distributed phase variables and $\varphi_j(t)$ are the stochastic phase variables. We make the rather standard assumption that the phases $\varphi_j(t)$ follow a Wiener-Levy diffusion process

[159,160]. The phase fluctuations statistics is thus characterized by the following random equation of motion:

$$\dot{\varphi}_j(t) = \mu_j(t), \quad (7.2)$$

with $\mu_j(t)$ as a Gaussian white noise satisfying the following properties:

$$\overline{\mu_j(t)} = 0, \quad (7.3a)$$

$$\begin{aligned} \overline{\mu_i(t)\mu_j(t')} &= 2\gamma_{ci} \delta(t-t') & i = j, \\ &= 2\gamma_{cicj} \delta(t-t') & i \neq j, \end{aligned} \quad (7.3b)$$

where $2\gamma_{ci}$ is the bandwidth of laser Ω_i and $2\gamma_{cicj}$ represent the cross-correlation that may exist between the lasers Ω_i and Ω_j . Here and subsequently, ‘bar’ denotes the ensemble average with respect to the distribution of the random process $\mu_j(t)$. Cross correlations arise when two lasers interact simultaneously with the atom. They may also arise naturally if the two fields are different modes of the same laser or if the second field is produced by splitting and frequency conversion from the other laser beam. For critical correlation of driving fields we have

$$\gamma_{cicj} = (\gamma_{ci} + \gamma_{cj}) / 2. \quad (7.4)$$

In order to obtain the atomic observables averaged over phase fluctuations, we generalize the procedure used by D’Souza *et al.* [148] for the study of laser fluctuation effects in ODR spectra. The advantage of Weiner-Levy model of phase fluctuations is that it is possible to derive the master equation for density operator averaged over the ensemble of phase fluctuations. To this end we introduce the transformed density operator W^{pqs} as

$$W^{pqs}(t) = \exp(-iY)\exp(-iZ)\rho(t)\exp(iZ), \quad (7.5)$$

$$Y = p\varphi_1 + q\varphi_2 + s\varphi_3, \quad Z = \varphi_1 A_{33} + (\varphi_2 - \varphi_3)A_{22} + \varphi_2 A_{44}. \quad (7.6)$$

Differentiating Eq. (7.5) we obtain the following equation for W^{pqs}

$$dW^{pqs} / dt = -i(p\mu_1 + q\mu_2 + s\mu_3)W^{pqs} - i[\dot{Z}, W^{pqs}] + e^{-iY} e^{-iZ} (\partial\rho / dt) e^{iZ}. \quad (7.7)$$

The equation of motion for W^{pqs} is thus given as

$$dW^{pqs} / dt = [L_0 - i\mu_1(p + L_1) - i\mu_2(q + L_2) - i\mu_3(s - L_3)]W^{pqs}, \quad (7.8)$$

$$\begin{aligned} L_0 W^{pqs} &= i\alpha_1[A_{13} + A_{31}, W^{pqs}] + i\alpha_2[A_{14} + A_{41}, W^{pqs}] + i\alpha_3[A_{24} + A_{42}, W^{pqs}] \\ &\quad - i\Delta_1[A_{33}, W^{pqs}] - i(\Delta_2 - \Delta_3)[A_{22}, W^{pqs}] - i\Delta_2[A_{44}, W^{pqs}] - \gamma_{ij}\{A_{ii}W^{pqs} \\ &\quad - 2A_{ji}W^{pqs}A_{ij} + W^{pqs}A_{jj}\} - \Gamma_{ij}\{A_{ii}\rho - 2A_{ji}W^{pqs}A_{ij} + W^{pqs}A_{jj}\}, \end{aligned} \quad (7.9)$$

$$L_1 W^{pqs} = [A_{33}, W^{pqs}], \quad L_2 W^{pqs} = [A_{22} + A_{44}, W^{pqs}], \quad L_3 W^{pqs} = [A_{22}, W^{pqs}]. \quad (7.10)$$

Eq. (7.8) is a special case of a multiplicative stochastic differential equation. Our next step is to obtain the master equation for transformed density operator $\chi^{pqs} = \overline{W^{pqs}}$ averaged over distributions of phase variables $\varphi_j(t)$, ($j=1,2,3$). Since $\varphi_j(t)$ represent δ -correlated Gaussian processes, it is possible to apply the theory of multiplicative stochastic processes [159,160] to obtain an exact evolution equation for $\chi^{pqs}(t)$. To this end we write Eq. (7.8) as

$$dW^{pqs} / dt = \{B_0 - i\mu_1(t)B_1 - i\mu_2(t)B_2 - i\mu_3(t)B_3\}W^{pqs}, \quad (7.11)$$

where B_i are fixed operators defined as follows:

$$B_0 = L_0, \quad B_1 = p + L_1, \quad B_2 = q + L_2, \quad B_3 = s - L_3. \quad (7.12)$$

In the interaction representation Eq. (7.11) simplifies to

$$dv(t) / dt = -iw(t)v(t), \quad (7.13)$$

where

$$v(t) = e^{-B_0 t} W^{pqs}(t), \quad w(t) = e^{-B_0 t} [\mu_1(t)B_1 + \mu_2(t)B_2 + \mu_3(t)B_3] e^{B_0 t}. \quad (7.14)$$

Formal solution of Eq. (7.13) can be written in terms of time-ordered exponential as

$$v(t) = T \exp\left\{-i \int_0^t d\tau w(\tau)\right\} v(0), \quad (7.15)$$

where T is the time ordering operator. Taking the average of Eq. (7.15) with a fixed value of $v(0)$ and using the fact that averaging commutes with time ordering we obtain

$$\overline{v(t)} = T \exp\left\{-i \int_0^t d\tau \overline{w(\tau)}\right\} v(0). \quad (7.16)$$

The characteristic function of a stochastic variable x is defined as

$$G(k) \equiv \overline{\exp(ikx)} = \int dx \exp(ikx) P(x), \quad (7.17)$$

where $P(x)$ is probability distribution of x . Taking logarithm of Eq. (7.17), we obtain

$$\ln G(k) \equiv \sum_{m=1}^{\infty} \frac{(ik)^m}{m!} \langle\langle x^m \rangle\rangle, \quad (7.18)$$

where $\langle\langle \dots \rangle\rangle$ are the cumulants [160]. For Gaussian processes all cumulants beyond the second order are zero. The first cumulant is just the average value. Using Eq. (7.18) in (7.16) we obtain

$$\begin{aligned} \overline{v(t)} &= T \exp\left\{-i \int_0^t d\tau \overline{w(\tau)} - \frac{1}{2} \int_0^t dt_1 \int_0^t dt_2 \langle\langle w(t_1)w(t_2) \rangle\rangle\right\} v(0) \\ &= T \exp\left\{-\int_0^t dt_1 \int_0^{t_1} dt_2 \overline{w(t_1)w(t_2)}\right\} v(0), \end{aligned} \quad (7.19)$$

where we have used $\overline{w(\tau)} = 0$. In this case the second cumulant is equal to the second order correlation $\overline{w(t_1)w(t_2)}$. Differentiating Eq. (7.19), we have

$$d\overline{v(t)} / dt = -\int_0^t d\tau \overline{w(t)w(\tau)} \overline{v(t)}. \quad (7.20)$$

Reverting back to the original representation we obtain

$$d\overline{W^{pqS}} / dt = \left\{ B_0 - \int_0^t d\tau \sum_{i=1}^3 \sum_{j=1}^3 B_i \exp(B_0\tau) \overline{\mu_i(t)\mu_j(t-\tau)} B_j \exp(-B_0\tau) \right\} \overline{W^{pqS}}. \quad (7.21)$$

Using Eq. (7.3) in (7.21) we obtain terms like

$$2\gamma_c \int_0^t d\tau B_i \exp(B_0\tau) B_j \exp(-B_0\tau) \delta(\tau) = \gamma_c B_i B_j. \quad (7.22)$$

Now using Eq. (7.22) and the fact that B_i 's commute we finally obtain

$$\begin{aligned} \overline{dW^{pqs}(t)/dt} = & [B_0 - \gamma_{c1} B_1^2 - \gamma_{c2} B_2^2 - \gamma_{c3} B_3^2 \\ & - 2\gamma_{c1c2} B_1 B_2 - 2\gamma_{c1c3} B_1 B_3 - 2\gamma_{c2c3} B_2 B_3] \overline{W^{pqs}(t)}, \end{aligned} \quad (7.23)$$

which is equivalent to the master equation

$$\begin{aligned} d\chi^{pqs}/dt = & [L_0 - \gamma_{c1}(p+L_1)^2 - \gamma_{c2}(q+L_2)^2 - \gamma_{c3}(s-L_3)^2 - 2\gamma_{c1c2}(p+L_1) \\ & (q+L_2) - 2\gamma_{c1c3}(p+L_1)(s-L_3) - 2\gamma_{c2c3}(q+L_2)(s-L_3)] \chi^{pqs}. \end{aligned} \quad (7.24)$$

χ^{pqs} may be directly used to compute one-time expectation values of atomic operators.

7.2.1 Numerical Analysis

Master equation (7.24) can be cast in a c-number representation by taking the matrix elements of the density operator $\chi^{pqs}(t)$ between the atomic states to obtain

$$dX^{pqs}/dt = M^{pqs} X^{pqs}, \quad (7.25)$$

where X^{pqs} is a column vector with 16 components given by $X_{j+4(i-1)}^{pqs} = \langle i | \chi^{pqs} | j \rangle$ and

M^{pqs} is a 16×16 matrix whose elements are given in *Appendix-7*. The general solution of the matrix equation (7.25) can be written as

$$X(t) = \sum_{k=1}^{16} \frac{[\tilde{V}_k^{pqs} \cdot X_k^{pqs}]}{C_k^{pqs}} U_k^{pqs} \exp(\lambda_k^{pqs} t), \quad (7.26)$$

where U_k^{pqs} and V_k^{pqs} are respectively the eigenvectors of M_k^{pqs} and \tilde{M}_k^{pqs} corresponding to eigenvalue λ_k^{pqs} . \tilde{V}_k^{pqs} and \tilde{M}_k^{pqs} are the transpose of V_k^{pqs} and M_k^{pqs} respectively.

Coefficients $C_k^{pqs} = (\tilde{V}_k^{pqs} \cdot U_k^{pqs})$ are normalization constants. These eigenvalues and eigenvectors can be easily obtained numerically. In general, eigenvalues λ_k^{pqs} are complex with negative real part. The computation of atomic averages and intensity-intensity correlation functions involves the distribution χ^{000} . For χ^{000} , a steady-state exists which corresponds to the existence of an eigenvalue $\lambda_k^{000} = 0$. With $p = q = s = 0$ this method is quite similar to the one used by Dalton and Knight [146] for obtaining the populations which are related to one time averages. However proper choice of parameters (p, q, s) in the density matrix χ^{pqs} leads to simplification of off-diagonal atomic averages which can be used to obtain atomic coherences and fluorescent spectra. For e.g. the fluorescent spectra require the distributions χ^{100} , χ^{010} and χ^{001} .

7.2.2 One Time Averages

Consider the averages of operators A_{kk} which correspond to atomic populations,

$$\begin{aligned} \langle \overline{A_{kk}(t)} \rangle &= Tr[\overline{A_{kk}\rho(t)}] = Tr[\overline{A_{kk} \exp(iY) \exp(iZ) W^{pqs}(t) \exp(-iZ)}] \\ &= Tr[\overline{\exp(iY) \exp(-iZ) A_{kk} \exp(iZ) W^{pqs}(t)}] \\ &= Tr[\exp\{i(p\varphi_1 + q\varphi_2 + s\varphi_3)\} A_{kk} W^{pqs}(t)]. \end{aligned} \quad (7.27)$$

Since $\exp(-iZ) A_{kk} \exp(iZ) = A_{kk}$, we choose $p = q = s = 0$ to take average over the phase

distribution and obtain $\langle \overline{A_{kk}(t)} \rangle = Tr[A_{kk} \chi^{000}(t)]$. Similarly the average of off-diagonal

operator A_{12} can be obtained as

$$\begin{aligned} \langle \overline{A_{12}(t)} \rangle &= Tr[\overline{A_{12}\rho(t)}] = Tr[\overline{A_{12} \exp(iY) \exp(iZ) W^{pqs}(t) \exp(-iZ)}] \\ &= Tr[\overline{\exp(iY) \exp(iZ) A_{12} \exp(-iZ) W^{pqs}(t)}] \\ &= Tr[\exp\{i(p\varphi_1 + q\varphi_2 + s\varphi_3)\} \exp\{i(\varphi_2 - \varphi_3)\} A_{12} W^{pqs}(t)], \end{aligned} \quad (7.28)$$

where we have used the cyclic property of trace operation and identity (a) in Chapter-2.

We now choose $p = 0$, $q = -1$ and $s = 1$ to obtain $\langle \overline{A_{12}(t)} \rangle = Tr[A_{12}\chi^{0(-1)1}(t)]$. Similarly

the phase averaged expectation values of the other off-diagonal operators A_{jk} ($j \neq k$)

involve distributions with $p, q, s \neq 0$ can be obtained as follows:

$$\begin{aligned}
 \langle \overline{A_{12}(t)} \rangle &= Tr[A_{12}\chi^{0(-1)1}(t)], & \langle \overline{A_{21}(t)} \rangle &= Tr[A_{21}\chi^{01(-1)}(t)], & \langle \overline{A_{13}(t)} \rangle &= Tr[A_{13}\chi^{(-1)00}(t)], \\
 \langle \overline{A_{31}(t)} \rangle &= Tr[A_{31}\chi^{100}(t)], & \langle \overline{A_{14}(t)} \rangle &= Tr[A_{14}\chi^{0(-1)0}(t)], & \langle \overline{A_{41}(t)} \rangle &= Tr[A_{41}\chi^{010}(t)], \\
 \langle \overline{A_{23}(t)} \rangle &= Tr[A_{23}\chi^{(-1)1(-1)}(t)], & \langle \overline{A_{32}(t)} \rangle &= Tr[A_{32}\chi^{1(-1)1}(t)], & \langle \overline{A_{24}(t)} \rangle &= Tr[A_{24}\chi^{00(-1)}(t)], \\
 \langle \overline{A_{42}(t)} \rangle &= Tr[A_{42}\chi^{001}(t)], & \langle \overline{A_{34}(t)} \rangle &= Tr[A_{34}\chi^{1(-1)0}(t)], & \langle \overline{A_{43}(t)} \rangle &= Tr[A_{43}\chi^{(-1)10}(t)].
 \end{aligned}
 \tag{7.29}$$

Thus within the phase diffusion model, fluctuations can be treated exactly.

Further the two-time correlation functions can be obtained from one-time expectation values of the atomic operators by invoking the quantum regression theorem.

7.3 Effect of Phase Fluctuations on Three- and 2+1- photon Resonances

While the driving fields can be chosen arbitrarily, for this analysis we consider the case of $^{40}\text{Ca}^+$ ion [227], where E_2 and E_3 are strong fields and the ground level $|1\rangle$ is connected to a metastable level $|3\rangle$ by weak field E_1 (*cf.* Fig. 2.1(c)). This scheme represents the type of system encountered in atomic clocks, where transition $|1\rangle \rightarrow |3\rangle$ is the clock transition of $^{40}\text{Ca}^+$ ion or ^{87}Sr atom [227]. Here levels $|1\rangle$, $|2\rangle$ and $|3\rangle$ are stable

(metastable) while the state $|4\rangle$ is unstable unlike the ^{87}Rb system studied in the previous chapter. Champenois *et al.* [227] have pointed out that due to the instability of state $|4\rangle$, the narrow lines at three-photon resonance in this system can only be explained in terms of population trapping and not transfer of coherence (TOC). To compare our results with Ref. [227], the only decay channels considered in this section are γ_{41} and γ_{42} . The system exhibits narrow resonances when the following two conditions are satisfied,

(i) Three-photon resonance condition

$$\Delta_2 - \Delta_3 - \Delta_1 = 0 \text{ and } \Delta_1 \neq 0, \quad (7.30)$$

in which states $|2\rangle$ and $|3\rangle$ are resonantly coupled by three-photon process, and

(ii) 2+1-photon resonance condition

$$\Delta_2 - \Delta_3 = 0 \text{ and } \Delta_1 = 0, \quad (7.31)$$

where the states $|1\rangle$ and $|2\rangle$ are coupled by two-photon process while states $|1\rangle$ and $|3\rangle$ are coupled by one-photon process. We now focus on the steady-state and time dependent behavior of the atom under the above two conditions.

7.3.1 Steady - State Population Distribution

(a) *Three-Photon Resonance*

For a clear perception of the three-photon resonance condition it is pertinent here to discuss briefly the dark state in the absence of phase fluctuations. Though it is difficult to obtain closed analytic expressions of the dressed states, for $\alpha_1 \ll \alpha_2, \alpha_3$ coupling between states $|1\rangle$ and $|3\rangle$ can be treated perturbatively by introducing the first order

perturbation parameter $\alpha_1 / \Delta_1 \ll 1$. The dressed states of the two-level system $|1\rangle \leftrightarrow |3\rangle$

are $|\psi_{\pm}\rangle = \sqrt{(\Omega_R \mp \Delta_1) / 2\Omega_R} |1\rangle \mp \sqrt{(\Omega_R \pm \Delta_1) / 2\Omega_R} |3\rangle$ corresponding to the energies

$\varepsilon_{1,2} = (\Delta_1 \pm \Omega_R) / 2$ where $\Omega_R = \sqrt{\Delta_1^2 + 4\alpha_1^2}$. Thus for $\Delta_1 \neq 0$ and $|\Delta_1| \gg \alpha_1$ we have

$$|\psi_+\rangle = n_1 [(\alpha_1 / \Delta_1)|1\rangle - |3\rangle], \quad \varepsilon_1 = \Delta_1 + \alpha_1^2 / \Delta_1 \quad (7.32a)$$

$$|\psi_-\rangle = n_1 [|1\rangle + (\alpha_1 / \Delta_1)|3\rangle], \quad \varepsilon_2 = -\alpha_1^2 / \Delta_1 \quad (7.32b)$$

where $n_1 = \Delta_1 / \sqrt{\alpha_1^2 + \Delta_1^2}$ is the normalization constant. States $|\psi_+\rangle$ and $|2\rangle$ are

resonantly coupled by an effective two-photon process [227]. Coupling between states

$|\psi_+\rangle$ and $|4\rangle$ is $\alpha_1\alpha_2 / \Delta_1$. Dressed states of N system therefore correspond to the

eigenvectors of Hamiltonian of the system formed by levels $|2\rangle$, $|\psi_+\rangle$ and $|4\rangle$, i.e.,

$$H = \begin{pmatrix} \Delta_2 - \Delta_3 & 0 & -\alpha_3 \\ 0 & \Delta_1 + \alpha_1^2 / \Delta_1 & \alpha_1\alpha_2 / \Delta_1 \\ -\alpha_3 & \alpha_1\alpha_2 / \Delta_1 & \Delta_3 \end{pmatrix}. \quad (7.33)$$

The effective dark state of the system corresponds to three-photon resonance at

$\Delta_3 = \Delta_2 - \Delta_1$ and the corresponding dressed state eigen vector is

$$|\psi_D\rangle \approx n_2 [(\alpha_1\alpha_2 / \alpha_3\Delta_1)|2\rangle + |\psi_a\rangle]. \quad (7.34)$$

The other two dressed (bright) states of the system are

$$|\psi_{B1,B2}\rangle = n_{B1,B2} \left[-\frac{\alpha_1^2\alpha_2n_1}{\Delta_1^2(\Delta_1 - \varepsilon_{B1,B2})} |1\rangle + \frac{\alpha_3}{\Delta_1 - \varepsilon_{B1,B2}} |2\rangle + \frac{\alpha_1\alpha_2n_1}{\Delta_1(\Delta_1 - \varepsilon_{B1,B2})} |3\rangle + |4\rangle \right] \quad (7.35)$$

which correspond to $\varepsilon_{B1,B2} = \left((\Delta_1 + \Delta_2) \pm \sqrt{(\Delta_1 + \Delta_2)^2 + 4((\alpha_1^2\alpha_2^2 / \Delta_1^2) - \alpha_3^2)} \right) / 2$. Here

$n_2 = \Delta_1\alpha_3 / \sqrt{\alpha_1^2\alpha_2^2 + \Delta_1^2\alpha_3^2}$ and $n_{B1,B2} = \Delta_1(\Delta_1 - \varepsilon_{B1,B2}) / \sqrt{\alpha_1^2\alpha_2^2 + \Delta_1^2\alpha_3^2 + \Delta_1^2(\Delta_1 - \varepsilon_{B1,B2})^2}$

are the normalization constants.

From Eq. (7.32) – (7.34) it is clear that under the weak coupling condition i.e. $\alpha_1/\Delta_1 \ll 1$, dark state $|\psi_D\rangle \approx |3\rangle$. Therefore under steady state almost all the population is transferred to state $|3\rangle$ while the remaining states are correspondingly empty. This results in a sharp resonance, the linewidth of which is dependent on $(\alpha_1^2\alpha_2/\Delta_1^2\alpha_3)^2$ [227]. The complete trapping of population in state $|3\rangle$ is referred to as dark resonance.

Fig. 7.1 displays the populations $\langle \overline{A_{ii}} \rangle$ ($i=1-4$) as a function of Δ_3 at the three-photon resonance condition when $\gamma_{c1} = \gamma_{c2} = \gamma_{c3}$ and $\gamma_{cij} = 0$. The data chosen is same as in Ref. [227]. In the absence of phase fluctuations (*cf.* curve A), the steady state of the system is characterized by two resonances, a sharp three-photon resonance at $\Delta_3 = \Delta_2 - \Delta_1$ corresponding to almost complete transfer of population to state $|3\rangle$ and a broad two-photon resonance at $\Delta_3 = \Delta_2$. Note in Fig. 7.1 that at two-photon resonance condition, the maximum population is in state $|2\rangle$ and this is what is expected in a three-level Λ system [146,147] formed by the levels $|1\rangle$, $|2\rangle$ and $|4\rangle$ in the present problem. Fig. 7.1 thus permits a direct comparison of the behavior of three-photon resonance in N system and two-photon resonance in Λ system under identical phase fluctuations. The effect of phase fluctuations on these resonances is represented by curves B – D in Fig. 7.1. It is clear from Fig. 7.1 that the three-photon resonance is strongly affected by laser bandwidths. Higher bandwidths lead to strong suppression of the population in the metastable level, while increasing the populations in the other levels. Thus the phase fluctuations dephase the atomic coherences thereby destroying the sharp resonance. It then follows that to obtain ultra-narrow three-photon absorptive resonance using three

independent lasers laser bandwidths must be extremely narrow. For example, for the data of Fig. 7.1 the population in level $|3\rangle$ decreases to 96% and 84% for laser linewidths of 1 kHz and 5 kHz respectively. It may also be seen from Fig. 7.1 that the suppression in the two-photon resonance is relatively insensitive to the increase in laser bandwidths.

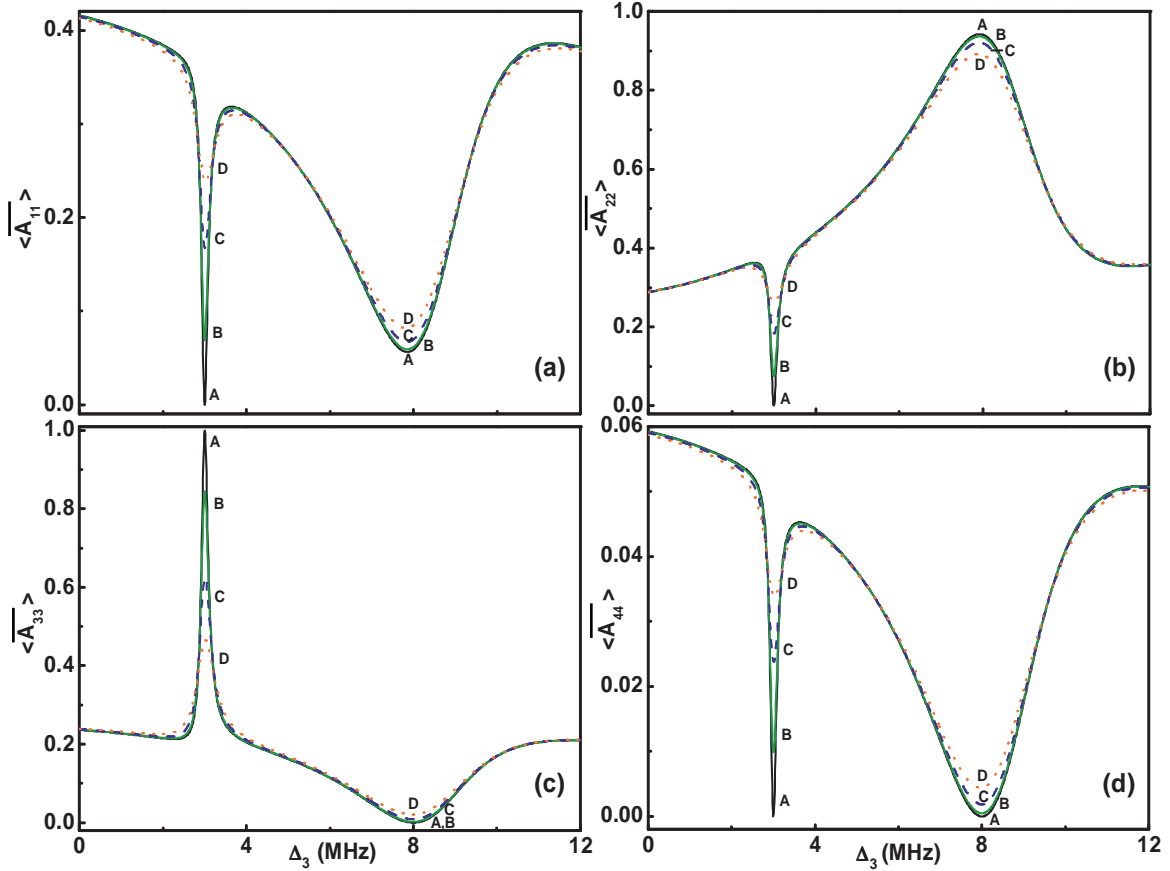


Fig. 7.1: Effect of laser bandwidths on level populations under three-photon resonance condition. Frames (a) – (d) correspond to the populations in levels $|1\rangle$, $|2\rangle$, $|3\rangle$ and $|4\rangle$ calculated for $(\alpha_1, \alpha_2, \alpha_3) = (0.025, 5.0, 1.25)$ MHz, $(\Delta_1, \Delta_2) = (5, 8)$ MHz and $(\gamma_{41}, \gamma_{42}) = (9.375, 0.625)$ MHz. Curves A–D in each frame correspond to bandwidths $\gamma_{c1} = \gamma_{c2} = \gamma_{c3} = 0, 5, 20$ and 50 kHz respectively and all the cross-correlation are assumed to be absent.

In Fig. 7.1 all laser bandwidths were assumed to be equal. Fig. 7.2 shows the effect of individual laser bandwidths on the behavior of two-photon and three-photon resonances respectively when no cross-correlations exist between the lasers. We observe

that the three-photon resonance is affected by all laser bandwidths equally. On the other hand, the suppression of two-photon resonance is dependent only on γ_{c_2} and γ_{c_3} similar to its behaviour in a Λ system.

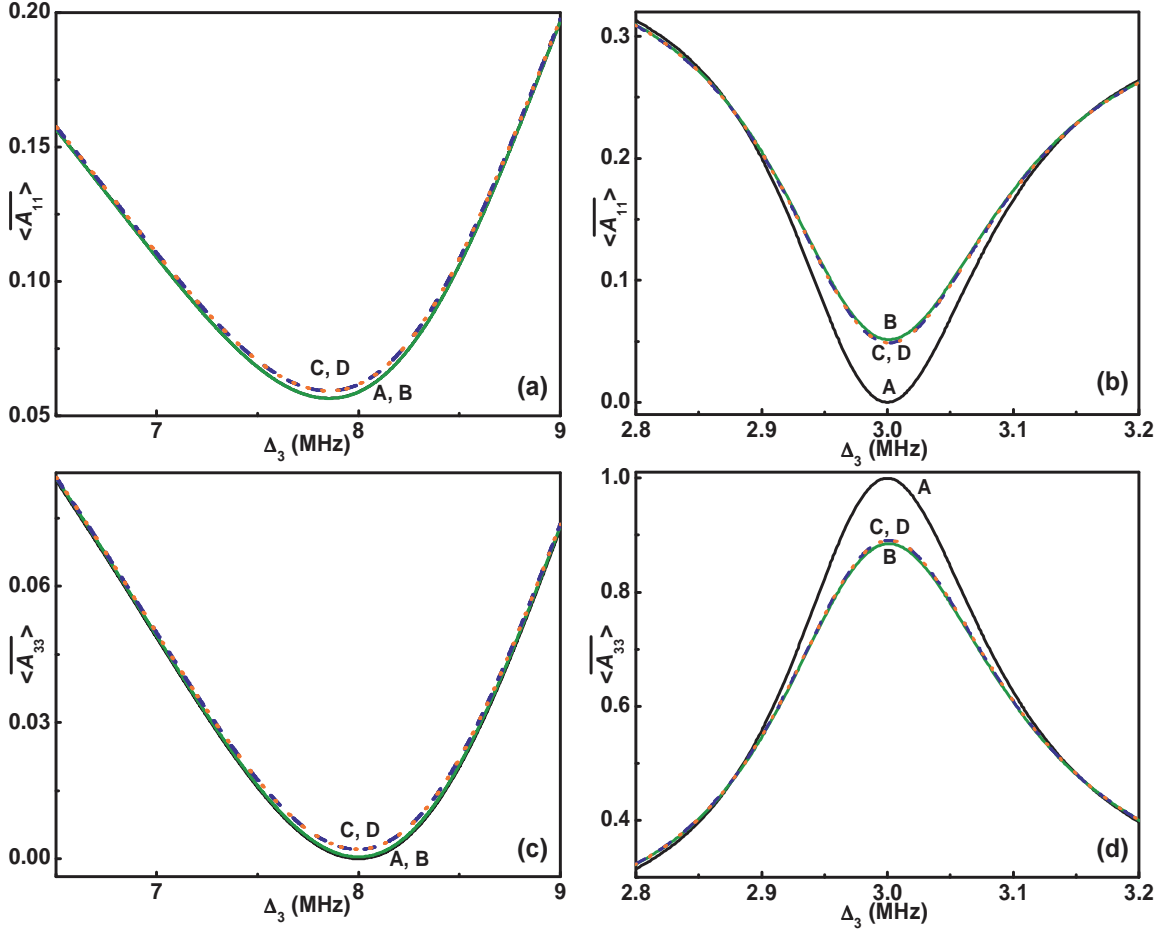


Fig. 7.2: Effect of individual laser bandwidths on the populations of levels $|1\rangle$ and $|3\rangle$ calculated for $(\alpha_1, \alpha_2, \alpha_3) = (0.025, 5.0, 1.25)$ MHz, $(\Delta_1, \Delta_2) = (5, 8)$ MHz and $(\gamma_{41}, \gamma_{42}) = (9.375, 0.625)$ MHz. Frames (a),(c) and (b),(d) highlight the behavior in the vicinity of two- and three-photon resonances respectively. Curves A – D in each frame correspond to $(\gamma_{c_1}, \gamma_{c_2}, \gamma_{c_3}) = (0,0,0), (10,0,0), (0,10,0)$ and $(0,0,10)$ kHz respectively. All cross-correlations are assumed to be zero.

The effect of cross correlations ($\gamma_{c_{ij}}$) in reviving the populations is shown in Fig. 7.3 where we have shown the two- and three-photon resonances when any two fields are critically correlated. It is well known that for Λ system if the driving fields are critically

correlated, the two-photon coherences are unaffected by laser fluctuations and coherence minimum persists [146]. This behavior may be seen in Fig. 7.3(a) and (c) where complete revival is observed when $\gamma_{c2c3} = (\gamma_{c2} + \gamma_{c3})/2$. Note also that the two-photon resonance is insensitive to cross-correlations γ_{c1c2} and γ_{c1c3} . The three-photon resonance, however, behaves very differently from the two-photon resonance, as is seen from Fig. 7.3(b) and (d). Firstly γ_{c1c2} and γ_{c2c3} help to revive three-photon resonance, but only partially even when the relevant fields are critically correlated. Secondly the effect of γ_{c1c3} is opposite, i.e., it results in deterioration of the resonance instead of its restoration.

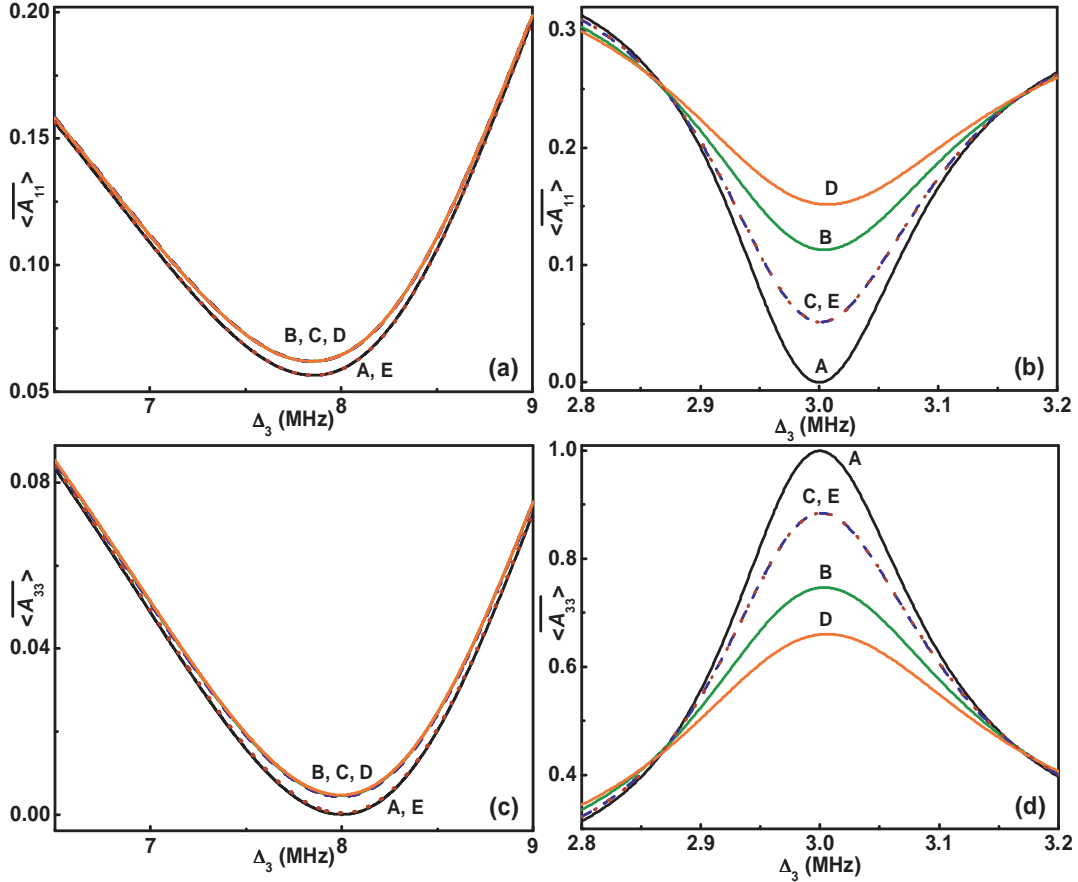


Fig. 7.3: Effect of cross-correlations on the population of levels $|1\rangle$ and $|3\rangle$. The basic atom-field interaction data is same as in Fig. 7.1. Frames (a), (c) and (b), (d) highlight the behavior in the vicinity of two- and three-photon resonances respectively. In each frame the curve A is for $\gamma_{ci} = \gamma_{cij} = 0$ and serves as the reference. For curves B – E, $\gamma_{c1} = \gamma_{c2} = \gamma_{c3} = 10$ kHz and $(\gamma_{c1c2}, \gamma_{c1c3}, \gamma_{c2c3}) = (0,0,0), (10,0,0), (0,10,0)$ and $(0,0,10)$ kHz respectively. Here each pair of fields is assumed to be critically correlated.

The distinctive features of three- and two-photon resonances of N system under laser phase fluctuations may be discussed in terms of the coherences associated with various processes. The coherence ρ_{23} between levels $|2\rangle$ and $|3\rangle$ is responsible for three-photon resonance, while the coherence ρ_{12} between levels $|1\rangle$ and $|2\rangle$ is related to two-photon resonance $\Delta_3 = \Delta_2$. Atomic coherences ρ_{23} and ρ_{12} are associated with the corresponding diagonal terms \wp_7 and \wp_2 given in Eq. (A7.15) and Eq. (A7.11) of Appendix-7 with $p = q = s = 0$, i.e.

$$\wp_7 = -i(\Delta_3 - \Delta_2 + \Delta_1) + \gamma_{c1} + \gamma_{c2} + \gamma_{c3} - 2\gamma_{c1c2} + 2\gamma_{c1c3} - 2\gamma_{c2c3} \quad (7.36)$$

$$\wp_2 = i(\Delta_3 - \Delta_2) + \gamma_{c2} + \gamma_{c3} - 2\gamma_{c2c3} \quad (7.37)$$

Thus the phase fluctuations modify the detunings of system as $\Delta_k \rightarrow \Delta_k + i\gamma_{ck}$, ($k = 1,3$) and $\Delta_2 \rightarrow \Delta_2 - i\gamma_{c2}$. It is clear from these equations that the three-photon resonance is affected by all γ_{ci} equally, while the two-photon resonance is broadened only by γ_{c2} and γ_{c3} . This is consistent with the observations made from Fig. 7.2. The revival of the two-photon resonance for critically correlated fields, i.e., $\gamma_{c2} + \gamma_{c3} = 2\gamma_{c2c3}$ is obvious from Eq. (7.37) and is shown in Fig. 7.3(a) and (c). On the contrary such exact cancellation is not possible in case of three-photon resonance (cf. Eq. (7.36)). Thus γ_{c1c2} and γ_{c2c3} revive the three-photon resonance only partially; see curves C and E of Fig. 7.3(b),(d). As expected the revival is better for small bandwidths of the three lasers. For example the population in metastable state $|3\rangle$ revives to 97% for $\gamma_{ci} = \gamma_{cij} = 1$ kHz (not shown here). One may also note from Eq. (7.36) that the effect of γ_{c1c3} is exactly opposite to that of γ_{c1c2} and γ_{c2c3} , i.e., it does not cancel the effect of γ_{c1} and γ_{c3} , but

rather adds. This results in further suppression of three-photon resonance as is exhibited by curve D of Fig. 7.3(b), (d). This analysis shows that cross-correlation of lasers coupling one of the common levels, i.e., $|1\rangle$ and $|4\rangle$, help to restore the resonance, and consequently these frequencies can be derived from a single laser source to obtain relatively sharp three-photon absorption resonance.

(b) 2+1-Photon Resonance

We now consider the 2+1-photon resonance which is a special case of three-photon resonance. The difference between 2+1- and three-photon resonance is that when the former condition is satisfied, the steady state response of the system is characterized by the Λ system formed by levels $|1\rangle$, $|2\rangle$ and $|4\rangle$ alone. This manifests into a remarkable difference in the response of the system under the two resonance conditions. In the absence of phase fluctuations the dynamics of the system may be conveniently discussed in terms of dressed states of the Λ system given in Table-6. Here the dark state ψ'_1 is a coherent superposition of levels $|1\rangle$ and $|2\rangle$, and the energy of this state is $\varepsilon = \Delta_2 (= \Delta_3)$. For $\alpha_2 > \alpha_3$, the dark state essentially retains the character of level $|2\rangle$. This dark state is resonantly coupled to $|3\rangle$ exhibiting an effective two-level behavior. At long times, however, the system is damped due to off-resonant coupling of $|3\rangle$ with other two dressed states of the Λ system and the rate of this damping is responsible for the width of 2+1-photon resonance [227]. Fig. 7.4 shows the effect of laser bandwidths on the populations $\langle \overline{A_{ii}} \rangle$ ($i = 1 - 4$) for 2+1-photon resonance condition. In the absence of phase fluctuations, almost all population is shared between levels $|2\rangle$ and $|3\rangle$ (*cf.* curve

A in Fig. 7.4). Note that, for $\alpha_2 < \alpha_3$ the steady state population is shared between the levels $|1\rangle$ and $|3\rangle$. The effect of bandwidths of driving fields ($\gamma_{ci} \neq 0$) in the absence of correlations ($\gamma_{cicj} = 0$) may be seen from the curves B, C and D of Fig. 7.4. We observe here that an increase in the laser bandwidths results in broadening of 2+1- photon resonance with no significant change in its height.

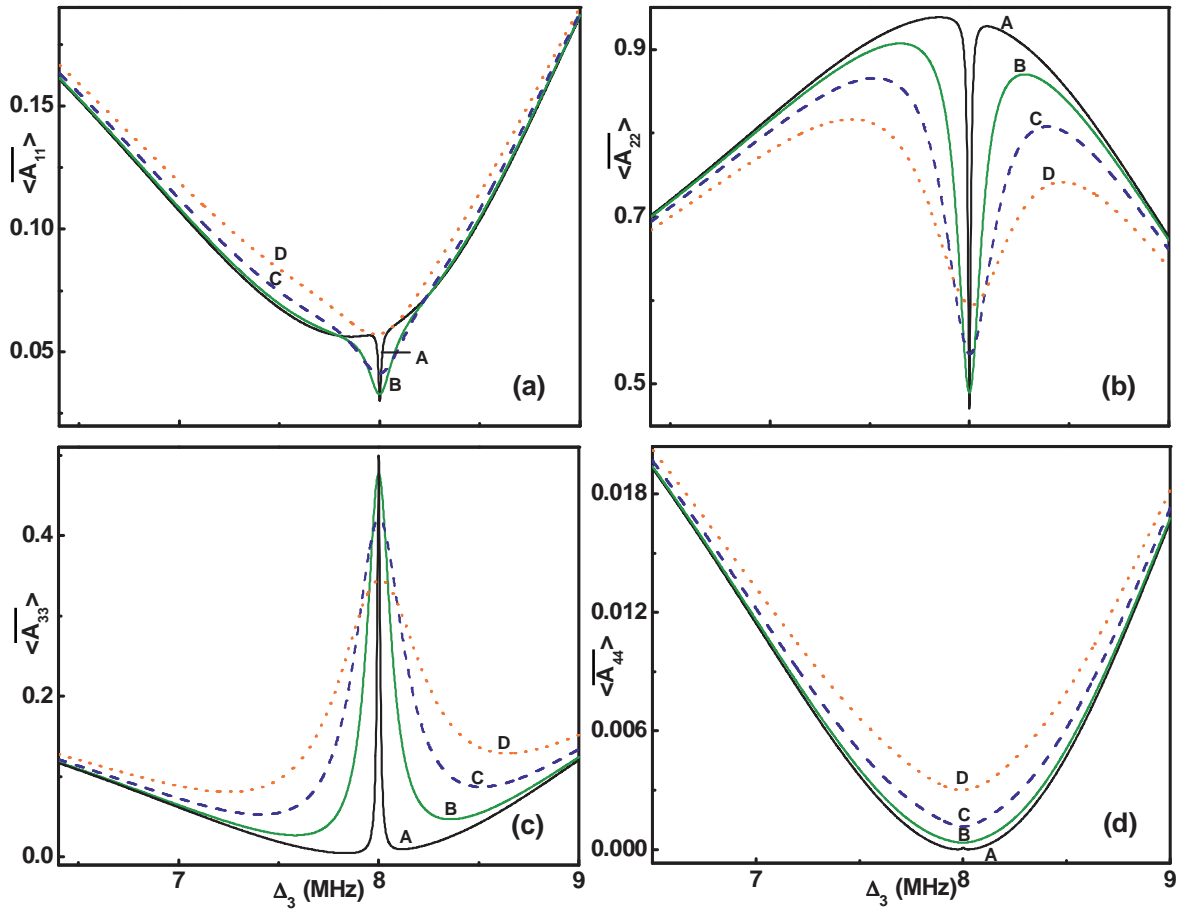


Fig. 7.4: Effect of laser phase fluctuations on the level populations under 2+1-photon resonance condition. Frames (a) – (d) correspond to the populations in levels $|1\rangle$, $|2\rangle$, $|3\rangle$ and $|4\rangle$ calculated for $(\alpha_1, \alpha_2, \alpha_3) = (0.025, 5.0, 1.25)$ MHz, $(\Delta_1, \Delta_2) = (0, 8)$ MHz and $(\gamma_{41}, \gamma_{42}) = (9.375, 0.625)$ MHz. Curves A – D in each frame correspond to bandwidths $\gamma_{c1} = \gamma_{c2} = \gamma_{c3} = 0, 5, 20$ and 50 kHz respectively and all the cross-correlation are assumed to be absent ($\gamma_{cicj} = 0$).

The effect of individual laser bandwidths on the populations of levels $|1\rangle$ and $|3\rangle$ is shown in Fig. 7.5. It is observed that all bandwidths γ_{c_i} affect the populations of levels $|2\rangle$ and $|3\rangle$ in equal measure. However γ_{c_1} has a relatively weaker effect than γ_{c_2} and γ_{c_3} on the populations of levels $|1\rangle$ and $|4\rangle$. The resonance is only slightly broadened in the vicinity of 2+1-photon resonance as shown in Fig. 7.5(a). Nonetheless the populations of these levels are very small and hence this result is of little consequence.

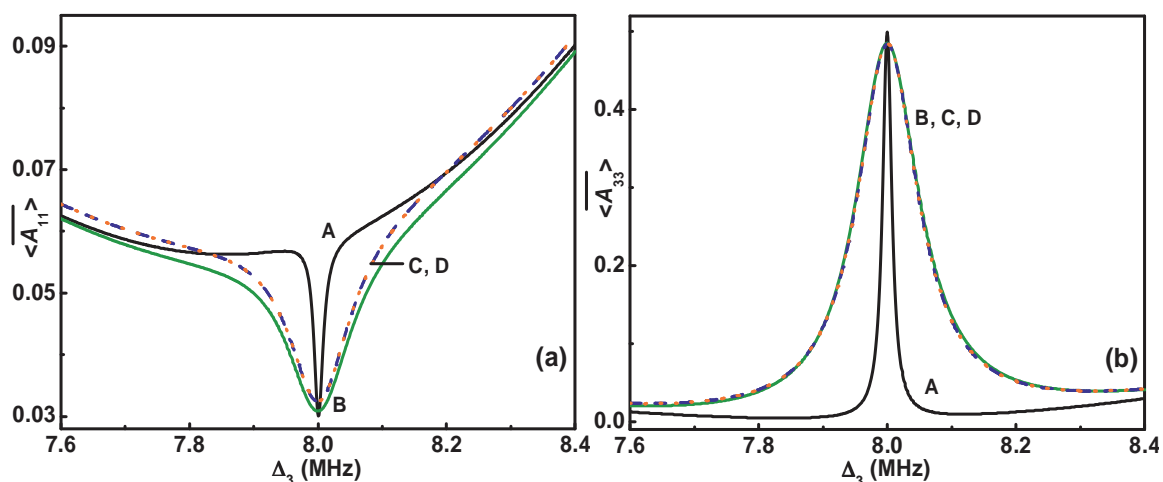


Fig. 7.5: Effect of individual laser bandwidths on the populations of levels $|1\rangle$ and $|3\rangle$ calculated for $(\alpha_1, \alpha_2, \alpha_3) = (0.025, 5.0, 1.25)$ MHz, $(\Delta_1, \Delta_2) = (0, 8)$ MHz and $(\gamma_{41}, \gamma_{42}) = (9.375, 0.625)$ MHz. Shown is the behavior in the vicinity of 2+1-photon resonance. Curves A – D correspond to $(\gamma_{c_1}, \gamma_{c_2}, \gamma_{c_3}) = (0, 0, 0), (10, 0, 0), (0, 10, 0)$ and $(0, 0, 10)$ kHz respectively and all cross-correlations are assumed to be zero.

Thus comparing the behavior of three-photon (*cf.* Fig. 7.2(b),(d)) and 2+1-photon resonances (*cf.* Fig. 7.5) under identical laser bandwidths, it may be concluded that both these resonances are deteriorated under finite bandwidths, however the manner in which this effect is exhibited is different, i.e., suppression for three-photon resonance while broadening for 2+1-photon resonance. The role of cross-correlations when the laser fields

are critically correlated is shown in Fig. 7.6. Correlation $\gamma_{c_2c_3}$ play a stronger role in reviving the populations of level $|1\rangle$ and $|4\rangle$ than $\gamma_{c_1c_2}$. However of interest are the populations of the levels $|2\rangle$ and $|3\rangle$ connected by 2+1-photon coupling, where it is seen that both $\gamma_{c_1c_2}$ and $\gamma_{c_2c_3}$ are effective in restoring the linewidth of the resonance albeit partially. The cross-correlation $\gamma_{c_1c_3}$, however, is found to exhibit detrimental effect. The effect of laser bandwidths and cross-correlations is thus similar to that observed in three-photon resonance, and is in tune with Eq. (7.36). In the absence of phase fluctuations, the damping of the two-state coherent dynamics is responsible for the linewidth of the 2+1-photon resonance [227]. As is discussed in Sec. 7.3.2, the laser phase fluctuations contribute an additional damping mechanism and that results in broadening of the resonance. The cross-correlations on the other hand appear to revive the coherent dynamics to some extent, which helps in restoring the linewidth to some extent.

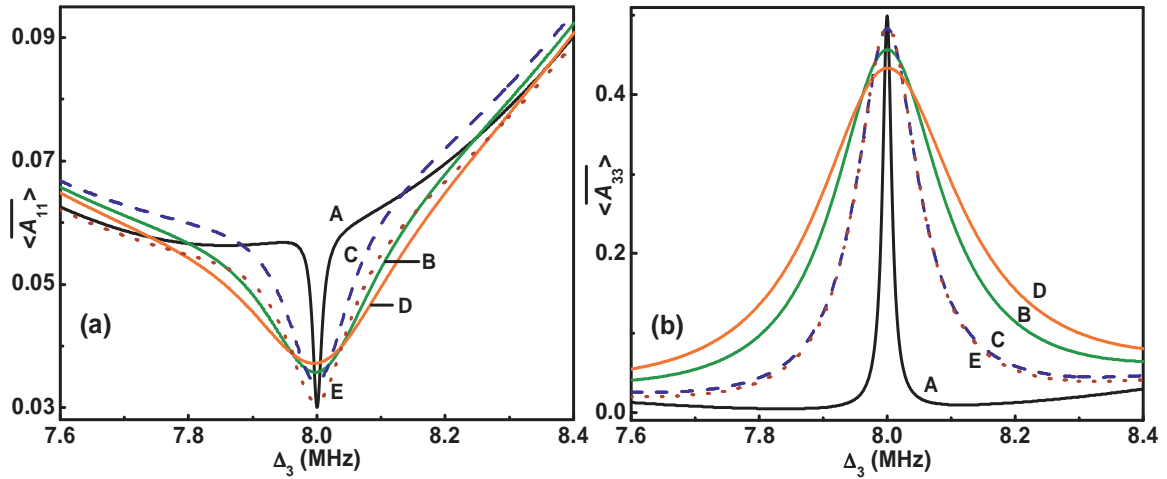


Fig. 7.6: Effect of cross-correlations on the populations of levels $|1\rangle$ and $|3\rangle$ in the vicinity of 2+1-photon resonance. The basic atom-field interaction data is same as in Fig. 7.4. Curve A is for $\gamma_{ci} = \gamma_{c_{ij}} = 0$ and serves as the reference. For curves B – E, $\gamma_{c_1} = \gamma_{c_2} = \gamma_{c_3} = 10$ kHz and $(\gamma_{c_1c_2}, \gamma_{c_1c_3}, \gamma_{c_2c_3}) = (0,0,0), (10,0,0), (0,10,0)$ and $(0,0,10)$ kHz respectively. Here each pair of fields is assumed to be critically correlated.

7.3.2 Time Dependent Behaviour of Population Distribution

Time evolution of the atomic populations under three-photon and 2+1-photon resonance conditions for a N system has been investigated in details in Ref. [227]. We present here the case studies which help us to understand the manner in which the phase fluctuations affect the three- and 2+1-photon resonances. For three-photon case, the time evolution of populations $\langle \overline{A_{ii}} \rangle$, ($i = 1-3$) is shown in Fig. 7.7 for two different initial conditions. In Fig. 7.7(a) – (c) the atom is considered to be in the ground level $|1\rangle$ initially. In the absence of phase fluctuations (curve A) the dynamical behavior of the system is analogous to quantum jumps i.e., an abrupt change of population from one energy level to another, with loss or gain of a quantum of energy [228,229]. In the short time scale (10^{-6} - 10^{-5} s) close to half the population is transferred to quasi steady state $|2\rangle$, i.e., steady state of the intrinsic Λ system. Subsequently in longer time scale (10^{-3} s) population is transferred to the metastable dark state $|3\rangle$, i.e., the steady state of N system, through three-photon coupling. In the steady state, almost all population resides in the dark state. It may be seen from Fig. 7.7(a) – (c) that the phase fluctuations do not affect the behavior of the system in the transient ($< 10^{-6}$ s) or intermediate (10^{-4} s) time scale. The effect of phase fluctuations is however seen in the slow time scale, wherein we find leakage of population from level $|3\rangle$ to levels $|1\rangle$ and $|2\rangle$ (curve B). Inclusion of critical cross-correlations helps to restore the population, albeit only partially (curve C). Fig. 7.7(d) – (f) shows the time dependent behavior when initial state is the metastable state $|3\rangle$. In the absence of phase fluctuations, system remains in the initial state at all times (curve A). However the presence of phase fluctuations results in redistribution of

population in the slow time scale (curve B). The cross-correlations help to revive the original behavior only partially (curve C). Increase in the laser bandwidths thus reduce the population in $|3\rangle$ while the critical cross-correlations result in its partial restoration.

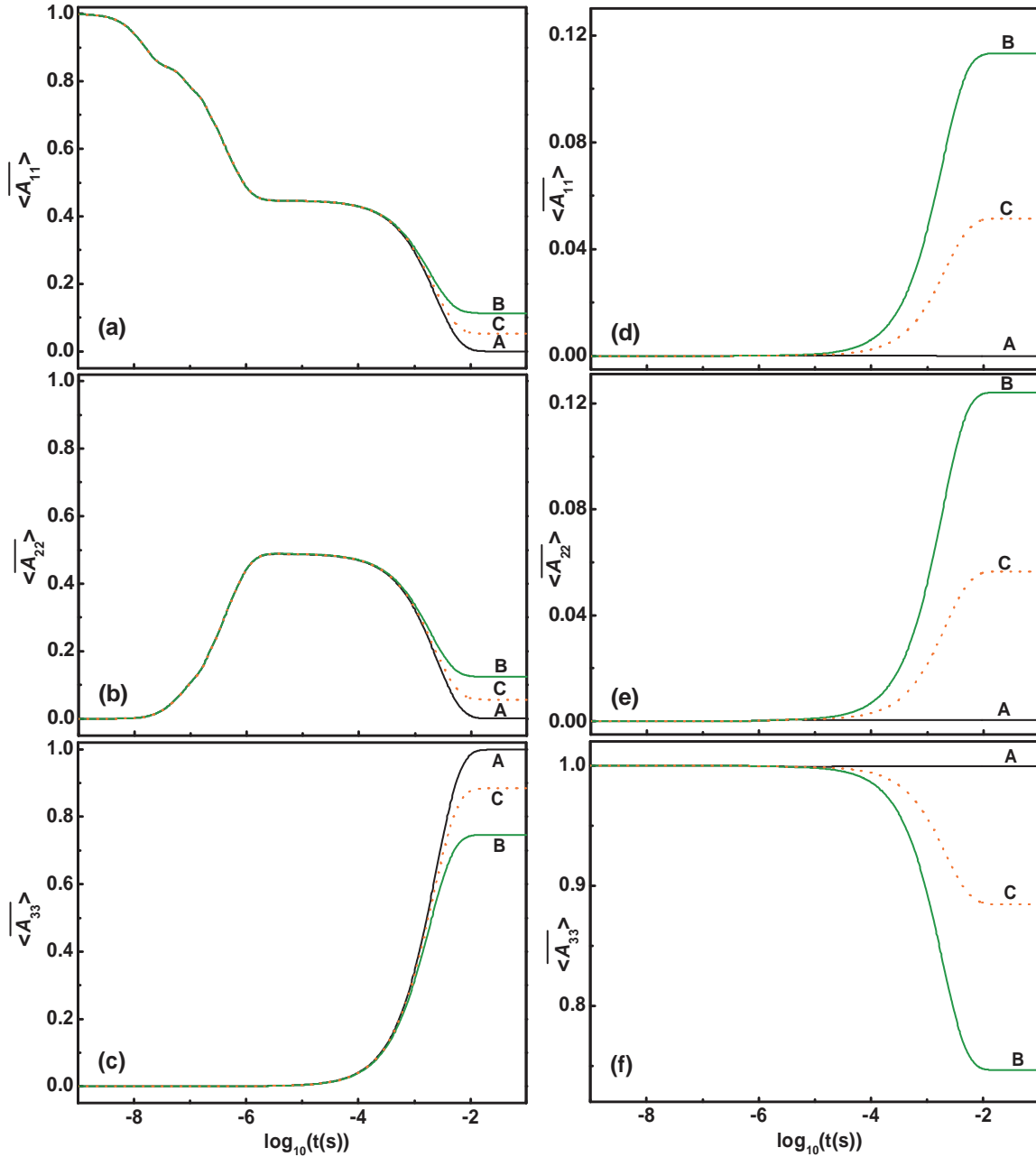


Fig. 7.7: Time evolution of populations at three-photon resonance calculated for $(\alpha_1, \alpha_2, \alpha_3) = (0.025, 5.0, 1.25)$ MHz, $(\Delta_1, \Delta_2, \Delta_3) = (5, 8, 3)$ MHz and $(\gamma_{41}, \gamma_{42}) = (9.375, 0.625)$ MHz. For frames (a) – (c) the initial condition is set as level $|1\rangle$ while for frames (d) – (f) it is level $|3\rangle$. Curves A – C correspond to $(\gamma_{c1}, \gamma_{c2}, \gamma_{c3}, \gamma_{c1c2}, \gamma_{c1c3}, \gamma_{c2c3}) = (0, 0, 0, 0, 0, 0)$, $(10, 10, 10, 0, 0, 0)$ and $(10, 10, 10, 10, 10, 10)$ kHz respectively.

The observations made on the steady state three-photon resonance under fluctuating laser fields are consistent with Fig. 7.7. Fig. 7.8 shows the time evolution of the populations $\langle A_{ii} \rangle$, ($i = 1-3$) for 2+1-photon resonance condition.

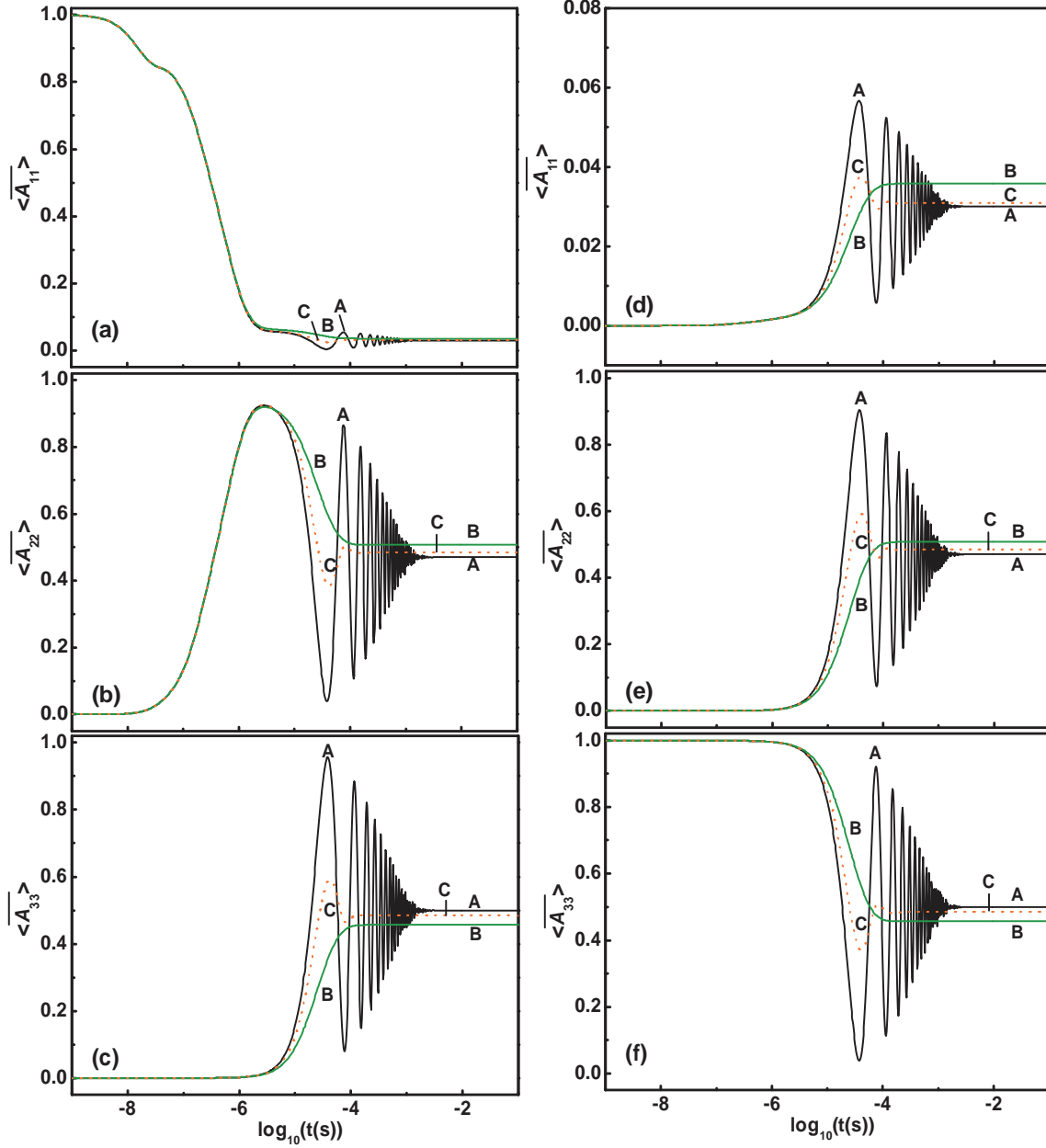


Fig. 7.8: Time evolution of populations in levels $|1\rangle$, $|2\rangle$ and $|3\rangle$ at 2+1-photon resonance calculated for $(\Delta_1, \Delta_2, \Delta_3) = (0, 8, 8)$ MHz. For frames (a) – (c) the initial condition is set as level $|1\rangle$ while for frames (d) – (f) it is level $|3\rangle$. Curves A – C correspond to $(\gamma_{c1}, \gamma_{c2}, \gamma_{c3}, \gamma_{c1c2}, \gamma_{c1c3}, \gamma_{c2c3}) = (0, 0, 0, 0, 0, 0)$, $(10, 10, 10, 0, 0, 0)$ and $(10, 10, 10, 10, 10, 10)$ kHz respectively. Other data are same as in Fig. 7.7.

The atom is considered to be initially in level $|1\rangle$ for frames (a) – (c). In the absence of phase fluctuations (*cf.* curve A), in the time scale of 10^{-6} s, the system jumps from $|1\rangle$ to $|2\rangle$ which is the trapped state of the Λ system. Thereafter the system exhibits two-state coherent dynamics involving levels $|2\rangle$ and $|3\rangle$ as may be seen from out of phase Rabi oscillations of these levels. However these oscillations are damped by off-resonant coupling of $|3\rangle$ and beyond 10^{-2} s the system attains steady state population. The effect of finite bandwidths of laser is to further damp the Rabi oscillations and cause only a marginal deviation in the steady state result (curve B). The transient behavior ($< 10^{-5}$ s) is unaffected by the bandwidths.

Inclusion of cross-correlations at their critical values helps to restore the coherent behavior to a limited extent (curve C). The critical cross correlations do not revive the coherent Rabi oscillations completely unlike the steady state populations which are almost completely revived. Very similar observations may be made from Fig. 7.8(d) – (f), where we have exhibited the time dependent behavior of the system when the atom is initially taken in level $|3\rangle$. Fig. 7.8 thus explicitly shows that the laser bandwidths primarily affect the coherent dynamics of the effective two-level system with little change in the steady state populations. The additional damping arising from the phase fluctuations is reflected in the increased linewidth of 2+1-photon resonance and very little change in its height. This is consistent with the observations made on the steady state 2+1-photon resonance under fluctuating laser fields.

For the sake of completeness we have also studied the effect of phase fluctuations and cross correlations on intensity-intensity correlation functions. In absence of phase

fluctuations the intensity-intensity correlation functions show the expected oscillations through bunching and anti-bunching cycles decaying to their steady-state value 1. The phase fluctuations tend to reduce the amplitudes of these oscillations but do not change the basic structure of the curves.

7.4 Effect of Phase Fluctuations on Absorption

In this section we examine the effect of laser phase fluctuations on the absorption spectra of N -system specifically on EIA resonance. We consider model C of Chapter-6 for this analysis where the weak probe laser E_2 drives $|1\rangle \rightarrow |4\rangle$ transition. This model is chosen as a representative of EIT/EIA resonances in N system. A similar behaviour is observed for the other models also and hence not shown here. The density operator χ^{pqs} is used to compute the one-time expectation values of the off-diagonal atomic operators averaged over the ensemble of the phase fluctuations as given in Eq. (7.29). A typical result for the effect of the independent laser fluctuations on the EIA resonance for the data of Fig. 6.9(a) is shown in Fig. 7.9. This figure shows that the effect of phase fluctuations on EIA resonance is in sync with the effect on populations. The effect of phase fluctuations on the EIT resonances is similar.

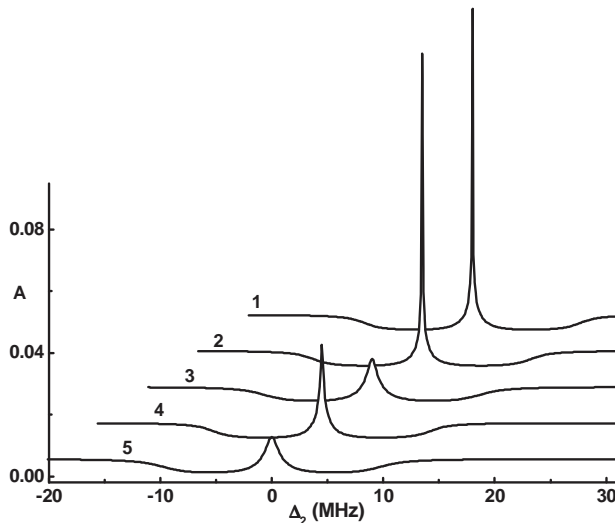


Fig. 7.9: Effect of individual laser bandwidths on the EIA resonance calculated for $\alpha_1 = \alpha_3 = 5$ MHz and $\Delta_1 = \Delta_3 = 0$. $(\gamma_{c1}, \gamma_{c2}, \gamma_{c3}) = (0,0,0)$, $(0.1,0,0)$, $(0,0.1,0)$, $(0,0,0.1)$ and $(0.1,0.1,0.1)$ MHz for curves 1 – 5 respectively. All cross-correlations are assumed to be zero.

In general the laser phase fluctuations broaden and destroy the EIA/EIT resonances, however the extent of this effect is critically dependent on the phase fluctuations associated with the pump, probe and control laser. For example, phase fluctuation γ_{c1} in the laser E_1 , which forms the V sub-system of the N-resonance, is found to be of very little consequence. However the fluctuations associated with the Λ sub-system i.e. the probe and pump lasers (γ_{c2} and γ_{c3}) matter a lot. Curve 5 shows the case when all the lasers have equal bandwidths. As seen from Fig. 7.9 curve 3 and 5 are almost identical which proves that the major suppression of the EIA resonance is caused by the fluctuations in the probe laser. The effect of individual cross-correlations on EIA resonance with fluctuating driving fields is shown in Fig. 7.10.

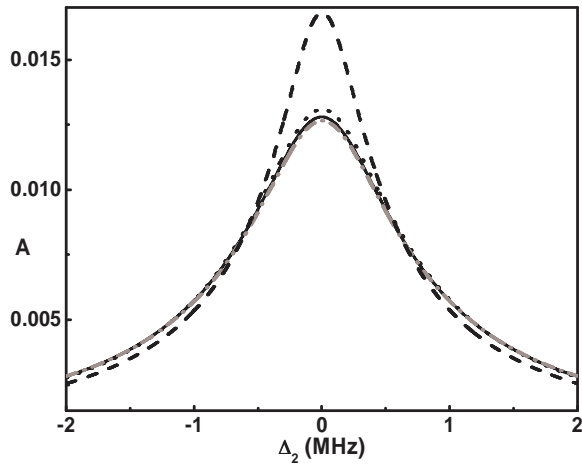


Fig. 7.10: Effect of cross-correlations on the EIA resonance. The basic atom-field interaction data is same as in Fig. 7.9. $\gamma_{c1} = \gamma_{c2} = \gamma_{c3} = 0.1$ MHz and, $(\gamma_{c1c2}, \gamma_{c1c3}, \gamma_{c2c3}) = (0,0,0), (0.1,0,0), (0,0.1,0)$ and $(0,0,0.1)$ MHz for solid, dotted, gray dash-dotted and dashed curves respectively. Here each pair of fields is assumed to be critically correlated.

Introduction of cross-correlations helps to revive the resonances, but here also the extent to which that happens depends on the specific cross-correlations. For example, cross-correlation between the two strong lasers γ_{c1c3} further spoils the EIA/EIT resonance similar to its effect on populations. The correlations between the probe and pump (control) laser helps in reviving the resonance. Out of these two cross correlations, the one between the two fields forming the inherent Λ system, i.e., γ_{c2c3} helps to a much greater extent in the revival as is shown by dashed curve in Fig. 7.10.

CHAPTER 8

COHERENCE INDUCED NEGATIVE REFRACTIVE INDEX IN FOUR-LEVEL ATOMIC MEDIUM

8.1 Introduction

The propagation of electromagnetic wave in a medium is governed by its refractive index $n_r = \sqrt{\epsilon_r \mu_r}$. Here ϵ_r and μ_r are relative dielectric permittivity and permeability which in general are complex functions of frequency. Depending on the value of refractive index, all the available media/materials can be characterized into four quadrants as shown in Fig. 8.1. Conventional optical materials belong to the first quadrant. These are known as right handed materials since electric vector \vec{E} , magnetic vector \vec{H} and wave vector \vec{k} form a right handed coordinate frame in them. The second and fourth quadrants constitute non-propagating evanescent waves. While the gaseous

and solid plasma materials belong to the second quadrant, materials which can be structured to behave like magnetic plasma belong to the fourth quadrant.

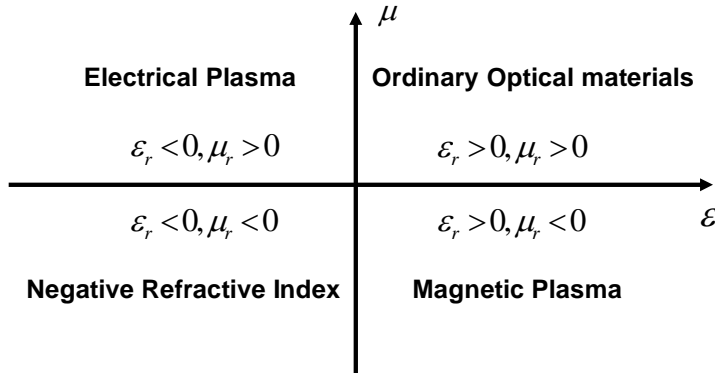


Fig. 8.1: Quadrant diagram illustrating the classification of materials based on the values of ε_r and μ_r .

Most interesting materials which offer possibilities of controlling light propagation within a medium belong to the third quadrant. These materials are characterized by simultaneous negative ε_r and μ_r and are referred to as negative refractive index (NRI) materials, double negative materials, backward wave media (having negative group velocity), left-handed materials (LHMs) or metamaterials. \vec{E} , \vec{H} and \vec{k} form a left-handed triad of vectors in NRI media. Further the Poynting vector is in opposite direction to wave propagation and hence the group velocity direction, which modifies the conventional route of refraction, diffraction and scattering of waves in these materials. The existence of LHMs was predicted by Veselago in 1968 [115]. He showed that LHMs do not violate any fundamental physical law and some of the most fundamental electromagnetic properties in these materials are opposite to that of ordinary materials, resulting in unusual optics. Some of the counter-intuitive electromagnetic and optical effects exhibited by these materials are reversed Snell's law, reversed Doppler shift, an obtuse angle for Cherenkov radiation, anomalous refraction, sub-wavelength focusing, negative Goos-Hanchen shift, intense enhancement of the local fields, distinct

phase matching conditions and nonlinear response, photon tunneling etc. [115-121]. Due to nonexistence of such materials naturally this field did not captured the attention of researchers for a long time. However following the demonstration of the key practical application of LHM i.e. perfect lens by Pendry in 2000 [117] the interest in these materials has grown tremendously. He showed that a NRI slab can focus all Fourier components and amplify evanescent modes allowing a complete reconstruction of a point source to a perfect point image, thus making it possible to achieve, in principle, unlimited resolution without any loss of energy [117]. Since then LHMs have become one of the frontline research area. The captivating optical properties of LHM not only bring new conceptual horizons in the basic understanding of physics but make them a potential candidate for diverse applications such as sub-wavelength imaging and beam refocusing, electromagnetic cloaking, slow and stopped light, stimulated Raman scattering, enhanced bio-sensing, quantum computation, in acoustics, photonics etc. [115-121].

8.2 Approaches for Realization of Negative Refraction Index

Several fascinating approaches have been developed for fabrication of LHMs. Most of the LHMs have been artificially realized in the microwave region using transmission line simulation, nanostructures, assembling composite lattice of metallic split ring resonators and metallic wires, or by using anomalous propagation properties of light in two-dimensional photonic crystal structures with periodicity of the order of or much smaller than the wavelength of the electromagnetic field [122,123]. All such materials, also known as artificial metamaterials, require delicate manufacturing of spatially periodic structures. Very recently Yoon *et al.* [124] have demonstrated NRI by

exploiting inertia of electrons in semiconductor two-dimensional electron gases which promises to open a path to miniaturization in the science and technology of these materials.

Of particular interest is the realization of NRI in optical region. However in this region refraction is always accompanied with absorption. Further it is difficult to realize negative μ_r with low loss, since magnetic dipole response to an oscillating magnetic field is smaller than the electric dipole response by a factor of α_{fs}^2 , where $\alpha_{fs} \approx 1/137$ is the fine structure constant. Several elegant suggestions such as magneto cross coupling technique or chirality induction have been made to alleviate this problem. A chiral media is an optically active media capable of producing negative refraction of circularly polarized wave [125]. Coupling a magnetic dipole transition coherently with an electric dipole transition may lead to electromagnetically induced chirality, which can show NRI with suppressed absorption without requiring negative permeability [118]. However such media suffer from losses due to environmental effects. Another proposal suggested a quantum optical approach in which, under certain conditions, electric-dipole and magnetic-dipole transitions in a multilevel EIT atomic/molecular system exhibit NRI [126-131]. As has been established in previous chapters EIT based dispersive media do not suffer from absorption at resonance, and offer low transmission losses even at high frequencies.

The realization of negative refraction in EIT based Λ system was first proposed by Oktel *et al.*, however with a stringent condition that the middle state ($|2\rangle$ in Fig. 1.2 (a)) is involved in both magnetic transition and electric transition at the same frequency [126]. A much realistic four-level EIT system was studied by Thommen and Mandel

[127] for the existence of left-handedness within a restricted domain of parameters and the requirement of degeneracy of the four levels. Further they suggested that atomic hydrogen and neon are good candidates for such experiments [127]. Since then several multilevel schemes based on quantum coherence and interference have been studied to realize NRI [128-131]. This method of coherently prepared atomic media offers various advantages such as realization of NRI in optical frequency range, electric and magnetic responses at atomic level and isotropic macroscopic electromagnetic structure as compared to artificial metamaterials.

In the chapter we demonstrate the use of laser induced coherent preparation of atomic medium to obtain simultaneous negative ϵ_r and μ_r with minimal absorption in four-level systems in two different configurations interacting with trichromatic coherent field. Such systems can be realized within the hyperfine energy level or Zeeman manifold of alkali atoms. The advantage of *rf* field coupling over the conventional three level Λ scheme [126] is the additional control of μ_r by regulating the *rf* field parameters. Further the *rf* field provides flexibility for adjusting frequency, depth and dispersion of the EIT resonance. We obtain ϵ_r and μ_r for a dense atomic medium in the framework of master equation and Clausius-Mossotti relation. Local field corrections (arising due to dipole-dipole interaction of the neighboring atoms) to the susceptibilities of the medium enhance the magnetic response and play an important role in reducing the absorptive losses. Our analysis shows that negative ϵ_r and μ_r can be realized simultaneously in certain probe frequency regions with transparent propagation due to EIT. The use of the dispersion property of the negative refractive index to control the group velocity of the probe beam from subluminal to superluminal is also discussed.

8.3 Description of the Models

We consider two Λ type four-level schemes coupled by three coherent fields as shown in Fig. 8.2.

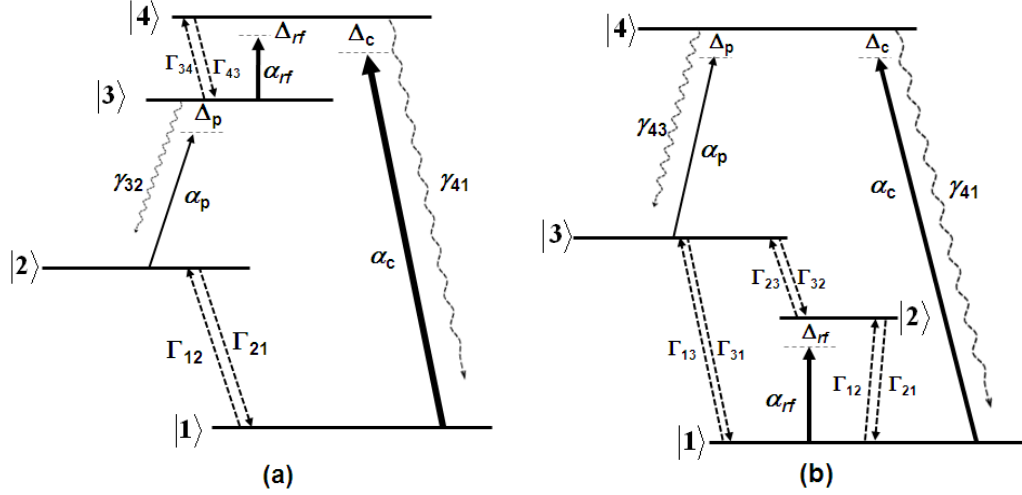


Fig. 8.2: Schematic representation of four-level systems coherently driven by three laser fields: control, rf and probe of Rabi frequencies $2\alpha_c$, $2\alpha_{rf}$ and $2\alpha_p$ respectively. The corresponding detunings are Δ_c , Δ_{rf} and Δ_p . Radiative and nonradiative decay rates associated with $|i\rangle \rightarrow |j\rangle$ transition are denoted by γ_{ij} and Γ_{ij} respectively.

Model (a): The scheme is similar to the DDL system studied in Chapters-4 and -5 with an additional rf field coupling the excited levels as shown in Fig. 8.2(a). Here transitions $|1\rangle \rightarrow |4\rangle$ and $|2\rangle \rightarrow |3\rangle$ are driven by control and probe lasers of Rabi frequencies $2\alpha_c$ and $2\alpha_p$ respectively. The electric dipole forbidden transition $|3\rangle \rightarrow |4\rangle$ is driven by a rf field of Rabi frequency $2\alpha_{rf}$. The relevant electric and magnetic dipole moments are $\vec{d}_{ij} = \langle i|\hat{d}|j\rangle$ and $\vec{m}_{ij} = \langle i|\hat{m}|j\rangle$ where \hat{d} and \hat{m} are the electric and magnetic dipole operators respectively. The detunings of control, rf and probe fields are $\Delta_c = \omega_{41} - \Omega_c$, $\Delta_{rf} = \omega_{43} - \Omega_{rf}$ and $\Delta_p = \omega_{32} - \Omega_p$ respectively. This scheme was earlier studied by Fu *et al.* [230] to show switching between EIT and EIA depending on the field detunings.

Model (b): This scheme consists of a triplet ground state $|1\rangle$, $|2\rangle$ and $|3\rangle$ and an excited state $|4\rangle$. Here transitions $|1\rangle \rightarrow |4\rangle$, $|3\rangle \rightarrow |4\rangle$ and $|1\rangle \rightarrow |2\rangle$ are driven by probe, control and *rf* fields of Rabi frequencies $2\alpha_p$, $2\alpha_c$ and $2\alpha_{rf}$ respectively. The detunings of these fields from the corresponding atomic resonances are $\Delta_p = \omega_{43} - \Omega_p$, $\Delta_c = \omega_{41} - \Omega_c$ and $\Delta_{rf} = \omega_{21} - \Omega_{rf}$. This scheme has been earlier studied in context of *rf* induced dynamic Stark effect [231], experimental realization of double dark resonances [232], sub-Doppler resonances [232,233] and other quantum interference effects [234].

8.4 Realization of Negative Refractive Index in Model (a)

8.4.1 Theoretical Formulation

In this section we obtain relative permittivity and permeability for a dense atomic medium in the framework of master equation and Clausius-Mossotti relation.

(a) Density Matrix Equations and Coherences

The time evolution of the system is described by the following master equation,

$$d\rho/dt = -\frac{i}{\hbar}[H_0, \rho] - \sum_{i,j} \gamma_{ij} (A_{ii}\rho - 2A_{ji}\rho A_{ij} + \rho A_{ii}) - \sum_{i,j} \Gamma_{ij} (A_{ii}\rho - 2A_{ji}\rho A_{ij} + \rho A_{ii}), \quad (8.1)$$

where γ_{ij} and Γ_{ij} represent the radiative and non radiative decay rates associated with transitions $|i\rangle \rightarrow |j\rangle$. The semi classical Hamiltonian of the system under RWA is

$$H_0 = -\alpha_c (A_{14} + A_{41}) - \alpha_p (A_{23} + A_{32}) - \alpha_{rf} (A_{34} + A_{43}) \\ + (\Delta_c - \Delta_{rf} - \Delta_p) A_{22} + (\Delta_c - \Delta_{rf}) A_{33} + \Delta_c A_{44}. \quad (8.2)$$

The elements of the density operator satisfy the following equations:

$$d\rho_{11}/dt = -2\Gamma_{12}\rho_{11} - i\alpha_c(\rho_{14} - \rho_{41}) + 2\Gamma_{21}\rho_{22} + 2\gamma_{41}\rho_{44}, \quad (8.3a)$$

$$d\rho_{12}/dt = -f_1\rho_{12} - i\alpha_p\rho_{13} + i\alpha_c\rho_{42}, \quad (8.3b)$$

$$d\rho_{13}/dt = -i\alpha_p\rho_{12} - f_2\rho_{13} - i\alpha_{rf}\rho_{14} + i\alpha_c\rho_{43}, \quad (8.3c)$$

$$d\rho_{14}/dt = -i\alpha_c(\rho_{11} - \rho_{44}) - i\alpha_{rf}\rho_{13} - f_3\rho_{14}, \quad (8.3d)$$

$$d\rho_{22}/dt = 2\Gamma_{12}\rho_{11} - 2\Gamma_{21}\rho_{22} - i\alpha_p(\rho_{23} - \rho_{32}) + 2\gamma_{32}\rho_{33}, \quad (8.3e)$$

$$d\rho_{23}/dt = -i\alpha_p(\rho_{22} - \rho_{33}) - f_4\rho_{23} - i\alpha_{rf}\rho_{24}, \quad (8.3f)$$

$$d\rho_{24}/dt = -i\alpha_c\rho_{21} - i\alpha_{rf}\rho_{23} - f_5\rho_{24} + i\alpha_p\rho_{34}, \quad (8.3g)$$

$$d\rho_{33}/dt = -i\alpha_p(\rho_{32} - \rho_{23}) - 2(\gamma_{32} + \Gamma_{34})\rho_{33} - i\alpha_{rf}(\rho_{34} - \rho_{43}) + 2\Gamma_{43}\rho_{44}, \quad (8.3h)$$

$$d\rho_{34}/dt = i\alpha_p\rho_{24} - i\alpha_c\rho_{31} - i\alpha_{rf}(\rho_{33} - \rho_{44}) - f_6\rho_{34}, \quad (8.3i)$$

$$d\rho_{44}/dt = i\alpha_c(\rho_{14} - \rho_{41}) + 2\Gamma_{34}\rho_{33} + i\alpha_{rf}(\rho_{34} - \rho_{43}) - 2(\gamma_{41} + \Gamma_{43})\rho_{44}, \quad (8.3j)$$

where the coefficients f_i are defined as

$$\begin{aligned} f_1 &= \Gamma_{12} + \Gamma_{21} + i(\Delta_c - \Delta_{rf} - \Delta_p), & f_2 &= \Gamma_{12} + \gamma_{32} + \Gamma_{34} + i(\Delta_c - \Delta_{rf}), \\ f_3 &= \Gamma_{12} + \gamma_{41} + \Gamma_{43} + i\Delta_c, & f_4 &= \Gamma_{21} + \gamma_{32} + \Gamma_{34} + i\Delta_p, \\ f_5 &= \Gamma_{21} + \gamma_{41} + \Gamma_{43} + i(\Delta_p + \Delta_{rf}), & f_6 &= \gamma_{32} + \Gamma_{34} + \gamma_{41} + \Gamma_{43} + i\Delta_{rf}. \end{aligned} \quad (8.4)$$

For weak probe laser steady state solutions of Eq. (8.3) can be obtained as follows:

$$\rho_{32}^{(1)} = \frac{\alpha_p[f_1\alpha_{rf}\rho_{43}^{(0)} + i\{(f_1f_5^* + \alpha_c^2)(\rho_{22}^{(0)} - \rho_{33}^{(0)}) + \alpha_c\alpha_{rf}\rho_{13}^{(0)}\}]}{f_1f_4^*f_5^* + \alpha_{rf}^2f_1 + \alpha_c^2f_4^*} = \rho_{23}^{(1)*}, \quad (8.5a)$$

$$\rho_{12}^{(1)} = \frac{\alpha_p[f_4^*\alpha_c\rho_{43}^{(0)} - i\{(f_4^*f_5^* + \alpha_{rf}^2)\rho_{13}^{(0)} + \alpha_c\alpha_{rf}(\rho_{22}^{(0)} - \rho_{33}^{(0)})\}]}{f_1f_4^*f_5^* + \alpha_{rf}^2f_1 + \alpha_c^2f_4^*} = \rho_{21}^{(1)*}, \quad (8.5b)$$

$$\rho_{43}^{(0)} = i\alpha_{rf}[(f_2f_3 + \alpha_{rf}^2)(\rho_{33}^{(0)} - \rho_{44}^{(0)}) - \alpha_c^2(\rho_{11}^{(0)} - \rho_{44}^{(0)})]/F_1, \quad (8.5c)$$

$$\rho_{13}^{(0)} = -\alpha_c\alpha_{rf}[f_6^*\rho_{11}^{(0)} + f_3\rho_{33}^{(0)} - (f_3 + f_6^*)\rho_{44}^{(0)}]/F_1, \quad (8.5d)$$

$$\rho_{11}^{(0)} = -\Gamma_{21}[\gamma_{32}\gamma_{41} + \Gamma_{34}\gamma_{41} + \gamma_{32}\Gamma_{43} - \alpha_c^4\alpha_{rf}^4 j_2^2 + \alpha_c^2\alpha_{rf}^2 \{j_1 j_3 - j_2(\Gamma_{34} - \Gamma_{43} + 2\gamma_{32})\} + \alpha_c^2 j_1(\gamma_{32} + \Gamma_{43}) + \alpha_{rf}^2 j_3(\gamma_{32} + \gamma_{41})]/F_2, \quad (8.6a)$$

$$\rho_{33}^{(0)} = -\alpha_c^2\Gamma_{21}[j_1\Gamma_{43} + \alpha_{rf}^2(j_1 j_3 + j_2\gamma_{41}) - \alpha_c^2\alpha_{rf}^4 j_2^2]/F_2, \quad (8.6b)$$

$$\rho_{44}^{(0)} = -\alpha_c^2\Gamma_{21}[j_1(\gamma_{32} + \Gamma_{34}) + \alpha_{rf}^2(j_1 j_3 - j_2\gamma_{32}) - \alpha_c^2\alpha_{rf}^4 j_2^2]/F_2, \quad (8.6c)$$

$$\rho_{22}^{(0)} = 1 - \rho_{11}^{(0)} - \rho_{33}^{(0)} - \rho_{44}^{(0)}, \quad (8.6d)$$

where

$$j_1 = \text{Re}[(f_2 f_6^* + \alpha_c^2)/F_1], \quad j_2 = \text{Re}(F_1)/|F_1|^2, \quad j_3 = \text{Re}[(f_2 f_3 + \alpha_{rf}^2)/F_1], \quad (8.7a)$$

$$F_1 = f_2 f_3 f_6^* + \alpha_c^2 f_3 + \alpha_{rf}^2 f_6^*, \quad (8.7b)$$

$$\begin{aligned} F_2 = & -[\alpha_c^4\alpha_{rf}^4 j_2^2(\Gamma_{12} + 3\Gamma_{21} + \gamma_{32}) + \alpha_c^2\alpha_{rf}^2 \{j_1 j_3(\Gamma_{12} + 3\Gamma_{21} + \gamma_{32}) \\ & - j_2[2\gamma_{32}\gamma_{41} + \Gamma_{12}(-2\gamma_{32} - \Gamma_{34} + \Gamma_{43}) + \Gamma_{21}(\gamma_{41} + \Gamma_{43} - 3\gamma_{32} - \Gamma_{34})\}] \\ & + \alpha_c^2 j_1[(\Gamma_{12} + 2\Gamma_{21})(\gamma_{32} + \Gamma_{34}) + \Gamma_{43}(\gamma_{32} + \Gamma_{21})] + \alpha_{rf}^2 j_3 \\ & (\Gamma_{12} + \Gamma_{21})(\gamma_{32} + \Gamma_{34}) + (\Gamma_{12} + \Gamma_{21})(\gamma_{41}\Gamma_{34} + \gamma_{32}\gamma_{41} + \gamma_{32}\Gamma_{43})]. \end{aligned} \quad (8.7c)$$

(b) Electric and Magnetic Response

The atomic coherences can be used to analyze the possibility of observing NRI in the medium. Transitions $|2\rangle \rightarrow |3\rangle$ and $|1\rangle \rightarrow |2\rangle$ are driven by electric and magnetic field of the weak probe respectively. Therefore the coherences related to the electric and magnetic response are $\rho_{32}^{(1)}$ and $\rho_{21}^{(1)}$ respectively. The induced electric dipole moment of an atom due to the interaction with probe field is given by

$$\vec{P}_e(\omega_p) = \text{Tr}(\hat{\rho} \vec{d}) = \vec{d}_{23}\rho_{32}^{(1)} + \vec{d}_{23}\rho_{23}^{(1)}. \quad (8.8)$$

Electric and magnetic response of the medium can also be given in terms of electric polarizability α_e and magnetizability α_m . We choose the probe field \vec{E}_p parallel

to the electric dipole moment \vec{d}_{23} ($=\vec{d}_{32}$) so that α_e is a scalar quantity. α_e is related to the induced dipole moment as $\vec{P}_e(\omega_p) = \varepsilon_o \alpha_e \vec{E}_p(\omega_p)$ where ε_o is permittivity of free space. We therefore obtain,

$$\alpha_e = \frac{|d_{23}|^2 \rho_{32}^{(1)}}{2\varepsilon_o \hbar \alpha_p}. \quad (8.9)$$

Similarly magnetization \vec{P}_m is given as

$$\vec{P}_m(\omega_p) = Tr(\hat{\rho} \vec{\mu}) = \vec{m}_{12} \rho_{12}^{(1)} + \vec{m}_{12} \rho_{21}^{(1)}, \quad \mu_o \vec{P}_m(\omega_p) = \alpha_m \vec{B}_p(\omega_p), \quad (8.10)$$

where μ_o is permeability of free space, and \vec{B}_p is the magnetic field given by

$$\vec{B}_p = \vec{k}_p \times \vec{E}_p / \omega_p. \quad (8.11)$$

We further assume that magnetic dipole moment is perpendicular to the induced electric dipole moment, i.e. \vec{m}_{12} is parallel to $\vec{k}_p \times \vec{E}_p$ so that $\vec{B}_p = \vec{E}_p / c$ and therefore we have,

$$\alpha_m = \frac{m_{12} d_{23} \mu_o c \rho_{21}^{(1)}}{2\hbar \alpha_p}. \quad (8.12)$$

The electric and magnetic Clausius-Mossotti relations connect the macroscopic and microscopic variables of a media. For macroscopic polarization electric susceptibility of the medium can be obtained as

$$\chi_e = N\alpha_e / (1 - N\alpha_e / 3). \quad (8.13)$$

The relative electric permittivity of the medium is therefore given as

$$\varepsilon_r = \frac{1 + 2N\alpha_e / 3}{1 - N\alpha_e / 3}. \quad (8.14)$$

Similarly relative permeability of the medium can be obtained as follows:

$$\mu_r = \frac{1 + 2N\alpha_m / 3}{1 - N\alpha_m / 3}, \quad (8.15)$$

where N is the atomic density. In order to modify ϵ_r and μ_r simultaneously the foremost condition is that the electric and magnetic dipoles should oscillate at the same frequency, which implies that ω_{32} and ω_{21} should be equal to the probe frequency. The relevant electric and magnetic dipole moments chosen for the subsequent studies are 2.534×10^{-29} Cm and 1.312×10^{-23} J/T respectively which correspond to ^{87}Rb atom.

For a dilute atomic vapor the microscopic local fields are very weak and hence neglected. However under this condition it is impossible to obtain negative permittivity and permeability as clear from Eqs. (8.9) – (8.15). Thus we consider a dense atomic media of closely packed atoms ($N = 10^{23} \text{ m}^{-3}$) where dipole - dipole interactions i.e the Lorentz-Lorenz local fields play a crucial role in the response of the medium. Finally for a left-handed media the absorption coefficient and refractive index are defined as $A = 2\pi \text{Im}[-\sqrt{\epsilon_r \mu_r}]$ and $n_r = \text{Re}[-\sqrt{\epsilon_r \mu_r}]$ respectively. The group velocity of the medium ($v_g = c/n_g$) becomes negative in certain frequency range of NRI. Thus by the tailoring the group index $n_g = n_r(\omega_p) + \omega_p [dn_r(\omega_p)/d\omega_p]$ one can tune the velocity of probe propagation from subluminal to superluminal.

8.4.2 Results and Discussion

We first consider that the control and rf fields are at resonance. Fig. 8.3 shows the effect of control strength on the permittivity, permeability and refractive index of the media. For $\alpha_c = 0$, the system effectively becomes a cascade type system comprising of levels $|2\rangle$, $|3\rangle$ and $|4\rangle$, therefore no coherence is established between levels $|1\rangle$ and $|2\rangle$

($\rho_{12} = 0$). This implies $\alpha_m = 0$ (cf. Eq. (8.12)) and hence $\mu_r = 1$. Thus left handedness of the medium is not possible in the absence of control field.

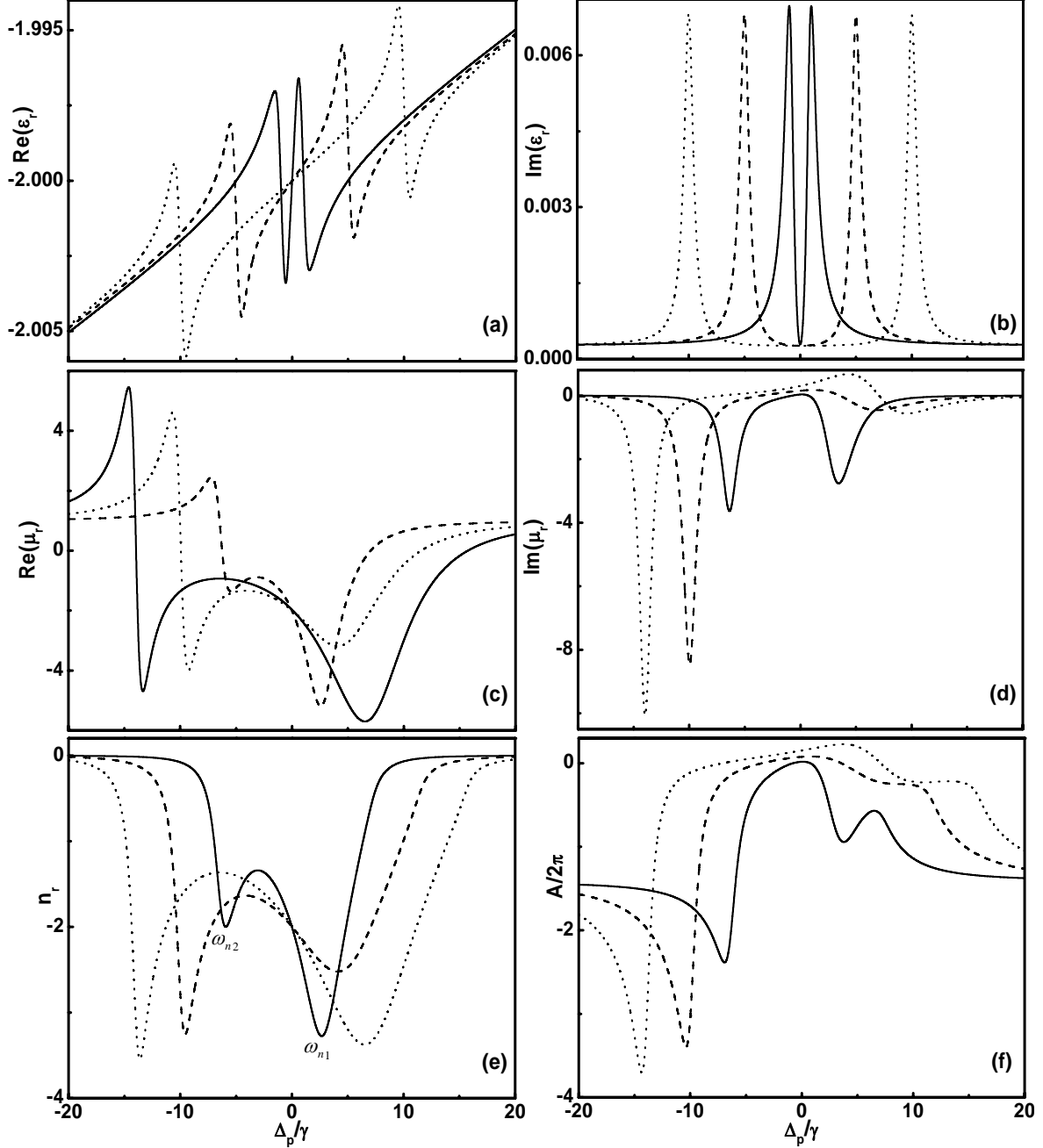


Fig. 8.3: Probe field dependence of (a): $\text{Re}(\varepsilon_r)$, (b): $\text{Im}(\varepsilon_r)$, (c): $\text{Re}(\mu_r)$, (d): $\text{Im}(\mu_r)$, (e): n_r and (f): A . Here $\Delta_c = \Delta_{rf} = 0$, $\alpha_{rf} = 5\gamma$, $\gamma_{ij} = \gamma$ and $\Gamma_{ij} = 0.001\gamma$. $\alpha_c = \gamma$ (solid curve), 5γ (dashed curve) and 10γ (dotted curve). ω_{n1} and ω_{n2} are indicated for solid curve in frame (e).

We observe that control field strength is proportional to the maximum amplitude of NRI and frequency range over which both ϵ_r and μ_r are negative. This is due to broadening of EIT resonance at $\Delta_p = 0$ with increase in α_c . We denote the frequency of maximum NRI as ω_{n1} and ω_{n2} (cf. solid curve in Fig. 8.3(e)). Further from Fig. 8.3(e) it is clear that in the region $\Delta_p > \omega_{n1}$ and $\Delta_p < \omega_{n2}$ refractive index increases with decreasing probe frequency ($dn_r/d\omega_p = -dn_r/d\Delta_p$) showing anomalous behavior. Thus v_g becomes negative in this region which indicates superluminal propagation. On the other hand for $\omega_{n2} < \Delta_p < \omega_{n1}$, group index $n_g \gg 1$ indicating subluminal velocity. Thus in the NRI region one can control the propagation of probe beam with proper choice of laser atom interaction parameters. In the probe region $\Delta_p < \omega_{n2}$, the refractive index rises steeply compared to the region $\Delta_p > \omega_{n2}$ which means that the velocity of light can be made much faster than c . Further in the vicinity of ω_{n2} absorption coefficient is negative. This region is of interest for obtaining probe amplification in the NRI media.

Another interesting observation is that one can tune the transparency region, and hence ω_{n1} , ω_{n2} and the range of NRI by controlling field detunings as shown in Fig. 8.4. This is an important advantage of coherent preparation method over artificial fabrication to realize NRI. Fig. 8.5 shows the dependence of rf field strength (α_{rf}) on refractive index and absorption coefficient. For $\alpha_{rf} = 0$, the system can be considered as two independent two-level systems comprising of levels $|1\rangle - |4\rangle$ and $|2\rangle - |3\rangle$. In this condition also, $\rho_{12} = 0$ which implies $\alpha_m = 0$ and hence $\mu_r = 1$. Thus it can be concluded that left handedness is possible in this scheme only if both electric and magnetic coupling

are present simultaneously. Further from Fig. 8.5(a) it is evident that as the rf field strength increases the maximum value of negative n_r attained increases. Fig. (8.3) – (8.5) thus which highlight the importance of choosing optimum values of field strengths and detunings to obtain desired NRI values and range.

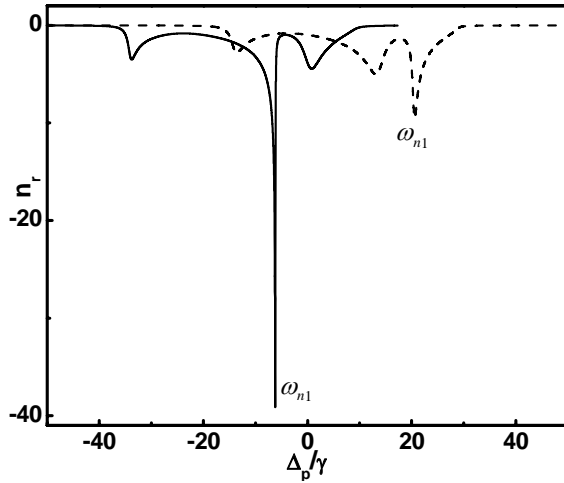


Fig. 8.4: Refractive index versus probe detuning for $\alpha_c = \alpha_{rf} = 10\gamma$. Solid and dashed lines correspond to $(\Delta_c, \Delta_{rf}) = (0, 20\gamma)$ and $(20\gamma, 0)$ respectively. Other data are same as in Fig. 8.3. $\omega_{n1} = -6.2\gamma$ and 20.58γ for solid and dashed curves.

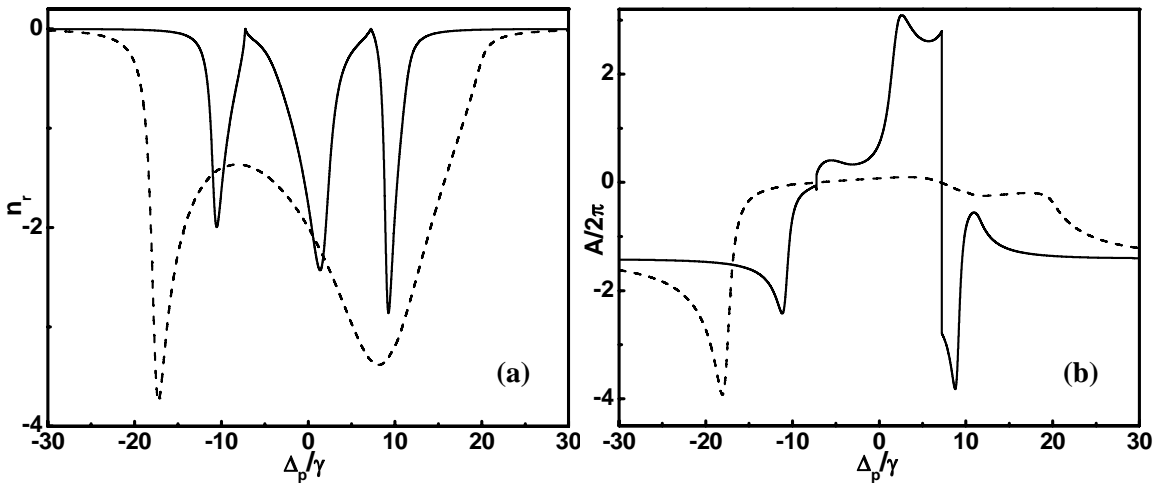


Fig. 8.5: Probe field dependence of (a): refractive index and (b): absorption coefficient. Here $\Delta_c = \Delta_{rf} = 0$, $\alpha_c = 10\gamma$, $\alpha_{rf} = \gamma$ (solid curve) and 10γ (dashed curve). Other data are same as in Fig. 8.3.

The effect of control and rf field parameters on the range of NRI and maximum value of n_r achieved is summarized in Table-7. It is observed that a very large NRI value can be obtained when the rf field is detuned.

Table-7: Dependence of strengths and detunings of control and *rf* fields on the range and maximum amplitude of negative refractive index

α_c	α_{rf}	Δ_c	Δ_{rf}	Range of negative ϵ_r and μ_r	n_r (max)
γ	5γ	0	0	-6.25γ to 7.05γ	-3.28
5γ	5γ	0	0	-9.94γ to 11.54γ	-3.26
10γ	5γ	0	0	-13.95γ to 15.73γ	-3.54
10γ	γ	0	0	-10.72γ to 11.29γ	-2.86
10γ	10γ	0	0	-17.62γ to 19.89γ	-3.74
10γ	10γ	20γ	0	-13.99γ to 13.76γ , 20.34γ to 29.02γ	-9.57
10γ	10γ	0	20γ	-34.06γ to -6.18γ , -0.35γ to 9.03γ	-39.12

8.5 Realization of Negative Refractive Index in Model (b)

8.5.1 Theoretical Formulation

The interaction Hamiltonian of this system under RWA is given as

$$\begin{aligned}
 H_0 = & -\alpha_{rf}(A_{12} + A_{21}) - \alpha_c(A_{14} + A_{41}) - \alpha_p(A_{34} + A_{43}) \\
 & - \Delta_{rf}A_{22} - (\Delta_c - \Delta_p)A_{33} - \Delta_c A_{44}.
 \end{aligned} \tag{8.16}$$

The elements of the density operator satisfy the following equations:

$$\begin{aligned}
 d\rho_{11}/dt = & -2(\Gamma_{12} + \Gamma_{13})\rho_{11} - i\alpha_{rf}(\rho_{12} - \rho_{21}) - i\alpha_c(\rho_{14} - \rho_{41}) \\
 & + 2\Gamma_{21}\rho_{22} + 2\Gamma_{31}\rho_{33} + 2\gamma_{41}\rho_{44},
 \end{aligned} \tag{8.17a}$$

$$d\rho_{12}/dt = -i\alpha_{rf}(\rho_{11} - \rho_{22}) - g_1\rho_{12} + i\alpha_c\rho_{42}, \tag{8.17b}$$

$$d\rho_{13}/dt = -g_2\rho_{13} - i\alpha_p\rho_{14} + i\alpha_{rf}\rho_{23} + i\alpha_c\rho_{43}, \tag{8.17c}$$

$$d\rho_{14}/dt = -i\alpha_c(\rho_{11} - \rho_{44}) - i\alpha_p\rho_{13} - g_3\rho_{14} + i\alpha_{rf}\rho_{24}, \tag{8.17d}$$

$$d\rho_{22}/dt = 2\Gamma_{12}\rho_{11} + i\alpha_{rf}(\rho_{12} - \rho_{21}) - 2(\Gamma_{21} + \Gamma_{23})\rho_{22} + 2\Gamma_{32}\rho_{33}, \quad (8.17e)$$

$$d\rho_{23}/dt = i\alpha_{rf}\rho_{13} - g_4\rho_{23} - i\alpha_p\rho_{24}, \quad (8.17f)$$

$$d\rho_{24}/dt = i\alpha_{rf}\rho_{14} - i\alpha_c\rho_{21} - i\alpha_p\rho_{23} - g_5\rho_{24}, \quad (8.17g)$$

$$d\rho_{33}/dt = 2\Gamma_{13}\rho_{11} + 2\Gamma_{23}\rho_{22} - 2(\Gamma_{31} + \Gamma_{32})\rho_{33} - i\alpha_p(\rho_{34} - \rho_{43}) + 2\gamma_{43}\rho_{44}, \quad (8.17h)$$

$$d\rho_{34}/dt = -i\alpha_c\rho_{31} - i\alpha_p(\rho_{33} - \rho_{44}) - g_6\rho_{34}, \quad (8.17i)$$

$$d\rho_{44}/dt = i\alpha_c(\rho_{14} - \rho_{41}) + i\alpha_p(\rho_{34} - \rho_{43}) - 2(\gamma_{41} + \gamma_{43})\rho_{44}, \quad (8.17j)$$

where the coefficients g_i are defined as

$$\begin{aligned} g_1 &= \Gamma_{12} + \Gamma_{13} + \Gamma_{21} + \Gamma_{23} + i\Delta_{rf}, & g_2 &= \Gamma_{12} + \Gamma_{13} + \Gamma_{31} + \Gamma_{32} + i(\Delta_p - \Delta_c), \\ g_3 &= \Gamma_{12} + \Gamma_{13} + \gamma_{41} + \gamma_{43} + i\Delta_p, & g_4 &= \Gamma_{21} + \Gamma_{23} + \Gamma_{31} + \Gamma_{32} + i(\Delta_p - \Delta_c - \Delta_{rf}), \\ g_5 &= \Gamma_{21} + \Gamma_{23} + \gamma_{41} + \gamma_{43} + i\Delta_{42}, & g_6 &= \Gamma_{31} + \Gamma_{32} + \gamma_{41} + \gamma_{43} + i\Delta_{43}. \end{aligned} \quad (8.18)$$

Under the weak probe approximation the solutions of Eq. (8.17) are obtained as

$$\rho_{43}^{(1)} = \frac{\alpha_p[g_4\alpha_c\rho_{14}^{(0)} + i\{(g_2g_4 + \alpha_{rf}^2)(\rho_{33}^{(0)} - \rho_{44}^{(0)}) + \alpha_c\alpha_{rf}\rho_{24}^{(0)}\}]}{g_2g_4g_6^* + \alpha_c^2g_4 + \alpha_{rf}^2g_6^*} = \rho_{34}^{(1)*}, \quad (8.19a)$$

$$\rho_{13}^{(1)} = \frac{\alpha_p[\alpha_cg_4(\rho_{44}^{(0)} - \rho_{33}^{(0)}) + \alpha_{rf}g_6^*\rho_{24}^{(0)} - ig_4g_6^*\rho_{14}^{(0)}]}{g_2g_4g_6^* + \alpha_c^2g_4 + \alpha_{rf}^2g_6^*} = \rho_{31}^{(1)*}, \quad (8.19b)$$

$$\rho_{14}^{(0)} = -i\alpha_c[(g_1^*g_5 + \alpha_c^2)(\rho_{11}^{(0)} - \rho_{44}^{(0)}) - \alpha_{rf}^2(\rho_{11}^{(0)} - \rho_{22}^{(0)})]/G_1, \quad (8.19c)$$

$$\rho_{24}^{(0)} = \alpha_c\alpha_{rf}[g_3(\rho_{11}^{(0)} - \rho_{22}^{(0)}) + g_1^*(\rho_{11}^{(0)} - \rho_{44}^{(0)})]/G_1, \quad (8.19d)$$

$$\begin{aligned} \rho_{11}^{(0)} &= \{\alpha_c^4\alpha_{rf}^4j_5^2(\Gamma_{31} + \Gamma_{32}) + \alpha_c^2\alpha_{rf}^2[j_5\Gamma_{32}\gamma_{43} - j_4j_6(\Gamma_{31} + \Gamma_{32})] - (\alpha_c^2j_4 \\ &\quad + \gamma_{41} + \gamma_{43})(\Gamma_{23}\Gamma_{31} + \Gamma_{21}\Gamma_{31} + \Gamma_{21}\Gamma_{32}) - \alpha_{rf}^2j_6(\Gamma_{31} + \Gamma_{32})(\gamma_{41} + \gamma_{43})\}/G_2, \end{aligned} \quad (8.20a)$$

$$\begin{aligned} \rho_{22}^{(0)} &= \{\alpha_c^4\alpha_{rf}^4j_5^2(\Gamma_{31} + \Gamma_{32}) + \alpha_c^2\alpha_{rf}^2\{j_5[\Gamma_{32}\gamma_{43} + (\Gamma_{31} + \Gamma_{32})(\gamma_{41} + \gamma_{43})] \\ &\quad - j_4j_6(\Gamma_{31} + \Gamma_{32})\} - (\alpha_c^2j_4 + \gamma_{41} + \gamma_{43})(\Gamma_{13}\Gamma_{32} + \Gamma_{12}\Gamma_{31} + \Gamma_{12}\Gamma_{32}) \\ &\quad - \alpha_{rf}^2j_6(\Gamma_{31} + \Gamma_{32})(\gamma_{41} + \gamma_{43}) - \alpha_c^2j_4\Gamma_{32}\gamma_{43}\}/G_2, \end{aligned} \quad (8.20b)$$

$$\rho_{44}^{(0)} = \{\alpha_c^4 \alpha_{rf}^4 j_5^2 (\Gamma_{31} + \Gamma_{32}) - \alpha_c^2 \alpha_{rf}^2 \{j_5 [\Gamma_{31} (\Gamma_{21} - \Gamma_{12} + \Gamma_{23}) + \Gamma_{32} (\Gamma_{21} - \Gamma_{12} - \Gamma_{13})] - j_4 j_6 (\Gamma_{31} + \Gamma_{32})\} - \alpha_c^2 j_4 (\Gamma_{21} \Gamma_{31} + \Gamma_{23} \Gamma_{31} + \Gamma_{21} \Gamma_{32})\} / G_2, \quad (8.20c)$$

$$\rho_{33}^{(0)} = 1 - \rho_{11}^{(0)} - \rho_{22}^{(0)} - \rho_{44}^{(0)}, \quad (8.20d)$$

where

$$G_1 = g_1^* g_3 g_5 + \alpha_c^2 g_3 + \alpha_{rf}^2 g_1^*, \quad j_4 = \text{Re}[(g_1^* g_5 + \alpha_c^2) / G_1], \quad (8.21a)$$

$$j_5 = \text{Re}(G_1) / |G_1|^2, \quad j_6 = \text{Re}[(g_3 g_5 + \alpha_{rf}^2) / G_1], \quad (8.21b)$$

$$\begin{aligned} G_2 = & -[\alpha_c^4 \alpha_{rf}^4 j_5^2 (\Gamma_{13} + \gamma_{43} + 2\Gamma_{31} + 2\Gamma_{32}) + (\alpha_c^2 j_4 + \gamma_{41} + \gamma_{43}) [\alpha_{rf}^2 \alpha_c^2 j_5 (\Gamma_{23} + \Gamma_{31} + \Gamma_{32}) \\ & - \alpha_{rf}^2 j_6 (2\Gamma_{31} + 2\Gamma_{32} + \Gamma_{13} + \Gamma_{23})] - (\Gamma_{21} + \Gamma_{23})(\Gamma_{13} + \Gamma_{31}) - \Gamma_{32}(\Gamma_{13} + \Gamma_{31}) - \Gamma_{12} \\ & (\Gamma_{23} + \Gamma_{31} + \Gamma_{32})] - \alpha_c^2 (j_4 - \alpha_{rf}^2 j_5) [\Gamma_{23} \Gamma_{31} + (\Gamma_{23} + \Gamma_{32}) \Gamma_{43} + \Gamma_{21} (\Gamma_{31} + \Gamma_{32} + \gamma_{43}) \\ & + \alpha_{rf}^2 \alpha_c^2 j_5 (\Gamma_{23} + \Gamma_{31} + \Gamma_{32}) + \alpha_{rf}^2 j_6 (\Gamma_{31} + \Gamma_{32} + \gamma_{43})] + \alpha_{rf}^2 \alpha_c^2 j_5 [\Gamma_{32} (\gamma_{43} - \Gamma_{31}) \\ & - \Gamma_{21} (\Gamma_{31} + \Gamma_{32} + \gamma_{43}) - \alpha_{rf}^2 j_6 (\Gamma_{31} + \Gamma_{32} + \gamma_{43})], \end{aligned} \quad (8.21c)$$

The electric and magnetic polarizability of the medium are obtained as

$$\alpha_e = \frac{|d_{34}|^2 \rho_{43}^{(1)}}{2\epsilon_0 \hbar \alpha_p}, \quad \alpha_m = \frac{m_{13} d_{34} \mu_o c \rho_{31}^{(1)}}{2\hbar \alpha_p}. \quad (8.22)$$

In this model the dipole synchronization restriction requires $\omega_{43} = \omega_{31}$. The relevant dipole moments and the atomic density are chosen similar to that in model (a).

8.5.2 Results and Discussion

For $\alpha_c = 0$, this configuration can be considered as two independent two-level systems comprising of levels $|1\rangle - |2\rangle$ and $|3\rangle - |4\rangle$. Thus no coherence is established between levels $|1\rangle$ and $|3\rangle$ which means $\alpha_m = 0$ (*cf.* Eq. (8.22)). Hence negative refraction is not possible. However when $\alpha_{rf} = 0$ the response of the system is similar to

that of a three-level Λ system formed by levels $|1\rangle$, $|3\rangle$ and $|4\rangle$ where one can find probe regions exhibiting NRI [126]. Fig. 8.6 show the effect of control strength on ε_r , μ_r , n_r and A .

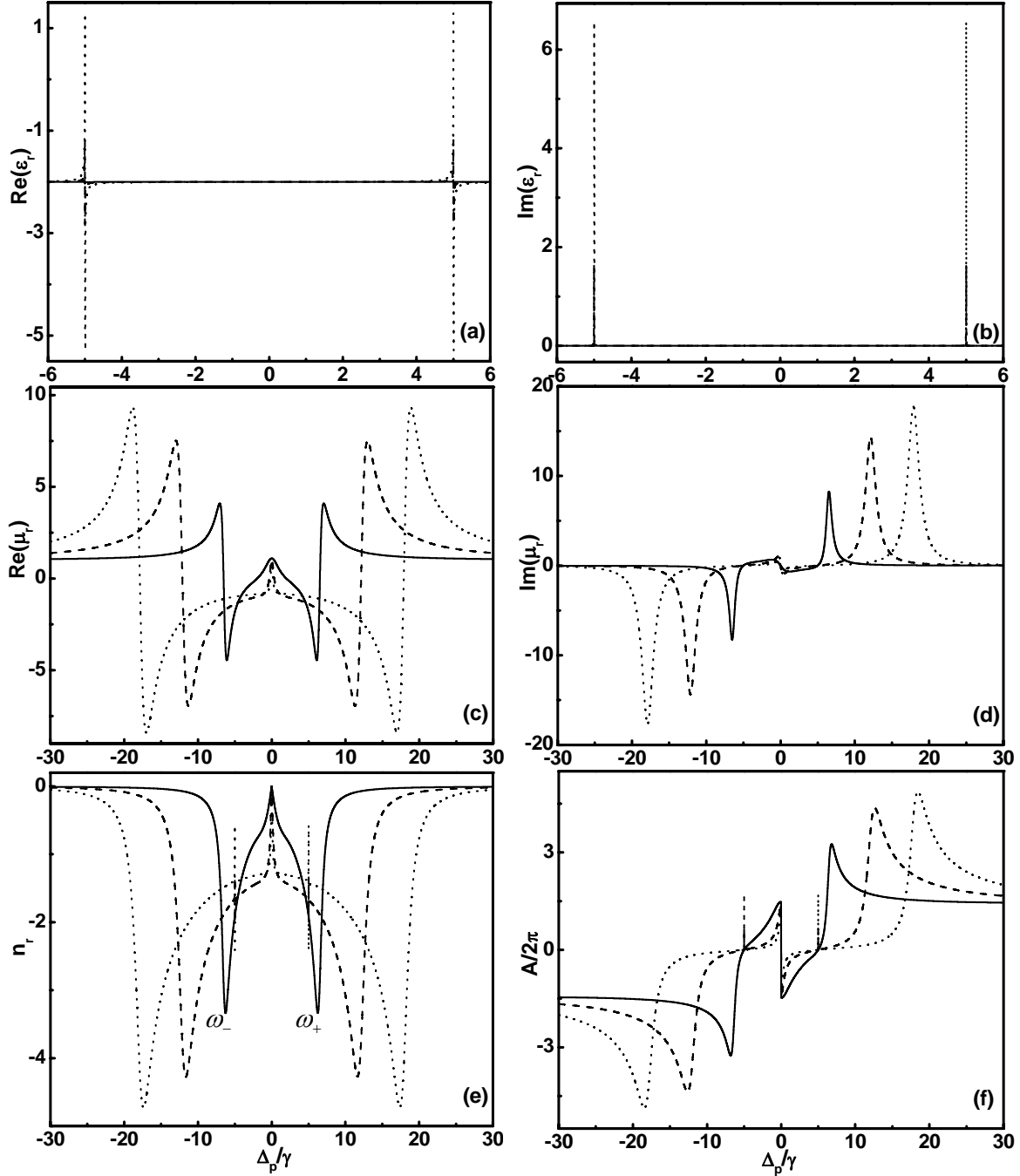


Fig. 8.6: Probe field dependence of (a): $\text{Re}(\varepsilon_r)$, (b): $\text{Im}(\varepsilon_r)$, (c): $\text{Re}(\mu_r)$, (d): $\text{Im}(\mu_r)$, (e): n_r and (f): A . Here $\Delta_c = \Delta_{rf} = 0$, $\alpha_{rf} = 5\gamma$, $\alpha_c = \gamma$ (solid curve), 5γ (dashed curve) and 10γ (dotted curve). ω_+ and ω_- are indicated for the solid curve in frame (e).

There exist two maxima in the NRI region located at $\Delta_p = \omega_+$ and $\Delta_p = \omega_-$ (cf. Fig. 8.6(e)). For $\Delta_p > \omega_+$ and $\Delta_p < \omega_-$, refractive index n_r increases sharply with increase in Δ_p thereby indicating anomalous behavior. Comparing Fig. 8.6(e) – (f) we can identify the frequency regions where $n_r < 0$ and $A \sim 0$, which is of significant interest experimentally. Interestingly in the region $\Delta_p \sim \omega_-$ we observe $A < 0$ and that corresponds to the amplification of the probe beam. Fig. 8.7 shows the effect of control and *rf* detunings on the refractive index of the media. Similar to the previous model, here also one can tune the range and amplitude of NRI by controlling the field detunings.

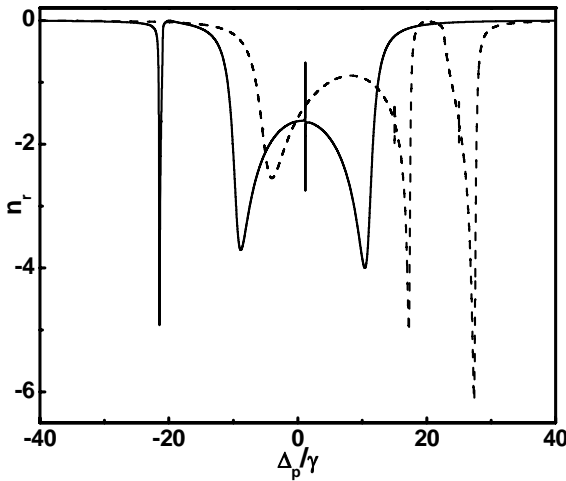


Fig. 8.7: Refractive index versus probe detuning for $\alpha_c = \alpha_{rf} = 10\gamma$. The solid and dashed curves correspond to $(\Delta_c, \Delta_{rf}) = (0, 20\gamma)$ and $(20\gamma, 0)$ respectively.

Fig. 8.8 show the effect of *rf* strengths and detunings on n_r and A. From Figs. 8.6(e) and 8.8(e) it is clear that the range and maximum amplitude of NRI increases with increase in strengths of both the fields. The effect of laser atom interaction parameters on NRI is summarized in Table-8.

Finally a comment on the group velocity (v_g) in this coherently driven system is appropriate at this stage. Here $v_g > 0$ in the region $\omega_- < \Delta_p < \omega_+$, while $v_g < 0$ in the anomalous dispersion region. This provides a prospect for observing both subluminal and

superluminal light propagation in the media similar to the previous model.

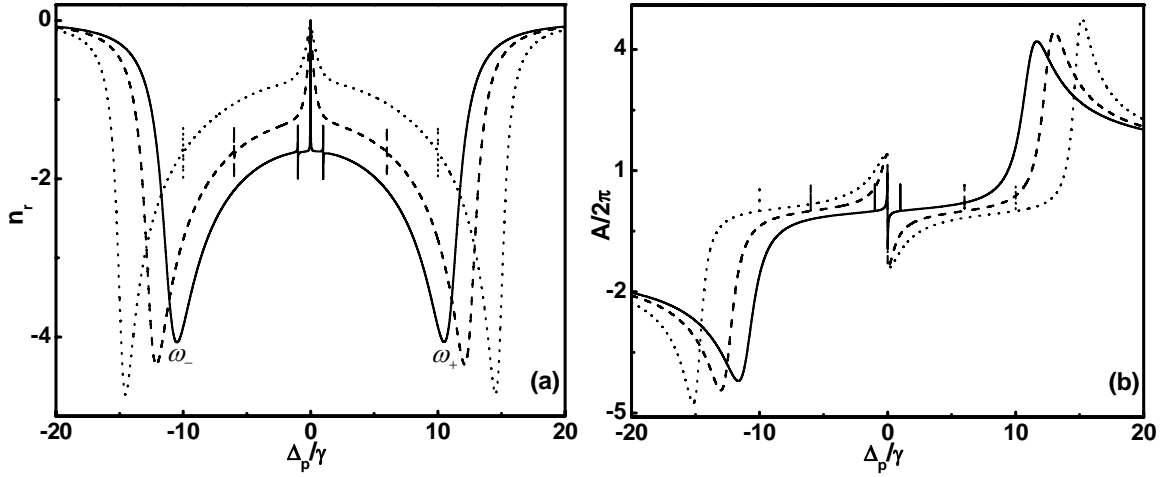


Fig. 8.8: Dependence of probe detuning on (a): refractive index and (b): absorption coefficient. Here $\Delta_c = \Delta_{rf} = 0$, $\alpha_c = 5\gamma$, $\alpha_{rf} = \gamma$ (solid curve), 6γ (dashed curve) and 10γ (dotted curve).

Table-8: Dependence of strengths and detunings of control and rf field on the maximum value and range of negative refractive index

α_c	α_{rf}	Δ_c	Δ_{rf}	Range of negative ϵ_r and μ_r	n_r (max)
γ	5γ	0	0	-6.53γ to 6.53γ	-3.34
5γ	5γ	0	0	-12.11γ to 12.11γ	-4.28
10γ	5γ	0	0	-17.88γ to 17.88γ	-4.73
5γ	γ	0	0	-11.03γ to 11.03γ	-4.07
5γ	6γ	0	0	-12.55γ to 12.55γ	-4.36
5γ	10γ	0	0	-14.85γ to 14.85γ	-4.73
5γ	5γ	20γ	0	-4.65γ to 17.32γ , 22.68γ to 27.46γ	-6.14
5γ	5γ	0	20γ	-21.49γ to -20.94γ , -9.39γ to 10.92γ	-4.92

CHAPTER 9

CONCLUSIONS AND FUTURE SCOPE OF THE WORK

9.1 Conclusions

Quantum coherence and interference provide an interesting outlook for designing strategies for control of optical response of atomic/molecular medium. This theme has been the main focus of the work reported in this thesis. We have considered here three- and four-level atomic/molecular systems in various configurations, i.e., Λ , double- Λ , tripod, N-resonance etc. under multi-chromatic coherent interaction. Specific issues addressed here are electromagnetically induced transparency (EIT), electromagnetically induced absorption (EIA), amplification without inversion (AWI), spontaneously generated coherence (SGC), Kerr nonlinearity and the effect of laser phase fluctuations. Also examined are the issues relating to permanent dipole moments in molecular systems, subluminal and superluminal light propagation, and realization of negative refractive index (NRI) in coherently prepared atomic medium. While the thesis mainly

concentrates on the theoretical development of light-matter interaction and analysis of the aforementioned effects, few experimental results are also reported to provide a flavor of coherent pump-probe spectroscopy. Thesis begins with Chapter-1 which provides a brief introduction to spectroscopy in a coherently prepared atomic medium. The requisite theoretical background is developed in Chapter-2 and specific studies are reported in Chapter-3 to Chapter-8. Main findings and conclusions of the work included in this thesis are as follows:

In our work on three-level dipolar molecules in Λ configuration reported in Chapter-3, we have provided an integrated view of coherent pump-probe spectroscopy of a medium of dipolar molecules. The objective here is to investigate the effect of diagonal dipole moments on the coherent response of the system, particularly in the context of AT doublet, EIT, dispersion and its connection to the issue of subluminal and superluminal light propagation. These issues have been discussed for medium of stationary molecules as well as Doppler broadened molecular medium. The presence of permanent dipole moments provides a mechanism for multi-photon absorption processes, and therefore the coherent dynamics of Λ system is discussed in terms of m - and n -photon absorption mediated by pump and probe fields respectively. Our study shows that the outcome of the general $(m+n)$ -photon pump-probe spectroscopy is independent of n and is solely determined by m . Recently Zhou *et al.* [173] have reported amplification without inversion in this system for reversal in the sign of the difference of the permanent moments of the excited and ground levels connected by the probe field for $n = 2$. We explicitly show that the prediction of Zhou *et al.* is erroneous and trace the underlying reasons for arriving at such a result. Our analysis shows that the permanent dipole

moments essentially damp the laser-molecule Rabi frequency to result in narrower EIT linewidth and larger group velocity index. These effects are further enhanced when the order of the multi-photon process is increased. We have further included the virtual mechanism in the treatment of multi-photon absorption based EIT phenomenon. Analysis based on 2+1-photon EIT shows that the inclusion of virtual mechanism has two effects: firstly it leads to modification of the laser-molecule coupling which has a bearing on EIT width and group velocity index, and secondly it results in the frequency shift of the EIT resonance. In order to test several of these effects experimentally, we have proposed two schemes of Λ systems based on the molecular data of ${}^7\text{LiH}$.

In Chapter-4 we have investigated coherent pump-probe spectroscopy of an atomic medium in Λ configuration with a closely placed adjacent excited level driven coherently by a pump and a probe laser. The presence of additional level results in two simultaneous Λ resonances with common ground levels, i.e., degenerate double lambda (DDL) resonance. Such resonances arise naturally in coherent pump-probe spectroscopy of D_1 and D_2 transitions of alkali atoms due to hyperfine interaction. We have used a DDL system formed using the hyperfine manifold of D_2 transition of ${}^{85}\text{Rb}$ for detailed analysis of this problem. We have established the dressed states associated with this problem and used them to identify the sub-natural resonances. We observe that the system can exhibit at least two sub-natural resonances in the dressed state spectroscopy. Another remarkable feature observed is the suppression of the sub-natural resonance under specific atom-field interaction parameters. This suppression is attributed to the coherence and ensuing interference developed in simultaneous excitation of two two-level systems with a common ground level. Doppler averaging of the probe absorption

spectrum gives rise to an EIT resonance, which differs in character from that of a Λ system. The effect of the neighboring level on the shape, linewidth and position of EIT resonance is discussed. The linewidth of EIT spectrum as a function of pump Rabi frequency shows two distinctive regions. For low pump saturation the EIT linewidth of DDL system is lower than that of a Λ system, whereas for high pump saturation the trend is reversed. This behavior is discussed in terms of the increase in the optical pumping rate due to the presence of a nearby level. The discussion is further augmented by the extension of the DDL scheme to a six-level level model as applicable to D_2 transitions of alkali atoms. The analysis presented here thus provides a realistic theoretical description of pump-probe spectroscopy of hyperfine transitions of alkali atoms. The chapter is completed with a discussion on experimental results on dressed state spectroscopy of DDL system in a Doppler broadened medium of ^{87}Rb atoms.

Chapter-5 is dedicated to the studies on quantum interference and its manifestation in the observation of AWI in a DDL system using master equation and quantum jump formalisms. A model DDL system formed using hyperfine manifold of D_1 transition of ^{87}Rb atom is discussed here as an example. It is shown here that near two-photon resonance, the probe is amplified without any inversion in the bare atomic levels and dressed levels. The inversionless amplification is a result of interference between two simultaneously excited Λ resonances and it exhibits a strong dependence on the low frequency coherence established in the pair of ground levels. We show that AWI in the present case is strongly dependent on the pump detuning, which governs the relative excitation amplitudes of two simultaneously excited Λ resonances. Consequently for the model system of D_1 transition of ^{87}Rb , AWI is tunable and it is maximized when the

pump detuning is at half the frequency separation between excited levels. This is in contrast to the earlier works on three-level Λ resonances, where AWI is shown to occur when pump and probe lasers are near resonant with the respective transitions. Further AWI is observed to persist in the presence of inhomogeneous broadening, albeit with deterioration at large Doppler widths. The results are substantiated with a closed form analytical expression for probe absorption obtained perturbatively in the weak probe limit. The analytical expressions permit to express AWI in terms of the relative magnitudes of the dipole matrix elements involved in the problem. The analysis is extended to the DDL system in D_2 transition of ^{87}Rb to explain the contrasting behavior of absorption instead of AWI, which develops into a full grown EIT after Doppler averaging. Quantum jump formalism is used to provide useful insight into the inherent physical mechanism responsible for AWI. This analysis shows that the interference between one-photon absorption processes is primarily responsible for AWI in the present system.

Chapter-6 deals with the analysis of interference effects in two four-level configurations, i.e., tripod system and N-resonance, interacting with coherent trichromatic field consisting of a pump, a probe and a control. The presence of additional resonant transition and field offers enhanced degrees of freedom for controlling the coherent dynamics and optical properties of the medium. The parametric dependence of dressed states and pair of EIT resonances in the tripod system are studied with an objective of controlling their linewidths, and the existence of an ultra-narrow absorptive resonance is demonstrated. N-system is studied to examine the choice of probe field in tailoring the response of the atomic medium. Some appealing traits studied are inversion

in dressed states, observation of multiple transparency windows and switching between EIT and EIA by controlling the field parameters. These effects are attributed to the competition between inherent Λ and V systems, and transfer of coherence (TOC) in the medium. Observation of both EIA and EIT provides an interesting prospect of controlling the light propagation from subluminal to superluminal with appropriate choice of field parameters. Further we have studied the effect of SGC on the linear and nonlinear response of the N- system. It is shown that the SGC transforms EIT to EIA and vice-versa, enhances the Kerr nonlinearity of the medium while suppressing the absorption. Further it is observed that enhanced Kerr nonlinearity enters the minimal absorption window with increase in SGC parameters and a large Kerr nonlinearity can be obtained for detuned driving fields. The chapter is completed with experimental results on comparison of EIT width in Λ and N systems. EIT signal in N-system is shown to be significantly narrower than that in Λ system.

Chapter-7 addresses the issue of laser phase fluctuations in the pump-probe spectroscopy of N-system. The laser phase variables are modeled by Wiener-Levy diffusion process to specify the bandwidths ($\gamma_{ci}, i = 1, 2, 3$) and cross-correlations ($\gamma_{cicj}, i \neq j$) that may exist between a pair of laser fields. The problem is analyzed in the framework of master equation and multiplicative stochastic processes. The technique developed here is general and can be applied to study the effect of phase fluctuations on populations, spectrum and intensity-intensity correlation function etc. for any arbitrary four-level system. Results are presented for steady state and time-dependent populations of levels under three-photon and 2+1-photon resonance conditions using the model N-system of $^{40}\text{Ca}^+$ ion [227]. It is observed that both three-photon and 2+1-photon

resonances are strongly affected by the phase fluctuations associated with all lasers, however, the manner in which the resonances are influenced is different, i.e., suppression of three-photon resonance and broadening of 2+1-photon resonance. The effect of cross-correlations between the laser fields is found to exhibit two distinctive effects. The cross-correlations between the adjacent pair of lasers, i.e. γ_{c1c2} and γ_{c2c3} , help to restore the resonances. However in contrast to the three-level Λ system, this revival is only partial even when the fields are critically correlated. On the other hand, the cross-correlation γ_{c1c3} between the lasers that are not coupled through a common level is observed to affect the resonances adversely. The observed behavior is explained in terms of the relevant atomic coherences and their dependence on γ_{ci} and γ_{cicj} . The steady state results are complimented by time dependent studies. In case of three-photon resonance, the phase fluctuations lead to leakage of population from the metastable level and this effect is only partially corrected when the fields are critically correlated. On the other hand in case of 2+1-photon resonance, the phase fluctuations tend to damp the two-state coherent behavior with little change in the steady state population distribution. The coherent behavior is revived to a limited extent when the relevant fields are critically correlated. The study of phase fluctuations is further extended to EIT/EIA resonances. We observe that while the phase fluctuations in all three driving lasers participate equally in the destruction of 2+1- and three-photon resonances, it is the fluctuations in the probe laser field that is crucial to EIT/EIA resonances. The critical cross correlations between two driving lasers coupled to a common level help in the revival in both the studies, however the cross correlation γ_{c2c3} between the lasers forming the intrinsic Λ system plays a

stronger role in the revival of probe absorption. These results, we believe, are useful in the context of coherent spectroscopy of N-system with finite laser bandwidths.

Chapter-8 examines the prospect of realizing negative refractive index (NRI) in the optical region using coherently driven medium consisting of multi-level atoms. We have considered four-level atomic system in two different configurations coherently driven by a control, a probe and an additional *rf* field. The *rf* field provides auxiliary control of magnetic permeability and flexibility for adjusting frequency, depth and dispersion of EIT resonance. In the framework of master equation and Classius-Mossotti relation, the relative permittivity and permeability are obtained for a dense medium of such atoms. We show here that these models exhibit simultaneous negative permittivity and permeability in certain frequency domains. Further by controlling the detunings of the control and *rf* fields, it is possible to tune the maximum value of NRI and the corresponding range in these configurations. The results are substantiated by discussing the possibility of subluminal and superluminal light propagation using anomalous dispersion in NRI media.

9.2 Future Scope of the Work

This thesis embodies studies on quantum coherence and interference effects in three- and four-level atomic/molecular systems and their ramifications. We believe that the work reported here provide opportunities for newer studies in this field.

Work reported here on the coherent pump-probe spectroscopy of molecular systems with permanent dipole moments builds the concrete background for testing multi-photon EIT, which is of significant current interest to the experimentalists. To this

end, we have identified suitable molecular configurations in ^7LiH molecule, which can be conveniently used by the experimentalists. Also of interest are the other phenomena such as subluminal and superluminal light propagation and negative refractive index in the medium of dipolar molecules. Work reported here on EIT, EIA and AWI in four-level atomic systems is important in the context of several contemporary applications such as metrology, optical switching and quantum information processing. The effect of SGC is another important issue, which can be explored in the studies relating to higher order optical nonlinearity and also in the domain of AWI. We have provided here a complete treatment for phase fluctuations in four-level systems, which is of significant interest in the development of time- and frequency standards. At the same time, we may point out that there exists a need to develop a complete treatment for laser amplitude fluctuations in the domain of coherent pump-probe spectroscopy of multi-level atomic systems. Inherent in these studies are the issues connected with amplitude noise to phase noise conversions and vice versa in such systems. We have explored here some issues relating to the observation of negative refractive index in coherently prepared atomic medium. This issue is gathering a significant momentum in very recent years and we believe that it will be one of the thriving areas in theoretical and experimental quantum optics in very near future.

APPENDIX-1

Zero Order Polarizations of Degenerate Double Λ System

The zero order coherences under the perturbative approach are obtained as follows:

$$\rho_{23}^{(0)} = -i\alpha_2[(\kappa_5\kappa_6 + \alpha_2^2)(\rho_{22}^{(0)} - \rho_{33}^{(0)}) - \alpha_1^2(\rho_{22}^{(0)} - \rho_{44}^{(0)})]/C_1, \quad (\text{A1.1})$$

$$\rho_{42}^{(0)} = i\alpha_1[(\kappa_4^*\kappa_6 + \alpha_1^2)(\rho_{22}^{(0)} - \rho_{44}^{(0)}) - \alpha_2^2(\rho_{22}^{(0)} - \rho_{33}^{(0)})]/C_1, \quad (\text{A1.2})$$

$$\rho_{43}^{(0)} = \alpha_1\alpha_2[\kappa_5(\rho_{22}^{(0)} - \rho_{33}^{(0)}) + \kappa_4^*(\rho_{22}^{(0)} - \rho_{44}^{(0)})]/C_1, \quad (\text{A1.3})$$

where

$$C_1 = \kappa_4^*\kappa_5\kappa_6 + \alpha_1^2\kappa_5 + \alpha_2^2\kappa_4^*. \quad (\text{A1.4})$$

Coefficients κ_i , ($i=1\dots6$) are as defined in Eq. (4.3). Similarly $\rho_{ii}^{(0)}$ are given as,

$$\rho_{22}^{(0)} = \Gamma_{12}[-\alpha_1^4\alpha_2^4\zeta_1^2 + (\gamma_3 + \alpha_2^2\zeta_2)(\gamma_4 + \alpha_1^2\zeta_3) - \Gamma_{34}\Gamma_{43} - \alpha_1^2\alpha_2^2\zeta_1(\Gamma_{34} + \Gamma_{43})]/C_2, \quad (\text{A1.5})$$

$$\rho_{33}^{(0)} = \Gamma_{12}\{\alpha_1^2(\zeta_3 - \alpha_2^2\zeta_1)\Gamma_{43} + \alpha_2^2[\gamma_4(\zeta_2 - \alpha_1^2\zeta_1) + \alpha_1^2(\zeta_2\zeta_3 - \alpha_1^2\alpha_2^2\zeta_1^2)]\}/C_2, \quad (\text{A1.6})$$

$$\rho_{44}^{(0)} = \Gamma_{12}\{\alpha_2^2(\zeta_2 - \alpha_1^2\zeta_1)\Gamma_{34} + \alpha_1^2[\gamma_3(\zeta_3 - \alpha_2^2\zeta_1) + \alpha_2^2(\zeta_2\zeta_3 - \alpha_1^2\alpha_2^2\zeta_1^2)]\}/C_2, \quad (\text{A1.7})$$

$$\rho_{11}^{(0)} = 1 - \rho_{22}^{(0)} - \rho_{33}^{(0)} - \rho_{44}^{(0)}, \quad (\text{A1.8})$$

where

$$\zeta_1 = \text{Re}(C_1)/|C_1|^2, \quad \zeta_2 = \text{Re}[(\kappa_5\kappa_6 + \alpha_2^2)/C_1], \quad \zeta_3 = \text{Re}[(\kappa_4^*\kappa_6 + \alpha_1^2)/C_1], \quad (\text{A1.9})$$

$$\begin{aligned} C_2 = & (\Gamma_{12} + \Gamma_{21})[\gamma_3\gamma_4 + \alpha_1^2\gamma_3\zeta_3 + \alpha_2^2\gamma_4\zeta_2 + \alpha_1^2\alpha_2^2(\zeta_2\zeta_3 - \zeta_1^2) - \Gamma_{34}\Gamma_{43}] + \\ & + \alpha_2^2(\zeta_2 - \alpha_1^2\zeta_1)[(\Gamma_{21} + \gamma_{31})(\gamma_4 + \alpha_1^2\zeta_3) + (\Gamma_{34} - \alpha_1^2\alpha_2^2\zeta_1)(\Gamma_{12} + \gamma_{41})] \\ & + \alpha_1^2(\zeta_3 - \alpha_2^2\zeta_1)[(\Gamma_{21} + \gamma_{41})(\gamma_3 + \alpha_2^2\zeta_2) + (\Gamma_{43} - \alpha_1^2\alpha_2^2\zeta_1)(\Gamma_{12} + \gamma_{31})] \\ & + \alpha_1^2\alpha_2^2(\Gamma_{12} + \Gamma_{21})(\Gamma_{34} + \Gamma_{43}). \end{aligned} \quad (\text{A1.10})$$

These coherences and populations are used in the analysis of Sec. 4.5 and 5.3.

APPENDIX-2

Absorption and Dispersion in Degenerate Double Λ System

Absorption and dispersion in a DDL system are related to real and imaginary components of \tilde{P} (cf. Eq. (4.5)). Using Eq. (4.5) – (4.8) we obtain,

$$\tilde{P} = (p_1 + ip_2)/(u_1 + iu_2), \quad (\text{A2.1})$$

$$p_1 = \alpha_1^2 \gamma_{31} + \alpha_2^2 \gamma_{41} + (\Gamma_{21} + \Gamma_{12})[\gamma_{31}(\gamma_4 + \Gamma_{12}) + \gamma_{41}(\gamma_3 + \Gamma_{12})] \\ - (\delta_1 \gamma_{31} + \delta_2 \gamma_{41})(\delta_1 - \Delta_1) - \frac{\alpha_1 \alpha_2}{\beta_1 \beta_2} (\beta_1^2 \gamma_{31} + \beta_2^2 \gamma_{41}), \quad (\text{A2.2})$$

$$p_2 = (\Gamma_{12} + \Gamma_{21})(\delta_1 \gamma_{31} + \delta_2 \gamma_{41}) + [\gamma_{31}(\gamma_4 + \Gamma_{12}) + \gamma_{41}(\gamma_3 + \Gamma_{12})](\delta_1 - \Delta_1), \quad (\text{A2.3})$$

$$u_1 = \alpha_1^2 \delta_2 + \alpha_2^2 \delta_1 + (\delta_1 - \Delta_1)[(\gamma_3 + \Gamma_{12})(\gamma_4 + \Gamma_{12}) - \delta_1 \delta_2] \\ + (\Gamma_{12} + \Gamma_{21})[(\gamma_3 + \Gamma_{12})\delta_1 + (\gamma_4 + \Gamma_{12})\delta_2], \quad (\text{A2.4})$$

$$u_1 = (\delta_1 - \Delta_1)[(\gamma_3 + \Gamma_{12})\delta_1 + (\gamma_4 + \Gamma_{12})\delta_2] - \alpha_1^2 (\gamma_3 + \Gamma_{12}) - \alpha_2^2 (\gamma_4 + \Gamma_{12}) \\ - (\Gamma_{12} + \Gamma_{21})[(\gamma_3 + \Gamma_{12})(\gamma_4 + \Gamma_{12}) - \delta_1 \delta_2]. \quad (\text{A2.5})$$

Therefore absorption and dispersion can be obtained as follows:

$$A = [(\delta_1 - \Delta_1)^2 \{(\gamma_4 + \Gamma_{12})\gamma_{41}[(\gamma_3 + \Gamma_{12})^2 + \delta_2^2] + (\gamma_3 + \Gamma_{12})\gamma_{31}[(\gamma_4 + \Gamma_{12})^2 + \delta_1^2]\} \\ + (\delta_1 - \Delta_1) \left\{ [(\gamma_3 + \Gamma_{12})\delta_1 + (\gamma_4 + \Gamma_{12})\delta_2] \frac{\alpha_1 \alpha_2}{\beta_1 \beta_2} (\beta_1^2 \gamma_{31} + \beta_2^2 \gamma_{41}) \right\} \\ \left. - 2[\gamma_{31}(\gamma_3 + \Gamma_{12})\alpha_1^2 \delta_1 + \gamma_{41}(\gamma_4 + \Gamma_{12})\alpha_2^2 \delta_2] \right\} \\ + (\Gamma_{12} + \Gamma_{21})^2 \{(\gamma_4 + \Gamma_{12})\gamma_{41}[(\gamma_3 + \Gamma_{12})^2 + \delta_2^2] + (\gamma_3 + \Gamma_{12})\gamma_{31}[(\gamma_4 + \Gamma_{12})^2 + \delta_1^2]\} \\ + (\Gamma_{12} + \Gamma_{21}) \left\{ \alpha_1^2 \gamma_{41}[(\gamma_3 + \Gamma_{12})^2 + \delta_2^2] + \alpha_2^2 \gamma_{31}[(\gamma_4 + \Gamma_{12})^2 + \delta_1^2] + 2(\gamma_3 + \Gamma_{12})(\gamma_4 + \Gamma_{12}) \right\} \\ \left. \left\{ (\alpha_1^2 \gamma_{31} + \alpha_2^2 \gamma_{41}) - [(\gamma_3 + \Gamma_{12})(\gamma_4 + \Gamma_{12}) - \delta_1 \delta_2] \frac{\alpha_1 \alpha_2}{\beta_1 \beta_2} (\beta_1^2 \gamma_{31} + \beta_2^2 \gamma_{41}) \right\} \right\} \\ + [\alpha_1^2 (\gamma_3 + \Gamma_{12}) + \alpha_2^2 (\gamma_4 + \Gamma_{12})] \left\{ \alpha_1^2 \gamma_{31} + \alpha_2^2 \gamma_{41} - \frac{\alpha_1 \alpha_2}{\beta_1 \beta_2} (\beta_1^2 \gamma_{31} + \beta_2^2 \gamma_{41}) \right\} / (u_1^2 + u_2^2), \quad (\text{A2.6})$$

$$\begin{aligned}
 \eta = & [(\delta_1 - \Delta_1)^2 \{ \delta_1 \gamma_{41} [(\gamma_3 + \Gamma_{12})^2 + \delta_2^2] + \delta_2 \gamma_{31} [(\gamma_4 + \Gamma_{12})^2 + \delta_1^2] \}] \\
 & - (\delta_1 - \Delta_1) \left\{ \alpha_1^2 \gamma_{41} [(\gamma_3 + \Gamma_{12})^2 + \delta_2^2] + \alpha_2^2 \gamma_{31} [(\gamma_4 + \Gamma_{12})^2 + \delta_1^2] + 2\delta_1 \delta_2 (\alpha_1^2 \gamma_{31} + \alpha_2^2 \gamma_{41}) \right. \\
 & \quad \left. + [(\gamma_3 + \Gamma_{12})(\gamma_4 + \Gamma_{12}) - \delta_1 \delta_2] \frac{\alpha_1 \alpha_2}{\beta_1 \beta_2} (\beta_1^2 \gamma_{31} + \beta_2^2 \gamma_{41}) \right\} \\
 & + (\Gamma_{12} + \Gamma_{21})^2 \{ \delta_1 \gamma_{41} [(\gamma_3 + \Gamma_{12})^2 + \delta_2^2] + \delta_2 \gamma_{31} [(\gamma_4 + \Gamma_{12})^2 + \delta_1^2] \} \\
 & + (\Gamma_{12} + \Gamma_{21}) \left\{ 2[\alpha_2^2 \delta_1 \gamma_{41} (\gamma_3 + \Gamma_{12}) + \alpha_1^2 \delta_2 \gamma_{31} (\gamma_4 + \Gamma_{12})] \right. \\
 & \quad \left. - [(\gamma_3 + \Gamma_{12})\delta_1 + (\gamma_4 + \Gamma_{12})\delta_2] \frac{\alpha_1 \alpha_2}{\beta_1 \beta_2} (\beta_1^2 \gamma_{31} + \beta_2^2 \gamma_{41}) \right\} \\
 & + (\alpha_1^2 \delta_2 + \alpha_2^2 \delta_1) \left\{ \alpha_1^2 \gamma_{31} + \alpha_2^2 \gamma_{41} - \frac{\alpha_1 \alpha_2}{\beta_1 \beta_2} (\beta_1^2 \gamma_{31} + \beta_2^2 \gamma_{41}) \right\} / (u_1^2 + u_2^2),
 \end{aligned} \tag{A2.7}$$

$$\begin{aligned}
 u_1^2 + u_2^2 = & \{ (\delta_1 - \Delta_1) [(\gamma_3 + \Gamma_{12})\delta_1 + (\gamma_4 + \Gamma_{12})\delta_2] - \alpha_1^2 (\gamma_3 + \Gamma_{12}) - \alpha_2^2 (\gamma_4 + \Gamma_{12}) \\
 & - (\Gamma_{12} + \Gamma_{21}) [(\gamma_3 + \Gamma_{12})(\gamma_4 + \Gamma_{12}) - \delta_1 \delta_2] \}^2 + \{ \alpha_1^2 \delta_2 + \alpha_2^2 \delta_1 + (\delta_1 - \Delta_1) \\
 & \quad [(\gamma_3 + \Gamma_{12})(\gamma_4 + \Gamma_{12}) - \delta_1 \delta_2] + (\Gamma_{12} + \Gamma_{21}) [(\gamma_3 + \Gamma_{12})\delta_1 + (\gamma_4 + \Gamma_{12})\delta_2] \}^2.
 \end{aligned} \tag{A2.8}$$

From equations (A2.6) – (A2.8) it is clear that at two-photon resonance condition $\delta_1 = \Delta_1$, $A \rightarrow 0$ and $\eta \rightarrow 0$. These expressions prove that susceptibility of DDL system remains finite though small at $\delta_1 = \Delta_1$, i.e., A does not go to exact zero at $\delta_1 = \Delta_1$ which causes the shift in EIT from exact two-photon resonance (*cf.* Sec. 4.5).

APPENDIX-3

Low Frequency Coherence in Degenerate Double Λ System

Of particular interest in the analysis of AWI is the low frequency coherence $\rho_{21}^{(1)}$.

In the limit of weak excitation, $\rho_{11}^{(0)} \approx 1$ and $\rho_{22}^{(0)} = \rho_{33}^{(0)} = \rho_{44}^{(0)} \approx 0$, we may write

$$\rho_{21}^{(1)} \approx (\phi_1 + i\phi_2)/C, \quad (\text{A3.1})$$

where

$$\begin{aligned} \phi_1 = & (-\alpha_1\beta_1\{[\delta_2^2 + (\gamma_3 + \Gamma_{12})^2][\alpha_1^2 - \delta_1(\delta_1 - \Delta_1) + (\Gamma_{12} + \Gamma_{21})(\gamma_4 + \Gamma_{12})] \\ & - \alpha_2^2[\delta_1\delta_2 + (\gamma_3 + \Gamma_{12})(\gamma_4 + \Gamma_{12})]\}) \\ & + (\alpha_1 \leftrightarrow \alpha_2, \beta_1 \leftrightarrow \beta_2, \Delta_1 \leftrightarrow \Delta_2, \delta_1 \leftrightarrow \delta_2, \gamma_3 \leftrightarrow \gamma_4), \end{aligned} \quad (\text{A3.2})$$

$$\begin{aligned} \phi_2 = & (\alpha_1\beta_1\{[\delta_2^2 + (\gamma_3 + \Gamma_{12})^2][(\delta_1 - \Delta_1)(\gamma_4 + \Gamma_{12}) + \delta_1(\Gamma_{12} + \Gamma_{12})] \\ & + \alpha_2^2[\delta_1(\gamma_3 + \Gamma_{12}) - \delta_2(\gamma_4 + \Gamma_{12})]\}) \\ & + (\alpha_1 \leftrightarrow \alpha_2, \beta_1 \leftrightarrow \beta_2, \delta_1 \leftrightarrow \delta_2, \Delta_1 \leftrightarrow \Delta_2, \gamma_3 \leftrightarrow \gamma_4), \end{aligned} \quad (\text{A3.3})$$

$$\begin{aligned} C = & \{(\delta_1 - \Delta_1)[(\gamma_3 + \Gamma_{12})\delta_1 + (\gamma_4 + \Gamma_{12})\delta_2] - \alpha_1^2(\gamma_3 + \Gamma_{12}) - \alpha_2^2(\gamma_4 + \Gamma_{12}) \\ & - (\Gamma_{12} + \Gamma_{21})[(\gamma_3 + \Gamma_{12})(\gamma_4 + \Gamma_{12}) - \delta_1\delta_2]\}^2 + \{\alpha_1^2\delta_2 + \alpha_2^2\delta_1 + (\delta_1 - \Delta_1) \\ & [(\gamma_3 + \Gamma_{12})(\gamma_4 + \Gamma_{12}) - \delta_1\delta_2] + (\Gamma_{12} + \Gamma_{21})[(\gamma_3 + \Gamma_{12})\delta_1 + (\gamma_4 + \Gamma_{12})\delta_2]\}^2. \end{aligned} \quad (\text{A3.4})$$

Using Eqs. (5.3) and (5.5) we have,

$$\begin{aligned} \zeta = & \left(\frac{\alpha_1}{\beta_1} \gamma_{41} \frac{(\gamma_4 + \Gamma_{12})}{(\gamma_4 + \Gamma_{12})^2 + \delta_1^2} + \frac{\alpha_2}{\beta_2} \gamma_{31} \frac{(\gamma_3 + \Gamma_{12})}{(\gamma_3 + \Gamma_{12})^2 + \delta_2^2} \right) \\ & - i \left(\frac{\alpha_1}{\beta_1} \gamma_{41} \frac{\delta_1}{(\gamma_4 + \Gamma_{12})^2 + \delta_1^2} + \frac{\alpha_2}{\beta_2} \gamma_{31} \frac{\delta_2}{(\gamma_3 + \Gamma_{12})^2 + \delta_2^2} \right), \end{aligned} \quad (\text{A3.5})$$

$$\text{Re}(\chi_2) = \text{Re}(\rho_{21}^{(1)}) \text{Re}(\zeta) - \text{Im}(\rho_{21}^{(1)}) \text{Im}(\zeta). \quad (\text{A3.6})$$

At two-photon resonance condition $\delta_1 = \Delta_1$ and for $\delta_1 \gg \alpha_1, \alpha_2, \gamma_3, \gamma_4, \Gamma_{12}$ we obtain

$$\operatorname{Re}(\zeta) = \frac{\alpha_1}{\beta_1} \gamma_{41} \frac{(\gamma_4 + \Gamma_{12})}{\delta_1^2} + \frac{\alpha_2}{\beta_2} \gamma_{31} \frac{(\gamma_3 + \Gamma_{12})}{\delta_2^2} \rightarrow 0, \quad (\text{A3.7})$$

$$\operatorname{Im}(\zeta) = -\frac{\alpha_1}{\beta_1} \gamma_{41} \frac{1}{\delta_1} - \frac{\alpha_2}{\beta_2} \gamma_{31} \frac{1}{\delta_2}. \quad (\text{A3.8})$$

Thus $A(\delta_1 = \Delta_1) \approx -\operatorname{Im}(\rho_{21}^{(1)}) \operatorname{Im}(\zeta)$.

We assume $\Gamma_{34} = \Gamma_{43}$, $\Gamma_{12} = \Gamma_{21}$ and $\gamma_3 = \gamma_4 = \gamma_d$. AWI is maximized when $\Delta_1 = S/2$, which also implies that $\Delta_2 = -S/2$. Under these approximations and at the two-photon resonance condition we can obtain $\operatorname{Im}(\zeta)$ and $\operatorname{Im}(\rho_{21}^{(1)})$ as

$$\operatorname{Im}(\zeta) = \gamma_d (\alpha_2 \beta_1 - \alpha_1 \beta_2) / S \beta_1 \beta_2, \quad (\text{A3.9})$$

$$\operatorname{Im}(\rho_{21}^{(1)}) = \frac{2S^3 (\Gamma_{12} + \Gamma_{21}) (\alpha_1 \beta_1 - \alpha_2 \beta_2) + 16S \alpha_1 \alpha_2 (\gamma_d + \Gamma_{12}) (\alpha_2 \beta_1 - \alpha_1 \beta_2)}{[S^2 (\Gamma_{12} + \Gamma_{21}) + 4(\gamma_d + \Gamma_{12} + \Gamma_{34}) (\alpha_1^2 + \alpha_2^2)]^2 + S^2 (\alpha_2^2 - \alpha_1^2)^2}. \quad (\text{A3.10})$$

These expressions are used in the analysis of Sec. 5.3 to obtain the expression for probe absorption at the two-photon resonance condition (*cf.* Eq. 5.9).

APPENDIX-4

Probability Amplitudes for Quantum Jump Approach

Probability amplitudes C_{ij} relevant to the analysis of Sec. 5.5 are obtained under the assumptions $\beta_1, \beta_2 \ll \alpha_1, \alpha_2$ and $\gamma_3, \gamma_4 \gg \Gamma_{12}, \Gamma_{21}, \beta_1, \beta_2$ so that γ_3, γ_4 represent the fastest time scales in the system. Thus for $t > 1/\gamma_3, 1/\gamma_4$ it is possible to eliminate fast oscillating variables C_{i3} and C_{i4} as compared to slow variables C_{i1} and C_{i2} . Under this adiabatic elimination, we obtain

$$\dot{C}_{i3}(\tau) = \dot{C}_{i4}(\tau) = 0. \quad (\text{A4.1})$$

$$C_{i3} = i(\beta_2 C_{i1} + \alpha_2 C_{i2}) / (\gamma_3 + i\delta_2), \quad (\text{A4.2})$$

$$C_{i4} = i(\beta_1 C_{i1} + \alpha_1 C_{i2}) / (\gamma_4 + i\delta_1). \quad (\text{A4.3})$$

Using the above equations in Eq. (5.22) we get the following coupled equations:

$$\dot{C}_{i1}(\tau) = -q_1 C_{i1}(\tau) - q_2 C_{i2}(\tau), \quad (\text{A4.4})$$

$$\dot{C}_{i2}(\tau) = -q_2 C_{i1}(\tau) - q_3 C_{i2}(\tau), \quad (\text{A4.5})$$

$$q_1 = \Gamma_{12} + \frac{\beta_1^2 \gamma_4}{\gamma_4^2 + \delta_1^2} + \frac{\beta_2^2 \gamma_3}{\gamma_3^2 + \delta_2^2} - i \left[\frac{\beta_1^2 \delta_1}{\gamma_4^2 + \delta_1^2} + \frac{\beta_2^2 \delta_2}{\gamma_3^2 + \delta_2^2} \right], \quad (\text{A4.6})$$

$$q_2 = \frac{\alpha_1 \beta_1 \gamma_4}{\gamma_4^2 + \delta_1^2} + \frac{\alpha_2 \beta_2 \gamma_3}{\gamma_3^2 + \delta_2^2} - i \left[\frac{\alpha_1 \beta_1 \delta_1}{\gamma_4^2 + \delta_1^2} + \frac{\alpha_2 \beta_2 \delta_2}{\gamma_3^2 + \delta_2^2} \right], \quad (\text{A4.7})$$

$$q_3 = \Gamma_{21} + \frac{\alpha_1^2 \gamma_4}{\gamma_4^2 + \delta_1^2} + \frac{\alpha_2^2 \gamma_3}{\gamma_3^2 + \delta_2^2} - i \left[\Delta_1 - \delta_1 + \frac{\alpha_1^2 \delta_1}{\gamma_4^2 + \delta_1^2} + \frac{\alpha_2^2 \delta_2}{\gamma_3^2 + \delta_2^2} \right]. \quad (\text{A4.8})$$

Eq. (A4.2) – (A4.5) can be easily solved under the initial condition $C_{ij}(0) = \delta_{ij}$.

APPENDIX-5

Steady State Populations in Tripod System

Considering all the non-radiative decays to be equal i.e. $\Gamma_{ij} = \Gamma$, we obtain the populations in tripod system as,

$$\rho_{11}^{(0)} = \Gamma [3\Gamma(\gamma_4 + h_1 + 2h_2 + h_3) + 2(h_1h_3 - h_2^2) + (h_3 - h_2)\gamma_4] / \mathfrak{S}, \quad (\text{A5.1})$$

$$\rho_{22}^{(0)} = \Gamma [3\Gamma(\gamma_4 + h_1 + 2h_2 + h_3) + 2(h_1h_3 - h_2^2) + (h_1 - h_2)\gamma_4] / \mathfrak{S}, \quad (\text{A5.2})$$

$$\rho_{44}^{(0)} = \Gamma [3\Gamma(h_1 + 2h_2 + h_3) + 2(h_1h_3 - h_2^2)] / \mathfrak{S}, \quad (\text{A5.3})$$

$$\rho_{33}^{(0)} = 1 - \rho_{11}^{(0)} - \rho_{22}^{(0)} - \rho_{44}^{(0)}, \quad (\text{A5.4})$$

where

$$h_1 = \alpha_1^2 \text{Re} \left(\frac{b_1 b_5^* + \alpha_1^2}{\mathfrak{S}_1} \right), \quad h_2 = -\alpha_1^2 \alpha_2^2 \text{Re} \left(\frac{1}{\mathfrak{S}_1} \right), \quad h_3 = \alpha_2^2 \text{Re} \left(\frac{b_1^* b_3^* + \alpha_2^2}{\mathfrak{S}_1} \right), \quad (\text{A5.5})$$

$$\mathfrak{S} = 3\Gamma^2(4h_1 + 8h_2 + 4h_3 + 3\gamma_4) + 2\Gamma\gamma_4(h_1 + h_3 - h_2) + (8\Gamma + \gamma_{43})(h_1h_3 - h_2^2), \quad (\text{A5.6})$$

$$\mathfrak{S} = b_1^* b_3^* b_5 + \alpha_1^2 b_3^* + \alpha_2^2 b_5, \quad (\text{A5.7})$$

where the coefficients b_i , ($i=1..6$) are defined in Eq. (6.2). These population terms are used in the analysis of Sec. 6.2.1.

APPENDIX-6

Steady State Populations in N System

For Model A

$$\rho_{11}^{(0)} = \Gamma_{21}[(\Gamma_{34}\Gamma_{43} - \Gamma_3\Gamma_4) + x_3(\Gamma_{34} + \Gamma_{43}) + (\Gamma_3x_4 + \Gamma_4x_2) + x_3^2 - x_2x_4]/x_1, \quad (\text{A6.1})$$

$$\begin{aligned} \rho_{22}^{(0)} = & [(x_3^2 - x_2x_4)(\Gamma_{12} + \gamma_{42} + \gamma_{32}) + \Gamma_{12}(\Gamma_{34}\Gamma_{43} - \Gamma_3\Gamma_4) \\ & + x_3\{\Gamma_4\gamma_{32} + \Gamma_3\gamma_{42} + \Gamma_{43}(\Gamma_{12} + \gamma_{32}) + \Gamma_{34}(\Gamma_{12} + \gamma_{42})\} \\ & + x_2(\Gamma_4(\Gamma_{12} + \gamma_{32}) + \gamma_{42}\Gamma_{34}) + x_4(\Gamma_3(\Gamma_{12} + \gamma_{42}) + \gamma_{32}\Gamma_{43})]/x_1, \end{aligned} \quad (\text{A6.2})$$

$$\rho_{33}^{(0)} = 2\Gamma_{21}[x_3^2 - x_2x_4 + \Gamma_4(x_2 + x_3) + \Gamma_{43}(x_3 + x_4)]/x_1, \quad (\text{A6.3})$$

$$\rho_{44}^{(0)} = 2\Gamma_{21}[x_3^2 - x_2x_4 + \Gamma_3(x_3 + x_4) + \Gamma_{34}(x_2 + x_3)]/x_1, \quad (\text{A6.4})$$

where

$$\begin{aligned} x_1 = & (x_3^2 - x_2x_4)(\Gamma_{12} + 3\Gamma_{21} + \gamma_{32} + \gamma_{42}) + (\Gamma_{12} + \Gamma_{21})(\Gamma_{34}\Gamma_{43} - \Gamma_3\Gamma_4) \\ & + x_2[\Gamma_{34}(\Gamma_{21} + \gamma_{42}) + \Gamma_4(\Gamma_{12} + 2\Gamma_{21} + \gamma_{32})] \\ & + x_3[\Gamma_3(\Gamma_{21} + \gamma_{42}) + \Gamma_4(\Gamma_{21} + \gamma_{32}) + \Gamma_{43}(\Gamma_{12} + 2\Gamma_{21} + \gamma_{32}) \\ & + \Gamma_{34}(\Gamma_{12} + 2\Gamma_{21} + \gamma_{42})] + x_4[\Gamma_{43}(\Gamma_{21} + \gamma_{32}) + \Gamma_3(\Gamma_{12} + 2\Gamma_{21} + \gamma_{42})], \end{aligned} \quad (\text{A6.5})$$

$$x_2 = -\alpha_1^2 \operatorname{Re}\left(\frac{a_4a_{12} + \alpha_1^2}{x_5}\right), \quad x_3 = \alpha_1^2\alpha_2^2 \operatorname{Re}\left(\frac{1}{x_5}\right), \quad x_4 = -\alpha_2^2 \operatorname{Re}\left(\frac{a_9a_{12} + \alpha_2^2}{x}\right), \quad (\text{A6.6})$$

$$x_5 = a_4a_9a_{12} + \alpha_1^2a_9 + \alpha_2^2a_4. \quad (\text{A6.7})$$

For Model B

$$\begin{aligned} \rho_{11}^{(0)} = & [\Gamma_3\Gamma_{21}(\gamma_{41} + \gamma_{42} - y_2 - 2y_3 - y_4) + \Gamma_3(y_2y_4 - y_3^2) + \Gamma_{21}\Gamma_{43}(\gamma_{31} + \gamma_{32}) \\ & + y_3(\Gamma_3\gamma_{42} + \Gamma_{43}\gamma_{32}) - y_4(\Gamma_3\gamma_{41} + \Gamma_{43}\gamma_{31})]/y_1, \end{aligned} \quad (\text{A6.8})$$

$$\begin{aligned} \rho_{22}^{(0)} = & [\Gamma_3\Gamma_{12}(\gamma_{41} + \gamma_{42} - y_2 - 2y_3 - y_4) + \Gamma_3(y_2y_4 - y_3^2) + \Gamma_{12}\Gamma_{43}(\gamma_{31} + \gamma_{32}) \\ & + y_3(\Gamma_3\gamma_{41} + \Gamma_{43}\gamma_{31}) - y_2(\Gamma_3\gamma_{42} + \Gamma_{43}\gamma_{32})]/y_1, \end{aligned} \quad (\text{A6.9})$$

$$\rho_{33}^{(0)} = \Gamma_{43}[(y_2 y_4 - y_3^2) - \Gamma_{12}(y_3 + y_4) - \Gamma_{21}(y_2 + y_3)] / y_1, \quad (\text{A6.10})$$

$$\rho_{44}^{(0)} = \Gamma_3[(y_2 y_4 - y_3^2) - \Gamma_{12}(y_3 + y_4) - \Gamma_{21}(y_2 + y_3)] / y_1, \quad (\text{A6.11})$$

where

$$\begin{aligned} y_1 = & (2\Gamma_3 + \Gamma_{43} + \Gamma_3)(y_2 y_4 - y_3^2) + \Gamma_3 \Gamma_{12}(\gamma_{41} + \gamma_{42} - y_2 - 3y_3 - 2y_4) \\ & + \Gamma_3 \Gamma_{21}(\gamma_{41} + \gamma_{42} - 2y_2 - 3y_3 - y_4) + \Gamma_{12} \Gamma_{43}(\gamma_{31} + \gamma_{32} - y_3 - y_4) \\ & + \Gamma_{21} \Gamma_{43}(\gamma_{31} + \gamma_{32} - y_2 - y_3) + (\Gamma_{43} \gamma_{32} + \Gamma_3 \gamma_{42})(y_3 - y_2) \\ & + (\Gamma_3 \gamma_{41} + \Gamma_{43} \gamma_{31})(y_3 - y_4), \end{aligned} \quad (\text{A6.12})$$

$$y_2 = -\alpha_2^2 \operatorname{Re}\left(\frac{a_2 a_{14} + \alpha_2^2}{y_5}\right), \quad y_3 = \alpha_2^2 \alpha_3^2 \operatorname{Re}\left(\frac{1}{y_5}\right), \quad y_4 = -\alpha_3^2 \operatorname{Re}\left(\frac{a_2 a_4 + \alpha_2^2}{y_5}\right), \quad (\text{A6.13})$$

$$y_5 = a_2 a_4 a_{14} + \alpha_2^2 a_4 + \alpha_3^2 a_{14}. \quad (\text{A6.14})$$

For Model C

$$\begin{aligned} \rho_{11}^{(0)} = & [\Gamma_{21}(\Gamma_3 \Gamma_4 - \Gamma_{34} \Gamma_{43}) + \alpha_1^2 z_2 \Gamma_{21} \Gamma_4 + \alpha_1^2 \alpha_3^2 z_2 z_3 (\Gamma_{21} + \Gamma_4 - \gamma_{42}) \\ & + \alpha_3^2 z_3 \{\Gamma_3 (\Gamma_{21} + \Gamma_4 - \gamma_{42}) - \Gamma_{43} (\gamma_{32} + \Gamma_{34})\}] / z_1, \end{aligned} \quad (\text{A6.15})$$

$$\begin{aligned} \rho_{22}^{(0)} = & [\Gamma_{12}(\Gamma_3 \Gamma_4 - \Gamma_{34} \Gamma_{43}) + \alpha_1^2 z_2 \{\Gamma_4 (\Gamma_{12} + \gamma_{32}) + \Gamma_{34} \gamma_{42}\} \\ & + \alpha_3^2 z_3 \Gamma_{12} \Gamma_3 + \alpha_1^2 \alpha_3^2 z_2 z_3 (\Gamma_{12} + \gamma_{32} + \Gamma_{34})] / z_1, \end{aligned} \quad (\text{A6.16})$$

$$\rho_{33}^{(0)} = [\alpha_1^2 z_2 \Gamma_{21} \Gamma_4 + \alpha_3^2 z_3 \Gamma_{12} \Gamma_{43} + \alpha_1^2 \alpha_3^2 z_2 z_3 (\Gamma_{21} + \gamma_{41} + \Gamma_{43})] / z_1, \quad (\text{A6.17})$$

$$\rho_{44}^{(0)} = [\alpha_1^2 z_2 \Gamma_{21} \Gamma_{34} + \alpha_3^2 z_3 \Gamma_{12} \Gamma_3 + \alpha_1^2 \alpha_3^2 z_2 z_3 (\Gamma_{12} + \gamma_{32} + \Gamma_{34})] / z_1, \quad (\text{A6.18})$$

$$\begin{aligned} \rho_{22}^{(j)} = & [z_5^{(j)} \{\Gamma_3 \Gamma_4 - \Gamma_{34} \Gamma_{43} + \alpha_1^2 z_2 (2\Gamma_4 + \Gamma_{34})\} - z_6^{(j)} \alpha_3^2 z_3 (\Gamma_3 + 2\alpha_1^2 k_2) + z_4^{(j)} \\ & \{\gamma_{32} \Gamma_4 + \gamma_{42} \Gamma_{34} - \Gamma_{12} \Gamma_{34} - \Gamma_{12} \Gamma_4 + \alpha_3^2 z_3 (\gamma_{32} - \Gamma_{12} + \Gamma_{34})\} + (z_5^{(j)} + z_6^{(j)}) \\ & \{\Gamma_{12} \Gamma_3 + \Gamma_{12} \Gamma_{43} - \gamma_{32} \Gamma_{43} - \gamma_{42} \Gamma_3 + \alpha_1^2 z_2 (\gamma_{32} - 2\gamma_{42} + \Gamma_{12})\}] / z_1, \end{aligned} \quad (\text{A6.19})$$

$$\begin{aligned} \rho_{33}^{(j)} = & [\{z_4^{(j)} \Gamma_4 - (z_5^{(j)} + z_6^{(j)}) \Gamma_{43}\} (\Gamma_{12} + \Gamma_{21}) + z_5^{(j)} \alpha_1^2 z_2 (\gamma_{42} - \Gamma_4 + \Gamma_{21}) \\ & + z_6^{(j)} (\alpha_1^2 z_2 \gamma_{42} + \alpha_1^2 z_2 \Gamma_{21} - \alpha_3^2 z_3 \Gamma_{43} + 2\alpha_1^2 k_2 \alpha_3^2 z_3) \\ & + z_4^{(j)} \alpha_3^2 z_3 (2\Gamma_{12} + \Gamma_{21} + \gamma_{41} + \Gamma_{43})] / z_1, \end{aligned} \quad (\text{A6.20})$$

$$\begin{aligned} \rho_{44}^{(j)} = & [\{z_4^{(j)}\Gamma_{34} - (z_5^{(j)} + z_6^{(j)})\Gamma_3\}(\Gamma_{12} + \Gamma_{21}) + z_4^{(j)}\alpha_3^2 z_3(\gamma_{32} + \Gamma_{34} - \Gamma_{12}) \\ & - z_6^{(j)}\{\alpha_1^2 z_2(\gamma_{32} + \Gamma_{12} + 2\Gamma_{21}) + \alpha_3^2 z_3\Gamma_3 + 2\alpha_1^2 z_2\alpha_3^2 z_3\} \\ & - z_5^{(j)}\alpha_1^2 z_2(\gamma_{32} + \Gamma_{34} - \Gamma_{12} - 2\Gamma_{21})] / z_1, \end{aligned} \quad (\text{A6.21})$$

$$\rho_{11}^{(j)} = -(\rho_{22}^{(j)} + \rho_{33}^{(j)} + \rho_{44}^{(j)}). \quad (\text{A6.22})$$

where

$$\begin{aligned} z_1 = & (\Gamma_{12} + \Gamma_{21})(\Gamma_3\Gamma_4 - \Gamma_{34}\Gamma_{43}) + \alpha_1^2 z_2[\Gamma_4(\Gamma_{12} + 2\Gamma_{21} + \gamma_{32}) + \Gamma_{34}(\Gamma_{21} + \gamma_{42})] \\ & + \alpha_3^2 z_3[\Gamma_3(\Gamma_4 + 2\Gamma_{12} + \Gamma_{21} - \gamma_{42}) + \Gamma_{43}(\Gamma_{12} - \gamma_{32} - \Gamma_{34})] \\ & + 2\alpha_1^2 \alpha_3^2 z_2 z_3(\Gamma_{12} + \Gamma_{21} + \Gamma_3 + \Gamma_4 - \gamma_{31} - \gamma_{42}), \end{aligned} \quad (\text{A6.23})$$

$$z_2 = \frac{\Gamma_3 + \Gamma_{12}}{(\Gamma_3 + \Gamma_{12})^2 + \Delta_1^2}, \quad z_3 = \frac{\Gamma_4 + \Gamma_{21}}{(\Gamma_4 + \Gamma_{21})^2 + \Delta_3^2}, \quad (\text{A6.24})$$

$$z_4^{(j)} = \alpha_1 \alpha_2 \operatorname{Re}(\rho_{34}^{(j)} / a_2^*), \quad z_5^{(j)} = \alpha_2 \alpha_3 \operatorname{Re}(\rho_{21}^{(j)} / a_5), \quad (\text{A6.25})$$

$$z_6^{(j)} = -\alpha_2 \operatorname{Im}(\rho_{14}^{(j)}), \quad (j = 1, 2, 3). \quad (\text{A6.26})$$

The populations in the three model schemes are used in the analysis of Sec. 6.3 and Sec 6.4.

APPENDIX-7

Non-Zero Elements of Matrix M^{pqs} in N system

$$M_{1,3}^{pqs} = M_{3,1}^{pqs} = M_{5,7}^{pqs} = M_{7,5}^{pqs} = M_{9,11}^{pqs} = M_{11,9}^{pqs} = M_{13,15}^{pqs} = M_{15,13}^{pqs} = -i\alpha_1, \quad (A7.1)$$

$$M_{1,9}^{pqs} = M_{9,1}^{pqs} = M_{2,10}^{pqs} = M_{10,2}^{pqs} = M_{3,11}^{pqs} = M_{11,3}^{pqs} = M_{4,12}^{pqs} = M_{12,4}^{pqs} = i\alpha_1, \quad (A7.2)$$

$$M_{1,4}^{pqs} = M_{4,1}^{pqs} = M_{5,8}^{pqs} = M_{8,5}^{pqs} = M_{9,12}^{pqs} = M_{12,9}^{pqs} = M_{13,16}^{pqs} = M_{16,13}^{pqs} = -i\alpha_2, \quad (A7.3)$$

$$M_{1,13}^{pqs} = M_{13,1}^{pqs} = M_{2,14}^{pqs} = M_{14,2}^{pqs} = M_{3,15}^{pqs} = M_{15,3}^{pqs} = M_{4,16}^{pqs} = M_{16,4}^{pqs} = i\alpha_2, \quad (A7.4)$$

$$M_{2,4}^{pqs} = M_{4,2}^{pqs} = M_{6,8}^{pqs} = M_{8,6}^{pqs} = M_{10,12}^{pqs} = M_{12,10}^{pqs} = M_{14,16}^{pqs} = M_{16,14}^{pqs} = -i\alpha_3, \quad (A7.5)$$

$$M_{5,13}^{pqs} = M_{13,5}^{pqs} = M_{6,14}^{pqs} = M_{14,6}^{pqs} = M_{7,15}^{pqs} = M_{15,7}^{pqs} = M_{8,16}^{pqs} = M_{16,8}^{pqs} = i\alpha_3, \quad (A7.6)$$

$$M_{1,6}^{pqs} = 2\Gamma_{21}, \quad M_{1,11}^{pqs} = 2\gamma_{31}, \quad M_{1,16}^{pqs} = 2\gamma_{41}, \quad (A7.7)$$

$$M_{6,1}^{pqs} = 2\Gamma_{12}, \quad M_{6,11}^{pqs} = 2\gamma_{32}, \quad M_{6,16}^{pqs} = 2\gamma_{42}, \quad (A7.8)$$

$$M_{11,16}^{pqs} = 2\Gamma_{43}, \quad M_{16,11}^{pqs} = 2\Gamma_{34}, \quad M_{k,k}^{pqs} = -\wp_k. \quad (A7.9)$$

Here \wp_k ($k=1,2,\dots,16$) are related to terms a_k defined in Eq. (6.12) as follows:

$$\wp_k = a_k + a(p, q, s), \quad (k = 1, 6, 11, 16), \quad (A7.10)$$

$$\wp_2 = a_2 + a(p, q-1, s+1), \quad (A7.11)$$

$$\wp_3 = a_3 + a(p-1, q, s), \quad (A7.12)$$

$$\wp_4 = a_4 + a(p, q-1, s), \quad (A7.13)$$

$$\wp_5 = a_5 + a(p, q+1, s-1), \quad (A7.14)$$

$$\wp_7 = a_7 + a(p-1, q+1, s-1), \quad (A7.15)$$

$$\wp_8 = a_8 + a(p, q, s-1), \quad (A7.16)$$

$$\wp_9 = a_9 + a(p+1, q, s), \quad (\text{A7.17})$$

$$\wp_{10} = a_{10} + a(p+1, q-1, s+1), \quad (\text{A7.18})$$

$$\wp_{12} = a_{12} + a(p+1, q-1, s), \quad (\text{A7.19})$$

$$\wp_{13} = a_{13} + a(p, q+1, s), \quad (\text{A7.20})$$

$$\wp_{14} = a_2 + a(p, q, s+1), \quad (\text{A7.21})$$

$$\wp_{15} = a_{15} + a(p-1, q+1, s), \quad (\text{A7.22})$$

$$a(p, q, s) = p^2\gamma_{c1} + q^2\gamma_{c2} + s^2\gamma_{c3} + 2pq\gamma_{c1c2} + 2ps\gamma_{c1c3} + 2qs\gamma_{c2c3}. \quad (\text{A7.23})$$

These elements are used for the analysis of three and 2+1-photon resonances in Sec. 7.3.

BIBLIOGRAPHY

- [1] *The theory of coherent atomic excitation: Vol. 1. Simple atoms and fields; Vol. 2. Multilevel atoms and incoherence.* B.W. Shore, Wiley-Interscience publication, New York (1990); B.W. Shore, *Acta Physica Slovaca* **58**, 243 (2008).
- [2] *Quantum Optics.* M.O. Scully and M.S. Zubairy, 6th edition, Cambridge university press, New York (2008).
- [3] *Quantum optics: an introduction.* M. Fox, 3rd edition, Oxford university press, New York (2009).
- [4] *The light fantastic.* I.R. Kenyon, Oxford University press, New York (2008).
- [5] B. Renaud, R.M. Whitley and C.R. Stroud Jr., *J. Phys. B: At. Mol. Opt. Phys.* **9**, L19 (1976).
- [6] G. Vemuri, G.S. Agarwal and B.D.N. Rao, *Phys. Rev. A* **53**, 2842 (1996).
- [7] J. Niu, L. Pei, X. Lu, R. Wang, L.-A. Wu and P. Fu, *Phys. Rev. A* **84**, 033853 (2011).
- [8] M. Wagner, H. Schneider, D. Stehr, S. Winner, A.M. Andrews, S. Schartner, G. Strasser and M. Helm, *Phys. Rev. Lett.* **105**, 167401 (2010).
- [9] E. Ahmed and A.M. Lyyra, *Phys. Rev. A* **76**, 053407 (2007).

- [10] *Coherent population trapping in laser spectroscopy*. E. Arimondo, edited by E. Wolf in *Progress in optics*, Elsevier Science, Amsterdam, vol. **XXXV**, chap. V, 258 (1996).
- [11] G. Alzetta, A. Gozzini, L. Moi and G. Orriols, *Nuovo Cimento Soc. Ita. Fis. B* **36**, 5 (1976).
- [12] P.M. Radmore and P.L. Knight, *J. Phys. B: At. Mol. Opt. Phys.* **15**, 561 (1982).
- [13] B.Lu, W.H. Burkett, M. Xiao, *Opt. Lett.* **23**, 804 (1998).
- [14] J.P. Marangos, *J. Mod. Opt.* **45**, 471 (1998).
- [15] M. Fleischhauer, A. Imamoglu and J.P. Marangos, *Rev. Mod. Phys.* **77**, 633 (2005).
- [16] S.E. Harris, *Phys. Today* **50**, 36 (1997).
- [17] M.D. Lukin and A. Imamoglu, *Nature* **413**, 273 (2001).
- [18] K.J. Boller, A. Imamoglu and S.E. Harris, *Phys. Rev. Lett.* **66**, 2593 (1991).
- [19] C.L.G. Alzar, M.A.G. Martinez and P. Nussenzveig, *Am. J. Phys.* **70**, 37 (2002).
- [20] P.M. Anisimov, J.P. Dowling and B.C. Sanders, *Phys. Rev. Lett.* **107**, 163604 (2011).
- [21] T.Y. Abi-Salloum, *Phys. Rev. A* **81**, 053836 (2010).
- [22] Y. Zhu and T.N. Wasserlauf, *Phys. Rev. A* **54**, 3653 (1996).
- [23] Niharika Singh, Q.V. Lawande, R. D'Souza, A. Ray and B.N. Jagatap, *Pramana -J. Phys.* **75**, 1151 (2010).
- [24] D. McGloin, D.J. Fullton and M.H Dunn, *Opt. Comm.* **190**, 221 (2001).
- [25] T. Li, M.-J Lu and J.D. Weinstein, *Phys. Rev. A* **84**, 023801 (2011).
- [26] N. Gavra, M. Rosenbluh, T. Zigdon, A.D. Wilson-Gordon, H. Friedmann, *Opt.*

- Comm. **280**, 374 (2007).
- [27] C. Goren, A.D. Wilson-Gordon, M. Rosenbluh and H. Friedmann, Phys. Rev. A **69**, 063802 (2004).
- [28] Niharika Singh and B.N. Jagatap, AIP Conf. Proc. **1391**, 16 (2011).
- [29] S.-J. Li, X.-D. Yang, X.-M. Cao, C.-D. Xie and H. Wang, J. Phys. B: At. Mol. Opt. Phys. **40**, 3211 (2007); Phys. Rev. Lett. **101**, 073602 (2008).
- [30] Niharika Singh, R. D'Souza, Q.V. Lawande and B.N. Jagatap, Asian J. Phys. **20**, 221 (2011).
- [31] M.G. Bason, A.K. Mohapatra, K.J. Weatherill and C.S. Adams, J. Phys. B: At. Mol. Opt. Phys. **42**, 075503 (2009).
- [32] S. Du, P. Kolchin, C. Belthangady, G.Y. Yin, S.E. Harris, Phys. Rev. Lett. **100**, 183603 (2008).
- [33] A. Sargsyan, C. Leroy, Y.P.-Leroy, D. Sarkisyan, D. Slavov and S. Cartaleva, Opt. Comm. **285**, 2090 (2012).
- [34] C.Y. Ye, A.S. Zibrov and Y.V. Rostovtsev, J. Mod. Opt. **49**, 391 (2002).
- [35] A. Javan, O. Kocharovskaya, H. Lee and M.O. Scully, Phys. Rev. A **66**, 013805 (2002).
- [36] H. Lee, Y.V. Rostovtsev, C.J. Bednar and A. Javan, Appl. Phys. B **76**, 33 (2003).
- [37] Y. Rostovtsev, I. Protsenko, H. Lee and A. Javan, J. Mod. Opt. **49**, 2501 (2002).
- [38] D.J. Fullton, S. Shepherd, R.R. Moseley, B.D. Sinclair and M.H. Dunn, Phys. Rev. A **52**, 2302 (1995).
- [39] J.R. Boon, E. Zekou, D. McGloin and M.H. Dunn, Phys. Rev. A **59**, 4675 (1999).

- [40] A. Lezama, S. Barreiro and A.M. Akulshin, *Phys. Rev. A* **59**, 4732 (1998).
- [41] C. Goren, A.D. Wilson-Gordon, M. Rosenbluh and H. Friedmann, *Phys. Rev. A* **67**, 033807 (2003); **69**, 053818 (2004).
- [42] A.V. Taichenachev, A.M. Tumaikin and V.I. Yudin, *Phys. Rev. A* **61**, 011802 (1999).
- [43] C. Goren, A.D. Wilson-Gordon, M. Rosenbluh and H. Friedmann, *Phys. Rev. A* **68**, 043818 (2003).
- [44] C.Y. Ye, A.S. Zibrov, Y.V. Rostovtsev and M.O. Scully, *J. Mod. Opt.* **50**, 2605 (2003).
- [45] E. Tilchin, A.D. Wilson-Gordon and O. Firstenberg, *Phys. Rev. A* **83**, 053812 (2011).
- [46] L.S. Molella, R.-H Rinkleff and K. Danzmann, *Phys. Rev. A* **72**, 041802 (2005).
- [47] H.S. Moon, S.K. Kim, K. Kim, C.H. Lee and J.B. Kim, *J. Phys. B: At. Mol. Opt. Phys.* **36**, 3721 (2003).
- [48] P. Valente, H. Failache and A. Lezama, *Phys. Rev. A* **67**, 013806 (2003).
- [49] J. Dimitrijevic, D. Arsenovic and B.M. Jelenkovic, *New J. Phys.* **13**, 033010 (2011).
- [50] A.M. Akulshin, A. Lezama, A.I. Sidorov, R.J. McLean and P. Hannaford, *J. Phys. B: At. Mol. Opt. Phys.* **38**, L365 (2005).
- [51] A.M. Akulshin, A. Cimmino and G.I. Opat, *Quantum Electron.* **32**, 567 (2002).
- [52] A.M. Akulshin, A.I. Sidorov, R.J. McLean and P. Hannaford, *Laser Physics* **15**, 1252 (2005).
- [53] *Lasing without inversion and electromagnetically induced transparency*. S.

- Alam, SPIE, Bellingham Washington (1999).
- [54] B.W. Shore, Contemporary physics **36**, 15 (1995).
- [55] J. Mompart and R. Corbalan, J. Opt B: Quantum Semiclass. Opt. **2**, R7 (2000).
- [56] J. Mompart, C. Peters and R. Corbalan, Phys. Rev. A **57**, 2163 (1998).
- [57] O. Kocharovskaya and P. Mandel, Quantum Opt. **6**, 217 (1994); Phys. Rev. A, **42**, 523 (1990).
- [58] O. Kocharovskaya, P. Mandel and Y.V. Radeonychev, Phys. Rev. A **45**, 1997 (1992).
- [59] O. Kocharovskaya, Hyperfine Interactions **107**, 187 (1997); Phys. Rep. **219**, 175 (1992).
- [60] D. Braunstein and R Shuker, J. Phys. B: At. Mol. Opt. Phys. **42**, 125401 (2009); Phys. Rev. A **68**, 013812 (2003).
- [61] G.S. Agarwal, Phys. Rev. A **44**, R28 (1991); Phys. Rev. Lett. **67**, 980 (1991).
- [62] K.M. Gheri and D.F. Walls, Phys. Rev. Lett. **68**, 3428 (1992); Phys. Rev. A **45**, 6675 (1992).
- [63] S.-Y. Zhu and M.O. Scully, Phys. Rev. Lett. **76**, 388 (1996).
- [64] M.O. Scully, S.-Y. Zhu and A. Gavrielides, Phys. Rev. Lett. **62**, 2813 (1989).
- [65] Y. Zhu, A.I. Rubiera and M. Xiao, Phys. Rev. A **53**, 1065 (1996).
- [66] M. Marthaler, Y. Utsumi, D.S. Golubev, A. Shnirman and G. Schon, Phys. Rev. Lett. **107**, 093901 (2011).
- [67] M.D. Frogley, J.F. Dynes, M. Beck, J. Faist and C.C. Philips, Nature materials **5**, 175 (2006).
- [68] G.A. Koganov, B. Shif and R. Shuker, Opt. Lett. **36**, 2779 (2011).

- [69] G.G. Padmabandu, G.R. Welch, I.N. Shubin, E.S. Fry, D.E. Nikonov, M.D. Lukin and M.O. Scully, *Phys. Rev. Lett.* **76**, 2053 (1996).
- [70] S. Ya. Kilin, K.T. Kapale and M.O. Scully, *Phys. Rev. Lett.* **100**, 173601 (2008).
- [71] A.S. Zibrov, M.D. Lukin, D.E. Nikonov, L. Hollberg, M.O. Scully, V.L. Velichansky and H.G. Robinson, *Phys. Rev. Lett.* **75**, 1499 (1995).
- [72] J. Kitching and L. Hollberg, *Phys. Rev. A* **59**, 4685 (1999).
- [73] S.E. Harris, *Phys. Rev. Lett.* **62**, 1033 (1989).
- [74] A. Imamoglu, J.E. Field and S.E. Harris, *Phys. Rev. Lett.* **66**, 1154 (1991).
- [75] G. Grynberg, M. Pinard and P. Mandel, *Phys. Rev. A* **54**, 776 (1996).
- [76] V. Ahufinger, J. Mompert and R. Corbalan, *Phys. Rev. A* **61**, 053814 (2000).
- [77] A. Hajibadali, K. Abbasian, Sh. Rahmatallahpur, *Optik* **123**, 1035 (2012).
- [78] Y. Zhu and J. Lin, *Phys. Rev. A* **53**, 1767 (1996).
- [79] G. Vemuri and G.S. Agarwal, *Phys. Rev. A* **53**, 1060 (1996).
- [80] H.S. Moon, L. Lee, K. Kim and J.B. Kim, *Appl. Phys. Lett.* **84**, 3001 (2004).
- [81] S.C. Bell, D.M. Heywood, J.D. White, J.D. Close and R.E. Scholten, *Appl. Phys. Lett.* **90**, 171120 (2007).
- [82] Y.B. Kale, A. Ray, R. D'Souza, Q.V. Lawande and B.N. Jagatap, *Appl. Phys. B* **100**, 505 (2010).
- [83] R. Wynands and A. Nagel, *Appl. Phys. B* **68**, 1 (1999).
- [84] I. Novikova, D.F. Phillips, A.S. Zibrov, R.L. Walsworth, A.V. Taichenachev and V.I. Yudin, *Opt. Lett.* **31**, 622 (2006); *Opt. Lett.* **31**, 2353 (2006).
- [85] J. Vanier, *Appl. Phys. B* **81**, 421 (2005); J. Vanier, M. Levine, S. Kendig, D. Janssen, C. Everson and M. Delaney, *Int. Freq. Control Symposium*, p.1 (2004).

- [86] J. Kitching, S. Knappe and E.A. Donley, IEEE sensors journal, **11**, 1749 (2011).
- [87] S. Knappe, V. Shah, P.D.D. Schwindt, L. Hollberg, J. Kitching, L.-A Liew and J. Moreland, Appl. Phys. Lett. **85**, 1460 (2004); S. Knappe, P.D.D. Schwindt, V. Shah, L. Hollberg and J. Kitching, Opt. Express **13**, 1249 (2005).
- [88] M. Stahler, S. Knappe, C. Affolderbach, W. Kemp and R. Wynands, Europhys. Lett. **54**, 323 (2001).
- [89] M.H. Acuna, Rev. Sci. Instrum. **73**, 3717 (2002).
- [90] P.D.D. Schwindt, S. Knappe, V. Shah, L. Hollberg, J. Kitching, L.-A Liew and J. Moreland, Appl. Phys. Lett. **85**, 6409 (2004).
- [91] D. Budker and M. Romalis, Nature physics **3**, 227 (2007).
- [92] A. Aspect, E. Arimondo, R. Kaiser, N. Vansteenkiste and C. Cohen-Tannoudji, Phys. Rev. Lett. **61**, 826 (1988).
- [93] M. Bienert and G. Morigi, New J. Phys. **14**, 023002 (2012).
- [94] M. Bayer, Nature Physics **4**, 678 (2008).
- [95] R. Rohlsberger, H.C. Wille, K. Schlage and B. Sahoo, Nature **482**, 199 (2012).
- [96] R.W. Boyd, J. Mod. Opt. **56**, 1908 (2009).
- [97] *Fast light, slow light and left-handed light*. P.W. Milonni, Series in Optics and optoelectronics, Institute of Physics Publishing, Bristol and Philadelphia (2004).
- [98] *Slow and fast light*. R.W. Boyd and D.J. Gauthier, edited by E. Wolf, in *Progress in optics*, Elsevier Science, Amsterdam, vol. **43** (2002); R.W. Boyd and D.J. Gauthier, Science **326**, 1074 (2009).
- [99] D.F. Phillips, A. Fleischhauer, A. Mair, R.L. Walsworth and M.D. Lukin, Phys. Rev. Lett. **86**, 783 (2001).

- [100] M.S. Bigelow, N.N. Lepeshkin and R.W. Boyd, *Science* **301**, 200 (2000).
- [101] M.M. Klein, M. Hohensee, Y. Xiao, R. Kalara, D.F. Phillips and R.L. Walsworth, *Phys. Rev. A* **79**, 053833 (2009).
- [102] A.B. Matsko, O. Kocharovskaya, Y.V. Rostovtsev, G.R. Welch, A.S. Zibrov and M.O. Scully, *Adv. At. Mol. Opt. Phys.* **46**, 191 (2001).
- [103] L.V. Hau, S.E. Harris, Z. Dutton and C.H. Behroozi, *Nature* **397**, 594 (1999).
- [104] A.H.S.-Naeini, T.P.M. Alegre, J. Chan, M. Eichenfield, M. Winger, Q. Lin, J.T. Hill, D.E. Chang and O. Painter, *Nature* **472**, 69 (2011).
- [105] M.D. Lukin and A. Imamoglu, *Phys. Rev. Lett.* **84**, 1419 (2000).
- [106] S.E. Harris, *Phys. Rev. Lett.* **85**, 4032 (2000).
- [107] B.S. Ham, *J. Mod. Opt.* **49**, 2477 (2002).
- [108] O. Kocharovskaya, Y.V. Rostovtsev and M.O. Scully, *Phys. Rev. Lett.* **86**, 628 (2001).
- [109] Yi.-H. Chen, M.-J. Lee, W. Hung, Y.-C. Chen, Y.-F. Chen and I.A. Yu, *Phys. Rev. Lett.* **108**, 173603 (2012).
- [110] A.S. Zibrov, A.B. Matsko, O. Kocharovskaya, Y.V. Rostovtsev, G.R. Welch and M.O. Scully, *Phys. Rev. Lett.* **88**, 103601 (2002).
- [111] J.P. Marangos, *Nature* **406**, 243 (2000).
- [112] L.J. Wang, A. Kuzmich and A. Dogariu, *Nature* **406**, 277 (2000).
- [113] G.M. Gehring, A. Schweinsberg, C. Barsi, N. Kostinski and R.W. Boyd, *Science* **312**, 895 (2006).
- [114] G.S. Agarwal, T.N. Dey and S. Menon, *Phys. Rev. A* **64**, 053809 (2001).
- [115] V.G. Veselago, *Sov. Phys. Usp.* **10**, 509 (1968).

- [116] V.G. Veselago, L. Braginsky, V. Shklover and C. Hafner, *J. Comput. Theor. Nanosci.* **3**, 189 (2006).
- [117] J.B. Pendry, *Phys. Rev. Lett.* **85**, 3966 (2000).
- [118] S.A. Ramakrishna, *Rep. Prog. Phys.* **68**, 449 (2005) and references therein.
- [119] J.B. Pendry and D.R. Smith, *Phys. Today* **57**, 37 (2004).
- [120] J.B. Pendry, D. Schurig and D.R. Smith, *Science* **23**, 1780 (2006).
- [121] K.L. Tsakmakidis, A.D. Boardman and O. Hess, *Nature* **450**, 397 (2007).
- [122] D.R. Smith, W.J. Padilla, D.C. Vier, S.C. Nemat-Nasser and S. Schultz, *Phys. Rev. Lett.* **84**, 4184 (2000).
- [123] E. Cubukcu, K. Aydin, E. Ozbay, S. Foteinopoulou and C.M. Soukoulis, *Nature* **423**, 604 (2003).
- [124] H. Yoon, K.Y.M. Yeung, V. Umansky and D. Ham, *Nature* **488**, 65 (2012).
- [125] S. Zhang, Y.S. Park, J. Li, X. Lu, W. Zhang and X. Zhang, *Phys. Rev. Lett.* **102**, 023901 (2009).
- [126] M.O. Oktel and O.E. Mustecaphoglu, *Phys. Rev. A* **70**, 053806 (2004).
- [127] Q. Thommen and P. Mandel, *Phys. Rev. Lett.* **96**, 053601 (2006).
- [128] J.C. Liu, J. Zhang, J. Liu and G. Jin, *Phys. B: At. Mol. Opt. Phys.* **42**, 095402 (2009).
- [129] X.M. Su, H.X. Kang, J. Kou, X.Z. Guo and J.Y. Gao, *Phys. Rev. A* **80**, 023805 (2009).
- [130] X.-Yu Yang and Y.-Yuan Jiang, *Opt. Comm.* **285**, 2161 (2012).
- [131] K.I. Osman and A. Joshi, *Opt. Comm.* **285**, 3162 (2012).
- [132] C. Goren, A.D. Wilson-Gordon, M. Rosenbluh and H. Friedmann, *Phys. Rev. A*

- 72, 023826 (2005).
- [133] X. Yang and S. Zhu, Phys. Rev. A **78**, 023818 (2008).
- [134] E. Figueroa, F. Vewinger, J. Appel and A.I. Lvovsky, Opt. Lett. **31**, 2625 (2006).
- [135] J.G. Coffey, M. Anderson and J.C. Camparo, Phys. Rev. A **65**, 033807 (2002).
- [136] M.A. Kumar and S. Singh, Phys. Rev. A **79**, 063821 (2009).
- [137] R.H. Dicke, Phys. Rev. **89**, 472 (1953).
- [138] J. Javanainen, Europhys. Lett. **17**, 407 (1992).
- [139] D. Wang and Y. Zheng, Phys. Rev. A **83**, 013810 (2011).
- [140] J.W. Gao, Q.Q. Bao, R.G. Wan, C.L. Cui and J.H. Wu, Phys. Rev. A **83**, 053815 (2011).
- [141] W.-J. Jiang, X. Yan, J. Song, H.-b. Zheng, C. Wua, B.-y. Yin and Y. Zhang, Opt. Comm. **282**, 101 (2009).
- [142] M.V.G. Dutt, J. Cheng, B. Li, X. Xu, X. Li, P.R. Berman, D.G. Steel, A.S. Bracker, D. Gammon, S.E. Economou, R.-B. Liu and L.J. Sham, Phys. Rev. Lett. **94**, 227403 (2005).
- [143] Y. Bai, H. Guo, H. Sun, D. Han, C. Liu and X. Chen, Phys. Rev. A **69**, 043814 (2004).
- [144] G.S. Agarwal, Phys. Rev. Lett. **37**, 1383 (1976).
- [145] G.S. Agarwal and P.A. Narayana, Opt. Comm. **30**, 364 (1979).
- [146] B.J. Dalton and P.L. Knight, J. Phys. B: At. Mol. Phys. **15**, 3997 (1982); Opt. Comm. **42**, 411 (1982).
- [147] B.J. Dalton, R. McDuff and P.L. Knight, Optica Acta **32**, 61 (1985).
- [148] R. D'Souza, Q.V. Lawande and S.V. Lawande, Opt. Comm. **50**, 342 (1984).

- [149] S.V. Lawande, R.R. Puri and R. D'Souza, Phys. Rev. A **33**, 2504 (1986); S.V. Lawande, R. D' Souza and R.R. Puri, Phys. Rev. A **36**, 3228 (1987).
- [150] P.A. Lakshmi and S. Swain, J. Mod. Opt. **38**, 2031 (1991).
- [151] J. Dalibard, J. Dupont-Roc and C. Cohen-Tannoudji, J. Physique **45**, 637 (1984).
- [152] K.D. Quoc, V.C. Long and W. Leonski, Phys. Scr. **T147**, 014008 (2012).
- [153] S. Sultana and M.S. Zubairy, Phys. Rev. A **49**, 438 (1994).
- [154] S.-Q. Gong, Z.-Z. Xu and S.-H. Pan, J. Mod. Opt. **42**, 1397 (1995).
- [155] Y. Xiao, T. Wang, M. Baryakhtar, M.V. Camp, M. Crescimanno, M. Hohensee, L. Jiang, D.F. Phillips, M.D. Lukin, S.F. Yelin and R.L. Walsworth, Phys. Rev. A **80**, 041805 (2009).
- [156] S. Qamar, S. Qamar and M.S. Zubairy, Opt. Comm. **283**, 781 (2010).
- [157] M. Fleischhauer, M.D. Lukin, D.E. Nikonov and M.O. Scully, Opt. Comm. **110**, 351 (1994).
- [158] K.I. Osman, Opt. Comm. **88**, 364 (1992).
- [159] N.G. Van Kampen, Physica **74**, 215; 239 (1974); *Stochastic processes in physics and chemistry*. N.G. Van Kampen, 3rd edition, North Holland, Amsterdam (2007).
- [160] *Quantum statistical properties of radiation*. W.H. Louisell, Wiley, New York (1973).
- [161] J.C. Petch, C.H. Keitel, P.L. Knight and J.P. Marangos, Phys. Rev. A **53**, 543 (1996).
- [162] Z. Zhang, X. Xue, C. Li, S. Cheng, L. Han, H. Chen, H. Zheng and Y. Zhang, Opt. Comm. **285**, 3627 (2012).

- [163] S.P. Tewari and G.S. Agarwal, Phys. Rev. Lett. **56**, 1811 (1986).
- [164] H. Schmidt and A. Imamoglu, Opt. Lett. **21**, 1936 (1996).
- [165] H. Wang, D. Goorskey and M. Xiao, Phys. Rev. Lett. **87**, 073601 (2001).
- [166] J. Wu, J.-B. Liu, H. Li, X.Y. Lu and A. Zheng, Opt. Comm. **285**, 1424 (2012).
- [167] R. Slusher, L. Hollberg, B. Yurke, J. Mertz and J. Valley, Phys. Rev. Lett. **55**, 2409 (1985).
- [168] T. Peyronel, O. Firstenberg, Q-Y Liang, S. Hofferberth, A.V. Gorshkov, T. Pohl, M.D. Lukin and V. Vuletić, Nature **488**, 57 (2012).
- [169] J.P. Poizat and P. Grangier, Phys. Rev. Lett. **70**, 271 (1993).
- [170] J. Guena, M. Lintz and M.-A Bouchiat, J. Opt. Soc. Am. B **22**, 21 (2005).
- [171] M.A. Anton, O.G. Calderon, S. Melle, I. Gonzalo and F. Carreño, Opt. Comm. **268**, 146 (2006).
- [172] M.A. Anton, F. Carreno, O.G. Calderon, S. Melle and I. Gonzalo, Opt. Comm. **281**, 6040 (2008).
- [173] F. Zhou, Y. Niu and S. Gong, J. Chem. Phys. **131**, 034105 (2009).
- [174] G. Ma, B. Shi, Y. Yao, H. Guo and W. Liu, J. Mod. Opt. **57**, 390 (2010).
- [175] A. Lazoudis, T. Kirova, E.H. Ahmed, L. Li, J. Qi and A.M. Lyyra, Phys. Rev. A **82**, 023812 (2010).
- [176] A. Lazoudis, T. Kirova, E.H. Ahmed, P. Qi, J. Huennekens and A.M. Lyyra, Phys. Rev. A **83**, 063419 (2011).
- [177] J. Qi, F.C. Spano, T. Kirova, A. Lazoudis, J. Magnes, L. Li, L.M. Narducci, R.W. Field and A.M. Lyyra, Phys. Rev. Lett. **88**, 173003 (2002).
- [178] L. Li, P. Qi, A. Lazoudis, E. Ahmed and A.M. Lyyra, Chem. Phys. Lett. **403**,

- 262 (2005).
- [179] H. Li, H. Chen, M.A. Gubin, Y.V. Rostovtsev, V.A. Sautenkov and M.O. Scully, *Laser Phys.* **20**, 1725 (2010).
- [180] Niharika Singh, Q.V. Lawande, R. D'Souza and B.N. Jagatap, *J. Chem. Phys.* **137**, 104309 (2012).
- [181] W.J. Meath and E.A. Power, *J. Phys. B: At. Mol. Opt. Phys.* **17**, 763 (1984); *Mol. Phys.* **51**, 585 (1984).
- [182] M.A. Kmetic and W.J. Meath, *Phys. Lett. A* **108**, 340 (1985); *Phys. Rev. A* **41**, 1556 (1990).
- [183] M.A. Kmetic, R.A. Thuraisingham and W.J. Meath, *Phys. Rev. A* **33**, 1688 (1986).
- [184] S. Nakai and W.J. Meath, *J. Chem. Phys.* **96**, 4991 (1992).
- [185] A.E. Kondo, W.J. Meath, S.H. Nilar and A.J. Thakkar, *Chem. Phys.* **186**, 375 (1994).
- [186] A. Brown and W.J. Meath, *J. Chem. Phys.* **109**, 9351 (1998).
- [187] B.N. Jagatap and W.J. Meath, *J. Opt. Soc. Am. B* **19**, 2673 (2002).
- [188] W.J. Meath, B.N. Jagatap and A.E. Kondo, *J. Phys. B: At. Mol. Opt. Phys.* **39**, S605 (2006).
- [189] W.J. Meath and B.N. Jagatap, *J. Phys. B: At. Mol. Opt. Phys.* **44**, 205401 (2011).
- [190] J.M. Bowman, S. Irle, K. Morokuma and A. Wodtke, *J. Chem. Phys.* **114**, 7923 (2001).
- [191] Y. Chen, X.G. Wei and B.S. Ham, *Opt. Express* **17**, 1781 (2009).
- [192] W.C. Stwalley and W.T. Zemke, *J. Chem. Phys. Ref. Data* **22**, 87 (1993).

- [193] W.T. Zemke and W.C. Stwalley, *J. Chem. Phys.* **73**, 5584 (1980).
- [194] H. Partridge, S.R. Langhoff, W.C. Stwalley and W.T. Zemke, *J. Chem. Phys.* **75**, 2299 (1981).
- [195] W.T. Zemke, J.B. Crooks and W.C. Stwalley, *J. Chem. Phys.* **68**, 4628 (1978).
- [196] W.T. Zemke and W.C. Stwalley, *J. Chem. Phys.* **68**, 4619 (1978).
- [197] H.R. Schlossberg and A. Javan, *Phys. Rev.* **150**, 267 (1966).
- [198] H. Xia, S.J. Sharpe, A.J. Merriam and S.E. Harris, *Phys. Rev. A* **56**, R3362 (1997).
- [199] I.E. Mazets, B.G. Matisov, E. Cerboneschi and E. Arimondo, *Phys. Lett.* **229**, 77 (1997).
- [200] C.Y. Ye and A.S. Zibrov, *Phys. Rev. A* **65**, 023806 (2002).
- [201] Y.B. Kale, A. Ray, Niharika Singh, Q.V. Lawande and B.N. Jagatap, *Eur. Phys. J. D* **61**, 221 (2011).
- [202] V. Wong, R.W. Boyd, C.R. Stroud, Jr., R.S. Bennink and A.M. Marino, *Phys. Rev. A* **68**, 012502 (2003).
- [203] H.-T. Tan, H.-X. Xia and G.-X. Li, *J. Phys. B: At. Mol. Opt. Phys.* **42**, 125502 (2009).
- [204] D.A. Steck, <http://steck.us/alkali data>, Revision 2.1, 1 (2008).
- [205] Niharika Singh, Y.B. Kale, A. Ray and B.N. Jagatap, *Indian J. Phys.* **84**, 1119 (2010).
- [206] C. Cohen-Tannoudji, B. Zambon and E. Arimondo, *J. Opt. Soc. Am. B* **10**, 2107 (1993).
- [207] J. Mompert and R. Corbalan, *Opt. Comm.* **156**, 133 (1998); *Eur. Phys. J. D* **5**,

- 351 (1999).
- [208] J. Mompart, R. Corbalan and R. Vilaseca, *Opt. Comm.* **147**, 299 (1998).
- [209] W.-H. Xu and J.-Y. Gao, *Phys. Rev. A* **67**, 033816 (2003).
- [210] M.B. Plenio and P.L. Knight, *Rev. Mod. Phys.* **70**, 101 (1998).
- [211] *Atom-photon interactions: basic processes and applications*. C. Cohen-Tannoudji, J.D.-Roc and G. Grynberg, Wiley-VCH, Weinheim (2004).
- [212] Y. Chen, X.G. Wei and B.S. Ham, *J. Phys. B: At. Mol. Opt. Phys.* **42**, 065506 (2009).
- [213] X.-X. Tian, D.-K. Lia and J.-H. Wu, *Opt. Comm.* **283**, 2561 (2010).
- [214] S.E. Harris and Y. Yamamoto, *Phys. Rev. Lett.* **81**, 3611 (1998).
- [215] M. Yan, E.G. Rickey and Y. Zhu, *Phys. Rev. Lett.* **64**, 041801 (2001)
- [216] L. Zhao, G. Yang and W. Duan, *Opt. Lett.* **37**, 2853 (2012).
- [217] X-Li Song, A.-J. Li, L. Wang, Z.-H. Kang, J. Kou, B. Zhang, C.-L. Wang, Y. Jiang and J.-Y. Gao, *Phys. Rev. A* **79**, 053857 (2012).
- [218] C.-Li Cui, J.-K. Jia, J.-W. Gao, Y. Xue, G. Wang and Jin-Hui Wu, *Phys. Rev. A* **76**, 033815 (2012).
- [219] T.N. Dey and G.S. Agarwal, *Phys. Rev. A* **76**, 015802 (2007).
- [220] C. Hang and G. Huang, *Opt. Express* **18**, 2952 (2010).
- [221] Y. Han, J. Xiao, Y. Liu, C. Zhang, H. Wang, M. Xiao and K. Peng, *Phys. Rev. A* **77**, 023824 (2008).
- [222] J. Sheng, X. Yang, H. Wu and M. Xiao, *Phys. Rev. A* **84**, 053820 (2011).
- [223] J.L. Ding, B.P. Hou and S.J. Wang, *J. Phys. B: At. Mol. Opt. Phys.* **43**, 225502 (2010).

- [224] S.-C. Tian, R.-G. Wan, Z.-H. Kang, H. Zhang, Y. Jiang, H.-N. Cui and J.-Yue Gao, *J. Opt. Soc. Am. B* **29**, 881 (2012).
- [225] R.-G. Wan, J. Kou, L. Jiang, S.-Q. Kuang, Y. Jiang and J.-Y. Gao, *Opt. Comm.* **284**, 1569 (2011).
- [226] T. Abi-Salloum, S. Meiselman, J.P. Davis and F.A. Narducci, *J. Mod. Opt.* **56**, 1926 (2009).
- [227] C. Champenois, G. Morigi and J. Eschner, *Phys. Rev.* **A74**, 053404 (2006).
- [228] W. Nagourney, I. Sandberg and H. Dehmelt, *Phys. Rev. Lett.* **56**, 2797 (1986).
- [229] R.J. Cook and H.J. Kimble, *Phys. Rev. Lett.* **54**, 1023 (1985); R.J. Cook, *Physica Scripta*. **T21**, 49 (1988); *Quantum jumps*. R.J. Cook, edited by E. Wolf, in *Progress in optics*, Elsevier, Amsterdam, vol. **XXVIII**, chap. V, 363 (1990).
- [230] G. Fu, X. Li, Z. Zhuang, L. Zhang, L. Yang, X. Li, H. Li, N.B. Manson and C. Wei, *Phys. Lett. A* **372**, 176 (2008).
- [231] L. Yang, L. Zhang, X. Li, L. Han, G. Fu, N.B. Manson, D. Suter and C. Wei, *Phys. Rev. A* **72**, 053801 (2005).
- [232] C.Y. Ye, A.S. Zibrov, Y.V. Rostovtsev and M.O. Scully, *Phys. Rev. A* **65**, 043805 (2002).
- [233] A.V. Sharypov, A.D. Wilson-Gordon, *Opt. Comm.* **282**, 3591 (2009).
- [234] M.D. Lukin, S.F. Yelin, M. Fleischhauer and M.O. Scully, *Phys. Rev. A* **60**, 3225 (1999).